The Incorporation and Controlled Release of Anionic Drugs from a Polypyrrole Membrane Film

NUI MAYNOOTH

Ollscoil na hÉireann Má Nuad

Eimear M. Ryan BSc. (Hons)

Department of Chemistry

National University of Ireland Maynooth

November 2010

Thesis submitted to the National University of Ireland in Fulfilment of the Requirements for the Degree of Doctor of Philosophy

Supervisor: Prof. Carmel B. Breslin

Head of Department: Prof. John P. Lowry

TABLE OF CONTENTS

This thesis is dedicated to my parents, with love.

This is where I have always been coming to. Since my time began. And when I go away from here, this will be the mid-point, to which everything ran, before, and *from* which everything will run.

A.S. Byatt, *Possession*

Declaration

I hereby certify that this thesis, which I now submit for assessment on the programme of study leading to the award of Ph.D., has not been submitted, in whole or part, to this or any other university for any degree, and is, except where otherwise stated the original work of the author.

Signed:_____ Date:_____

Acknowledgements

First and foremost, I'd like to thank my supervisor, Prof. Carmel Breslin. Over the last number of years, she has offered me guidance, support and encouragement. Even with such a large research group she was always been generous with her time and I couldn't have asked for a better mentor. No problem was too small and I have learned so much from her in the last three years.

During the course of this work, I was funded by Irish Research Council for Science, Engineering and Technology (IRCSET) and by an Endeavour Research Fellowship for my time in Australia.

I'd also like to thank Dr. Denise Rooney and Dr. John Colleran. To the technical staff, especially Ken and Ollie, thanks for all the help throughout the years. A special thank you to Mr. Noel Williams, who goes above and beyond the call of duty, helping all the postgrads in the department - I don't think he realises how lost we'd all be without him. Thanks also to Prof. Gordon Wallace and Dr. Simon Moulton for the time I spent in the Intelligent Polymer Research Institute in the University of Wollongong and to staff of the pathology lab in Wollongong Hospital. The experience was even more enhanced by the great friendships I made; Dr. Scott 'Scottie' McGovern, Troy, Willo, Bec and Cameron, we had some great laughs and those are memories I will always treasure.

I can't go any further without mentioning my former lab colleagues Dr. Claire Harley, Catherine 'Foxy' Fox and Dr. Gillian Hendy. They were not only there to lend a helping hand in the lab but they have become some of my closest friends and I know that will still be the case many years from now. A huge thanks to the postgrads and postdocs in the chemistry department for all the laughs and coffee room banter. I can't name everyone but I would like to mention Dr. Valeria Annibaldi, Dr. Sinéad McDermott, Enrico, Roisín, Conor, John Murphy, Owen and Declan. I wish you all the best of luck in the future.

The most important people to thank are my family and friends who supported me through all of my studies; my parents, John and Audrey for their unequivocal belief in my abilities and unconditional support. To my 'twin' sister Caoimhe and my brother Barry, his wife Kelly and their children Sadhbh and Cormac. To all the girls Gráinne, Sinéad, Rebecca, James, Elaine, Edel, Yvonne and of course Sarah who I've shared many of my world travels with including Australia. To all my Galway Cycle friends especially Ann Marie, friend for life is an apt phrase.

Finally, Fiachra. Thank you for your patience and understanding. You were always there and I will never forget that.

Abstract

In this thesis, results are presented and discussed on the synthesis and characterisation of polypyrrole (PPy) doped with various anionic drugs. The drugs, which were small to medium-large in size, included the aqueous soluble dexamethasone 21-phosphate disodium (NaDex) and valproic acid sodium (NaVPA) salts, and the less soluble diclofenac sodium (NaDF) salt. Two other drugs, indomethacin sodium (NaIndo) and sulindac sodium (NaSul) with very limited solubility in aqueous solution, were chosen.

The incorporation of dexamethasone (Dex^{2-}) and diclofenac anions (DF^{-}) within the PPy membrane was achieved by a potentiostatic mode of growth from an aqueous solution of pyrrole and the drug under investigation. For the PPy doped with Dex^{2-}, characterisation and release studies found the doping level of the polymer to be about 0.30, and approximately 31 μmol cm^{-2} of Dex^{2-} was incorporated into the polymer upon polymerisation. Furthermore, it was observed that the rate of release could be controlled by the potential applied with approximately 89 % of the Dex^{2-} released within 60 min at an applied potential of – 0.900 V vs SCE.

For the PPy doped with DF^{-}, unusual patterns in growth and morphology were observed. During the deposition of the polymer, the rate of polymerisation decreased with increasing time and higher applied potentials. The polymer had features of an insulating film, as evident from electrochemical impedance measurements, while SEM confirmed the presence of crystal-like shards on the surface of the polymer. These findings suggest that insoluble drug crystals are formed during polymerisation. DF^{-} displays a limited solubility in aqueous solutions and during the oxidation of the monomer and drop of pH at the surface, the equilibrium is shifted from the soluble DF^{-} towards the insoluble HDF causing insoluble crystals of the drug to deposit on the surface of the polymer, which hinders further polymerisation.

The incorporation of two insoluble medium sized drugs, NaIndo and NaSul, into the PPy film was also investigated. Deposition of PPy doped with either of the

drugs in question was carried out in ethanol and tetrabutylammonium perchlorate (TBAP) was added to increase the conductivity. It was found that the PPy films formed in this organic medium were not as conducting as those formed in the aqueous solution, and doping levels were considerably lower than those previously reported for PPy. The addition of the TBAP introduces the small and mobile, ClO_4^-, anion which is well known to dope PPy. UV-visible spectroscopy was used to calculate that approximately 2.19 x 10^{-6} mol cm^{-2} of ClO_4^- was present in the polymer. However, this is quite minute compared to the estimated amount of drug doped within the polymer; 260 μmol cm^{-2} and 60 μmol cm^{-2} of $Indo^-$ and Sul^-, respectively. As seen with the other polymers the rate of release was controlled by the applied potential.

Finally, the formation of PPy doped with a small soluble anionic drug, VPA^-, was studied. Although this was the smallest of all the drugs studied, it was not possible to incorporate this drug into the PPy membrane electrochemically. This was explained in terms of the solubility of the anion at low pH values. At pH values below 5.6 the equilibrium of the VPA^- is shifted towards the insoluble HVPA. As the monomer is oxidised, there is a decrease in the local pH in the vicinity of the electrode and this causes the HVPA to precipitate from solution. This, in turn, prevents any PPy from being deposited at the electrode. Vapour phase polymerisation is offered as an alternative approach to immobilise this drug into the PPy film.

Chapter 1

Introduction and Literature Review

1.1 Introduction

The aim of this research work was to examine the use of polypyrrole (PPy), a well known conducting polymer (CP), for the incorporation and controlled release of anionic drugs. The drugs studied in this work, were chosen based on their size and solubility. All drugs are FDA approved and currently on the market. They include anti-inflammatory drugs; dexamethasone 21-phosphate disodium, diclofenac sodium salt, indomethacin sodium salt and sulindac sodium salt as well as valproic acid sodium salt, which is used in the treatment of epilepsy and bipolar disorder. Further details on the applications and pharmacokinetics of each of these drugs are given in the appropriate results chapters. In this introductory chapter, the concept of controlled drug release is first introduced and the advancements that have occurred in this area over the last number of years are described. This is then followed by a description of CPs, particularly PPy and how this polymer can be used in drug delivery. Finally, a brief overview of the work presented and discussed in this thesis is given.

1.2 Controlled drug release

The first controlled release systems were produced in the early 1970s and since then there has been great interest in their development. Such systems have been employed in a wide variety of areas including cosmetics, food and pesticides[1-3]. Controlled release systems are focused on carrying out the release of the material in question, over a certain time without an external influence from any other potential release factor[4]. Another important research area under consideration is the development of drug delivery systems (DDS). The focus of research efforts in the drug delivery field has been on developing systems that can deliver a drug at a predictable release rate independent of their environment[5].

Several drug delivery devices have been under development since the 1970s. In 1979, the first scopolamine patch was approved and by 2004 a number of transdermal patches for drugs, such as nicotine, clonidine, fentanyl, estradiol, testosterone, lidocaine and oxybutin were in existence with the annual US market

for transdermal patches at more than $3 billion[6, 7]. Like a transdermal patch, polymeric coated tablets offer a straightforward, but effective, approach in providing a continuous sustained release of drugs[8-11]. However, during the 1980s many researchers began to focus on more sophisticated means of drug delivery that could be controlled[12]. Companies currently developing drug delivery devices aim to meet particular goals mostly related to the state of the patient[13]. These goals include:

- Improved efficiency
- Reduced side effects
- Continuous dosing
- Reduced pain administration
- Increased ease of use
- Increased compliance
- Improved mobility
- Decreased involvement with healthcare workers

With these criteria in mind, implants are an attractive prospect for controlled drug delivery devices. In 2004, the FDA announced that the world's first implantable radio frequency identification (RFID) microchip for humans had been cleared for medical uses in the United States[14]. About the size of a grain of rice, 'VeriChip' is a subdermal radio frequency microchip. The device has no power supply and it is activated when a scanning device is moved along the skin above it. A tiny transmitter on the chip then releases patient-specific information. Although not capable of carrying out arithmetic operations, such technology is available, and one of the biggest regulatory thresholds was surpassed. Thus, it is only a matter of time before new generations of similar devices seek FDA approval[15]. Many types of implantable controlled delivery devices are in various stages of production and clinical evaluation[16]. These devices have been designed to release drugs at various dosages and for both intermittent and continuous delivery.

Controlled release DDS offer advantages over conventional therapies by maintaining drug concentrations at effective levels while simultaneously improving patient adherence[17]. Patients with chronic health conditions are known to be poorly adherent to medication regimes[18, 19]. Such patients would benefit from the medication they require being made available in controlled release systems. Uhrich *et al*.[20] described how two types of control over drug release can be achieved, temporal and distribution control. In temporal control, the objective is to deliver the drug over an extended duration or at a specific time during treatment. Controlled release over longer time periods is highly advantageous for drugs that are rapidly metabolised and eliminated from the body after administration. An example of this is shown in Figure 1.1A, in which the concentration of drug at the site of activity within the body is compared after the immediate release from 4 injections administered at 6 h intervals to the continuous release from the controlled release system. With conventional methods of drug administration, i.e., injections or oral, drug levels rise after the initial administration, which can lead to potential toxicity problems. The concentrations then decrease until the next dosage, which has consequences in the efficiency of the dosage. This means that for only a portion of the treatment time the drug concentration is within the therapeutic window, i.e., the drug concentration that produces positive effects without harmful side effects. With the controlled release system, the rate of drug release matches the rate of drug elimination and therefore the drug concentration is within the therapeutic window for the vast majority of the 24 h period.

In distribution control, the drug delivery systems aim to target the release of the drug to the precise site of activity within the body. The advantage of this type of control is seen in Figure 1.1B, in which drug concentrations at the site of activity and side-effect production is compared. There are two situations in which distribution control can be beneficial. The first is when the natural distribution causes drug molecules to encounter tissues and cause major side effects that prohibit further treatment. This situation is often the cause of chemotherapy failure when bone marrow cell death prevents the patient from undergoing a complete drug treatment. The second situation is when the natural distribution of the drug does not allow drug molecules to reach their molecular site of action. For

example, a drug molecule that acts on a receptor in the brain will not be active if it is distributed by the patient's blood system but cannot cross the blood-brain barrier[21].

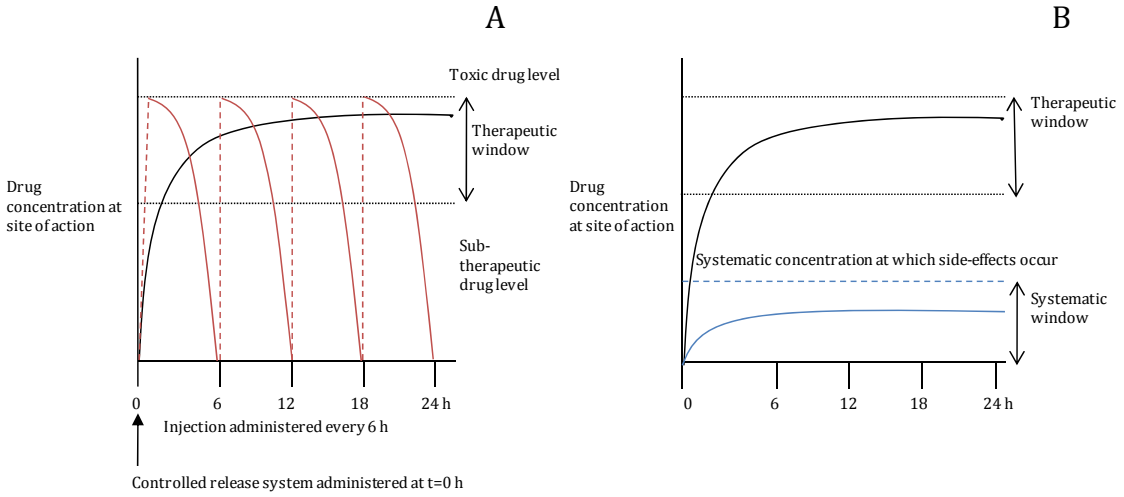

Figure 1.1: A Drug concentrations at site of therapeutic action after delivery as a conventional injection (—) and as a temporal release system (—). **B** Drug delivery from an ideal distribution controlled release system; — Drug concentrations at site of therapeutic action and — systematic levels at which side effects occur. These plots were taken from Uhrich *et al.*[20].

Currently, there are several materials under consideration for drug delivery, these include micelles[22-25], poly(lactide)/poly(lactide-co-glycolide) (PLA/PLGA)[26], albumin microspheres[27], nanoparticles[28, 29] and hydrogels[30-32]. Polymers that display a physiochemical response to stimuli are of particular interest and possible stimuli include pH, temperature and the application of an electrical field[17]. An ideal drug delivery device should fulfil two important requisites; i) the ability to control the rate of release and ii) the possibility of switching on/off the release[33]. Murdan[34] comprehensively reviewed electrically-responsive drug delivery from 'smart' drug delivery devices which were comprised of polyelectrolyte hydrogels. In the body, drug release can only be accomplished if the drug carrier responds to some class of stimuli, be it chemical, physical or biological. Conversely, an implanted 'smart' drug delivery device should be non-responsive to all other types of stimuli once in the body and one way of achieving this is through electrical stimulus. In the case of these devices, the hydrogels were loaded with a bioactive compound and both *in vitro* and *in vivo* release studies were carried out with the

application of an electrical field. However, one problem reported from the use of hydrogels in electrically-responsive drug delivery in these studies, was that they display deswelling or bending which affects the drug release.

In the search for improvements in biomaterials, CPs are receiving much attention in the field of drug delivery. Lira *et al.*[33] reported the synthesis of a conducting polymer-hydrogel hybrid material for the electrically controlled release of Safranin, a cationic dye. By combining the properties of these two 'smart materials', it has been shown that further control of the drug release could be achieved than seen with hydrogels on their own. However, Kim *et al.*[35] found that the blend had a negative effect on the electrical conductivity of the conducting polymer as it caused both physical and chemical changes in the polymer. CPs on their own are promising materials for biomedical devices not only due to their light weight, good biocompatibility and ability to function at body temperature, but also their ability to exhibit a reversible electrochemical response. Electrochemical switching of a CP is accompanied by charge compensation through ion movement into or out of the polymer. Therefore, it can be made work as an ion-gate which, in turn, allows the polymer film to bind and expel ions in response to electrical signals[36]. This makes CPs ideal for applications in controlled drug delivery.

1.3 Conducting polymers (CPs)

The electrically CP, polypyrrole (PPy), dates back to the early 1960s but little was understood about the polymer at this time and the discovery was essentially lost[37]. In 1977, Shirakawa *et al.*[38] reported that by doping polyacetylene (PA), the organic polymer could be altered to exhibit metal-like properties. The successful doping of PA encouraged the same scientists to test PA as a rechargeable active battery electrode[39, 40]. Their promising results prompted world-wide efforts to construct a polymer battery.

In the course of these studies, CPs with properties similar to PA were recognised and discovered. These include polypyrrole, polyaniline and polythiophene and the chemical structures for these are shown in Figure 1.2. These polymers are

comprised of C, H and simple heteroatoms such as N and S. A number of CPs are now used in a variety of applications, ranging from corrosion protection of materials to many biomedical applications, such as drug delivery, biosensors and tissue engineering[36, 41-43]. For their work Alan J. Heeger, Alan G. MacDiarmid and Hideki Shirakawa were awarded the Nobel Prize in Chemistry in 2000 for the discovery and development of CPs.

A

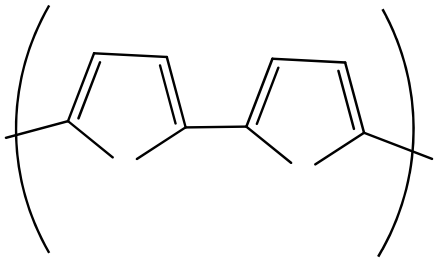

B

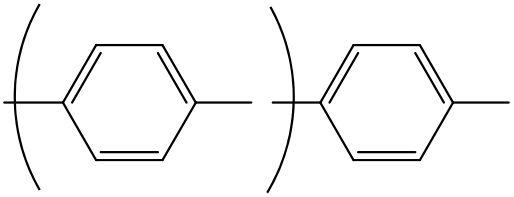

C

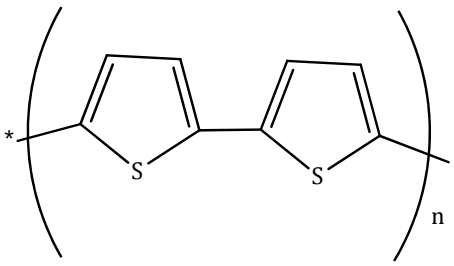

Figure 1.2: Chemical structures of **A** polypyrrole, **B** polyaniline and **C** polythiophene. All polymers are shown in the dedoped state.

Polymers and indeed, materials in general, can be categorised based on their electrical conductivity as insulators, semiconductors or conductors. In 1985, Bredas and Street[44] used the band theory of solids to describe the conductivity of conducting polymers. The highest occupied electronic levels constitute the valance band (VB) and lowest unoccupied level, the conduction band (CB). The band gap, E_g, between the VB and the CB determines the conductive properties of the

polymer, as shown in Figure 1.3. If E_g > 10 eV, it is difficult to excite electrons into the CB and an insulator band forms. In semiconductors, E_g ~ 1.0 eV, which means the gap is small enough that electrons can be excited between the VB and CB. For conductors, the VB overlaps the CB resulting in the CB being partially filled with electrons and metallic conduction is observed.

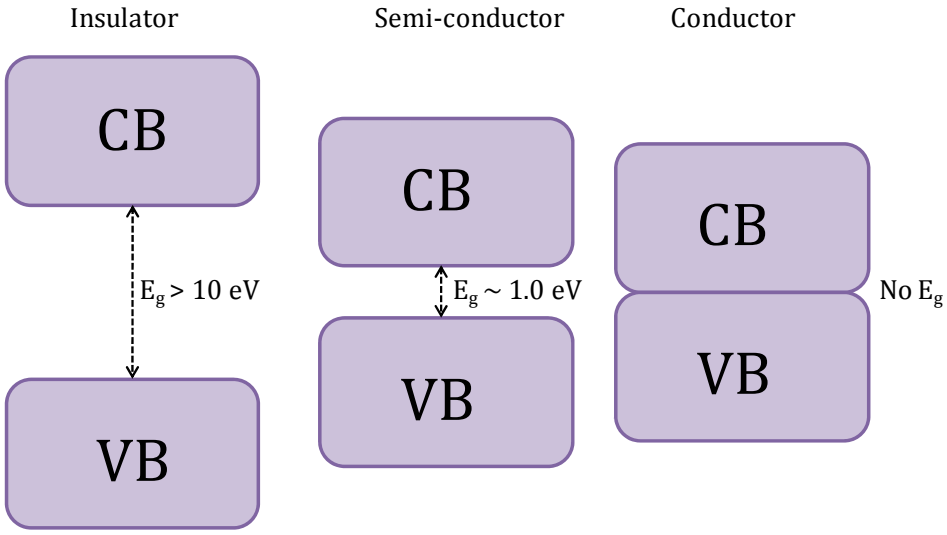

Figure 1.3: The difference in the band gap, E_g, for insulators, semi-conductors and conductors.

For most conducting polymers, the band gap energy is generally close to 1.0 eV, and consequently they can be categorised as semi-conductors. However, the conductivity can vary over a very broad range, from insulators to metals and cover the entire range of semiconductors, due to the number of different conducting polymers, dopants and doping levels, as shown in Figure 1.4.

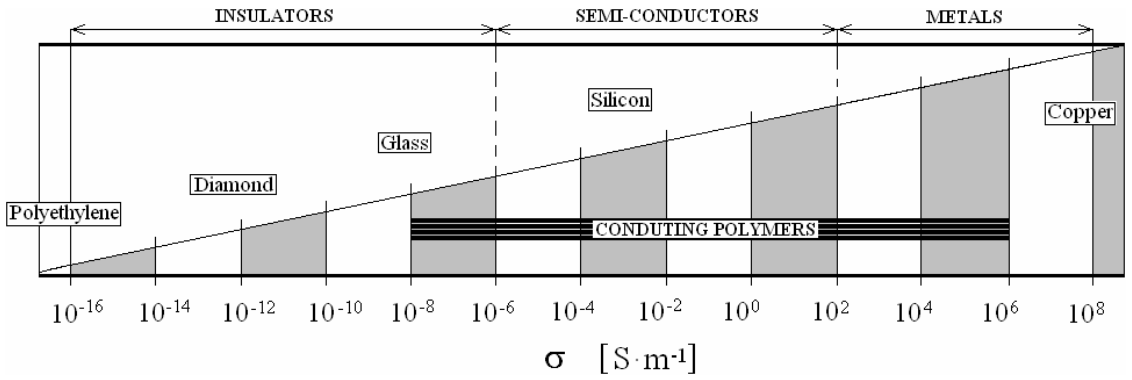

Figure 1.4: Classification of materials in order of electrical conductivity, σ.

However, the conductivity associated with CPs cannot be explained entirely using this band theory model. CPs are organic chains of alternating double- and single-bonded sp^2 hybridised atoms, which endow the polymer with metal-like semi-conductive properties. The series of alternating single and double bonds, which is generated by electron cloud overlap of p-orbitals to form π molecular orbitals, is referred to as a conjugated or π-system. This π-system can be described in terms of electronic wave functions that are delocalised over the entire chain. This delocalisation allows charge mobility across the polymer backbone[45]. Generally, this process occurs in 1 in every 4 monomer units and the introduction of counter ions (dopants) to compensate and reform the charge neutrality is required.

The concept of doping is a unique, central, underlying and unifying theme which distinguishes CPs from all other types of polymers[46]. During the doping process, an organic polymer, either an insulator or semiconductor having a small conductivity, typically in the range 10^{-8} to 10^{-3} S m^{-1}, is converted into a polymer which is in the 'metallic' conducting range[47] of 10^{2} to 10^{-2} S m^{-1}. Upon doping, the conducting polymer system with a net charge of zero is produced due to the close association of counter ions with the charged CP backbone[48, 49]. This process introduces charge carriers, in the form of charged polarons, i.e., radical ions, or bipolarons, i.e., dications or dianions, into the polymer, as shown in Figure 1.5. The attraction of electrons in one repeat-unit to the nuclei in the neighbouring units yields charge mobility along the chains and between the chains[50]. The ordered movement of these charge carriers along the conjugated CP backbone produces electrical conductivity. Doping can be performed chemically or electrochemically. The

chemical nature of the dopant affects electroactivity as well as surface and bulk structural properties of the polymer[50]. In addition, small and large dopants can both alter electrical conductivities and morphologies, but larger dopants, such as hyaluronic acid (HA), can change polymer density and more dramatically affect characteristics such as surface topography and physical handling properties[51].

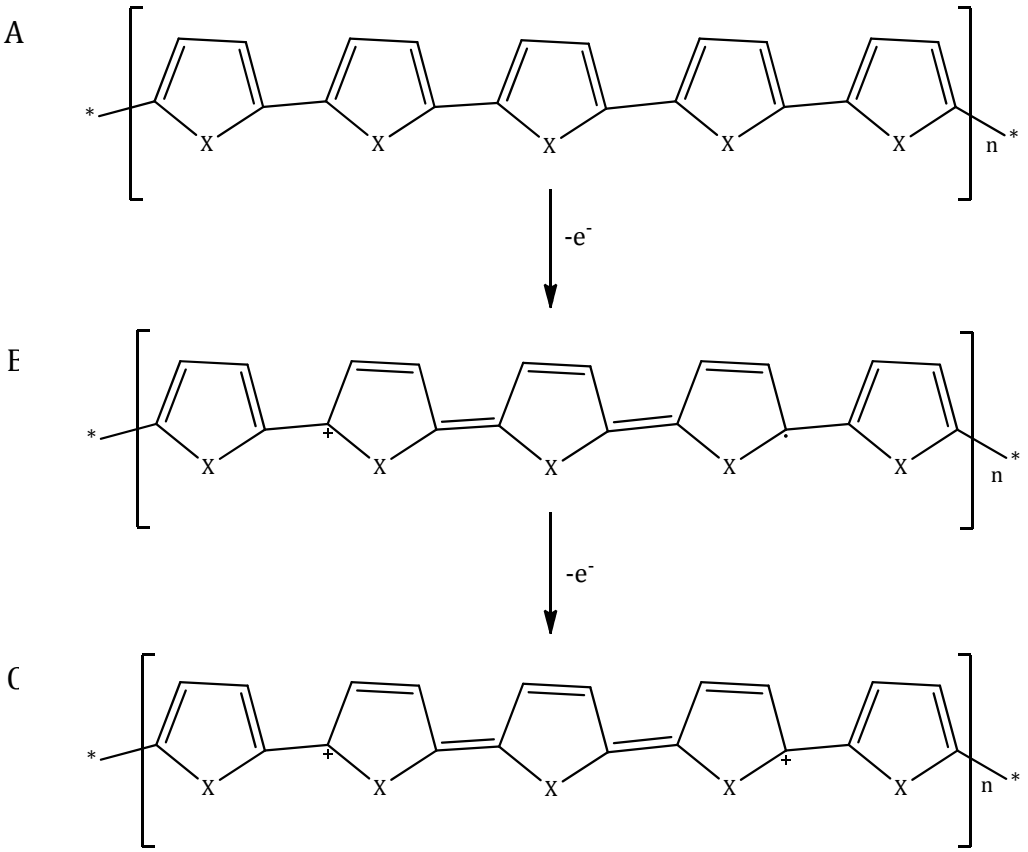

Figure 1.5: Formation of polaron and bipolaron where A is the neutral polymer, B is the partially oxidised polymer - polaron and C is the fully oxidised polymer –bipolaron.
X = S, N or O.

Polarons and bipolarons can also be described in terms of the band gap model and an example of one CP, polypyrrole, is shown Figure 1.6. At a hypothetical zero doping level, the polymer is neutral and its band structure is that of a standard semiconductor. The removal of one electron produces a polaron, as shown in Figure 1.6b, with two polaron levels about 0.5 eV from the valence and conduction band edges[44]. On removal of a second electron, a bipolaron is produced, Figure

1.6c, with the bipolaron levels being further removed from the VB and CB. It has been calculated that the bipolaron levels are about 0.75 eV from the band edges[44]. It is important to note that in an actual CP structure, the entire CP chain would first have to become nearly saturated with polarons before bipolaron formation would begin[48]. As the doping levels increase, the individual bipolaron states coalesce into bipolaron bands, as shown in Figure 1.6d. These bipolaron bands arise from electronic states 'scavenged' from the VB and CB edges. At high dopant concentrations, the bipolarons, which are spinless, can become mobile under the application of an electrical field, thus giving rise to the high conductivity observed in CPs.

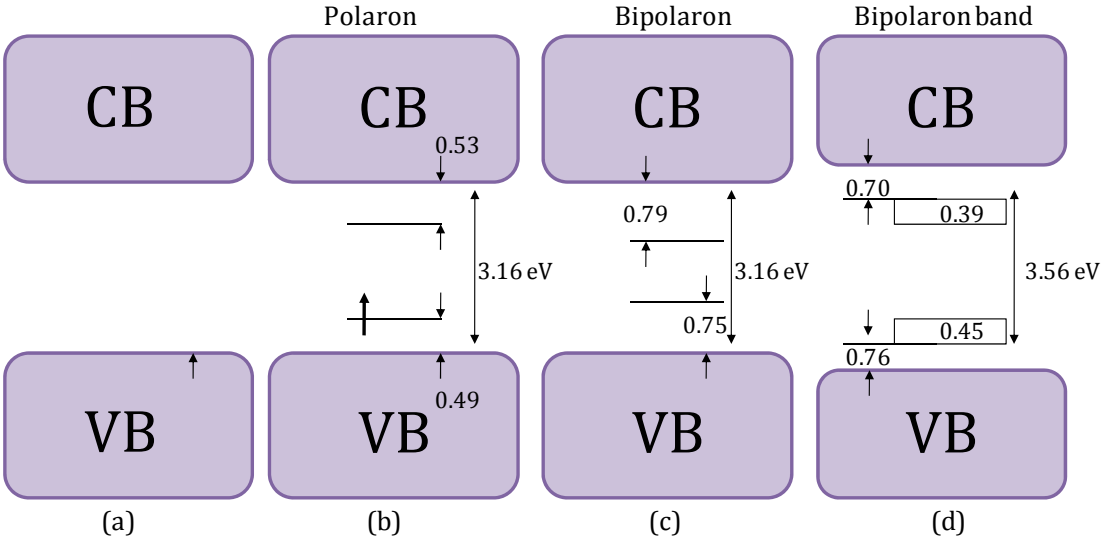

Figure 1.6: Band structure evolution for PPy. The evolution from (a) to (d) is with progressively increasing doping[48].

The chemical synthesis of CPs involves the use of a chemical oxidant, such as ammonium peroxydisulfate (APS), ferric ions, permanganate or dichromate anions. The monomer can be oxidised in the appropriate solution leading to chemically active cation radicals of the monomer used. These cation radicals then react with monomer molecules and this results in the formation of an insoluble polymer[52]. However, with this method it is difficult to deposit the CP onto a surface, as most of the CP precipitates within the solution phase.

Chemical deposition of CPs can also be achieved using techniques such as vapour phase polymerisation (VPP). In VPP, the oxidising agent, or monomer, is applied directly onto the surface before being exposed to the vapour of the monomer or oxidiser, respectively[53-55]. This ensures that polymerisation only occurs at the desired surface with no bulk polymerisation taking place in the solution. The advantage of VPP is that CP layers can be obtained on insulating surfaces unlike electrochemical polymerisation which is restricted to metal, carbon or other conducting materials[52]. CPs can also be synthesised photochemically[56]. Photochemical polymerisation takes place in the presence of sunlight. This technique utilises photons to initiate a polymerisation reaction in the presence of photosensitisers. Typical photosensitisers that have been used include copper and ruthenium (II) complexes[57].

Electrochemical polymerisation occurs when a suitable anodic potential or current is applied to a conducting substrate that has been immersed in a monomer electrolyte. A two- or three- electrode cell is used to prepare CPs with a working electrode and an auxillary electrode, with or without a reference electrode. A diagram of a three-electrode cell set-up is given in Section 2.2.2. The electropolymerisation is generally achieved by potentiostatic (constant potential) or galvanostatic (constant current) methods. Potentiodynamic techniques such as cyclic voltammetry (CV) can also be employed and are useful in obtaining qualitative information about the redox processes involved in the early stages of the polymerisation reaction[58]. Electrochemical polymerisation is often favoured over chemical polymerisation in the preparation of CP-based drug delivery systems as it allows tighter control of the quantity and properties of the polymer produced[59].

Once the CPs are formed they can be characterised using a number of techniques, including CV[60-63], electrochemical quartz crystal microbalance (EQCM)[64-66], electrochemical impedance spectroscopy (EIS)[67-69] and scanning electron microscopy (SEM)[70, 71]. All of these techniques were used throughout this study and are described and discussed further in Chapter 2, Section 2.4.

1.4 Polypyrrole (PPy)

As previously mentioned, in 1968 Dall'Olio *et al.*[37] published the first report on the electrochemical synthesis of PPy. They observed the formation of brittle, film-like pyrrole (Py) black on a platinum (Pt) electrode during the anodic oxidation of Py in dilute sulphuric acid[45]. In 1979, Diaz *et al.*[72] produced the first flexible, stable PPy film with high conductivity. The substance was polymerised on a Pt electrode by anodic oxidation in acetonitrile. This known chemical method of synthesis usually produced low conductivity powders from the monomers but instead a smooth, manageable film with good conductivity was formed[45]. Since these discoveries, the developments in this area have accelerated at an unexpectedly rapid rate.

PPy is by far the most extensively investigated CP not only due to the fact that the Py monomer, shown in Figure 1.7, is easily oxidised, water soluble and commercially available but also because of its environmental stability, good redox properties and the ability to give high electrical conductivities[73]. PPy can be prepared both chemically and electrochemically and a general description of these techniques has been given in Section 1.3. The first report of the deposition of PPy by VPP was described by Salaneck and co-workers[74]. They used $FeCl_3$ or H_2O_2 as oxidants to polymerise PPy films. The electrochemical synthesis method is a one step synthesis method that results in simple deposition of polymer films. The intrinsic properties of PPy are highly dependent on the electropolymerisation conditions. In this section, the electropolymerisation mechanism is first described and the parameters affecting its polymerisation, i.e., pH, temperature and solvent choice, are discussed followed by how the properties of PPy make it a suitable material for drug delivery.

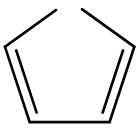

Figure 1.7: Schematic illustration of a monomer unit of pyrrole (Py).

1.4.1 Electropolymerisation mechanism of pyrrole

Various mechanisms for the electropolymerisation of pyrrole have been proposed over the last 30 years[75-77]. One of the principal difficulties encountered in the determination of the different stages of reaction is the rapidity of the polymerisation[58]. There is still not one mechanism that is universally accepted but the mechanism encountered most often in the literature is described by Diaz and his colleagues[75]. Waltman and Bargon[78] have confirmed this mechanism by theoretical studies based on correlation between reactivity and the unpaired electron density of the radical cations. This mechanism is demonstrated in Figure 1.8. The initial step involves the oxidation of the monomer which results in the formation of a radical cation. In chemical polymerisation, the radical cation then attacks another monomer molecule, generating a dimer radical cation. However, in the electrochemical case, the concentration of the radical cations at the electrode surface is much larger than that of the neutral monomer and radical-radical coupling leads to a radical dication. The coupling between the two radicals is generally between their α-positions and the loss of two protons then results in the formation of a neutral dimer. This is then followed by the oxidation of the dimer to form a radical cation where the unpaired electron is delocalised over the two rings. As a result, the oxidation potential of the dimer is lower than that of the monomer. Therefore the dimer is more easily oxidised at the applied potential at which the monomer was oxidised. The radical dimer couples with a radical monomer to form a trimer dication which deprotonates to give the neutral trimer.

The trimer can undergo coupling reactions at both the α- and β-positions even if the β-positions are sterically unattainable, but during the early stages of propagation the α-coupling will dominate. However, as the oligomer chain progresses the α-coupling will no longer be the only coupling possible. The longer the chain length the higher the number of β-bonds formed. Street showed that one Py in three is affected by this structural disorder[79, 80]. These β-couplings are responsible for the poor crystallinity that is associated with PPy. The propagation continues in the same manner of oxidation, coupling, deprotonation until the final polymer product is obtained.

There are a number of reasons why this mechanism is believed to be the best one representing this reaction. For one, the loss of H from the α-position indicated in the mechanism is in good agreement with the observed drop in pH of the solution during polymerisation[81, 82]. Furthermore, Diaz and co-workers[75] used chronoabsorption studies to demonstrate that the rate-determining step during film growth is a coupling process and not monomer diffusion towards the electrode.

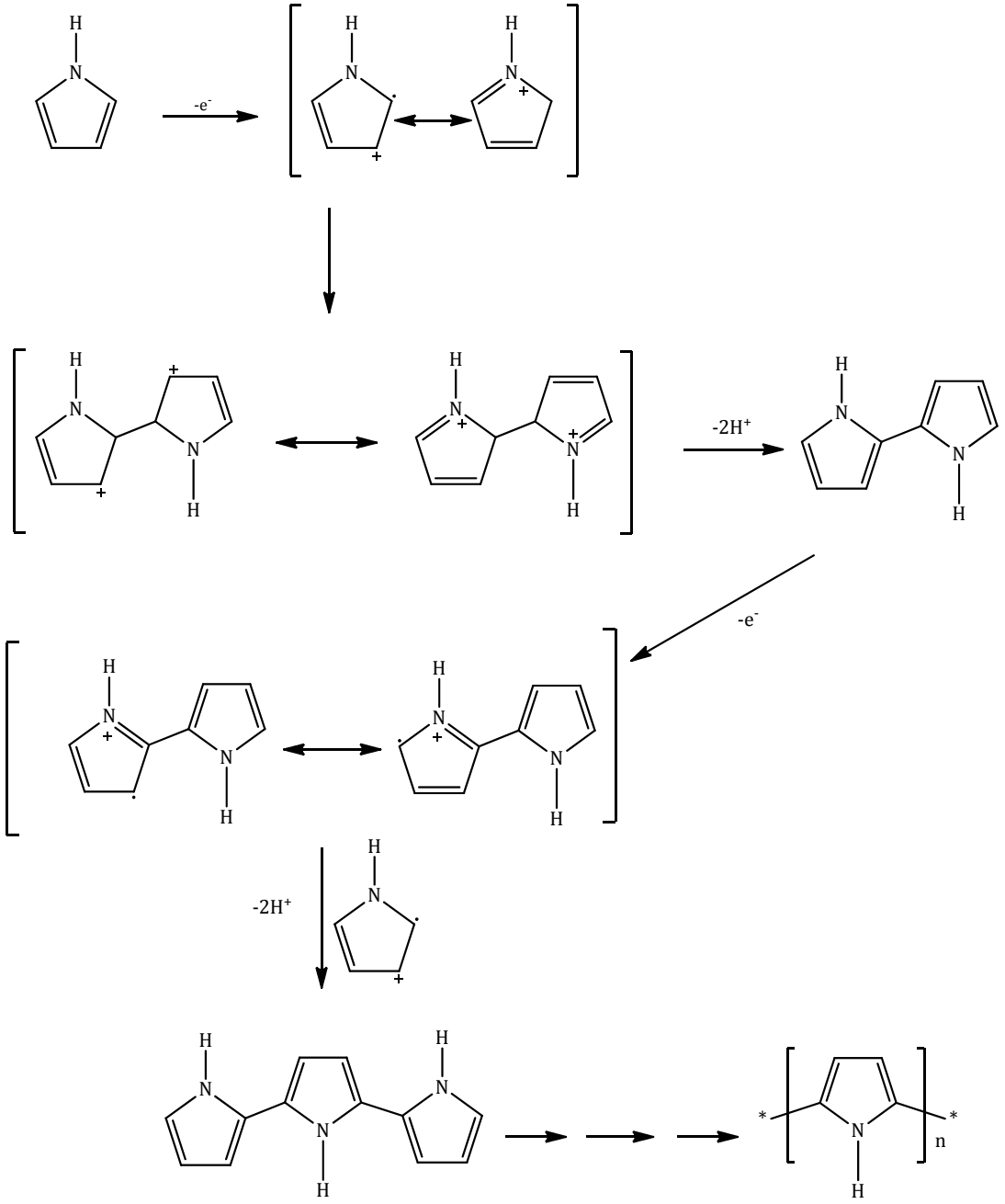

Figure 1.8: Mechanism of the electrochemical polymerisation of pyrrole (Py).

1.4.2 Synthesis parameters affecting the polypyrrole film

The nature of the electrode is of major importance for the synthesis of PPy films. Ideally both the working and counter electrode selected are inert in the solvent being used, corrosion resistant and stable over the potential ranges being worked within[59]. This ensures that the oxidation of the electrode is not competing with the oxidation of the monomer. Generally, substrates such as platinum, gold and glassy carbon are chosen as the working electrode, however, a range of active metals which form oxides have also been used[61, 70, 71, 83, 84]. In these circumstances, the potential of the pyrrole oxidation increases and the current density usually decreases[84]. Apart from metals, PPy has also been electrodeposited on a wide variety of other materials, including indium tin oxide glass (ITO)[85] and silicon[86].

As previously mentioned, the electrochemical oxidation of CPs can be achieved using different electrical forms including constant current, constant potential and CV. Otero and DeLarreta[87] noted that the choice of electrochemical method has an influence on the morphology, appearance and adhesion of the PPy film. The films formed from a constant current or constant potential mode of polymerisation are generally more porous and uneven than those achieved by CV, which are smooth and compact. However, more recent studies have shown that PPy films formed potentiostatically have a smooth surface morphology and the growth of the polymer is easier to control[88].

The morphology of the polymer can also be influenced by controlling the magnitude of the electrical stimulus. PPy prepared at lower current densities (< 1.0 mA cm^{-2}), or at lower anodic potentials (< + 0.800 V), is more dense and compact with homogeneous surfaces. While polymers deposited at higher current densities (> 5.0 mA cm^{-2}) or higher anodic potentials (> + 0.900 V), form open, porous structures with less regular surfaces[36, 89, 90]. However, if the anodic potential is too high, over-oxidation can occur, reducing the conductivity and electroactivity of the polymer with a loss in mechanical properties and decreased adhesion to the substrate[91-93]. The mechanism for over-oxidation still remains unclear but it is generally accepted that the over-oxidation of PPy is due to the

nucleophillic attack of PPy by strong aqueous nucleophiles such as OH^-, Br^- and H_2O[93]. This results in the formation of carbonyl groups on the α-carbons of the pyrrole ring which breaks the conjugation of the polymeric chain[91].

Different dopant anions can also affect the morphology of the PPy and therefore care must be taken when choosing a supporting electrolyte as any anions present during electropolymerisation could be incorporated[63]. The size of the anions can also affect the porosity and the redox properties of the polymer[94]. Dopants of various sizes have been studied including Cl^-, ClO_4^-, NO_3^-, para-toluene sulfonate (pTS^-) and dodecyl benzene sulfonate (DBS^-)[62, 63, 95-98]. When PPy is doped with smaller anions, such as Cl^-, ClO_4^- and NO_3^-, anion exchange is mainly displayed due to the high mobility of these ions in the polymer matrix. Cation exchange generally takes place on PPy modified with large and bulky shaped anions, such as DBS^-. However, when counterions are medium in size, like pTS^-, PPy exhibits both anion and cation exchange behaviour. The electrolyte concentration is also important. Li and Yang[99] reported that the doping, conductivity and tensile strength of a NO_3^- doped PPy film increase as the electrolyte concentration increases until a concentration of 1.0 mol dm^{-3} is reached. Beyond that no improvement was observed.

The choice of solvent has a strong influence on the electrochemical polymerisation of Py. Aqueous solutions usually require a reasonably high amount of supporting electrolyte to achieve the desired conductivity while for organic solutions the addition of an organic salt is often necessary. Acetonitrile is a common choice for an organic system[100, 101]. Several studies have been carried out comparing the electrodeposition of PPy in the presence of water, acetonitrile and mixtures of both water and acetonitrile[102-105]. There is a general agreement that films prepared in aqueous or mixed solutions are more porous than those prepared in organic medium and the amount of water in the mixed solutions has a big influence on the kinetics and properties of the polymer formed. Ko *et al.*[106] also found that PPy films prepared in acetonitrile/tetrabutylammonium perchlorate had more superior electron transfer characteristics and conductivities than those prepared in aqueous medium. However, a number of parameters were responsible for these

observations. These parameters included better contacts between the metal electrode and the polymer film, and better contacts between active sites inside the film itself for the PPy films prepared in acetonitrile.

Although the monomer oxidation potential is independent of the pH, the pH has an effect on the reactivity and stability of the PPy formed at the electrode[107]. In general, protons are produced after each oxidation at the electrode which consequently decreases the pH near the electrode. Zhou and Heinze[108] investigated the influence of pH on electropolymerisation of Py from acetonitrile and found that neutral or weakly acidic pH favours polymerisation. This is consistent with Pletcher and co-workers[109] who also found this to be the case when preparing a PPy film at a Pt electrode from solutions of varying pH. In addition, pH affects the speed of polymerisation with PPy forming most rapidly in acidic conditions, slower in neutral pH, and not forming at all in basic solutions. A very low pH results in the formation of a film of low conductivity. This is due to the acid catalysed formation of non-conjugated trimers which further react to form a partly conjugated PPy or become incorporated into the film[110]. While at basic conditions, cation radicals become deprotonated to neutral radicals which interferes with the radical-radical coupling reaction[111]. During synthesis the pKa of all species must be considered as the pH selected will influence which ions are present. It may be necessary to select a pH which compromises between polymerisation rate and maintaining species in the desired ionic form.

Finally, temperature plays an important role in the electropolymerisation of Py. A decrease in redox properties of PPy is observed as the temperature increases[58]. Although the rate of the electropolymerisation reaction is increased with increasing temperatures, the PPy that is deposited on the electrode is more likely to become over-oxidised and this has an insulating effect which hinders the further growth of the PPy.

In addition to affecting the rate of polymerisation, the nature of the dopant, solvent, electrolyte pH, polymerisation potential and electrode substrate all influence the morphology of PPy films. The most common morphology is the

'cauliflower' structure, but as detailed earlier, the surface roughness and porosity depend on the experimental conditions used in fabricating the polymer and these can lead to changes in the cauliflower morphology.

1.4.3 Electroactivity of polypyrrole

In Section 1.3, the movement of ions along the CP backbone was described and the switching of the polymer between the neutral, partially oxidised (polaron) and fully oxidised (bipolaron) states was shown in Figure 1.5. This is one of the most important properties of PPy. It would appear from the mechanism in Figure 1.8 that the final PPy chain is neutral; however, this is not the case. The final PPy chain is actually in an oxidised/doped state[58].

Burgmayer and Murray[112] demonstrated that PPy functions very well as an ion-gate membrane, which is positively charged in the oxidised state and neutral and hydrophobic in its reduced state. As previously mentioned, an important application of the ion-gate membrane is the controlled delivery of drugs which can be accumulated in the membrane. During this switching process the dopants move in and out of the polymer in order to create charge balance within the polymer. If the drug is anionic, the doping process occurs during polymerisation, to give the anion doped PPy. Provided the anion is not too large, the anion is expelled on reduction of the film, as shown in Figure 1.9A. Some anionic drugs that have been studied include naproxen, salicylate and nicoside[36]. For a cationic drug to be incorporated the properties of the polymer must be modified[113]. A large anion is initially doped within the polymer and remains entrapped in the polymer matrix. This allows the polymer to behave as a cation exchanger, where the charge of the polymer system can only be compensated through the uptake of cations. The cations are, therefore, taken up during the reduction of the polymer and released upon oxidation, as seen in Figure 1.9B.

Typical anionic dopants are Cl^-, ClO_4^- and pTS^- and the extent of the oxidation/ reduction is given by the doping level. This, expressed as the ratio of dopant anions, A^-, incorporated per monomer unit, i.e., 1 A^- per 4 monomer unit, generally gives a doping level of 0.25 or 25 %. The maximum doping level achievable with

PPy is 1 A^- per 3 pyrrole units or 0.33[114, 115]. It should be noted that doping may not always be uniform. There can be islands with high doping levels surrounded by regions with much lower doping levels[116]. In general, the rate determining step of the doping-dedoping process in PPy is governed by the ion migration, as the electron transfer is usually much faster during the redox switching.

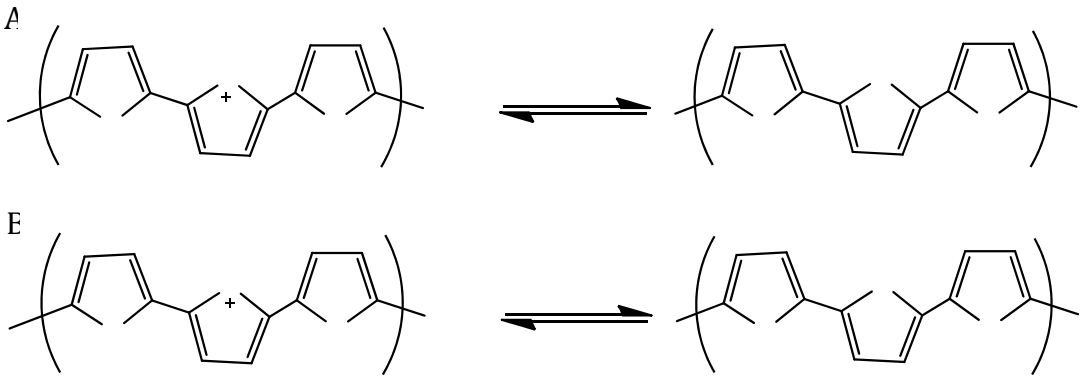

Figure 1.9: Interconversion between the oxidation and reduction states of PPy. **A** Anion (A^-) incorporation and release which is notably observed in small mobile anions. **B** Cation (C^+) insertion and liberation from the polymer films doped with larger anions which remain entrapped in the polymer matrix.

1.4.4 Polypyrrole in drug delivery

1.4.4.1 Biocompatibility

PPy was one of the first CPs studied, by Ingber and co-workers[117], for its effects on mammalian cells. The authors demonstrated through *in vivo* studies that extracellular matrix molecules, such as fibronectin, absorb efficiently onto PPy thin films and support cell attachment under serum-free conditions. Since then, PPy has been reported to support cell adhesion and growth of a number of different cell types including endothelial cells[118, 119], primary neurons[120, 121] and mesenchymal stem cells[122]. Several studies have shown cell and tissue compatibility of PPy *in vitro* and *in vivo,* with one early study showing PPy doped with pTS^- films are cytocompatible with mouse fibroblasts and neuroblastoma cells[123]. The biocompatibility of PPy prepared from both chemical and electrochemical means was thoroughly evaluated by Wang *et al.*[124]. They carried out a series of systematic toxicity tests by applying a solution of extracts from PPy powder to cell cultures

and animal models. They found that extract solutions did not have adverse effects on cell cultures or on the animals tested.

Minimal tissue response to implanted PPy has also been observed. Cui *et al.*[125] reported good recordings of electrical activity with PPy-synthetic peptide coated electrodes when implanted in guinea pig brain over two weeks with better nerve cell integration than uncoated electrodes. Ateh *et al.*[126] have extensively reviewed the developments in utilising PPy for biomedical purposes, such as tissue engineering, and it is obvious from the scope of this research that PPy is a promising biomaterial[127].

The anionic dopant and any other excipients present must be considered in addition to the PPy itself. It has been shown that electrical signalling *via* the polymer can be used to modulate cellular reactions[128, 129], which in turn, could limit the toxicity of the implanted device. Specific bioactive molecules can be entrapped in the polymer to influence compatibility[32]. Polymer properties including roughness, surface energy (hydrophobicity), conductivity, mechanical actuation and dopant retention will all influence biocompatibility[50, 130].

1.4.4.2 Biodegradability

PPy is not classified as biodegradable and this is a major drawback for an implanted material. This means that two procedures would need to be carried out; one to administer the drug delivery device and another for its removal. However, Rivers *et al.*[131] have shown that biodegradability can be accomplished through chemical modification of PPy. Pyrrole-thiophene oligomers (Py-Th-Py) were prepared using degradable ester linkages. These linkages can be cleaved by enzymes found *in vivo*. After enzyme digestion, the oligo segments can be engulfed and disposed of by macrophages. This modified film was still conductive although less so than the unmodified PPy.

1.4.4.3 Drug selection

Not all drugs are suitable for use in PPy-based DDS and the assessment of drugs is based on a number of factors. Firstly, the drug in question should not be

electroactive at the potentials the system will experience during either manufacture or working life. If the drug is electroactive in this range, the biological activity of the drug may be compromised[59]. The pKa of the drug should also be considered as the charge of the drug molecule will influence the loading and release from the polymer. Ideally the drug should be highly potent (require 1 mg release per day), as this lowers the loading requirements[132]. Drugs with short half lives are advantageous in minimising the risk of accumulation. If the drug requires frequent administration by conventional methods, an implanted controlled release system may improve the drug's efficiency. This is achieved in two ways; firstly implanted systems can improve non-adherence issues frequently observed with patients requiring chronic medication therapy[19]. Secondly, controlled release from an implantable system is able to reduce the peak to trough ratio providing desirable and constant levels of drug in the body[17]. Drugs with poor oral bioavailability may benefit from intravenous delivery, as less drug is required to achieve the same blood concentrations in a more predictable manner. After implantation of the delivery system local tissues may be exposed to higher concentrations of drug, and so preferably the drug should be non toxic to the surrounding area[59].

1.4.4.4 Drug incorporation

As previously mentioned, anionic drugs can be incorporated into the PPy during polymerisation. In 1984 Zinger and Miller[133] demonstrated the incorporation of ferrocyanide into PPy. They also investigated the use of glutamate as a dopant but found that the PPy would not form. Instead, a film of PPy doped with ClO_4^- was first deposited and glutamate was loaded into the PPy by stepping the film between 0.000 V and - 1.000 V vs SCE in a 0.10 mol dm^{-3} glutamate solution. Since then the entrapment of several anionic drugs in PPy films has been reported. These include adenosine 5'-triphosphate (ATP^-)[90], naproxen[36] and dexamethasone disodium phosphate[89].

Hepal and Mahdavi[113] reported the post-synthesis incorporation of chloropromazine into a PPy film, however, there have been some reports of the incorporation of cationic drugs in PPy during synthesis[92, 134]. Thompson *et al.*[92]

described the mechanism of the incorporation of NT-3^+ into PPy which involved a combination of electrostatic and hydrophobic interactions between drug, anionic dopant (pTS^-) and polymer, along with physical entrapment.

Gadelle and co-workers[135] reported the incorporation of a neutral drug into PPy. Anionic β-cyclodextrins (CD) were used as dopants to prepare PPy and this allowed for subsequent incorporation of neutral drugs. The uncharged antipsychotic drug, N-methylphenothiazine (NMP), was loaded into CD doped PPy by immersing the film in a 0.10 mol dm^{-3} NMP solution. The NMP was loaded into PPy through encapsulation as the drug preferentially moves into the hydrophobic interior of the CD. George *et al.*[136] presented a novel approach to increase the range of drugs that could be bound to PPy. Anionic biotin was incorporated into PPy during synthesis. The polymer was incubated with streptavidin which formed strong bonds to the biotin in the film. As streptavidin has multiple binding sites the polymer could now bind any biotin labelled compound.

Some difficulties have been reported when bioactive molecules are incorporated during synthesis. These include interference with polymer growth and decreased adherence of polymer to the underlying electrode[92, 133]. Adherence is an extremely important factor for electrically stimulated drug release. To overcome this issue a two-layered synthesis approach was reported whereby a layer of PPy doped with pTS^- was initially deposited onto the electrode before the second layer of PPy containing the pTS^- and a bioactive molecule was deposited[92]. This maintained the mechanical properties of PPy and greatly improved adhesion of the polymer to the underlying electrode.

1.4.4.5 Drug release and parameters affecting it

The mechanism of electrochemical drug release from PPy is described in Section 1.4.3. The first reported controlled release system based on PPy was reported by Zinger and Miller[133] when glutamate anions were released on reduction of PPy. More than 14 times the amount of glutamate was released when PPy was exposed to a reduction potential of – 1.000 V vs SCE than if no electrical stimulation was applied. In 1987, Zhou and co-workers[137, 138] demonstrated the release of dopamine from PPy derivatives. By the 1990s several accounts in the literature

were available on the release of anionic molecules such as ATP^{-}[139], pTS^{-}[36] and anthraquinone-2,6-disulfonic acid (ASQA)[140] from PPy films, and today progress is still being made in this field of research with attention focused on the release of drugs that are currently on the market, such as dexamethasone 21-disodium phosphate[89]. Methods of increasing the amount of drug that can be loaded into the polymers are continually being developed and these include increasing the surface area by forming 'nanotenacles' on the surface of the polymer[141], creating bubbles in the polymer that act as micro-containers or nanopores in which the drug can be sealed and released when mechanical pressure is applied[142, 143].

Polymer thickness is one parameter that affects drug release. The rate of charge passed during electrochemical polymerisation affects the speed of polymer deposition and subsequently the density, thickness and morphology of the film[59]. Numerous research groups have shown that an increase in polymer thickness correlates with an increase in total amount of drug that can be released[36, 92, 144, 145]. Most of these studies compared films prepared under the same synthesis parameters. Assuming the doping level remains fairly constant, then a higher amount of polymer corresponds with more drug incorporated, and subsequently more drug available for release. However, the level of drug release does not increase linearly with increasing film thickness; thinner films release a greater percentage of the incorporated drug than thicker films[133, 144, 145]. This may be due to thicker films being less electroactive[144] and changes in the diffusion coefficient with changing film thickness[145].

Wallace and co-workers[140] studied the factors influencing the release of ASQA from PPy films. The authors demonstrated that media characteristics such as pH, ionic strength, polarity and hydrophobicity all affect PPy properties and the release of the drugs. For example, ion transport at neutral pH involves both anion and cation movement, while below pH 3-4 anionic movement dominates[129, 146]. In general, to correlate *in vitro* and *in vivo* release the media used should mimic the targeted local environment where the system will be used. For implants intended to be in contact with extracellular fluid, studies are carried out at a pH of 7.4. However, if

the polymer films were designed for use in different conditions, for example an animal's rumen, the effect of pH would need to be considered[59].

The electrochemical parameters applied during the drug release have a significant effect on the drug release. Various forms of electrical stimulation can be applied to PPy in an attempt to control the release of drugs, including constant potential[147], step potential[36] or CV[89]. Step potential involves changing the potentials instantaneously between set potentials. CV involves sweeping the potential between two limits at a set rate. As the PPy redox state is altered a charged bioactive molecule will alternately experience attraction forces and an absence of attraction forces. Actuation can occur as the PPy is switched between its redox states which may also influence drug movement[148, 149].

Several papers have compared step potentials against CV to release drugs. CV appears to be the more proficient method to release ions of choice[36, 89, 90, 139, 144], however, there are several drawbacks to this method. Thompson *et al.*[92] reported that CV released NT-3^{+} at faster rates than using either rapidly alternating potential steps or current pulses but the PPy film delaminated away from the electrode upon handling. Contact with the underlying electrode was maintained when stimulation in the form of pulses, current or pulsed potential, was applied. Wadhwa *et al.*[89] also found CV to be the more efficient method to stimulate drug release but after 30 CV cycles at 100 mV s^{-1} cracks appeared in the PPy. This cracking is likely to be due to polymer actuation. Polymer delamination from the electrode and polymer cracking are both serious limitations for devices designed to release drugs over an extended period of time. Furthermore, a drug release device that relies on CV is a far more complex electronic device than one relying on alternating pulses of potential or current[59]. For these reasons, electrically stimulated release by CV may not necessarily be the best option. The most important electrochemical parameters to be considered, therefore, are the potential limits selected, the length of time spent at these limits and the corresponding redox states of the polymer.

1.4.4.6 Further applications

An ideal *in vivo* DDS should be able to determine when and if a dose is needed and then deliver it automatically. To do this, sensors are required to monitor both physical and biochemical conditions. PPy has been recognised as a highly efficient biosensor[42, 150]. One of the long term goals for *in vivo* drug delivery is to couple smart drug delivery devices to other implants. To date the limiting step in the creation of feedback-controlled drug delivery systems has been the development of stable sensors[16]. The focus of many of the early studies into coupling drug delivery with sensors was in the treatment of diabetes, with systems to sense blood glucose levels and release insulin in response[151]. However, no fully automatic long-term *in vivo* system has reached the market due to problems with the stability of *in vivo* glucose sensors[152]. Other electrochemical sensors which are used to measure mixed venous oxygen pressure, have functioned *in vivo* for as long as 4 years[153].

The coupling of drug delivery to sensors is only one aspect in which *in vivo* drug delivery could be linked to hardware. Each year a variety of medical devices are implanted and each has the potential to be coupled to drug delivery. Arbizzani *et al.*[154] demonstrated that PPy could be used as a drug-eluting membrane for coronary stents. The polymer was deposited onto a metal surface and the incorporated drug was released over 7 to 30 days which is a suitable time range for a drug-eluting stent. Cochlear implants are another biomedical device where the electrically stimulated release of drug could be of benefit. O'Leary and co-workers[155] showed that by coating cochlear implants with a polymer comprising of PPy/pTS/NT-3, the release of NT-3 promoted preservation of the spiral ganglion neurons without adversely affecting the function of the implant itself.

1.5 Research presented in this thesis

From the literature review, it is clear that there is a real need for DDS whereby the release of a drug can be controlled by an external stimulus and that PPy is a promising material for this application. The drugs, which were small to medium-

large in size, included the aqueous soluble dexamethasone 21-phosphate disodium (NaDex) and valproic acid sodium (NaVPA) salts, and the less soluble diclofenac sodium (NaDF) salt. Two other drugs, indomethacin sodium (NaIndo) and sulindac sodium (NaSul) with very limited solubility in aqueous solution, were chosen.

The incorporation of dexamethasone (Dex^{2-}) and diclofenac anions (DF^{-}) within the PPy membrane was achieved by a potentiostatic mode of growth from an aqueous solution of pyrrole and the drug under investigation. For the PPy doped with Dex^{2-}, characterisation and release studies found the doping level of the polymer to be about 0.30, and approximately 31 μmol cm^{-2} of Dex^{2-} was incorporated into the polymer upon polymerisation. Furthermore, it was observed that the rate of release could be controlled by the potential applied with approximately 89 % of the Dex^{2-} released within 60 min at an applied potential of – 0.900 V vs SCE.

For the PPy doped with DF^{-}, unusual patterns in growth and morphology were observed. During the deposition of the polymer, the rate of polymerisation decreased with increasing time and higher applied potentials. The polymer had features of an insulating film, as evident from electrochemical impedance measurements, while SEM confirmed the presence of crystal-like shards on the surface of the polymer. These findings suggest that insoluble drug crystals are formed during polymerisation. DF^{-} displays a limited solubility in aqueous solutions and during the oxidation of the monomer and drop of pH at the surface, the equilibrium is shifted from the soluble DF^{-} towards the insoluble HDF causing insoluble crystals of the drug to deposit on the surface of the polymer, which hinders further polymerisation.

The incorporation of two insoluble medium sized drugs, NaIndo and NaSul, into the PPy film was also investigated. Deposition of PPy doped with either of the drugs in question was carried out in ethanol and tetrabutylammonium perchlorate (TBAP) was added to increase the conductivity. It was found that the PPy films formed in this organic medium were not as conducting as those formed in the aqueous solution, and doping levels were considerably lower than those previously reported for PPy. The addition of the TBAP introduces the small and

mobile, ClO_4^-, anion which is well known to dope PPy. UV-visible spectroscopy was used to calculate that approximately 2.19 x 10^{-6} mol cm^{-2} of ClO_4^- was present in the polymer. However, this is quite minute compared to the estimated amount of drug doped within the polymer; 260 μmol cm^{-2} and 60 μmol cm^{-2} of $Indo^-$ and Sul^-, respectively. As seen with the other polymers the rate of release was controlled by the applied potential.

Finally, the formation of PPy doped with a small soluble anionic drug, VPA^-, was studied. Although this was the smallest of all the drugs studied, it was not possible to incorporate this drug into the PPy membrane electrochemically. This was explained in terms of the solubility of the anion at low pH values. At pH values below 5.6 the equilibrium of the VPA^- is shifted towards the insoluble HVPA. As the monomer is oxidised, there is a decrease in the local pH in the vicinity of the electrode and this causes the HVPA to precipitate from solution. This, in turn, prevents any PPy from being deposited at the electrode. Vapour phase polymerisation is offered as an alternative approach to immobilise this drug into the PPy film.

1.6 References

1. N. A. Peppas and D. J. Am Ende, *Journal of Applied Polymer Science,* **66**:509 (1997).
2. B. Singh, D. K. Sharma, and A. Gupta, *Journal of Environmental Science & Health, Part B -- Pesticides, Food Contaminants, & Agricultural Wastes,* **44**:113 (2009).
3. U. R. Pothakamury and G. V. Barbosa-Cánovas, *Trends in Food Science & Technology,* **6**:397 (1995).
4. N. A. Peppas and R. Langer, *Science,* **263**:1715 (1994).
5. P. Shivanand and O. L. Sprockel, *International Journal of Pharmaceuticals,* **167**:83 (1998).
6. R. Langer, *Advanced Drug Delivery Reviews,* **56**:557 (2004).
7. M. R. Prausnitz, S. Mitragotri, and R. Langer, *Nature Reviews,* **2**:115 (2001).
8. U. Conte, P. Colombo, C. Caramella, and A. La Manna, *Press-coated systems for drug release control.,*Phenum, 1983.
9. J. Verhoeven, S. C. Schutte, L. J. C. Peschier, M. Danhof, and H. E. Junginger, *Journal of Controlled Release,* **10**:205 (1989).
10. F. Siepmann, J. Siepmann, M. Walther, R. J. MacRae, and R. Bodmeier, *Journal of Controlled Release,* **125**:1 (2008).
11. L. K. Fung and W. M. Saltzman, *Advanced Drug Delivery Reviews,* **26**:209 (1997).

12. P. Tyle, *Drug delivery devices: fundamentals and applications,*Marcel Dekker, Inc., **32**, 1988.
13. C. S. Bruner, *Product Genesis Inc.,* (2004).
14. J. Halamka, A. Juels, A. Stubblefield, and J. Westhues, *Journal of the American Medical Informatics Association,* **13:**:601 (2006).
15. L. G. Bleris, P. D. Vouzis, J. G. Garcia, M. G. Arnold, and M. V. Kothare, *Control Engineering Practice,* **15**:1280 (2007).
16. D. A. LaVan, T. McGuire, and R. Langer, *Nature Biotechnology,* **21**:1184 (2003).
17. R. Langer, *Science,* **249**:1527 (1990).
18. M. Valenstein, L. Copeland, R. Owen, F. Blow, and S. Visnic, *Journal of Clinical Psychiatry,* **62**:545 (2001).
19. M. S. Turner and D. W. Stewart, *Journal of Psychopharmacology,* **20**:20 (2006).
20. K. E. Uhrich, S. M. Cannizzaro, R. S. Langer, and K. M. Shakesheff, *Chemical Reviews,* **99**:3181 (1999).
21. A. De Boer and D. Breimer, *Journal of Royal College Physicians London,* **28**:502 (1994).
22. J. M. J. Fréchet, *Proceedings of the National Academy of Sciences of the United States of America,* **99**:4782 (2002).
23. S. Y. Kim, I. L. G. Shin, Y. M. Lee, C. S. Cho, and Y. K. Sung, *Journal of Controlled Release,* **51**:13 (1998).
24. M. Liu, K. Kono, and J. M. J. Fréchet, *Journal of Controlled Release,* **65**:121 (2000).
25. C. J. F. Rijcken, O. Soga, W. E. Hennink, and C. F. v. Nostrum, *Journal of Controlled Release,* **120**:131 (2007).
26. R. A. Jain, *Biomaterials,* **21**:2475 (2000).
27. M. Tuncay, S. Calis, H.S. Kas, M.T. Ercan, I. Peksoy, and A. A. Hincal, *Journal of Microencapsulation* **17**:145 (2000).
28. T. M. Allen and P. R. Cullis, *Science,* **303**:1818 (2004).
29. Laura Mora, Karin Y. Chumbimuni-Torres, Corbin Clawson, Lucas Hernandez, Liangfang Zhang, and J. Wang, *Journal of Controlled Release,* **140**:69 (2009).
30. S. Dreve, I. Kacso, I. Bratu, and E. Indrea, *Journal of Physics: Conference Series* **182** (2009).
31. C. Wang, R. R. Varshney, and D.-A. Wang, *Advanced Drug Delivery Reviews,* **62**:699 (2010).
32. Sean Brahim and A. Guiseppi-Elie, *Electroanalysis,* **17**:556 (2005).
33. L. M. Lira and S. I. Córdoba de Torresi, *Electrochemistry Communications,* **7**:717 (2005).
34. S. Murdan, *Journal of Controlled Release,* **92**:1 (2003).
35. B. C. Kim, G. M. Spinks, G. G. Wallace, and R. John, *Polymer,* **41**:1783 (2000).
36. K. Kontturi, L. Murtomäki, P. Pentti, and G. Sundholm, *Synthetic Metals,* **92**:179 (1998).
37. A. Dall'Olio, Y. Dascola, V. Vanacca, and V. Bocchi, *Comptes Rendus de l'Academie des Sciences,* **C267**:433 (1968).
38. Hideki Shirakawa, Edwin J. Louis, Alan G. MacDiarmuid, Chwan K. Chiang, and A. J. Heeger, *Journal of Chemistry Society Chemical Communications,* (1977).

39. C. K. Chiang, M. A. Druy, S. C. Gau, A. J. Heeger, E. J. Louis, A. G. MacDiarmid, Y. W. Park, and H. Shirakawa, *Journal of the American Chemical Society,* **100**:1013 (1978).
40. P. J. Nigrey, J. D. MacInnes, D. P. Nairns, A. G. MacDiarmid, and A. J. Heeger, *Journal of The Electrochemical Society,* **128**:1651 (1981).
41. M. Biondi, F. Ungaro, F. Quaglia, and P. A. Netti, *Advanced Drug Delivery Reviews,* **60**:229 (2008).
42. T. Ahuja, I. A. Mir, D. Kumar, and Rajesh, *Biomaterials,* **28**:791 (2007).
43. M. A. L. García and M. A. Smit, *Journal of Power Sources,* **158**:397 (2006).
44. J. L. Bredas and G. B. Street, *Accounts of Chemical Research,* **18**:309 (1985).
45. J. Heinze, *Electronically Conducting Polymers*, **152**, 1990.
46. C. K. Chiang, C. R. Fincher, Y. W. Park, A. J. Heeger, H. Shirakawa, E. J. Louis, S. C. Gau, and A. G. MacDiarmid, *Physical Review Letters,* **39**:1098 (1977).
47. A. G. MacDiarmid, *Angewandte Chemie International Edition,* **40**:2581 (2001).
48. P. Chandrasekhar, *Conducting Polymers, Fundamentals and Applications: A practical approach,*Kluwer Academic Publishers, 1999.
49. B. Scrosati, *Applications of Electroactive Polymers,*Chapman & Hall, 1993.
50. N. K. Guimard, N. Gomez, and C. E. Schmidt, *Progress in Polymer Science,* **32**:876 (2007).
51. J. H. Collier, J. P. Camp, T. W. Hudson, and C. E. Schmidt, *Journal of Biomedical Materials Research,* **50**:574 (2000).
52. A. Malinauskas, *Polymer,* **42**:3957 (2001).
53. J. C. Bjorn Winther - Jenson, Keld West and Gordon Wallace, *Macromolecules,* **37**:5930 (2004).
54. J. Chen, B. Winther-Jensen, C. Lynam, O. Ngamna, S. Moulton, W. Zhang, and G. G. Wallace, *Electrochemical and Solid-State Letters,* **9**:H68 (2006).
55. J. Kim, E. Kim, Y. Won, H. Lee, and K. Suh, *Synthetic Metals,* **139**:485 (2003).
56. V. Bavastrello, S. Carrara, M. K. Ram, and C. Nicolini, *Langmuir,* **20**:969 (2004).
57. S. Annapoorni, N. S. Sundaresan, S. S. Pandey, and B. D. Malhotra, *J. Appl. Phys.,* **74**:2109 (1993).
58. S. Sadki, P. Schottland, N. Brodie, and G. Sabourand, *Royal Society of Chemistry,* **29**:283 (2000).
59. D. Svirskis, J. Travas-Sejdic, A. Rodgers, and S. Garg, *Journal of Controlled Release,* **146**:6 (2010).
60. J. L. Anderson and I. Shain, *Analytical Chemistry,* **50**:163 (1978).
61. S. B. Saidman and J. B. Bessone, *Journal of Electroanalytical Chemistry,* **521**:87 (2002).
62. L. Sheng, Q. Yubing, and G. Xingpeng, *Journal of Applied Polymer Science,* **114**:2307 (2009).
63. M. D. Levi, C. Lopez, E. Vieil, and M. A. Vorotyntsev, *Electrochimica Acta,* **42**:757 (1997).
64. V. Syritski, A. Opik, and O. Forsen, *Electrochimica Acta,* **48**:1409 (2003).
65. M. S. V. Carlier, C. Buess- Herman, *Journal of Electroanalytical Chemistry,* **456**:139 (1998).
66. C. Debiemme-Chouvy, H. Cachet, and C. Deslouis, *Electrochimica Acta,* **51**:3622 (2006).
67. X. Ren and P. G. Pickup, *The Journal of Physical Chemistry,* **97**:3941 (1993).

68. E. Barsoukov and J. R. MacDonald, *Impedance Spectroscopy. Theory, Experiment and Applications.,*Wiley, 2005.
69. C. Deslouis, M. M. Musiani, and B. Tribollet, *Synthetic Metals,* **84**:827 (1997).
70. M. Bazzaoui, L. Martins, E. A. Bazzaoui, and J. I. Martins, *Electrochimica Acta,* **47**:2953 (2002).
71. A. S. Liu and M. A. S. Oliveira, *Journal of Brazilian Chemistry Society,* **18**:143 (2007).
72. A. F. Diaz and K. K. Kanazawa, *Journal of Chemistry Society Chemical Communications*:635 (1979).
73. J. Simonet and J. Rault-Berthelot, *Progress in Solid State Chemistry,* **21**:1 (1991).
74. A. Mohammadi, M. A. Hasan, B. Liedberg, I. Lundström, and W. R. Salaneck, *Synthetic Metals,* **14**:189 (1986).
75. E. M. Genies, G. Bidan, and A. F. Diaz, *Journal of Electroanalytical Chemistry,* **149**:101 (1983).
76. K. J. Kim, H. S. Song, J. D. Kim, and J. K. Chon, *Bulletin of the Korean Chemical Society,* **9**:248 (1988).
77. Y. J. Qiu and J. R. Reynolds, *Journal of Polymer Science Part A: Polymer Chemistry,* **30**:1315 (1992).
78. R. J. Waltman and J. Bargon, *Tetrahedron,* **40**:3963 (1984).
79. P. Pfluger and G. B. Street, *The Journal of Chemical Physics,* **80**:544 (1984).
80. P. Pfluger, M. Krounbi, G. B. Street, and G. Weiser, *The Journal of Chemical Physics,* **78**:3212 (1983).
81. Q. Pei and R. Qian, *Journal of Electroanalytical Chemistry,* **322**:153 (1992).
82. C. S. C. Bose, S. Basak, and K. Rajeshwar, *The Journal of Physical Chemistry,* **96**:9899 (1992).
83. S. T. Earley, D. P. Dowling, J. P. Lowry, and C. B. Breslin, *Synthetic Metals,* **148**:111 (2005).
84. D. E. Tallman, C. Vang, G. G. Wallace, and G. P. Bierwagen, *Journal of Electrochemical Society,* **149**:C173 (2002).
85. L. Tian, Y. Qi, and B. Wang, *Journal of Colloid and Interface Science,* **333**:249 (2009).
86. R. K. Sharma, A. C. Rastogi, and S. B. Desu, *Physica B: Condensed Matter,* **388**:344 (2007).
87. T. F. Otero and E. De Larreta, *Synthetic Metals,* **26**:79 (1988).
88. T. Hernandez-Perez, M. Morales, N. Batina, and M. Salmon, *Journal of The Electrochemical Society,* **148**:C369 (2001).
89. R. Wadhwa, C. F. Lagenaur, and X. T. Cui, *Journal of Controlled Release,* **110**:531 (2005).
90. J.-M. Pernaut and J. R. Reynolds, *The Journal of Physical Chemistry B,* **104**:4080 (2000).
91. H. Ge, G. Qi, E.-T. Kang, and K. G. Neoh, *Polymer,* **35**:504 (1994).
92. B. C. Thompson, S. E. Moulton, J. Ding, R. Richardson, A. Cameron, S. O'Leary, G. G. Wallace, and G. M. Clark, *Journal of Controlled Release,* **116**:285 (2006).
93. F. Beck, P. Braun, and M. Oberst, *Berichte der Bunsen-Gesellschaft* **91**:967 (1987).
94. E. Beelen, J. Riga, and J. J. Verbist, *Synthetic Metals,* **41**:449 (1991).
95. J. Chengyou, Y. Fenglin, and Y. Weishen, *Journal of Applied Polymer Science,* **101**:2518 (2006).

96. S. Jing, T.-S. Jadranka, C. Shu Yi, L. Kwong Chi, and A. K. Paul, *Journal of Applied Polymer Science,* **111**:876 (2009).
97. H. Masuda and D. K. Asano, *Synthetic Metals,* **135-136**:43 (2003).
98. Y. Shen and M. Wan, *Synthetic Metals*:127 (1998).
99. Y. Li and J. Yang, *Journal of Applied Polymer Science,* **65**:2739 (1997).
100. A. F. Diaz and B. Hall, *IBM Journal of Research and Development,* **27**:342 (1983).
101. M. Zhou, M. Pagels, B. Geschke, and J. Heinze, *The Journal of Physical Chemistry B,* **106**:10065 (2002).
102. F. Beck, *Electrochimica Acta,* **33**:839 (1988).
103. F. Beck and M. Oberst, *Synthetic Metals,* **28**:C43 (1989).
104. F. Beck, M. Oberst, and R. Jansen, *Electrochimica Acta,* **35**:1841 (1990).
105. S. Carquigny, O. Segut, B. Lakard, F. Lallemand, and P. Fievet, *Synthetic Metals,* **158**:453 (2008).
106. J. M. Ko, H. W. Rhee, S. M. Park, and C. Y. Kim, *Journal of Electrochemistry Society,* **137** (1990).
107. M. Satoh, K. Imanishi, and K. Yoshino, *Journal of Electroanalytical Chemistry,* **317**:139 (1991).
108. M. Zhou and J. Heinze, *The Journal of Physical Chemistry B,* **103**:8443 (1999).
109. S. Asavapiriyanont, G. K. Chandler, G. A. Gunawardena, and D. Pletcher, *Journal of Electroanalytical Chemistry,* **177**:245 (1984).
110. T. F. Otero and J. Rodríguez, *Electrochimica Acta,* **39**:245 (1994).
111. S. Shimoda and E. Smela, *Electrochimica Acta,* **44**:219 (1998).
112. P. Burgmayer and R. W. Murray, *Handbook of Conducting Polymers,*Marcel Dekker, **1**, 1986.
113. M. Hepel and F. Mahdavi, *Microchemical Journal,* **56**:54 (1997).
114. M. C. Pedro, C. Milagros, O. Estibalitz, C. Elena, and A. P. José, *Surface and Interface Analysis,* **39**:26 (2007).
115. K. K. Kanazawa, A. F. Diaz, R. H. Geiss, W. D. Gill, J. F. Kwak, J. Anthony Logan, J. F. Rabolt, and G. B. Street, *Journal of Chemistry Society Chemical Communications,* **19**:854 (1979).
116. A. B. Kaiser, *Reports on Progress in Physics,* **64**:1 (2001).
117. J. Y. Wong, Robert Langer, and D. E. Ingberi, *Proceedings of the National Academy of Sciences of the United States of America,* **91**:3201 (1994).
118. B. Garner, A. Georgevich, A. J. Hodgson, L. Liu, and G. G. Wallace, *Journal of Biomedical Materials Research,* **44**:121 (1999).
119. B. Garner, A. J. Hodgson, G. G. Wallace, and P. A. Underwood, *Journal of Materials Science: Materials in Medicine,* **10**:19 (1999).
120. W. R. Stauffer and X. T. Cui, *Biomaterials,* **27**:2405 (2006).
121. N. Gomez, J. Lee, J. Nickels, and C. Schmidt, *Advanced Functional Materials,* **17**:1645 (2007).
122. H. Castano, E. A. O'Rear, P. S. McFetridge, and V. I. Sikavitsas, *Macromolecular Bioscience,* **4**:785 (2004).
123. R. L. Williams and P. J. Doherty, *Journal of Materials Science: Materials in Medicine,* **5**:429 (1994).
124. X. Wang, X. Gu, C. Yuan, S. Chen, P. Zhang, T. Zhang, J. Yao, F. Chen, and G. Chen, *Journal of Biomedical Materials Research Part A,* **68A**:411 (2004).
125. X. Cui, J. Wiler, M. Dzaman, R. A. Altschuler, and D. C. Martin, *Biomaterials,* **24**:777 (2003).

126. D. D. Ateh, H. A. Navsaria, and P. Vadgama, *Journal of The Royal Society Interface,* **3**:741 (2006).
127. B. Paczosa-Bator, T. Blaz, J. Migdalski, and A. Lewenstam, *Bioelectrochemistry,* **71**:66 (2007).
128. G. Wallace and L. Kane-Maguire, *Advanced Materials,* **14**:953 (2002).
129. Q. Xie, S. Kuwabata, and H. Yoneyama, *Journal of Electroanalytical Chemistry,* **420**:219 (1997).
130. J. M. Fonner, L. Forciniti, H. Hguyen, J. D. Byrne, Y. F. Kou, J. Syeda-Nawaz, and C. E. Schmidt, *Biomedical Materials,* **3**:034124 (2008).
131. T. Rivers, T. Hudson, and C. Schmidt, *Advanced Functional Materials,* **12**:33 (2002).
132. M. Staples, K. Daniel, M. Cima, and R. Langer, *Pharmaceutical Research,* **23**:847 (2006).
133. B. Zinger and L. L. Miller, *Journal of American Chemistry Society,* **106**:6861 (1984).
134. D. Svirskis, B. Wright, J. Travas-Sejdic, A. Rodgers, and S. Garg, *Electroanalysis,* **22**:439 (2010).
135. G. Bidan, C. Lopez, F. Mendes-Viegas, E. Vieil, and A. Gadelle, *Biosensors and Bioelectronics,* **10**:219 (1995).
136. P. M. George, D. A. LaVan, J. A. Burdick, C.-Y. Chen, E. Liang, and R. Langer, *Advanced Materials,* **18**:577 (2006).
137. L. L. Miller, G. A. Smith, C. An-Cheng, and Z. Qin-Xin, *Journal of Controlled Release,* **6**:293 (1987).
138. L. L. Miller and Q. X. Zhou, *Macromolecules,* **20**:1594 (1987).
139. M. Pyo and J. R. Reynolds, *Chemistry of Materials,* **8**:128 (1996).
140. Y. Lin and G. G. Wallace, *Journal of Controlled Release,* **30**:137 (1994).
141. Y. Xiao, J. Che, C. M. Li, C. Q. Sun, Y. T. Chua, V. S. Lee, and J. H. Luong, *Journal of Biomedical Materials Research Part A,* **80A**:925 (2007).
142. V. Bajpai, P. He, and L. Dai, *Advanced Functional Materials,* **14**:145 (2004).
143. X. Luo and X. T. Cui, *Electrochemistry Communications,* **11**:1956 (2009).
144. L. Li and C. Huang, *Journal of the American Society for Mass Spectrometry,* **18**:919 (2007).
145. Q.-X. Zhou, L. L. Miller, and J. R. Valentine, *Journal of Electroanalytical Chemistry,* **261**:147 (1989).
146. L. Yongfang and Q. Renyuan, *Journal of Electroanalytical Chemistry,* **362**:267 (1993).
147. B. Massoumi and A. Entezami, *Journal of Bioactive and compatible polymers,* **17** (2002).
148. P. M. M.R. Gandhi, G.M. Spinks, G.G. Wallace, *Synthetic Metals,* **73**:247 (1995).
149. C. W. Han Xu, Chunlei Wang, Jim Zoval, Marc Madou, *Biosensors and Bioelectronics,* **21**:2094 (2005).
150. S. Geetha, C. R. K. Rao, M. Vijayan, and D. C. Trivedi, *Analytica Chimica Acta,* **568**:119 (2006).
151. T. Nagakura, K. Ishihara, T. Furukawa, K. Masuda, and T. Tsuda, *Sensors and Actuators B: Chemical,* **34**:229 (1996).
152. W. Kerner, *Experimental and Clinical Endocrinology & Diabetes* **109**:S341 (2001).

153. N. Holmström, P. Nilsson, J. Carlsten, and S. Bowald, *Biosensors and Bioelectronics,* **13**:1287 (1998).
154. C. Arbizzani, M. Mastragostino, L. Nevi, and L. Rambelli, *Electrochimica Acta,* **52**:3274 (2007).
155. R. T. Richardson, A. K. Wise, B. C. Thompson, B. O. Flynn, P. J. Atkinson, N. J. Fretwell, J. B. Fallon, G. G. Wallace, R. K. Shepherd, G. M. Clark, and S. J. O'Leary, *Biomaterials,* **30**:2614 (2009).

Chapter 2

Experimental

2.1 Introduction

The experimental techniques and procedures employed in this study are outlined in this chapter. The electrochemical set up is described followed by an outline of the chemical preparation and experimental techniques employed to electrosynthesise and characterise the polymers. Finally, the techniques utilised to measure the controlled drug release are discussed. The experimental parameters used in the polymerisation and drug release studies are not described as these vary with each drug. The relevant details are given in Chapters 3, 4, 5 and 6.

2.2 Electrochemical set up

2.2.1 Instruments, software and ancillary equipment

All potentiostatic, galvanostatic and open-circuit potential experiments described in this chapter were carried out using one of two potentiostats; a Solartron (Model SI 1285) or an eDAQ Potentiostat with a standard three-electrode cell. Each potentiostat was controlled by a computer and the various software packages used were CorrWare for Windows™ Version 2.1 and eDAQ Echem Version 2.0.2, respectively. A photograph of the electrochemical equipment is shown in Figure 2.1.

The electrochemical quartz crystal microbalance (EQCM) experiments were performed with a CHi440 instrument (Model EA 160) linked to a crystal oscillator which in turn was connected to the quartz crystal working electrode in a specially designed electrochemical cell. This was controlled by CHi440 software Version 1.0.0.1. Further details on the electrochemical set-up are given in Section 2.4.2.1.

Electrochemical impedance spectroscopy (EIS) measurements were carried out using a Solartron Frequency Response Analyser (Model SI 1250) in conjunction with an electrochemical interface (Solartron Model SI 1287). The Frequency Response Analyser was controlled by ZPlot Version 2.1 for Windows™ and the resulting data were analysed with ZView Version 2.3 for Windows™.

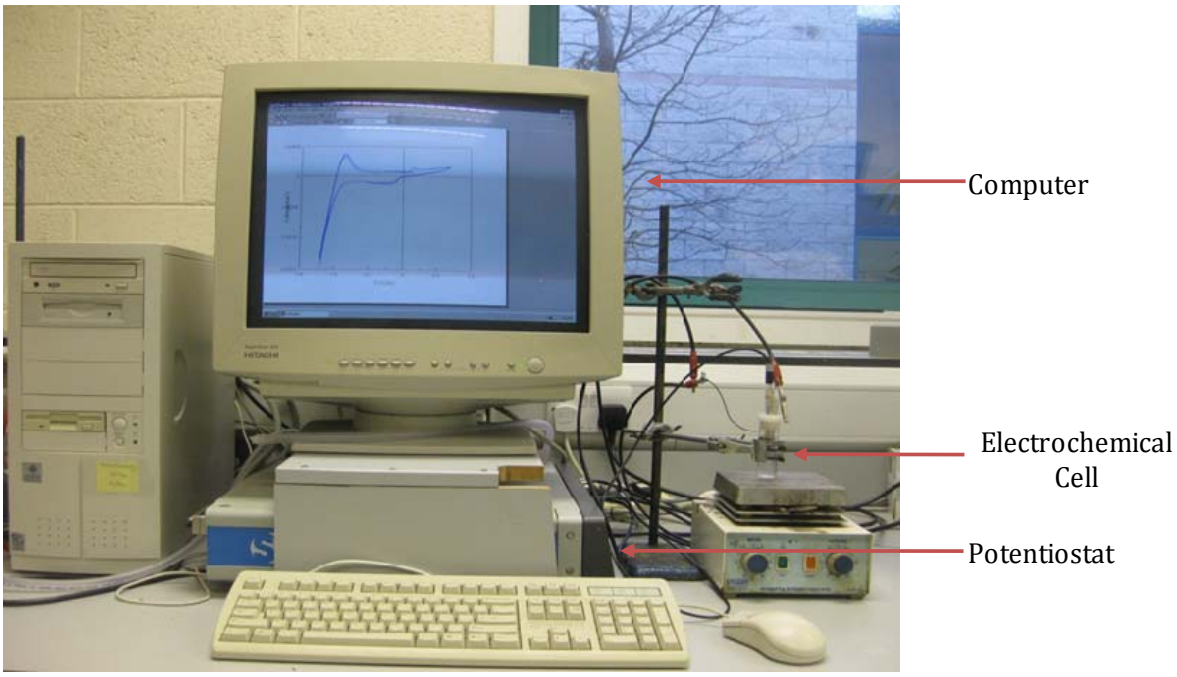

Figure 2.1: Experimental set up used to record all electrochemical measurements.

Differential scanning calorimetry (DSC) was performed with Perkin Elmer Pyris 6.0 apparatus and the results were recorded and analysed by means of Pyris Data software. Conductivity measurements were carried out using a Jenway 4510 conductivity meter while pH measurements were carried out using an Orion Model 720A pH meter. Optical images were taken using an Olympus BX51M system using Leica application suite and Olympus DP Version 3.2 software. Scanning electron microscopy (SEM) was performed on a Hitachi S2200N instrument using INCA software. However, the SEM micrographs discussed in Chapter 6 were taken using a JEOL 7500 field emission scanning electron microscope (FESEM).

2.2.2 The electrochemical cell

As previously stated, a three-electrode cell consisting of a working electrode (WE), an auxiliary or counter electrode (CE) and a reference (RE) was used**.** This set up is shown in Figure 2.2. A platinum wire/mesh, with a high surface area, was used as the auxiliary electrode. A standard saturated calomel electrode (SCE) was utilised for the majority of this work with some exceptions. Firstly, during the polymer formation studies with diclofenac sodium salt, indomethacin sodium salt and sulindac sodium salt, a silver wire pseudo reference electrode was used. Secondly, for the studies of valproic acid sodium salt (NaVPA), a silver/silver chloride

(Ag|AgCl) electrode (3.0 mol dm^{-3} NaCl filling solution) was used. For the majority of these studies, a platinum (Pt) disc electrode was used as the working electrode. In other work, a gold (Au) disc electrode and a gold coated mylar substrate were employed. The electrodes were connected to the potentiostat using coloured wires. All experiments were computer controlled.

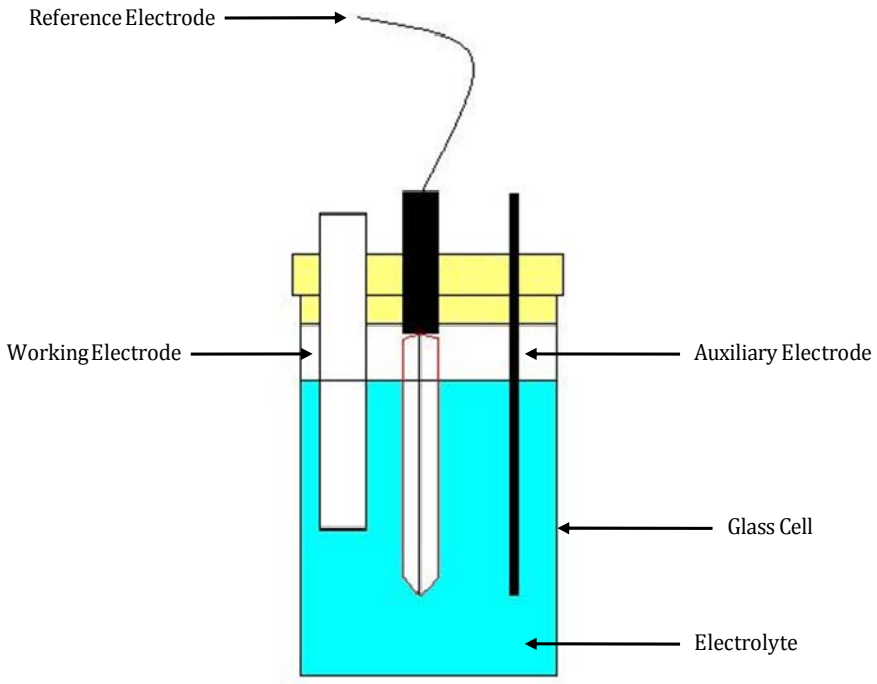

Figure 2.2: Schematic diagram of a three-electrode electrochemical cell.

2.2.3 Preparation of the working electrode

All electrode materials were supplied by Goodfellow Metals and Alfa Aesar in rod form and were sliced into discs with lengths of about 1 cm. The Pt disc comprised of a purity grade of 99.9 % and was 4 mm in diameter. The electrical contact was achieved by means of a copper wire at the base of the electrode. It was then encased in Teflon and secured in place by epoxy resin, a schematic of which is illustrated in Figure 2.3. It was polished with successively finer grades (30 μm, 15 μm, 6 μm and 1 μm) of diamond polishes (Buehler MetaDi Monocrystalline Diamond suspension) on a Buehler micro-cloth, sonicated and rinsed with distilled water to ensure a clean surface. The Au disc electrode (99.99% purity) was encased, as outlined for the Pt disc electrode, but had a smaller diameter of 3 mm.

It was polished as described above for the platinum disc electrode. In some electropolymerisation experiments, a glassy carbon rod (4 mm) was utilised and again it was encased as illustrated previously for the Pt electrode. In Chapter 6, gold mylar, masked to a 1 cm^2 area, was the substrate of choice for the working electrode. The gold mylar pieces were cut to the appropriate size, washed in ethanol and pretreated in a UV-Ozone cleaner (UV PRO 2800) for 20 min to remove any contaminants from the surface.

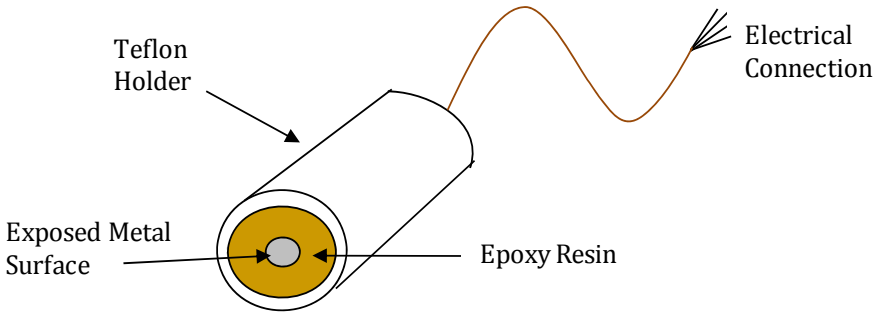

Figure 2.3: Schematic diagram of electrode assembly.

2.3 Chemicals

All chemicals were purchased from Sigma Aldrich and used without further purification except for the pyrrole (Py) monomer (98 %). The monomer was distilled and stored in the dark at low temperatures prior to use. All other chemicals were Analar grade reagents. In general, 0.20 mol dm^{-3} (0.35 ml in 25 ml supporting electrolyte) of Py was dissolved in the electrolyte solution for all electrochemical deposition experiments. Polypyrrole (PPy) film fabrication was carried out using electrosynthesis methods, which deposited the polymer film at the working electrode. In all cases, the monomer/drug solution was kept in a sealed electrochemical cell that was wrapped in aluminium foil between experiments. In Chapter 3 and 4, all polymers were doped with the drug upon formation from an aqueous electrolyte. The concentration of each drug can be seen in Table 2.1 with the higher concentrations corresponding to the electrolyte in which the polymer was placed whilst attempting to reuse the polymer. The electrodeposition of PPy doped with Dex^{2-} was carried out at room temperature at a Pt electrode, while the deposition of DF^{-} doped PPy was achieved under heated

conditions using Au as the working electrode. Further details are provided in the relevant chapters.

In Chapter 5, the electrodeposition of PPy doped with two different drugs was performed in ethanol using a Pt electrode as the working electrode. Again, the polymers were doped with the drug upon polymerisation under heated conditions. The conductivity of the ethanol was increased by adding tetrabutylammonium perchlorate (TBAP). The concentrations of each drug and TBAP are shown in Table 2.2. As before, the higher concentrations of drug correspond to the electrolyte in which the polymer was placed whilst attempting to reuse the polymer.

Table 2.1: Summary of the electrolyte used for the deposition of PPy from an aqueous solution.

Drug	Concentration / mol dm^{-3}
Dexamethasone disodium phosphate (NaDex)	0.05, 0.06
Diclofenac sodium salt (NaDF)	0.10, 0.12

Table 2.2: Summary of the electrolyte used for the polymerisation of Py in ethanol.

Drug or Salt	Concentration / mol dm^{-3}
Indomethacin sodium salt (NaIndo)	0.20, 0.30
Sulindac sodium salt (NaSul)	0.12, 0.20
Tetrabutylammonium perchlorate (TBAP)	0.08, 0.20

In Chapter 6, the studies on the incorporation of valproic acid (VPA^-) into the PPy membrane film were more complicated than the studies in Chapters 3, 4 and 5. Several electrochemical techniques were employed in an attempt to deposit PPy doped with VPA^- as well as vapour phase polymerisation. The concentrations of both the drug and monomers were varied throughout the study and for this reason all parameters are described in Chapter 6.

For the bulk drug release, the drug was released and measured in the presence of 0.10 mol dm^{-3} sodium chloride (NaCl). In the studies of VPA^-, artificial cerebral

spinal fluid (aCSF) was used as the release medium, the composition of which is shown in Table 2.3.

Table 2.3: Reagents and amounts required to make up 1 L of aCSF.

Reagent	Amount for 1 L / g
NaCl	8.660
KCl	0.224
$CaCl_2.2H_2O$	0.206
$MgCl_2.6H_2O$	0.163
$Na_2HPO_4.7H_2O$	0.214
$NaH_2PO_4.2H_20$	0.027

2.4 Experimental techniques

Polymerisation, characterisation and controlled release studies were carried out using various electrochemical and chemical techniques. These techniques are described in this section; however, specific parameters are not given as these vary throughout the study and will be provided and discussed in the appropriate results chapters.

2.4.1 Potentiostatic measurements

This technique was utilised to electrochemically deposit PPy doped with the drug of interest onto the working electrode. These measurements were carried out by applying a constant potential to the electrode for a given time or until a desired charge was passed. The current density was recorded as a function of time. To achieve the electropolymerisation of Py, the applied potential to the electrode of interest must exceed +0.500 V vs SCE. The anodic voltages used in this work ranged from +0.700 V vs SCE to +0.900 V vs SCE. Higher potentials were not employed as they are well known to give rise to over-oxidation of the polymer[1]. The thickness of the polymer films was controlled by monitoring the charge. Further details on the potentials and charges employed are given in the experimental sections of the relevant chapters.

This technique was also employed during the release studies. It is well known that PPy is reduced with the application of a cathodic potential and the dopant (depending on size) is forced out of the polymer so the polypyrrole can maintain its neutrality[2]. In this work the polymers were reduced by applying cathodic potentials in the range of –0.200 V vs SCE to –1.000 V vs SCE.

2.4.2 Open-circuit potential

This technique was used to monitor the rest potential of the doped polypyrrole films. The technique is very useful in a variety of areas including analysis of the stability of the polymer and measuring the potential in the cell during the drug release studies.

2.4.3 Cyclic voltammetry

Cyclic voltammetry (CV) is one of the most useful and widely applied techniques in electrochemistry[3, 4]. It was employed for two purposes, firstly as an alternative technique to electrochemically deposit PPy on the working electrode and secondly as an investigative tool to study the properties of the polymers[5]. CV involves sweeping the potential applied to the working electrode between two chosen potential limits and the change in current is monitored. This is done at a constant rate known as the scan rate. The initial applied potential, E_i, is swept to a vertex potential, E_v, where the scan is reversed and swept back to the final potential, E_f, which usually equals the original potential, E_i. This process creates a cyclic effect and is typically repeated a number of times. For a simple redox reaction, Equation 2.1, where only R is present, the current response of the forward scan is the linear potential sweep voltammogram as R is oxidised to O which produces an anodic peak. On the reverse scan, the reduction of O to R occurs, resulting in a cathodic peak. The resulting cyclic voltammogram plots the applied potential as a function of current, as shown in Figure 2.4.

$$O + ne^- \rightleftharpoons R \qquad 2.1$$

The working electrode provides the surface where the electron transfer of the redox reaction takes place and an electrical current is created. This is known as the

faradic current. At the counter electrode, electron transfer takes place in the opposite direction which balances the faradaic process (e.g., if oxidation takes place at the WE, reduction takes place at the CE). The redox reaction takes place within the potential range defined by the two chosen potential limits and the potentials at which reduction or oxidation take place provide qualitative information about the electroactive species under investigation. Therefore, depending on the applied potential to the surface, the working electrode can act as either an electrochemical reductant or oxidant. As the applied potential becomes more negative, the electrode becomes a better reducing agent. Equally, as the applied potential becomes more positive, the electrode becomes a better oxidising agent.

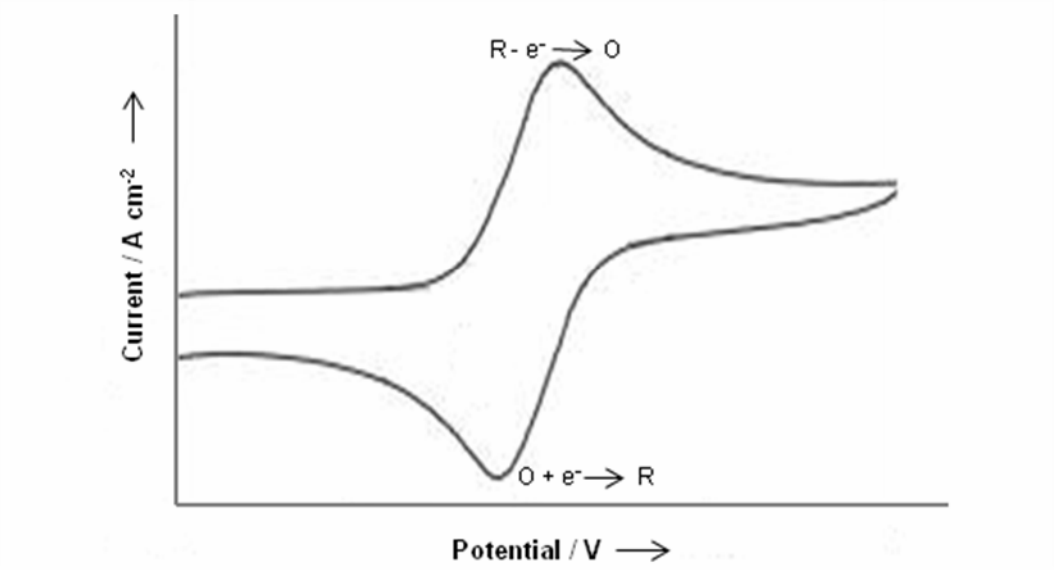

Figure 2.4: Typical current-potential profile for a cyclic voltammogram of a reversible redox species.

The voltammogram response at different scan rates can provide kinetic information concerning the electron transfer process as well as the electrocatalytic process, i.e. diffusion and adsorption effects. Furthermore, it can be used to determine the reversible behaviour of the system. The factors that influence the behaviour and magnitude of the peak current can be described by the Randles-Sevcik equation, Equation 2.2. The use of this equation is limited to processes that are reversible. The cyclic voltammogram shown in Figure 2.4 is an example of a reversible reaction. A reversible cyclic voltammogram can only be observed if both

the oxidation and reduction species are stable and if the kinetics of the electron transfer process are fast[6].

$$i_p = (2.69 \times 10^5)\, n^{\frac{3}{2}} A D^{\frac{1}{2}} C v^{\frac{1}{2}} \qquad 2.2$$

In this equation, n=number of electrons, F= Faraday's constant, A = electrode area (cm^2), C^*_0 = bulk concentration of the electrolyte (mole cm^{-3}), v = scan rate ($V\ s^{-1}$) and D = apparent diffusivity of the electrolyte in the polymer film ($cm^2\ s^{-1}$), with the assumption that the charge-compensation step is rate-limiting.

It can be seen in this equation that the peak current is proportional to the concentration of the electroactive species and the square-root of the scan rate and diffusion coefficient. Therefore, a linear relationship between the current and the square-root of the scan rate indicates that the redox reaction of the electroactive species conforms to the Randles-Sevcik equation and is governed by some extent by a diffusion-controlled process. For reversible reactions, the peak separation between the forward and reverse peaks is close to 59/n mV.

For a quasi-reversible system, the peak currents increase with the square-root of the scan rate but are not always proportional to it. Furthermore the peaks are separated by more than 59/n mV and this separation increases and the peak potential shifts with increasing scan rate[6].

2.4.4 Galvanostatic measurements

This technique was employed to electrochemically deposit PPy onto gold coated mylar in the studies of NaVPA. This technique involves the application of a constant current to the electrochemical cell. In the case of the pre-layers/polymers grown during the post-doping studies, a current density of 0.50 mA cm^{-2} was applied and the potential was recorded as a function of time, or until a suitable charge was passed. A pulsed galvanostatic technique was also employed, which involved applying current pulses of 0.10 mA cm^{-2} for a set time with a rest time in between each pulse.

2.4.5 Vapour phase polymerisation (VPP)

This technique was employed in the studies of NaVPA, in Chapter 6, when traditional electrochemical deposition proved difficult. VPP is a simple alternative to deposit PPy on various substrates and is useful for the deposition of polymers onto insulating substrates. Bjorn Winther-Jensen *et al.*[7] reported the successful VPP of Py and the same protocol was followed in this work. The most important parameter that was varied was the amount of the oxidising agent, ferric toluenesulfonate (Fe(III) [TOS]) deposited on the substrate. When higher concentrations or volumes of the oxidising agent were used, it proved difficult to obtain a uniform surface layer. For this reason, 40 % Fe(III) [TOS] was used and it was much easier to obtain an even film across the surface and less volume was required. The optimised parameters entailed the deposition of 7.5 µl of 40 % Fe (III) [TOS] in ethanol onto 1 cm^2 of indium tin oxide (ITO) glass. This was then heated to approximately 65 °C until the ethanol evaporated off. The surface was then exposed to pyrrole vapour at room temperature in a closed chamber. The resulting polymer, which nucleated onto the modified surface, was allowed to stand for 60 min and was then rinsed twice in ethanol containing different concentrations of NaVPA (0.5 to 2.0 %). Each rinse was 20 min long. Finally, the polymer was rinsed in pure ethanol.

2.4.6 Electrochemical quartz crystal microbalance (EQCM)

EQCM is a very useful tool in electrochemistry as it can monitor extremely small mass changes at the electrode surface during electrochemical experiments[8]. This technique was utilised to obtain additional information about the polymers including estimates of the mass and doping levels of the drugs within the polymers. As stated previously, all EQCM experiments were carried out on a CHi440 EQCM and the equipment consisted of a quartz crystal oscillator, a frequency counter, a fast digital function generator, a high resolution and high speed data acquisition circuitry, a potentiostat and a computer. A schematic indicating the various components of the EQCM set-up is shown in Figure 2.5.

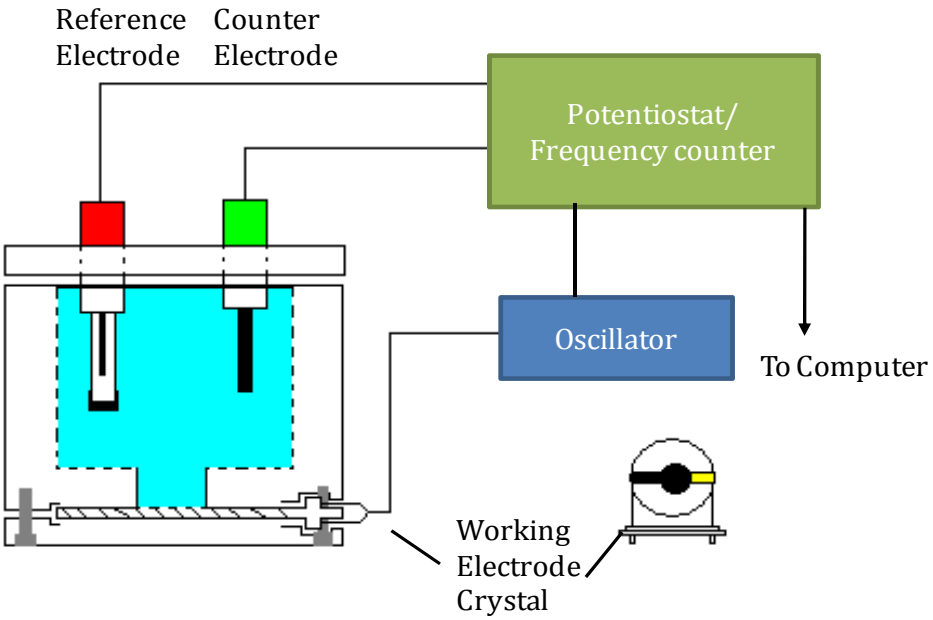

Figure 2.5: A schematic diagram of the EQCM set-up.

The polymers were deposited onto polished Au quartz crystal electrodes (Cambria Scientific) with an exposed surface area of 0.203 cm^2. The electrochemical cell consisted of a specially made Teflon holder in which the crystal was placed between two o-rings, a picture of which is shown in Figure 2.6. During each experiment only one of the metal electrode surfaces is in contact with the electrolyte. The quartz crystal is supported by two wires, one to carry current to the gold layer and the other to allow for crystal vibration and to record the frequency. The set up is completed using a platinum wire counter and a custom-made Ag|AgCl reference electrode.

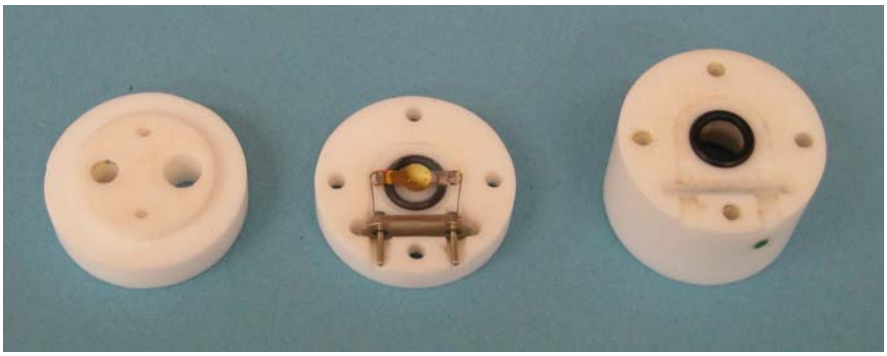

Figure 2.6: Picture of the Teflon holder including o-rings where the crystal is placed during the EQCM.

In EQCM measurements, the frequency of the oscillating quartz crystal is monitored. Changes in the frequency are observed as the mass of the crystal changes. The changes in frequency are related to the changes in mass through the Sauerbrey equation, Equation 2.3[9, 10].

$$\Delta f = -\frac{2f_0^2 \Delta M}{A\sqrt{\rho\mu}} \qquad 2.3$$

Here, f_0 is the resonant frequency, ΔM is the mass change, A is the surface area of the electrode, 0.203 cm^2, ρ is the density of the quartz, 2.648 g cm^{-3}, and μ is the shear modulus of the quartz, 2.947 x 10^{11} g cm^{-1} s^{-2}. In this equation the change of frequency (Δf) is equal to minus the change in mass (ΔM) per unit area (A) times a constant. The frequency, therefore, decreases as the mass increases.

During an electropolymerisation of Py, a forming polymer backbone is charged positively. Anions are incorporated into the PPy to balance the positive charges on the oxidised polymer. Generally it can be expressed as follows:

$$nPy + nxA^- \rightarrow [Py^{x+}xA^-]_n + n(2+x)e^- \qquad 2.4$$

In Equation 2.4, n is the degree of polymerisation and x is the doping level. The doping level is defined as the number of unit charges per Py ring[11-14]. As it follows from Equation 2.4, for the one monomer unit formation (2 + x) electrons are required. Thus, the mass of PPy film originating from the process shown in Equation 2.5 can be calculated using Faraday's law:

$$\frac{M}{Q} = \frac{(M_m) + (M_{dop})x}{(2+x)F} \qquad 2.5$$

Here, M is the total mass of the deposited polymer, Q is the charge reached, M_m is the mass of the monomer, M_{dop} is the mass of the dopant, x is the doping level ($x \leq 0.33$) and *F* is Faraday's constant, 96,484.56 C mol^{-1}.

Studies into the polymerisation of the Py by EQCM, have reported that the value of the doping level is independent of the experimental conditions such as pH, potential, temperature and relative permittivity assuming that no neutral species are transported[2].

2.4.7 Electrochemical impedance spectroscopy (EIS)

This technique was used to explore the properties and stability of the PPy doped with various drug molecules. Experiments were recorded at open-circuit potential and at a reduction potential of –0.900 V vs SCE with a small sinusoidal excitation voltage of 10 mV. The frequency of the AC wave was varied from 65,000 to 0.008 Hz allowing the impedance of the system to be obtained as a function of frequency. All experiments were performed over extended periods of time, usually 6-8 h, to ensure that the system was under steady-state conditions.

Impedance data can be plotted as a result of the imaginary impedance (Z'') versus the real impedance (Z') at each sampled frequency giving a complex plane plot, or it may be plotted as the logarithm of the total impedance, |Z|, and the phase angle, θ, versus the logarithm of the frequency giving a Bode plot, as seen in Figure 2.7. Equation 2.6 shows the relationship between the total impedance, |Z|, and the real, Z', and imaginary, Z'', impedance values.

$$|Z| = \sqrt{Z_{real}^{2} + Z_{Imag}^{2}} \qquad 2.6$$

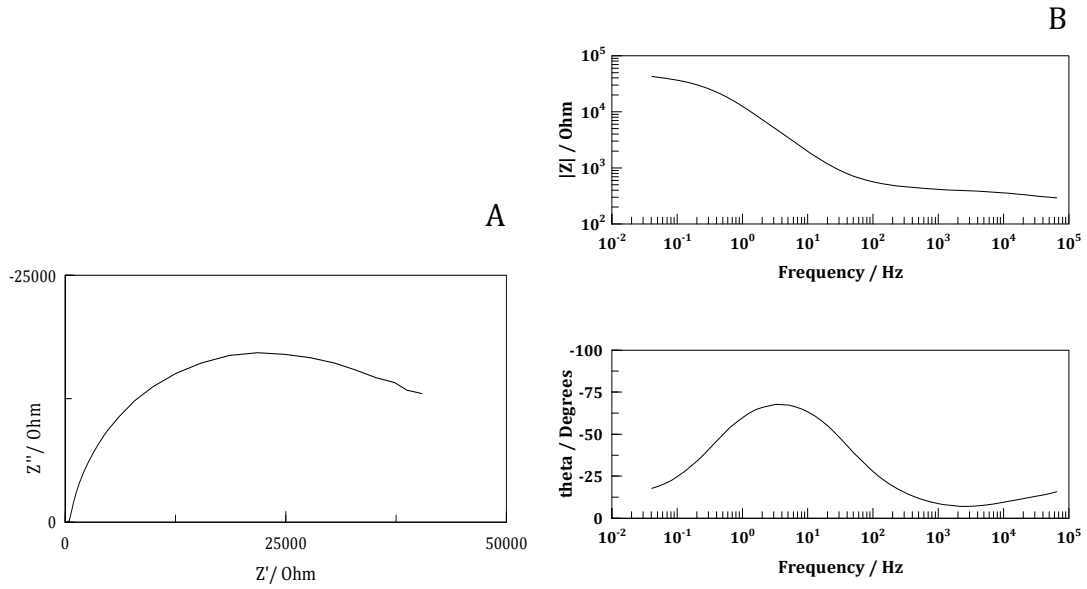

Figure 2.7: A Complex plane and **B** Bode plot. Typical example of the impedance plots leading to a simple Randles circuit fit.

The experimental data were fitted to equivalent electrical circuits using ZView software. In this analysis, initial estimates for the required parameters are obtained and are then refined using a non-linear least squares iterative process to improve the fit to the experimental data. The elements used in the fitting of the equivalent circuit are representative of a number of real physical attributes in the system. Two main circuit elements were used in fitting the data; these were resistors and constant phase elements. A resistor has no imaginary component and therefore its magnitude is equal to the impedance of the real component. Resistors represent the physical magnitude of resistive elements in the experimental system, for example, solution resistance and the resistance of charge transfer. Constant phase elements, CPEs, are often used in fitting impedance data and are generally attributed to distributed surface reactivity, surface inhomogeneity, roughness or fractal geometry and electrode porosity[15]. Equation 2.7 defines the impedance of a constant phase element where T represents the magnitude of the impedance, ω is the angular frequency (2πf), f is the frequency of the signal and P is an exponent. When P exhibits a value of 1.0, the constant phase element corresponds to a true capacitor, when the value is between 0.8 and 1.0 it is regarded as a non-ideal capacitor and when it has a value of 0.5 it corresponds to a diffusional process[16] and coincides with a phase angle of 45 °.

$$Z - \frac{1}{T\sqrt{(-1\omega)^{p}}} \qquad 2.7$$

Using various components, in series or in parallel, an appropriate model based on the physical system is created. Figure 2.8 shows the two models used to evaluate impedance data in the present thesis. Figure 2.9 shows the data printout obtained on fitting an equivalent circuit to the impedance plots shown in Figure 2.7. The program computes values for each parameter from initial estimates and then estimates the error and the % error by testing several solutions close to the 'best fit' value and by determining how much the values must change before the goodness of fit begins to decrease. As the system becomes more complex further circuit elements are added, however, as a result the % error increases also. In general, the errors were confined to < 3.0 %. If errors higher than 3.0 % were achieved, then an alternative circuit was considered. In addition, all data were recorded under steady-state or nearly steady-state conditions throughout the duration of the measurement to ensure that the system satisfied the condition of stability.

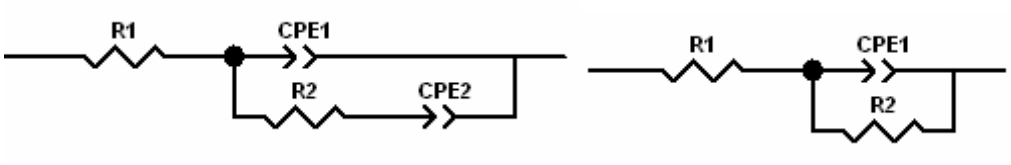

Figure 2.8: Equivalent circuits used to fit impedance data in this thesis.

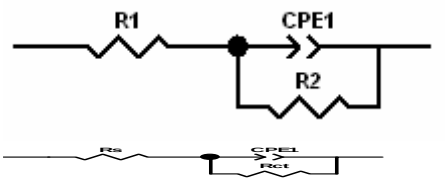

Element	Freedom	Value	Error	Error %
Rs	Free(+)	100.9	1.724	1.7086
CPE1-T	Free(+)	0.00013415	2.3356E-06	1.741
CPE1-P	Free(+)	0.46444	0.00345986	0.75329
Rct	Free(+)	11646	272.91	2.3434

Chi-Squared:	0.0050163
Weighted Sum of Squares:	0.69225
Data File:	C:\Documents and Settings\Eimear\My Documents\
Circuit Model File:	
Mode:	Run Fitting / Selected Points (0 - 70)
Maximum Iterations:	100
Optimization Iterations:	0
Type of Fitting:	Complex
Type of Weighting:	Calc-Modulus

Figure 2.9: Equivalent circuit and parameter fitting obtained for the impedance plots shown in Figure 2.7. This type of circuit is referred to as a Randles Cell.

2.4.8 Differential scanning calorimetry (DSC)

DSC is used to study the thermal transitions of polymers such as glass transitions, crystallisation, melting interval, decomposition and even purity[17]. Figure 2.10 shows the different parts of the apparatus for DSC analysis. The sample and reference are enclosed in a single furnace and connected by a low-resistance heat-flow path. The furnace is set to increase or decrease the temperature at a fixed rate and the arrangement of the furnace and pans ensure that both pans are at identical temperature at any given time. The difference in heat flow (mW) to the sample and to the reference is monitored against the temperature (°C). Enthalpy or heat capacity changes in the sample cause a difference in temperature, ΔT, compared to the reference. This temperature difference between the sample and the reference is recorded and used to generate a thermogram.

In this work, DSC was employed to gain further information on the properties and stability of the drugs. Pans containing approximately 3 mg of sample were heated from 50 °C to 300 °C at a rate of 10 °C min^{-1} under a nitrogen atmosphere to prevent oxidation phenomena. The reference was an empty aluminium pan.

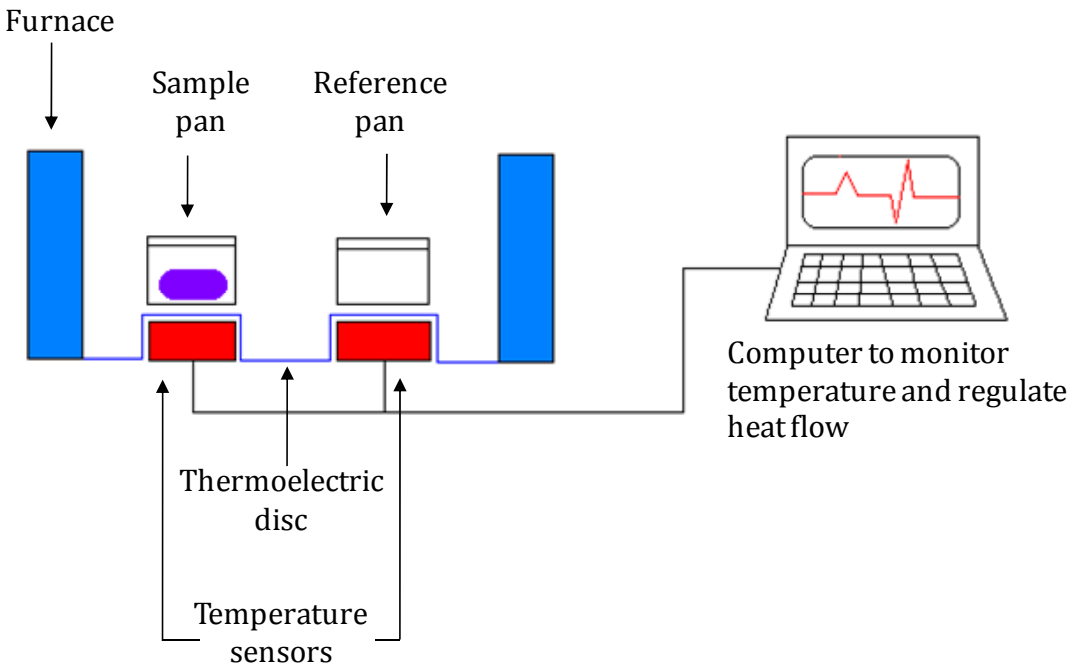

Figure 2.10: Schematic of differential scanning calorimeter

2.4.9 Optical and scanning electron microscopy

Optical microscopy allows the observation and characterisation of samples on a micrometre scale (μm), while higher resolution micrographs on a nanometre (nm) scale can be obtained using scanning electron microscopy (SEM). These techniques were used to analyse the morphology of the polymer films. Flat Pt or Au electrodes encased within a Teflon support, as detailed in Section 2.2.3, were used as the working electrodes. These electrodes were specifically designed for both the optical and SEM microscopes, in order to fit on the flat stage where the samples were placed. The polymer films were grown at their optimum conditions on the electrodes and then analysed. In the case of SEM, all samples were sputter coated with Au using an Emitech K550x gold sputter coater prior to analysis.

2.5 Controlled drug release measurements

Most release samples were analysed using a Varian Cary Series UV-visible spectrophotometer, by recording the absorbance of the drug as a function of the release conditions. In Chapter 6, for release studies of VPA^-, samples were analysed using a valproic acid reagent in conjunction with a Beckman Coultar Synchron Clinical System, model Unicel DxC600.

2.5.1 UV-visible spectroscopy

UV-visible spectroscopy measures the amount of ultraviolet and visible light transmitted or absorbed by a sample placed in a spectrometer. The wavelength at which a chemical absorbs light is a function of its electronic structure and the intensity of the light absorption is related to the amount of the chemical between the light source and the detector, so a UV-visible spectrum can be used to identify some chemical species[18]. The spectrometer used throughout these studies comprises of a Xenon lamp and has a maximum scan rate of 24 000 nm min^{-1}.

This technique was used to measure the amount of drug released from the polymer. Spectra were collected and analysed to calculate the amount of drug released upon application of a reduction/oxidation potential or at open-circuit potential. In all cases, a quartz cuvette with a diameter of 1 cm was used. The amount of drug released was determined by measuring the absorbance at a

particular wavelength, generally the wavelength of maximum absorption (λ_{max}) for the drug in question and applying the Beer-Lambert law, Equation 2.8.

$$A = \varepsilon cd \quad 2.8$$

Here, A is the absorbance, ε is the molar absorptivity, d is the path length and c is the concentration of the compound in solution. The slope was calculated from the linear relationship between the concentration and the absorbance. This was done for all drugs and representative absorbance spectra as well as calibration curves for NaDex and NaDF in water can be seen in Figure 2.14. The λ_{max} of the drug, the concentration range used to achieve these calibration curves and the slope of these lines are shown in Table 2.4. The slope was then used, in conjunction with the measured absorbance to calculate the concentration of the released drug. For example, Figure 2.14C shows a calibration curve of Dex which has a λ_{max} of 242 nm. Equation 2.9 gives the equation of the line, where y is the absorbance and x is the concentration, providing a direct correlation between absorbance and concentration.

$$y = 9459.1x \quad 2.9$$

Table 2.4: Summary of the λ_{max}, the concentration ranges at which the calibration curves were plotted and the slope of these lines for NaDex and NaDF.

Drug	**λ_{max} / nm**	**Concentration range / mol dm^{-3}**	**Slope /mol^{-1} dm^3**
Dexamethasone disodium phosphate (NaDex)	242	7.04 x 10^{-6} - 1.02 x 10^{-4}	9459.1
Diclofenac sodium salt (NaDF)	276	7.12 x 10^{-6} – 9.80 x 10^{-5}	9751.5

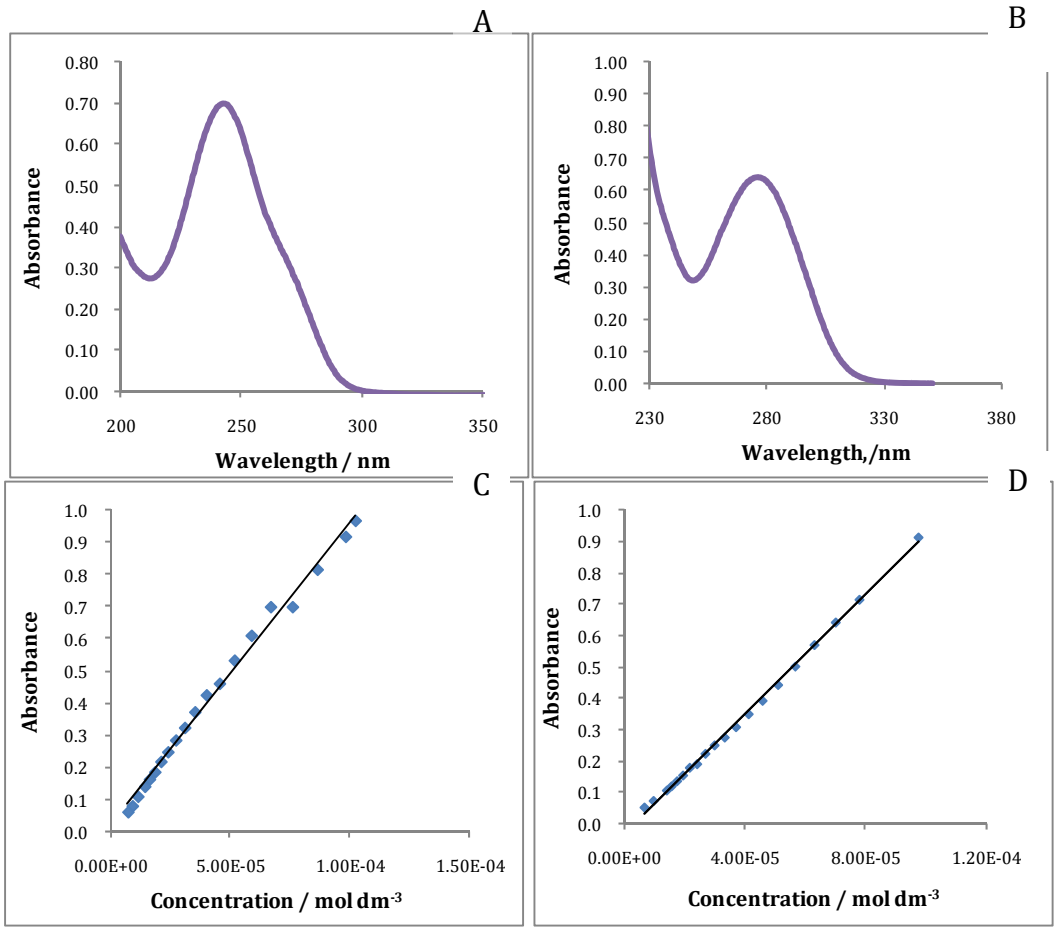

Figure 2.11: Representative absorbance spectra of **A** dexamethasone disodium phosphate (NaDex) (λ_{max} =242 nm, 7.6 x 10^{-5} mol dm^{-3}) and **B** diclofenac sodium salt (NaDF) (λ_{max} =276 nm, 7.05 x 10^{-5} mol dm^{-3}). Also calibration curves for **C** NaDex in water and **D** NaDF in water. Absorbance is a function of concentration. From the data, the slope was obtained.

Representative absorbance spectra for NaIndo and NaSul are shown in Figure 2.12. Calibration curves for NaIndo and NaSul were carried out in ethanol and can be seen in Figure 2.13A and Figure 2.13B. Again, the λ_{max} of the drugs, the concentration range used to achieve these calibration curves and the slope of these lines are shown in Table 2.5. The slopes of these calibration curves were calculated as 6653.5 and 11684.5 mol^{-1} dm^3 for NaIndo and NaSul, respectively. However, the release measurements were carried out in the presence of 0.10 mol dm^{-3} NaCl and for this reason a second calibration curve was then performed in 0.10 mol dm^{-3} NaCl. The poor solubility of the drugs limited the concentration that could be measured. The resulting calibration curves, presented in Figure 2.13C and Figure

2.13D, show a considerable change in the slopes calculated. These significant changes in the slope do not occur for those drugs that are soluble in water, for example, calibration curves for NaDF were performed in water and NaCl and the corresponding slopes were calculated as 9751.5 and 9656.1 mol^{-1} dm^3, respectively, which is not notably different. The difference seen between the absorbance measured in ethanol and NaCl must then be due to the difference in the molar absorptivity, ε, of the drug dissolved in the two solutions.

Table 2.5: Summary of the λ_{max}, the linear concentration ranges of the calibration curves and the slope of these lines for NaIndo and NaSul.

Drug	**λ_{max} / nm**	**Concentration range / mol dm^{-3}**	**Slopes in ethanol or NaCl/ mol^{-1} dm^3**
Indomethacin sodium salt (NaIndo)	320	3.77×10^{-5} – 1.80×10^{-4}	6653.5/ 293.7
Sulindac sodium salt (NaSul)	330	3.22×10^{-5} – 2.40×10^{-4}	11684.5/1146.2

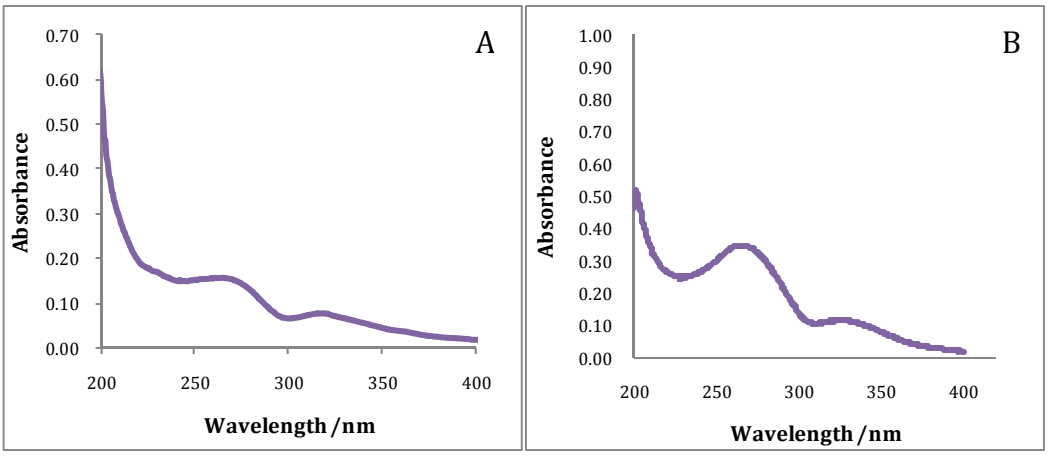

Figure 2.12: Representative absorbance spectra of **A** indomethacin sodium salt (NaIndo) (λ_{max} =320 nm, 1.80×10^{-4} mol dm^{-3}) in 0.10 mol dm^{-3} NaCl **B** sulindac sodium salt (NaSul) (λ_{max} =330 nm, 2.40×10^{-4} mol dm^{-3}) in 0.10 mol dm^{-3} NaCl.

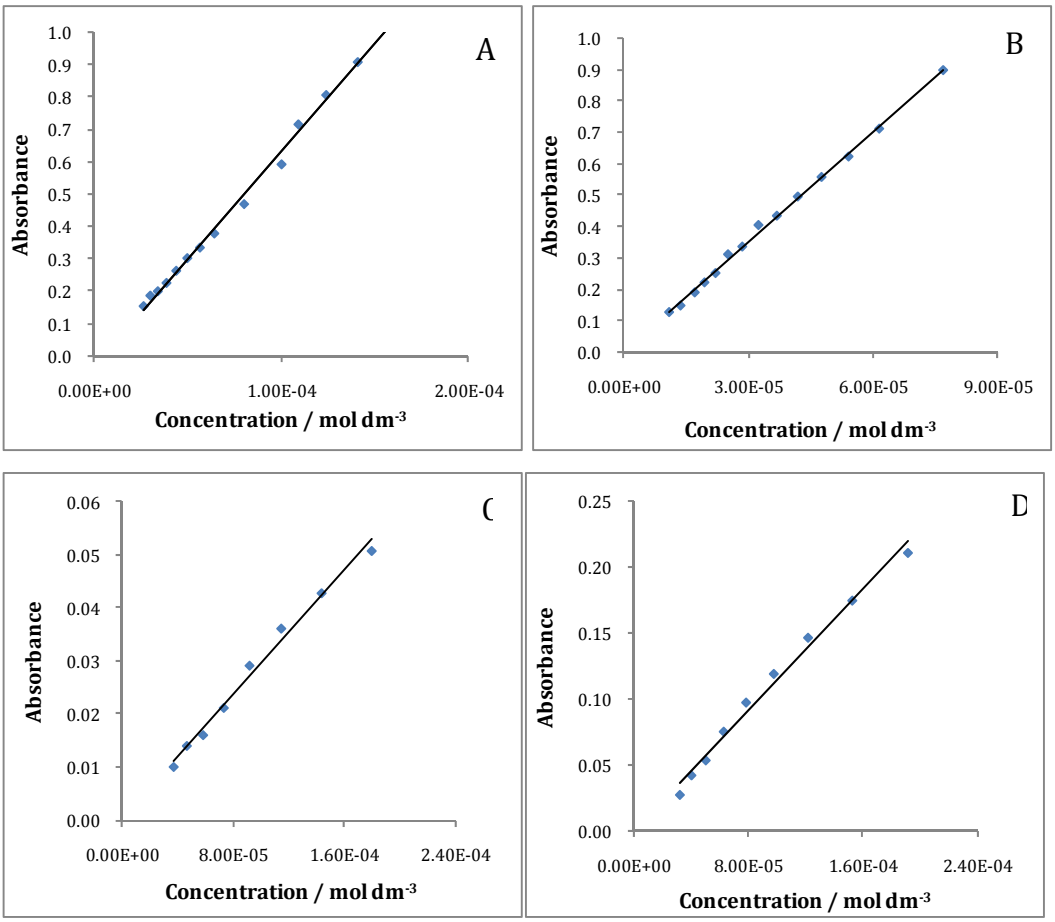

Figure 2.13: Calibration curve of **A** indomethacin sodium salt (NaIndo) in ethanol, **B** sulindac sodium salt (NaSul) in ethanol, **C** indomethacin sodium salt (NaIndo) in 0.10 mol dm^{-3} NaCl and **D** sulindac sodium salt (NaSul) in 0.10 mol dm^{-3} NaCl. Absorbance is plotted as a function of concentration.

In Chapter 6, sodium para-toluenesulfonate (NapTS) and valproic acid sodium salt (NaVPA) were measured by UV-vis spectroscopy and the calibration curves are shown in Figure 2.14. It is well documented in the literature that the detection of valproic acid by UV-vis spectroscopy is difficult and is generally achieved by carrying out esterification prior to detection[19-21]. In this study a calibration curve was achieved by measuring the absorbance of NaVPA at 205 nm. A slope of 114.98 mol^{-1} dm^3 along with an R^2 value of 0.996 was calculated. The wavelength at which the absorbance was measured, the concentration range used to achieve these calibration curves and the slopes of the linear relationships are shown in Figure 2.14. The VPA^- release was measured by UV-vis spectroscopy for one set of experiments only, and all further VPA^- detection was carried out using a valproic acid assay, as described in Section 2.5.2.

Table 2.6: Summary of the λ_{max}, the linear concentration ranges of the calibration curves and the slope of these lines for sodium para-toluenesulfonate (NapTS) and valproic acid sodium salt (NaVPA).

Drug	λ_{max} / nm	Concentration range / mol dm^{-3}	Slope/ mol^{-1} dm^3
Sodium para-toluenesulfonate (NapTS)	261	1.00 x 10^{-4} - 3.11 x 10^{-3}	262.44
Valproic acid sodium salt (NaVPA)	205	1.14 x 10^{-3} – 7.16 x 10^{-3}	114.98

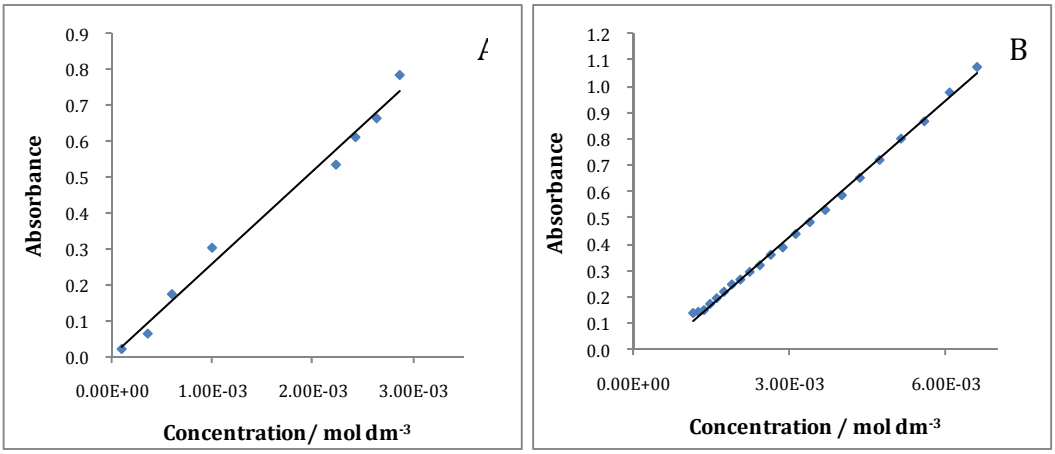

Figure 2.14: Calibration curve of **A** sodium para-toluenesulfonate (NapTS) in water and **B** valproic acid sodium salt (NaVPA) in water. Absorbance is plotted as a function of concentration.

2.5.2 The SYNCHRON valproic acid reagent

The SYNCHRON valproic acid assay was used to measure valproic acid concentration by a competitive particle enhanced turbidimetric immunoassay method[22]. Particle-bound drug (PBD) binds to the valproic acid specific antibody (Ab) forming insoluble aggregates causing turbidity. Non-particle-bound valproic acid in the sample competes with the PBD for the antibody binding sites, inhibiting the formation of aggregates. The rate of particle aggregation is inversely proportional to the concentration of valproic acid in the sample. The reaction scheme can be seen in Equation 2.10.

$$VPA_{sample} + PBD + Ab \rightarrow PBDAb_{Aggregates} + VPA_{sample}\,Ab \qquad 2.10$$

In this work, release studies were carried out in triplicate in 10 ml of artificial cerebral spinal fluid (aCSF) with a sample of 300 µL taken at certain time intervals. The volume of the release electrolyte was maintained at 10 ml for the entire length of release. The dilution factor was taken into account when the data were analysed.

2.6 References

1. F. Beck, P. Braun, and M. Oberst, *Berichte der Bunsen-Gesellschaft* **91**:967 (1987).
2. K. Kontturi, P. Pentti, and G. Sundholm, *Journal of Electroanalytical Chemistry,* **453**:231 (1998).
3. P. R. Unwin, *Instrumental and Electroanalytical Chemistry*,A. J. Bard and M. Stratmann,Wiley, **3**, 2003.
4. A. J. Bard and L. R. Faulkner, *Electrochemical Methods: Fundamentals and Applications.* ,John Wiley & Sons Inc, 2001.
5. A. F. Diaz, J. I. Castillo, J. A. Logan, and W.-Y. Lee, *J. Electroanal Chem,* **129**:115 (1981).
6. R. Greef, R. Peat, L. M. Peter, D. Pletcher, and J. Robinson, *Instrumental Methods in Electrochemistry*,T. J. Kemp,Ellis Horwood Limited, **443**, 1985.
7. J. C. Bjorn Winther - Jenson, Keld West and Gordon Wallace, *Macromolecules,* **37**:5930 (2004).
8. I. Rubinstein, *Physical Chemistry: Principles, Methods and Applications.,*CRC Press, 1995.
9. G. Sauerbrey, *Zeitschrift für Physik,* **155**:206 (1959).
10. Y. Xiao, J. Che, C. M. Li, C. Q. Sun, Y. T. Chua, V. S. Lee, and J. H. Luong, *Journal of Biomedical Materials Research Part A,* **80A**:925 (2007).
11. G. A. Snook and G. Z. Chen, *Journal of Electroanalytical Chemistry,* **612**:140 (2008).
12. V. Syritski, A. Öpik, and O. Forsén, *Electrochimica Acta,* **48**:1409 (2003).
13. Q. Xie, S. Kuwabata, and H. Yoneyama, *Journal of Electroanalytical Chemistry,* **420**:219 (1997).
14. M. C. Pedro, C. Milagros, O. Estibalitz, C. Elena, and A. P. José, *Surface and Interface Analysis,* **39**:26 (2007).
15. E. Barsoukov and J. R. MacDonald, *Impedance Spectroscopy. Theory, Experiment and Applications.,*Wiley, 2005.
16. A. C. Fisher, *Electrode Dynamics* Oxford Science Publications 1996.
17. G. W. H. Höhne, *Thermochimica Acta,* **330**:45 (1999).
18. B. G. Liptak, *Analytical Instrumentation,*Chilton Book Company, 1994.
19. C. Lucarelli, P. Villa, E. Lombaradi, P. Prandini, and A. Brega, *Chromatograph,* **33**:37 (1992).
20. K. Kondo, M. Nakamura, R. Nishioka, and S. Kawai, *Analytical Sciences,* **1**:385 (1985).
21. J. P. Moody and S. M. Allan, *Clinica Chimica Acta,* **127**:263 (1983).
22. H. H. Newman DJ, Price CP, *Ann. Clin. Biochem.* , **29**:22 (1992).

Chapter 3

Inclusion and Controlled Release of a Medium-Large Size Drug from Polypyrrole:

Dexamethasone 21-Phosphate Disodium Salt

3.1 Introduction

Corticosteroids are naturally produced by the adrenal gland in the body and have many important functions on every organ system. If the adrenal glands are not producing enough hormones, such as cortisol and aldosterone, treatment with replacement therapy is used to allow the body to function normally. Dexamethasone is used specifically to treat a disorder of the adrenal glands called congenital adrenal hyperplasia[1].

Dexamethasone is classified as a synthetic glucocorticosteroid and is used in several other treatments, including the reduction of inflammation in the central nervous system and in the treatment of cancer[2]. It is thought to act through the glucocorticosteroid receptors found in most neurons and glial cells throughout the brain[3]. These receptors' pathways are involved in the inhibition of astrocyte proliferation[4] and microglial activity[5]. Brand names of dexamethasone include Decadron®, Dexasone®, Diodex®, Hexadrol® and Maxidex®. The medication comes in several forms, including daily pills with a dose usually less than 10 mg[6]. It can also be given intravenously. Patients with leukaemia or lymphoma undergoing chemotherapy are often given dexamethasone eye drops to prevent many eye conditions and dexamethasone lotions to treat skin disorders.

With regards to the pharmacokinetics of dexamethasone, the half life, $t_{1/2}$, was found to be significantly different in males and females. Males demonstrated an average $t_{1/2}$ of 201.5 min while females had an average $t_{1/2}$ of 142.3 min[6, 7]. The prolonged $t_{1/2}$ in males however did not appear to affect the elimination of the drug as the total plasma clearance did not differ between males and females, with mean values of 247.5 ml min^{-1} and 242.9 ml min^{-1}, respectively. The difference in the body weight between the genders seems to be the contributing factor to the difference observed in $t_{1/2}$[6, 7].

Over the last 30 years, there has been keen interest in the development of a cochlear ear implant[8]. Cochlear implants provide auditory perception to profoundly deaf individuals with a sensorineural hearing loss by electronically stimulating ganglion neurons *via* an electrode array implanted into the scala

tympani of the coclea[9]. However, cochlear implantation itself can cause the loss of residual hair cells that may otherwise provide supplementary acoustic hearing and improved speech recognition after cochlear implantation, especially in the presence of background noise[10]. Consequently, the preservation of hearing in the implanted ear has become an objective of the implant surgery. Although several precautions are taken to minimise the intracochlear trauma during the insertion of the implant, residual hearing is lost or incompletely preserved in a third of cases[11, 12]. Several reports show that cochlear protection with steroids is achieved and is presumed to be due to the suppression of the inflammatory response initiated by cochlear implant surgery[13]. Steroids have also been used in treatments for other ear problems, such as Menière's disease[11, 14, 15]. Dexamethasone has been identified as one such steroid and studies show that the application of the drug to the round-window, prior to cochlear implant surgery, can protect hearing across the frequency range[11] as well as protect against noise-induced trauma in the guinea pig cochlea[15].

Systematic injections have the obvious disadvantage of exposing the whole body to high dosages of the drug and its potential toxicity[16]. Local drug delivery at the implant/tissue interface would be most effective. Various methods and materials are being investigated as a way to deliver this important drug to particular parts of the body, including poly(lactide)/poly(lactide-co-glycolide) (PLA/PLGA) biodegradable implants, chemical delivery systems and delivery *via* the transdermal by iontophoresis[14, 17-20].

There is a choice of different pro-drug forms of dexamethasone used for the treatments mentioned earlier in this section[21-25]. This study investigates the controlled release of dexamethasone 21-phosphate disodium salt (NaDex) which acts as a pro-drug and can be converted to the active dexamethasone within 40 min[25, 26]. It has a pKa of 6.4 and its chemical structure is shown in Figure 3.1. The presence of the phosphate group on the dexamethasone steroid ring structure imparts a negative charge to the drug (Dex^{2-}) making it suitable for incorporation as a dopant in polypyrrole (PPy)[27, 28].

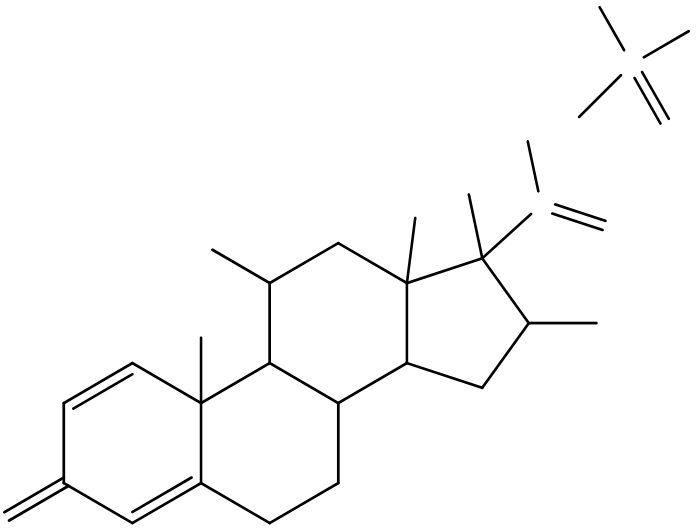

Figure 3.1: Dexamethasone disodium phosphate.

There have been some reports in the literature of the use of this pro-drug form of dexamethasone in controlled release studies. Wadhwa *et al.*[27] studied the controlled release of Dex^{2-} from PPy. The drug was incorporated into the polymer using a one-step electropolymerisation, while its release was carried out using cyclic voltammetry. In this work, very high potentials of 1.800 V relative to the counter electrode were used to deposit the PPy doped with Dex^{2-}. Moreover, the Dex^{2-} was released by cycling the polymer from –0.800 V vs SCE to 1.400 V vs SCE. These high potentials are likely to give rise to over-oxidation of PPy. Moulton *et al.*[28] also investigated the controlled release of Dex^{2-} from PPy using a novel approach of galvanically coupling the polymer to a magnesium (Mg) alloy *via* a salt bridge. An estimated 15 % of the drug was released after 5 h using this method.

Wallace and co-workers[29] reported the electrochemical release of therapeutic levels of Dex^{2-} from polyterthiophene film. Although the rate of release could be decreased dramatically by applying an oxidation potential, it was found that by applying a reduction potential the rate of drug release was not significantly increased when compared to an unstimulated film. A possible explanation for this is that polyterthiophene undergoes auto-reduction upon immersion in solution. This suggests that PPy is a more suitable polymer for this type of drug delivery system.

In this research and chapter, four successful methods of doping PPy with Dex^{2-} (PPyDex) and the optimum release conditions were developed. Investigations were also conducted into the possibility of reusing the polymer and exploiting the switch on/off capabilities of the PPy ion gate membrane. In all cases, the applied potentials were selected to avoid the over-oxidation of the PPy film.

3.2 Experimental

3.2.1 Materials

Dexamethasone 21-phosphate disodium salt (NaDex) was purchased from Sigma Aldrich and used as received. Pyrrole monomer (98%) was purchased from Aldrich and distilled prior to being used. All potentiostatic and cyclic voltammetry (CV) experiments were carried out on a Solartron (Model SI 1285) potentiostat. All Dex^{2-} release studies were measured using a Varian Cary Series UV-vis spectrophotometer. Electrochemical impedance spectroscopy (EIS), electrochemical quartz crystal microbalance (EQCM), differential scanning calorimetry (DSC) and scanning electron microscopy (SEM) were carried out using equipment described in Section 2.2.1.

3.2.2 Electrochemical experiments

An electrochemical cell was set up to include a platinum (Pt) electrode as the working electrode; a Pt wire as the auxiliary electrode and a standard calomel electrode (SCE) as the reference electrode. The PPyDex was electrosynthesised in four different ways using a combination of constant potential and CV in the presence of 0.05 mol dm^{-3} NaDex and 0.20 mol dm^{-3} pyrrole (Py). The pH of this electrolyte was approximately 8.2. The drug was released by applying a reduction potential in the presence of 120 ml of 0.10 mol dm^{-3} NaCl. During the release, all electrolytes were constantly stirred. As discussed in Chapter 2, Section 2.5.1, a calibration curve for NaDex was obtained using UV-vis spectroscopy and used to determine the amount of drug released. Dexamethasone has a λmax of 242 nm and UV-vis spectra recorded with different concentrations of NaDex can be seen in Figure 3.2. A typical calibration curve is shown in Chapter 2, Figure 2.10.

The drug and polymer were characterised using techniques that included CV, EQCM, EIS and SEM. All these techniques are described in Chapter 2 in Section 2.4.2.

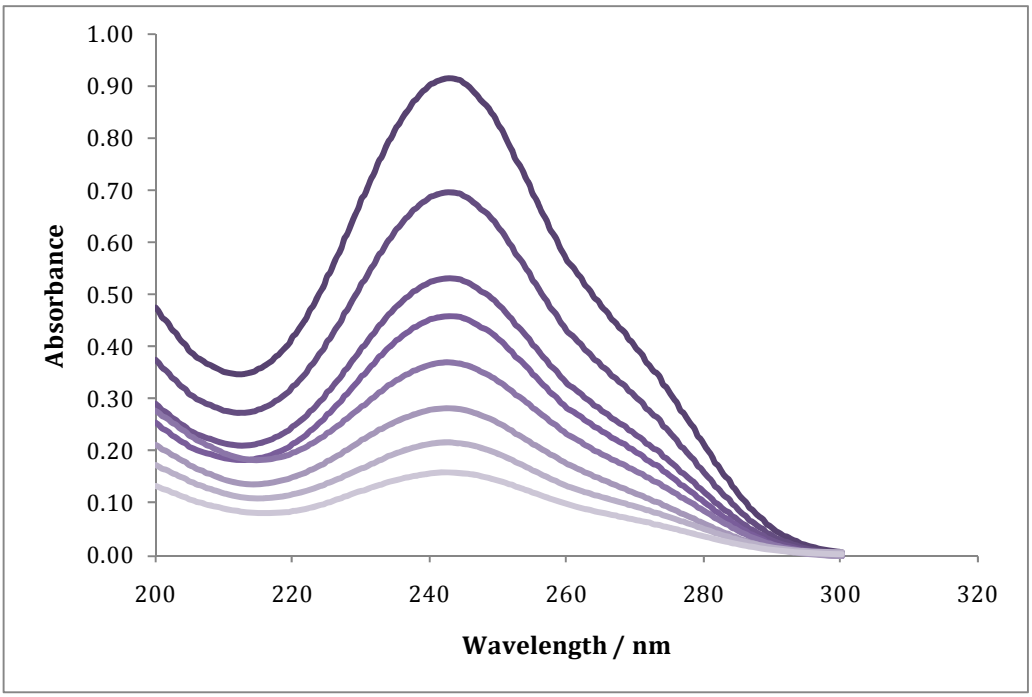

Figure 3.2: UV-vis spectra of NaDex with a concentration range of 7.04 x 10^{-6} to 1.02 x 10^{-4} mol dm^{-3} in water showing a λmax at 242 nm.

3.3 Results and discussion

3.3.1 Properties of Dex

Differential scanning calorimetry (DSC) was carried out on the dry NaDex powder and the resulting thermogram is shown in Figure 3.3. The sample was held at 50 °C for 5 min before it was heated to 300 °C at a rate of 10 °C min^{-1}. It is important to highlight that the experiment was performed under N_2 atmosphere to prevent oxidation phenomena. The first broad endothermic peak, from 50 to 100 °C, with a maximum around 85 °C, is due to loss of water from the sample. There is a sharp exothermic peak between 220 °C and 238 °C with a maximum at 232 °C. This corresponds to a recrystallisation process[30]. This is followed by an endothermic peak at 242 °C which is due to the melting of NaDex. The documented melting point for NaDex is 233-235 °C[31]. This is slightly lower than the value determined in

Figure 3.3. However, the large exothermic peak centred at 232 °C makes it difficult to accurately measure the melting point. The peaks recorded above 250 °C correspond to the decomposition of NaDex.

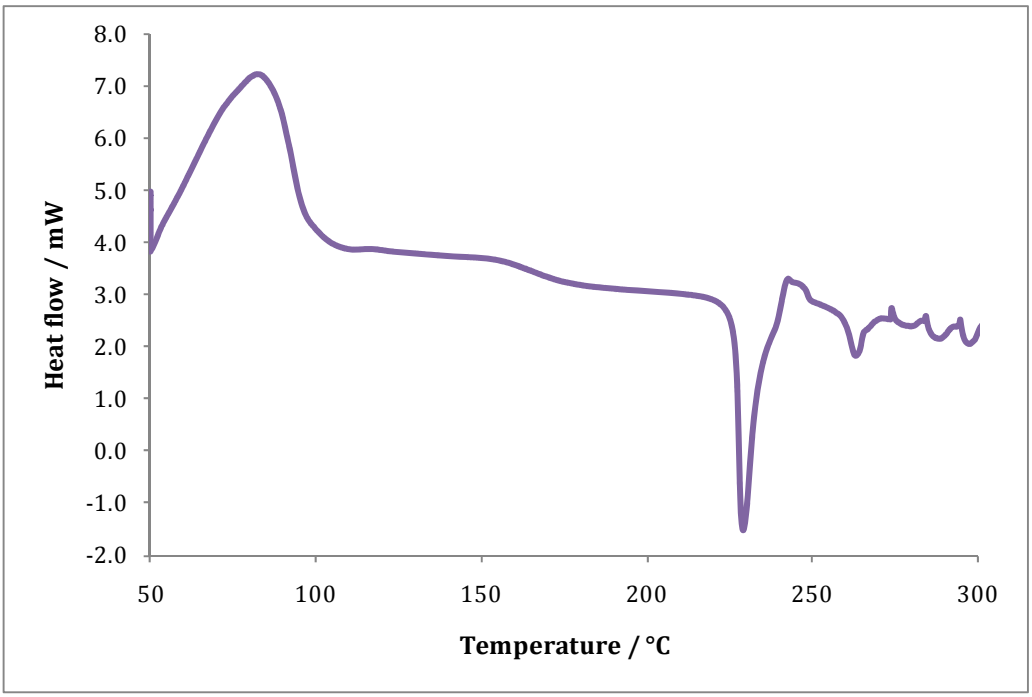

Figure 3.3: DSC thermogram of 3.20 mg sample of NaDex, isothermal pretreatment at 50 °C for 5 min. The temperature was scanned from 50 °C to 300 °C at a rate of 10 °C min^{-1}.

CV was used to gain information on the stability of NaDex towards oxidation and reduction as this has not been previously shown in the literature. The experiments were carried out on a bare Pt electrode by cycling between –1.200 V vs SCE and +0.700 V vs SCE at a scan rate of 25 mV s^{-1}, in 0.05 mol dm^{-3} NaDex. Typical cyclic voltammograms are shown in Figure 3.4. For comparison, a CV was carried out using the same parameters in the presence of 0.10 mol dm^{-3} NaCl. The pH of the NaCl electrolyte was adjusted to 8.5 using NaOH in order to have a similar pH to that of the NaDex electrolyte. Both cyclic voltammagrams display similar redox properties which are dominated by H^+ adsorption and $H_{2(g)}$ evolution from approximately –0.900 V vs SCE to –1.200 V vs SCE. This indicates the electrochemistry of the Pt is dominant and NaDex is a stable compound. The slight shift in the positions of the adsorption peaks and the rate of $H_{2(g)}$ evolution are due to variations in the nature of the electrolytes[32].

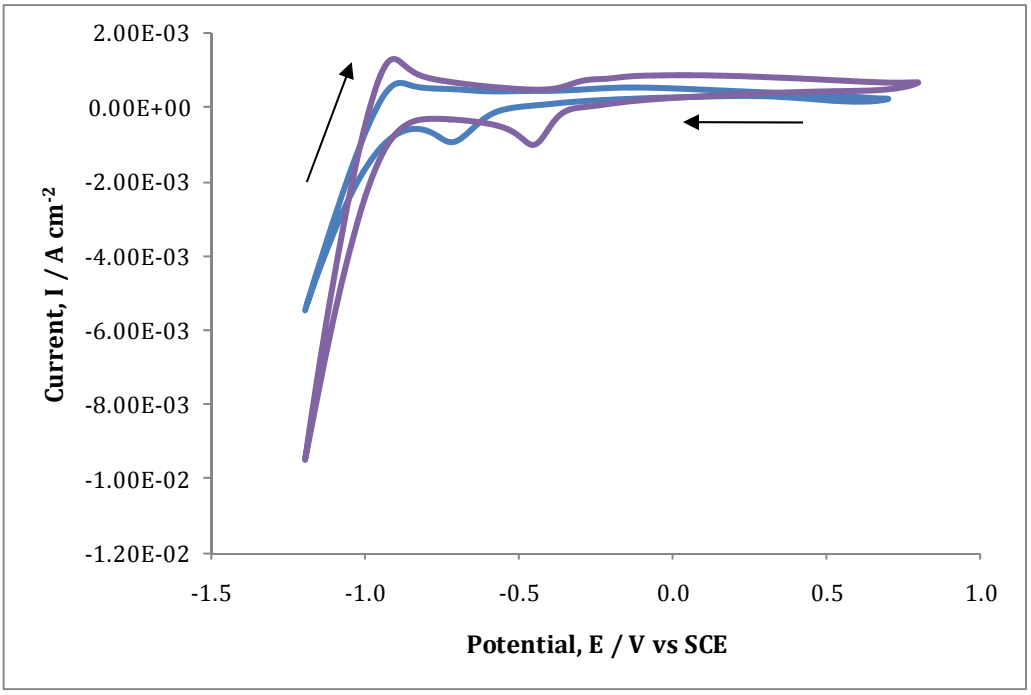

Figure 3.4: Cyclic voltammograms, 20th cycle, of bare Pt in — 0.05 mol dm^{-3} NaDex and — 0.10 mol dm^{-3} NaCl (pH = 8.5), carried out between –1.200 V vs SCE and +0.700 V vs SCE at 25 mV s^{-1}.

3.3.2 Electrosynthesis of the polymer

3.3.2.1 Constant potential

As stated in the experimental section of this chapter, the electrodeposition of the Dex^{2-} doped polypyrrole (PPyDex) was achieved in four different ways. The first and most straight-forward method was carried out by applying a constant potential. To investigate which potential yielded the best growth, various potentials were applied; +0.750 V vs SCE, +0.800 V vs SCE and +0.850 V vs SCE. The polymer failed to grow at these potentials and the potentiostatic plots of these attempts are shown in Figure 3.5. Although no polymer was visible on the surface of the electrode, the potentiostatic plots show an increase in the current within 10 s of the potential being applied, but this current increases slowly over the time frame of the experiment (1200 s). This indicates that some polymerisation occurs but not enough for significant deposition of the polymer to form on the electrode. The potential was then increased to +0.900 V vs SCE and the polymer grew rapidly in the same time period. The potentiostatic current-time plot can be seen in Figure 3.6.

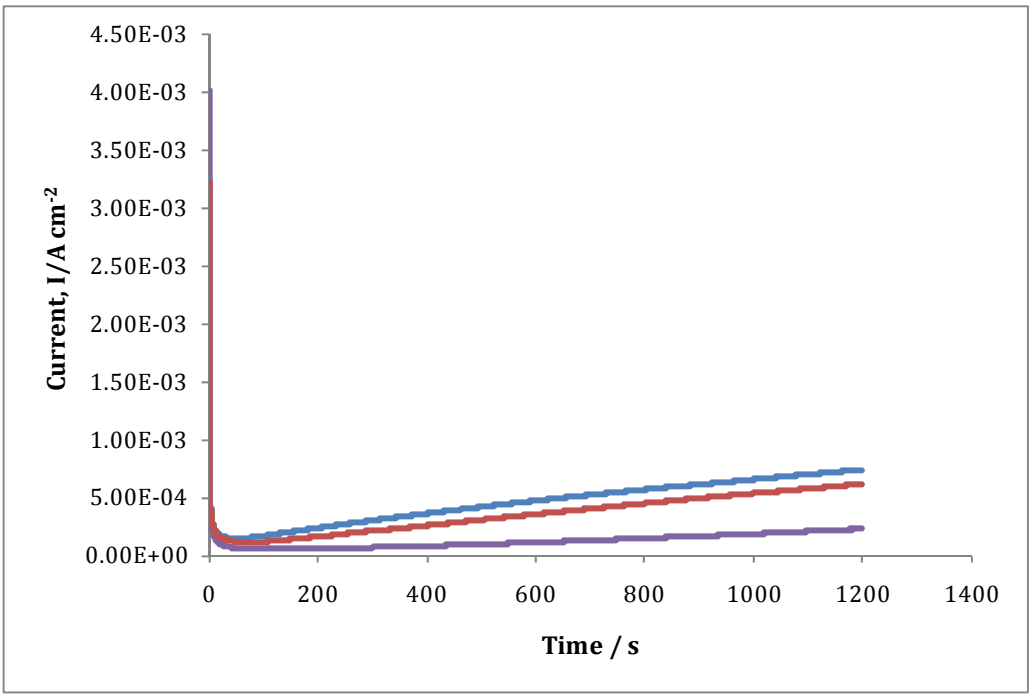

Figure 3.5: Potentiostatic current-time plots for the attempted growth of PPyDex at applied potentials of +0.850 V vs SCE, +0.800 V vs SCE and +0.750 V vs SCE from a solution of 0.05 mol dm^{-3} NaDex and 0.20 mol dm^{-3} Py.

In contrast to the plots seen in Figure 3.5, there is a rapid increase in the current when the potential is increased to +0.900 V vs SCE and within 200 s the current plateaus suggesting that a constant rate of growth is achieved. Not only did the polymer grow at a fast rate but the amount of polymer that was deposited varied from experiment to experiment which meant that growing to a set time was not a viable way to achieve reproducible electrosynthesis of the polymer. It is also apparent from the potentiostatic plots in both Figure 3.5 and Figure 3.6 that the initial growth of the polymer requires the application of a high potential but once this initial growth is achieved the polymer can grow quite easily. From this, the second method of growth was developed.

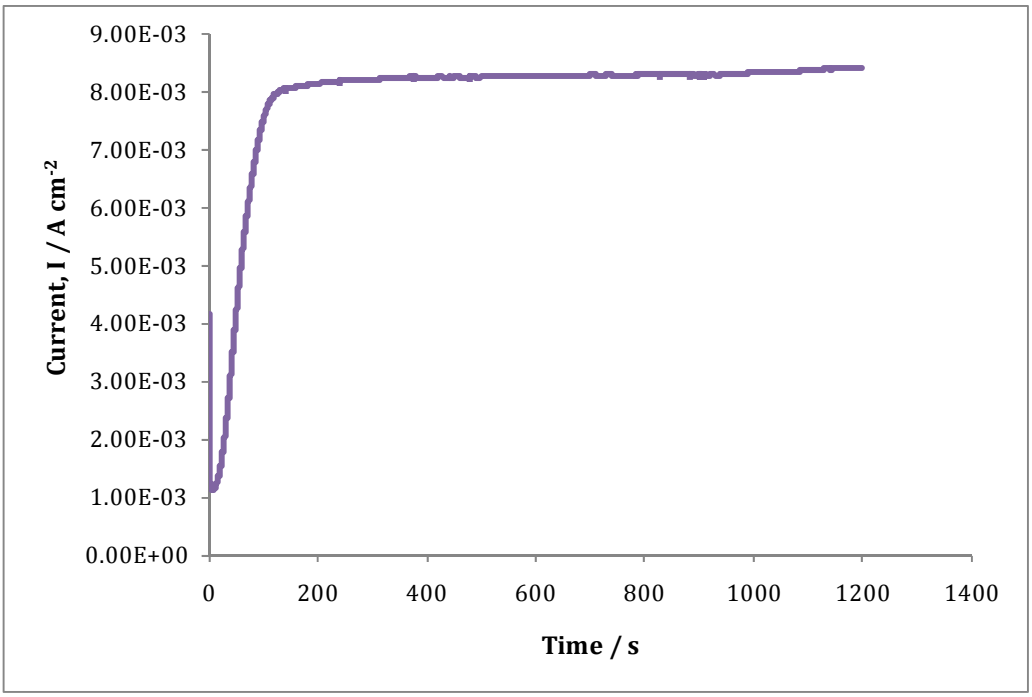

Figure 3.6: Potentiostatic current-time plot recorded for the deposition of PPyDex at +0.900 V vs SCE in an electrolyte of 0.05 mol dm^{-3} NaDex and 0.20 mol dm^{-3} Py.

3.3.2.2 Two step - constant potential

The second method of growth involved the application of two different potentials. A potential of +0.900 V vs SCE was applied until a charge of 0.8 C cm^{-2} was reached. This meant that there was sufficient polymer on the surface of the electrode to allow further growth to occur at a potential of +0.800 V vs SCE, until a charge of 2.0 C cm^{-2} was reached. Therefore, the total charge of the polymer was 2.8 C cm^{-2}. The potentiostatic plots corresponding to these two steps are shown in Figure 3.7A, with current as a function of time, and in Figure 3.7B, with charge as a function of time. From these plots, it is clear that at the higher potential the polymer grows slowly at first on the bare Pt electrode. The current and charge remain low for the first 30 s, but then there is a significant increase in the rate of polymer growth, giving an exponential like growth profile. Once the lower potential is applied the polymer grows in a more controlled manner and the relationship between charge and time is linear.

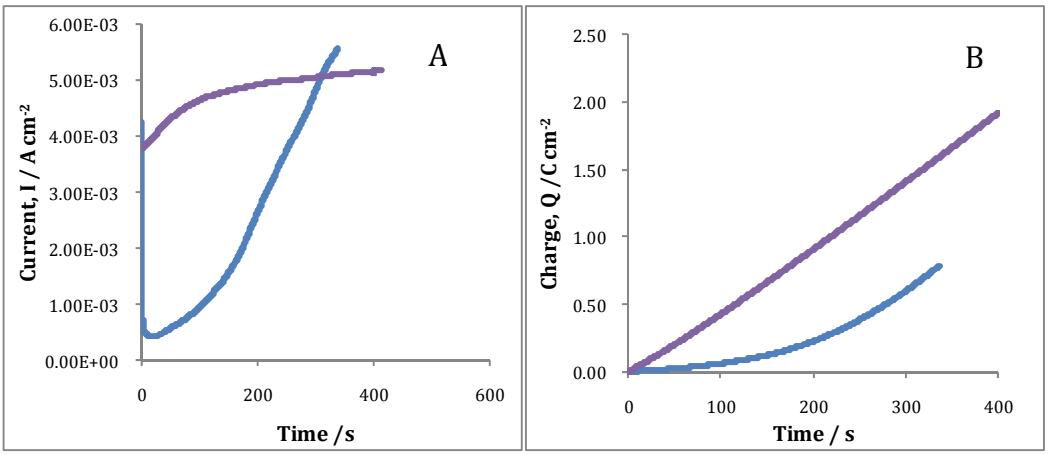

Figure 3.7: Potentiostatic plots for the electrodeposition of PPyDex in two steps; — first at a constant potential of +0.900 V vs SCE until a charge of 0.8 C cm^{-2} had passed and — secondly at +0.800 V vs SCE until a charge of 2.0 C cm^{-2} was consumed in the presence of 0.05 mol dm^{-3} NaDex and 0.20 mol dm^{-3} Py. Plot **A** shows current as a function of time while plot **B** shows charge as a function of time.

The polymer films were grown in this manner several times throughout the course of this study and Figure 3.8 shows five examples of the potentiostatic plots recorded. Although the plots do not overlap as expected for good reproducibility, they have relatively the same shape and take a similar length of time to reach the same charge. By plotting the charge-time plots of these polymers, Figure 3.9, the slope and subsequently the rate at which the polymers grow can be compared. For the initial step of the polymerisation at +0.900 V vs SCE, the slope was calculated from 200 s to finish and varied from 2.43 x 10^{-3} C cm^{-2} s^{-1} to 4.13 x 10^{-3} C cm^{-2} s^{-1}. For the second step of the growth, at +0.800 V vs SCE, the slopes ranged from 3.3 x 10^{-3} C cm^{-2} s^{-1} to 4.8 x 10^{-3} C cm^{-2} s^{-1}. These slope values suggest that once the first layer of PPyDex is deposited, the subsequent rate of electropolymerisation is similar at both +0.800 V vs SCE and +0.900 V vs SCE. In summary, the data show that the polymer grows in a similar manner each time and comparing release studies from one polymer with another is acceptable. This method was a very proficient way of growing the PPyDex and a variation of this method was further investigated.

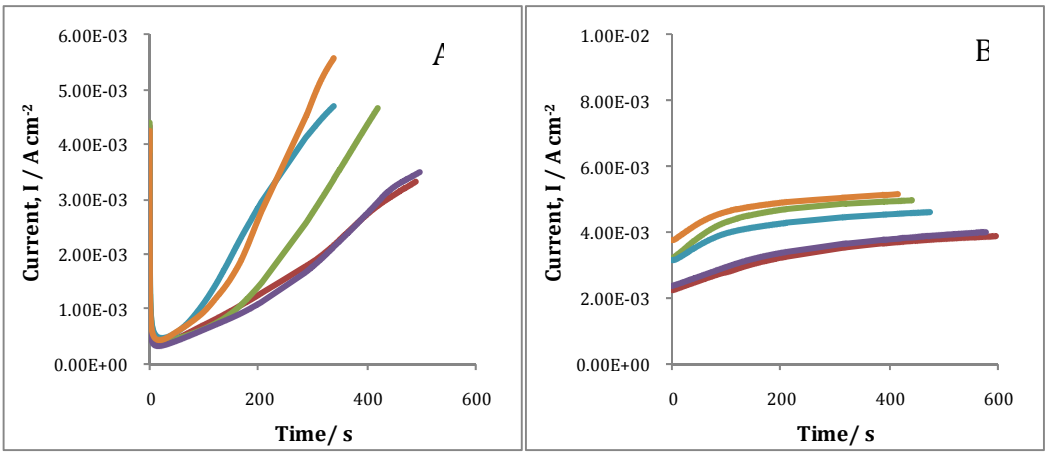

Figure 3.8: Representative potentiostatic plots recorded on different occasions for the electrodeposition of PPyDex in two steps; in **A** a constant potential of +0.900 V vs SCE was applied until a charge of 0.8 C cm^{-2} was consumed and in **B** a potential of +0.800 V vs SCE was applied until a charge of 2.0 C cm^{-2} was passed in the presence of 0.05 mol dm^{-3} NaDex and 0.20 mol dm^{-3} Py.

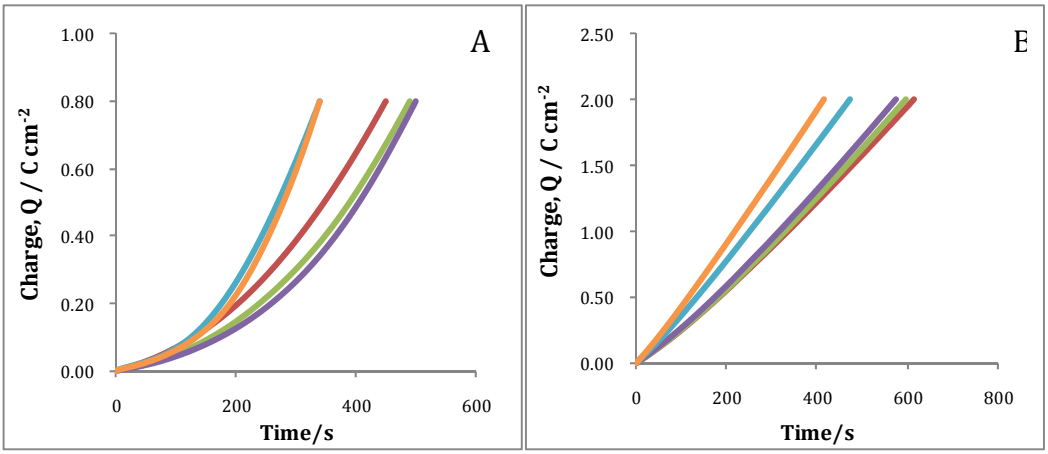

Figure 3.9: Representative charge-time plots recorded on different occasions during the electrodeposition of PPyDex in two steps from a solution of 0.05 mol dm^{-3} NaDex and 0.20 mol dm^{-3} Py; **A** at a constant potential of +0.900 V vs SCE until a charge of 0.8 C cm^{-2} was passed and **B** at a constant potential of +0.800 V vs SCE until a charge of 2.0 C cm^{-2} was reached.

3.3.2.3 Two step - cyclic voltammetry and constant potential

CV was then explored as a means of electrodepositing the polymer. However, as expected the polymer failed to grow as it was difficult to instigate the initial growth on the electrode. This was believed to be simply due to the fact that the potential was being swept over a potential window and not being held at an oxidation

potential that would promote polymer growth. A third method was then developed based on the promising results presented in Section 3.3.2.2. The PPyDex was grown as before to a charge of 0.8 C cm^{-2} at +0.900 V vs SCE and the CV was employed to electrodeposit more polymer. Figure 3.10 shows the corresponding cyclic voltammograms. The currents reached in these cyclic voltammograms were quite low regardless of the upper potential limit, indicating little or no further polymer growth.

However, successful growth was achieved when a thick polymer, grown to a charge of 1.2 C cm^{-2}, was deposited onto the electrode prior to the CV experiment. The potential was scanned between –0.100 V vs SCE and +0.800 V vs SCE at a scan rate of 50 mV s^{-1}. A typical plot showing different cycles is presented in Figure 3.11. It can be seen that oxidation of the Py occurs at +0.600 V vs SCE and although the currents decrease with repeated cycling, they indicate further polymer growth.

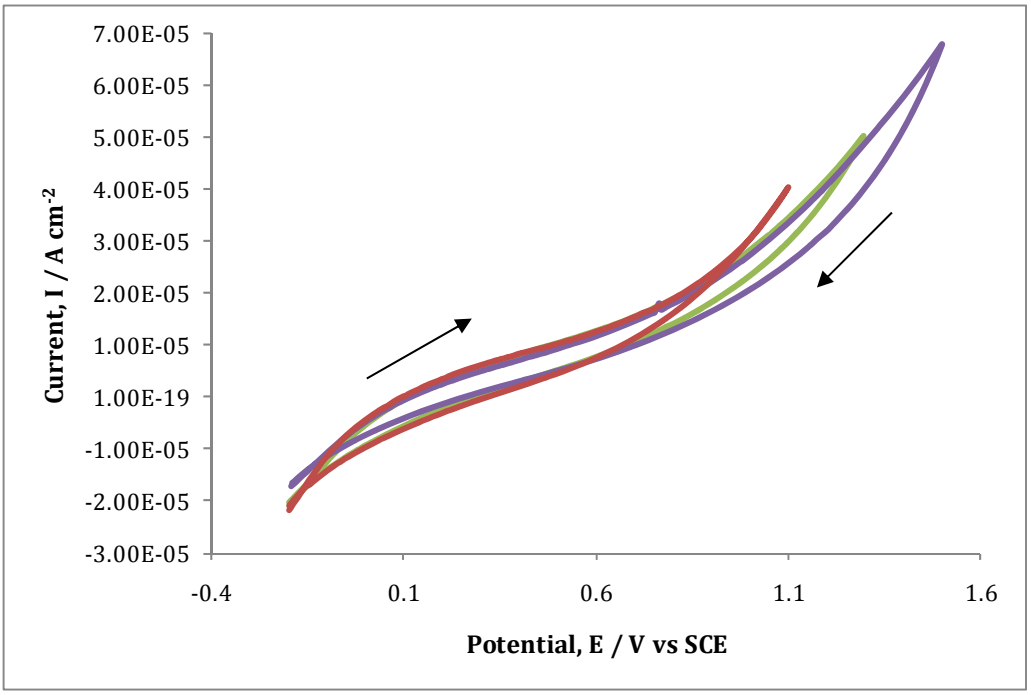

Figure 3.10: Cyclic voltammograms, 20th cycle, for the unsuccessful growth of PPyDex from a solution of 0.05 mol dm^{-3} NaDex and 0.20 mol dm^{-3} Py at various potential windows, swept between –0.200 V vs SCE and — 1.00 V vs SCE, — 1.300 V vs SCE and — 1.500 V vs SCE at 50 mV s^{-1}. The Pt electrode was already coated with PPyDex that was grown potentiostatically at +0.900 V vs SCE to a charge of 0.8 C cm^{-2}.

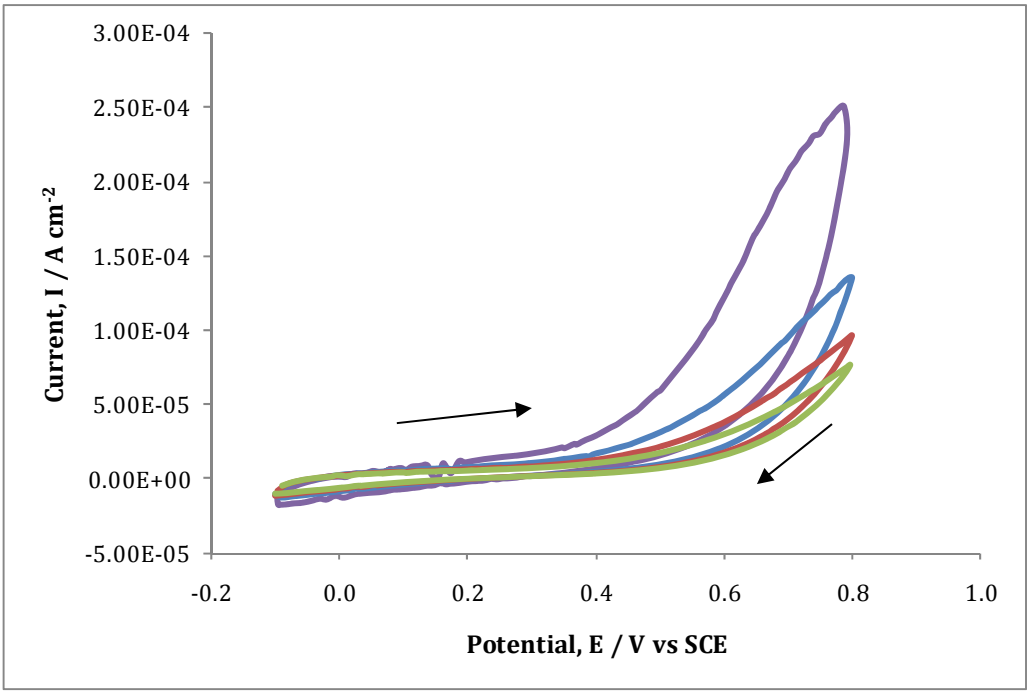

Figure 3.11: Cyclic voltammograms recorded between –0.100 V and +0.800 V vs SCE at 50 mV s^{-1} in 0.05 mol dm^{-3} NaDex and 0.20 mol dm^{-3} Py; — cycle 5, — cycle 10, — cycle 15 and — cycle 20. The Pt electrode was already coated with PPyDex that was grown potentiostatically to a charge of 1.2 C cm^{-2}.

3.3.2.4 Two step - PPyCl film and constant potential

The fourth and final method of growing the polymer was another variation of the two-step growth. A thin film of PPy doped with a chloride anion (PPyCl) was deposited onto the electrode surface and PPyDex was grown on top of this using a potentiostatic mode of polymerisation. The PPyCl easily grew at +0.600 V vs SCE until a charge of 0.16 C cm^{-2} had been reached. This is the minimum amount of PPyCl required to enable the deposition of PPyDex. The PPyDex was then grown at +0.800 V vs SCE until the total charge of the polymer was 2.8 C cm^{-2}. This arrangement meant that there was less Dex^{2-} in this polymer than in the previous polymers grown. The potential at which the PPyDex was grown was also investigated at +0.700 V vs SCE, however better release profiles were seen when the polymer was grown at +0.800 V vs SCE.

Figure 3.12 shows the potentiostatic current-time plots and corresponding charge-time plots of the growth of PPyDex at +0.700 vs SCE and +0.800 V vs SCE on a film of PPyCl grown to a charge of 0.16 C cm^{-2}. At the lower potential of +0.700 V vs

SCE, the currents begin to plateau after 500 s. However, at +0.800 V vs SCE the current increases throughout all the electropolymerisation period.

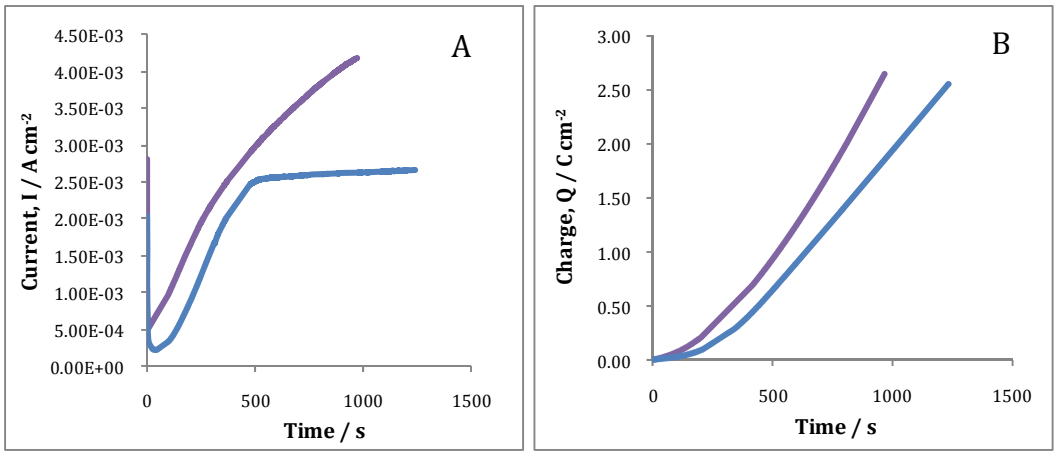

Figure 3.12: A Potentiostatic current-time plots and **B** Charge-time plots recorded during the formation of PPyDex on a film of PPyCl, which was grown to a charge of 0.16 C cm^{-2}, from a solution of 0.05 mol dm^{-3} NaDex and 0.20 mol dm^{-3} Py, at — +0.800 V vs SCE and — +0.700 V vs SCE until the total charge of 2.8 C cm^{-2} was reached.

Comparing these plots to the potentiostatic plots seen in Figure 3.5, it is clear that the rate of PPyDex deposition is increased by the presence of the thin layer of PPyCl. This reiterates the point that the initial growth of the polymer requires the application of high potentials but once a layer of polymer is deposited at the surface of the electrode, be it PPyCl or PPyDex, further electropolymerisation occurs at lower potentials. However, using a PPyCl layer will decrease the amount of Dex^{2-} available for release.

3.3.3 Characterisation of the PPyDex film

3.3.3.1 Redox properties of the polymer determined by CV

CV is a technique widely used for the characterisation of the electroactivity of conducting polymers. Redox properties of PPy films are associated with the exchange of ions, be it anionic, cationic or both. These exchange properties are significantly dependent on the dopant used during polymerisation[38-40]. There is a general agreement in the literature that in the presence of large anionic dopants, which remain immobilised in the polymer films, small cations from the electrolyte

enter it to maintain electroneutrality, but if dopants are medium-large in size, there is mixed ion transport across the polymer with exiting anion and entering cations[41]. Wadhwa *et al.*[27] utilised CV as a method to control the release of Dex^{2-} from PPy in a two-electrode cell. They measured the oxidation and reduction peaks of PPyDex at +0.490 V and –0.340 V, respectively, in the presence of 0.10 mol dm^{-3} PBS scanning between –0.800 V and +1.400 V at a scan rate of 100 mV s^{-1}. These peaks correspond to that of anion insertion and anion ejection[27].

In this work, CV experiments were carried out in the presence of 0.10 mol dm^{-3} NaCl. The pH of the NaCl electrolyte was adjusted to 3.0 as CV carried out at lower pH values tend to display more distinct peaks which have a higher current amplitude than those at higher pH values[42]. The potential was swept between –1.200 V vs SCE and +0.700 V vs SCE at 25 mV s^{-1} so that the redox properties could be monitored over a wide potential window. At high scan rates, hysteresis can occur due to limitations in the charge transfer[43]. By scanning at a lower scan rate, hysteresis is less likely to occur as there is more time available for electrolysis particularly if the rate of diffusion is slow[44] and this allows for more sensitive changes in current as it is swept across the potential window.

PPyDex was prepared in one step by applying +0.900 V vs SCE until a polymer of 2.0 C cm^{-2} was deposited and it was then cycled in 0.10 mol dm^{-3} NaCl. Figure 3.13 shows the resulting voltammograms. The first oxidation and reduction peaks occur at +0.250 V vs SCE and –0.600 V vs SCE, respectively. The second oxidation peak manifests at –0.500 V vs SCE at cycle 6 and becomes more evident with increasing cycle number. The presence of a distinct second reduction peak is also clear from the first cycle but with increasing cycle number this peak broadens and is no longer apparent by cycle 12. The four distinct peaks seen in these voltammograms are labelled A, B, C and D. These correspond to four ion exchange processes. They are cation ejection, anion insertion, anion ejection and cation insertion and are represented in Equations 3.1, 3.2, 3.3 and 3.4, respectively[38, 45]. Although these equations are not balanced, they demonstrate how the charged ions move across the polymer membrane.

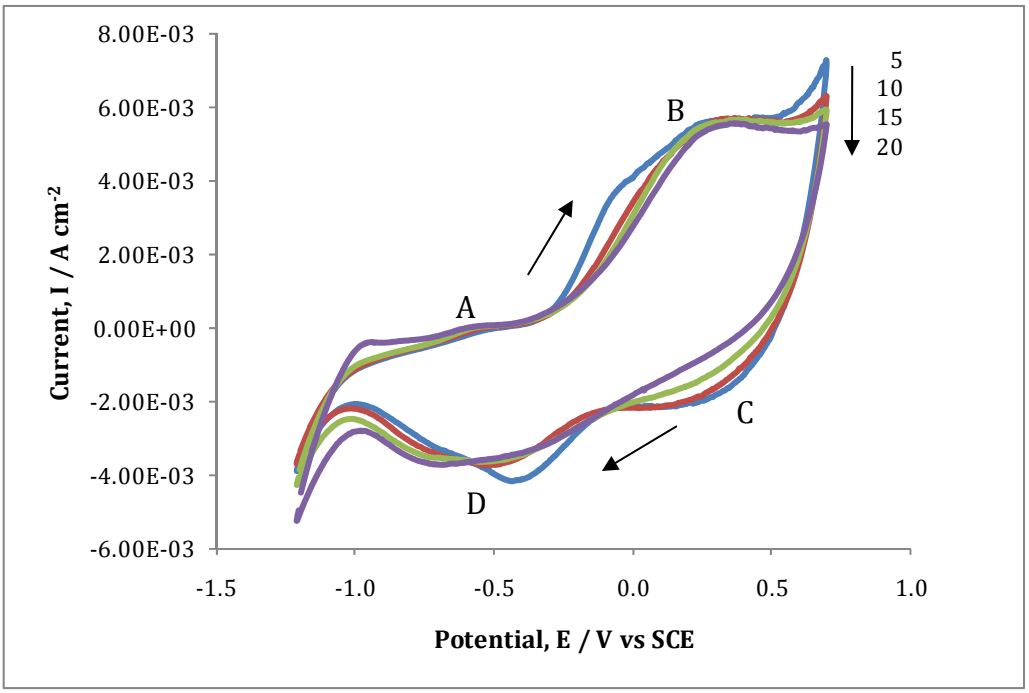

Figure 3.13: Cyclic voltammograms recorded for PPyDex in 0.10 mol dm^{-3} NaCl, pH 3.0, between –1.200 V vs SCE and +0.700 V vs SCE at 25 mV s^{-1} at — cycle 5, — cycle 10, — cycle 15 and — cycle 20. The peaks, labelled A, B, C and D, correspond to cation ejection, anion insertion, anion ejection and cation insertion, respectively. PPyDex was deposited at +0.900 V vs SCE from a solution of 0.05 mol dm^{-3} NaDex and 0.20 mol dm^{-3} Py until 2.0 C cm^{-2} of charge was consumed.

A: $PPy_n^0 Dex^{2-} 2Na^+ - e^- \rightarrow PPy_n^0 PPy_n^+ Dex^{2-} + 2Na^+$ 3.1

B: $PPy_n^0 PPy_n^+ Dex^{2-} + Cl^- - e^- \rightarrow PPy_n^+ Dex^{2-} Cl^-$ 3.2

C: $PPy_n^+ Dex^{2-} Cl^- + e^- \rightarrow PPy_n^0 PPy_n^+ Dex^{2-} + Cl^- + Dex^{2-}$ 3.3

D: $PPy_n^0 PPy_n^+ Dex^{2-} + 2Na^+ + e^- \rightarrow PPy_n^0 Dex^{2-} 2Na^+ + Dex^{2-}$ 3.4

The shape of the voltammograms seen in Figure 3.13 indicates that Dex^{2-} behaves like a medium-large size anion even though it is much larger in size than other dopants, such as para-toluene sulfonate (pTS^-), which display this mixed ion exchange. To fully comprehend the electrochemical properties of the polymer, further CV experiments were carried out under the same conditions as before but

at several scan rates; 50, 75, 100, 125 and 150 mV s^{-1}. The resulting cyclic voltammograms are shown in Figure 3.14.

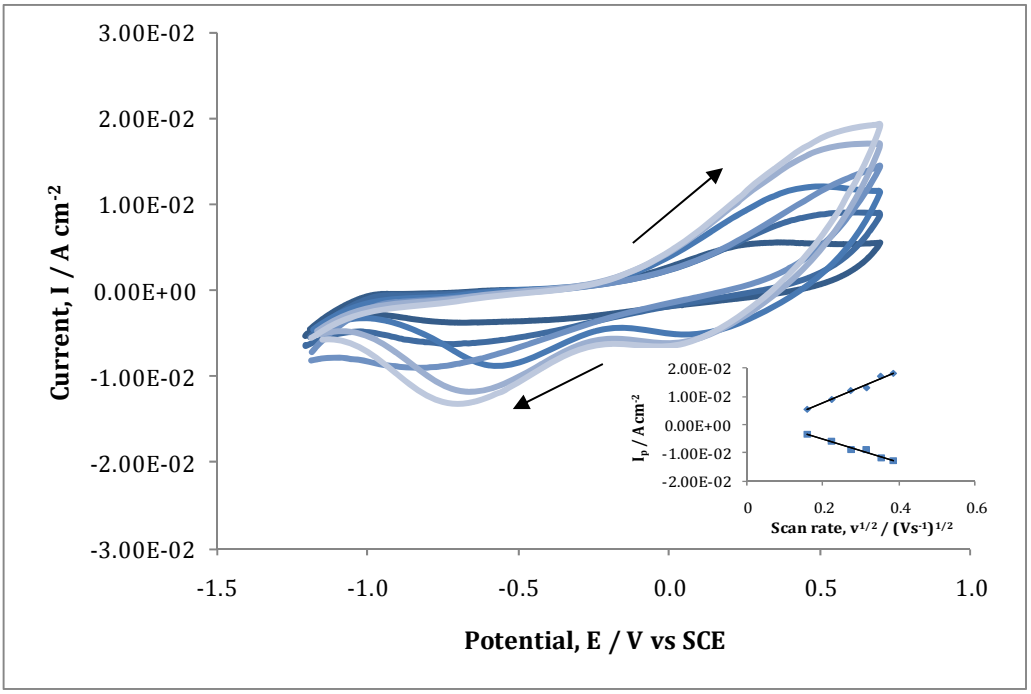

Figure 3.14: Cyclic voltammograms, 20th cycle, recorded in the presence of 0.10 mol dm^{-3} NaCl (pH 3.0) at 25, 50, 75, 100, 125 and 150 mV s^{-1} on PPyDex formed at +0.900 V vs SCE to 2.0 C cm^{-2} in 0.05 mol dm^{-3} NaDex and 0.20 mol dm^{-3} Py. Potentials were swept between –1.200 V vs SCE and +0.700 V vs SCE. Inset shows the peak current of the oxidation and reduction peaks plotted as a function of the square root of scan rate.

From Figure 3.14, it is seen that at the higher scan rates the oxidation peak is broad and no longer as well defined as it was at the lower scan rates. There is no evidence of the peak corresponding to cation ejection (peak A) that was seen at 25 mV s^{-1} (Figure 3.13). However, the two peaks corresponding to anion ejection and cation insertion are still present. It is apparent from both Figure 3.13 and Figure 3.14, that the reduction processes are faster than the oxidation process. The inset in Figure 3.14 plots the peak current of the oxidation (peak B) and reduction (peak D) peaks, i_p, as a function of the square root of the scan rate, $v^{1/2}$. R^2 values of 0.98 and 0.97 were achieved for the oxidation and reduction peak currents, respectively, indicating a linear relationship.

Cyclic voltammograms were also recorded on PPy doped with Cl^- which was formed in the presence of 0.10 mol dm^{-3} NaCl and 0.20 mol dm^{-3} Py until a charge of 2.0 C cm^{-2} was consumed, Figure 3.15. The polymer exhibits only one oxidation and reduction peak corresponding to anion insertion and anion ejection. Since the Cl^- is a smaller and more mobile dopant than Dex^{2-}, the polymer mainly exhibits anionic exchange properties[45]. The reduction peak at 100 mV s^{-1} is very similar to the peak seen at 125 mV s^{-1} which could be due to slight hysteresis. As observed with PPyDex there is again a linear relationship between the oxidation and reduction peak currents and the square root of the scan rate, as evident in the inset of Figure 3.15. R^2 values of 0.98 and 0.97 were calculated for the oxidation and reduction peak currents, respectively.

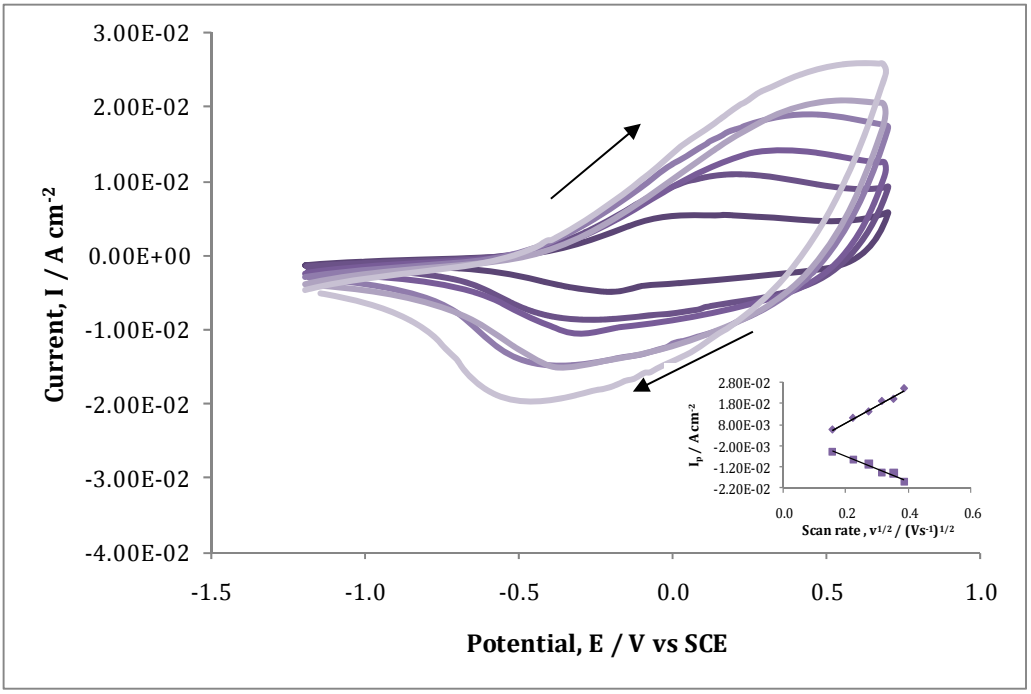

Figure 3.15: Cyclic voltammograms, 20th cycle, recorded in the presence of 0.10 mol dm^{-3} NaCl (pH 3.0) at 25, 50, 75, 100, 125 and 150 mV s^{-1} on PPyCl formed at +0.800 V vs SCE to 2.0 C cm^{-2} in 0.10 mol dm^{-3} NaCl and 0.20 mol dm^{-3} Py. Potentials were swept between –1.200 V vs SCE and +0.700 V vs SCE. Inset shows the peak current plotted as a function of the square root of scan rate.

Interestingly, the linear relationship between the peak currents and the square root of the scan rate suggests that the oxidation and the reduction processes follow the Randles-Sevcik equation, Equation 3.5[46]. The slopes of the linear plots were

determined and used to estimate the apparent diffusivity of the electrolyte species in the polymer film.

$$i_p = (0.4463)nFAC^*_0\left(\frac{nFvD}{RT}\right)^{0.5} \quad 3.5$$

In this equation, n=number of electrons, F= Faraday's constant, A = electrode area (cm^2), C^*_0 = bulk concentration of the electrolyte (mole cm^{-3}), v = scan rate (V s^{-1}) and D = apparent diffusivity of the electrolyte in the polymer film (cm^2 s^{-1}), with the assumption that the charge-compensation step is rate-limiting. Equation 3.5 can also be written in a more concise form, Equation 3.6[47-49].

$$i_p = (2.69 \times 10^5)\, n^{\frac{3}{2}} A D^{\frac{1}{2}} C v^{\frac{1}{2}} \quad 3.6$$

Martin *et al.*[46] applied the Randles-Sevcik equation in the characterisation of poly(TP-OEG-sulfonate) and poly(DMPT). The calculated D for the poly(DMTP) ranged from 10^{-9} cm^2 s^{-1} to 10^{-4} cm^2 s^{-1} in the oxidised state and from 10^{-10} cm^2 s^{-1} to 10^{-4} cm^2 s^{-1} in the reduced state. Using Equation 3.6 and taking n=2.3 with C^*_0=0.10, the diffusivity for PPyDex and PPyCl in the oxidised state ranged from 1.08 x 10^{-9} to 2.36 x 10^{-9} cm^2 s^{-1} and in the reduced state, D values ranged from 5.80 x 10^{-10} and 1.25 x 10^{-9} cm^2 s^{-1}.

Although the Randles-Sevcik equation has previously been used to determine diffusion coefficients of the electrolyte species in conducting polymer films[47, 48], this analysis has several shortcomings. Firstly, the Randles-Sevcik equation is valid for reversible electrochemical systems, displaying sharp redox peaks and peak-to-peak separations close to the ideal value of 59 mV. The peak-to-peak separations for PPyDex vary from 800 to 1000 mV as the scan rate increases from 25 to 150 mV s^{-1}. In the case of PPyCl, the peak-to-peak separations range from 300 to 800 mV. Clearly these are not reversible processes. Another complication in applying the Randles-Sevcik equation to conducting polymers is that two different diffusion processes are involved; diffusion of species within the electrolyte to the

electrode surface and solid-state diffusion within the polymer film. Diffusion coefficients are typically 1 x 10^{-5} cm^2 s^{-1} for diffusion within the electrolyte solutions, but are much lower for solid-state diffusion[50], typically 10^{-8} to 10^{-10} cm^2 s^{-1}. The values computed in this work for PPyDex and PPyCl suggest that solid state diffusion occurs in these systems. However as stated earlier, the experimental conditions are far removed from the ideal conditions on which the classical Randles-Sevcik equation is based.

3.3.3.2 The redox properties of the polymer determined by EQCM

EQCM measurements is one of the most common techniques employed to follow the charging and discharging reactions that take place in conducting polymer films[44, 51]. The Sauerbrey equation relates the mass change, ΔM, expressed in g, to the resonant frequency shift of the crystal, Δf, expressed in Hz, Equation 3.7[52].

$$\Delta f = -\frac{2f_0^2 \Delta M}{A\sqrt{\rho\mu}} \qquad 3.7$$

Here f_0 is the resonant frequency of the unloaded crystal; A is the surface area of the electrode (0.203 cm^2), ρ is the density of the quartz (2.648 g cm^{-3}) and μ is the shear modulus of the quartz, (2.947 x 10^{11} g cm^{-1} s^{-2}).

This equation is only valid under certain conditions[53]; the polymer film must behave as a rigid and perfectly elastic layer. The rigid film approximation is valid if the polymer thickness is small compared to the thickness of the crystal and if the overall mass loading results in a change in frequency that is small with respect to the resonant frequency of the unloaded crystal. Accordingly the analysis was confined to thin PPyDex films. It is also important to note that the equation to calculate theoretical mass assumes the current efficiency for the electropolymerisation of pyrrole is 100% and that no water is incorporated into the film[54].

CV and EQCM were employed as a tool to monitor both the current and the change in mass during the switching of the polymer. In these studies, the PPyDex was grown in one step to a charge of 3.5 x 10^{-2} C (0.16 C cm^{-2}) by applying a constant potential of +0.900 V vs Ag|AgCl. Figure 3.16 shows the first cycle for both the cyclic voltammogram recorded at 4.0 mV s^{-1} and the corresponding mass change involved during the cycling in 0.10 mol dm^{-3} NaCl. The current and the mass change were recorded simultaneously while the polymer was swept from +0.800 V vs Ag|AgCl to a reduction potential of –1.000 V vs Ag|AgCl. The redox peaks seen in Figure 3.16 have shifted, by approximately +0.200 V, from those recorded in the voltammogram of the bulk polymer, illustrated in Figure 3.13. This is due to the decrease in scan rate[44] from 25 mV s^{-1} to 4.0 mV s^{-1}. In addition, this PPyDex film is considerably thinner, deposited to a charge of 0.16 C cm^{-2} compared to 2.0 C cm^{-2}, Figure 3.13. Accordingly, the redox peaks have lower current densities.

It is evident from the mass data that during the reduction scan an increase in mass occurs, corresponding to the insertion of cations. This mass increase is observed to begin at approximately +0.000 V vs Ag|AgCl and continues to increase, reaching a maximum value at –0.400 V vs Ag|AgCl, close to the potentials at which the reduction peak is observed in the voltammogram. On the reverse cycle, the mass decreases corresponding to the ejection of the cations. Presuming the mass change is predominantly due to the uptake of cations, the mass increase is equivalent to ~ 3.04 x 10^{-8} mol of Na^{+}. On closer inspection of Figure 3.16, it can be seen that the rate of the mass increase (forward cycle) is higher than the rate of the mass loss (reverse cycle), again highlighting the fact that the reduction process is faster than the oxidation process. It is also noticeable from Figure 3.16 that a small mass increase occurs between +0.200 V vs Ag|AgCl and +0.800 V vs Ag|AgCl on the reverse scan. This is probably related to the uptake of Cl^{-} anions from the supporting electrolyte.

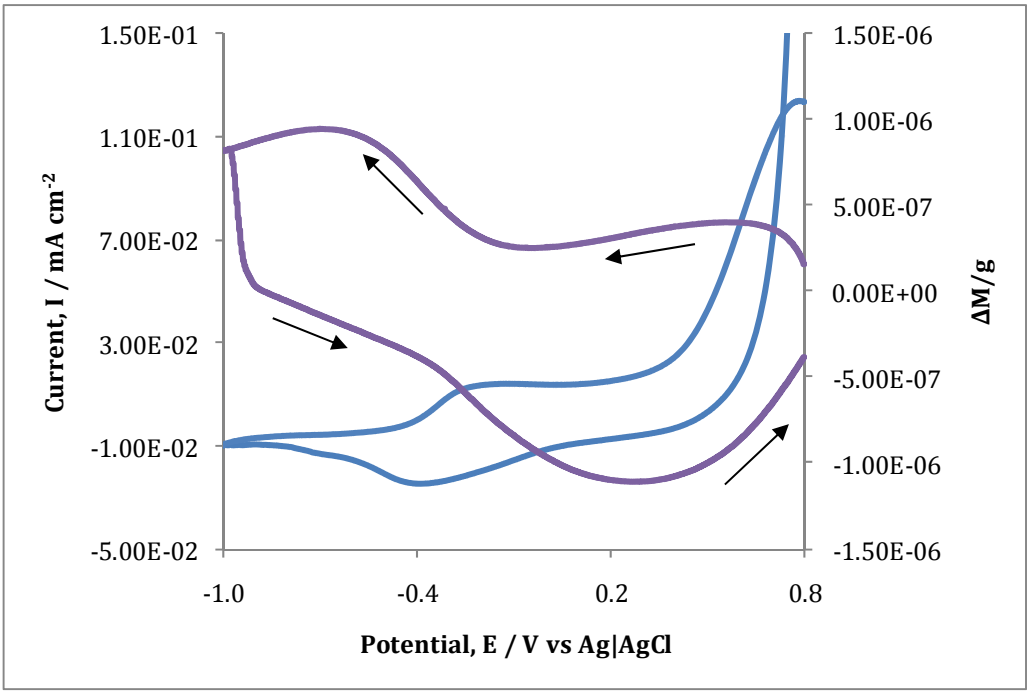

Figure 3.16: Current (—) and the mass change (—) plotted as a function of applied potential obtained for a PPyDex film, deposited to a charge of 3.2 x 10^{-2} C at a constant potential of +0.900 V vs Ag|AgCl. The potential was swept from +0.800 V vs Ag|AgCl to –1.000 vs Ag|AgCl at a scan rate of 4.0 mV s^{-1} in 0.10 mol dm^{-3} NaCl.

3.3.3.3 Mass and doping levels of the polymer

Additional EQCM measurements were performed and analysed to obtain information on the mass of the deposited polymer film and the doping level. In these studies, the PPyDex was grown to a charge of 3.5 x 10^{-2} C by applying a constant potential of +0.900 V vs Ag|AgCl. Figure 3.17 shows the frequency-charge and mass-charge plots for two polymers grown under the same conditions. As shown in the Saurbrey equation, Equation 3.7, a decrease in frequency is related to an increase in mass. It can be seen that the mass increases sharply once the charge of the polymer reaches values between 1.5 x 10^{-2} C and 2.0 x 10^{-2} C. The mass-to-charge ratio measured once these charges are reached is approximately 1.2 x 10^{-3} g C^{-1} for both polymers. It is again clear from these plots that the initial growth of the polymer is a slow step but once the electrode surface is covered with a thin polymer layer, the rate at which polymerisation occurs and the PPyDex is deposited increases.

The data also indicate that while charge is consumed during the very early stages of electropolymerisation, it does not lead to the deposition of the polymer. The mass-to-charge ratio during this early stage of deposition is approximately 3.6 x 10^{-4} g C^{-1}. One possible explanation for this low mass-to-charge ratio is the formation of soluble polymer oligomers that do not deposit.

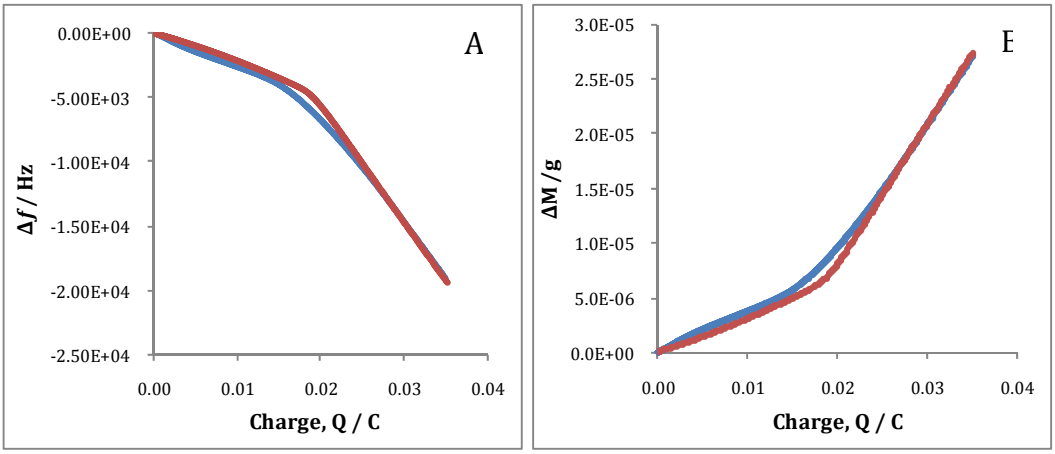

Figure 3.17: A Frequency-charge plots and **B** mass-charge plots for the deposition of PPyDex, recorded by EQCM measurements, in the presence of 0.50 mol dm^{-3} NaDex and 0.20 mol dm^{-3} Py. (Area = 0.203 cm^2).

The charge-time plots for the films grown by ECQM are shown in Figure 3.18. These plots appear to only adopt the more usual linear relationship (as seen for PPyCl, in Figure 3.19) at longer times; a linear charge-time relationship is observed for deposition times higher than about 150 s. The slopes of these linear segments were calculated between 3.0 x 10^{-4} C s^{-1} and 6.0 x 10^{-4} C s^{-1}. Obviously, the charge-time ratio is considerably lower at earlier deposition times.

The plots in Figure 3.17 and Figure 3.18 are very different from those seen for the formation of PPyCl, Figure 3.19. In this case, the growth is at a constant rate, 3.9 x 10^{-4} C s^{-1}, and a linear relationship is observed in the charge-time plot, as shown in Figure 3.19. Furthermore, the mass-to-charge ratio is constant at 2.3 x 10^{-4} g C^{-1}, indicating good efficiency in the deposition of the PPyCl.

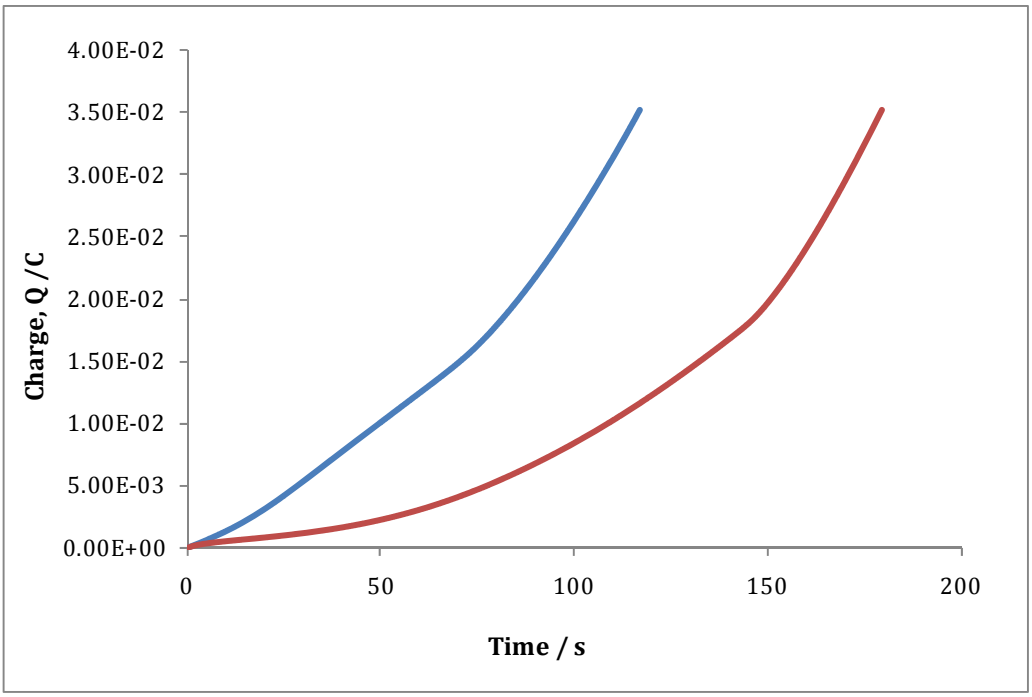

Figure 3.18: Charge-time plots of the formation of PPyDex in the presence of 0.50 mol dm^{-3} NaDex and 0.20 mol dm^{-3} Py at +0.900 V vs Ag|AgCl. (Area = 0.203 cm^2).

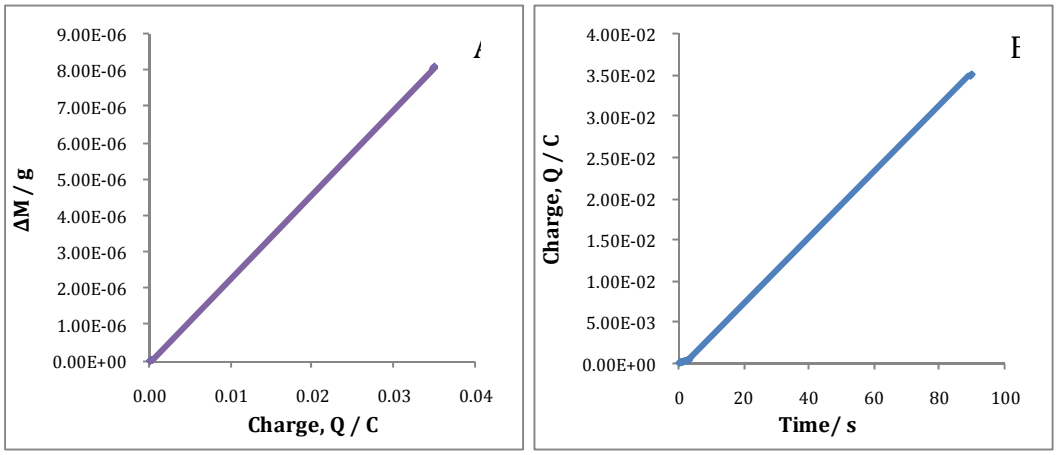

Figure 3.19: A mass-charge plots and **B** charge-time plots for the formation of PPyCl in the presence of 0.10 mol dm^{-3} NaCl and 0.20 mol dm^{-3} Py at +0.700 V vs Ag|AgCl. (Area = 0.203 cm^2).

The EQCM measurements can also be used along with Equations 3.8 and 3.9, a derivation of Faraday's law, to estimate the doping levels of the drugs for polypyrrole. In these equations, M is the total mass of the deposited polymer, Q is the charge reached, M_m is the mass of the monomer, M_{dop} is the mass of the dopant, x is the doping level ($x \leq 0.33$) and F is Faraday's constant, 96484.56 C mol^{-1}. Using

the slope of the mass-charge data, $\frac{M}{Q}$, for the PPyCl system, the doping level was calculated as 0.33. This is in good agreement with several previous studies[55-57].

$$M/Q = ((M_{\downarrow}m) + (M_{\downarrow}(dop)))x)/(2 + x)F \quad 3.8$$

$$M = \frac{Q(M_m)}{(2+x)F} + \frac{Q(M_{dop})x}{(2+x)F} \quad 3.$$

However, the mass-charge of PPyDex does not have this simple linear relationship, as shown in Figure 3.17B. This makes using Equation 3.8 to calculate the doping levels of the polymer more complex. The initial mass-charge slope of 3.6 x 10^{-4} g C^{-1} indicates inefficient electrodeposition and the mass-charge slope at the later times is more representative of the bulk polymer deposition of PPyDex. However, both sets of data were used to compute the doping levels at the different stages of growth. These parameters calculated for the profile of the PPyDex polymers grown on a quartz crystal are shown in Table 3.1. This results in a doping level of about 0.30, once the initial growth period has elapsed. However, considerably lower doping levels are estimated during the initial growth period.

Again, it should be noted that the equation used to calculate the theoretical mass does not take into account solvent participation and it also assumes the current efficiency for the electropolymerisation of the monomer is 100 %.

Table 3.1: Data values calculated for the profile of PPyDex grown by EQCM, (n=3).

Parameters	Initial growth / Average values	Bulk growth / Average values
Charge, Q / C	$1.86 \times 10^{-2} \pm 1.4 \times 10^{-3}$	$1.25 \times 10^{-2} \pm 5 \times 10^{-3}$
Mass, M / g	$7.56 \times 10^{-6} \pm 4.3 \times 10^{-3}$	$1.35 \times 10^{-5} \pm 6.3 \times 10^{-6}$
Doping levels, x	0.025 ± 0.005	0.30 ± 0.03
Mass contributed by Dex / g	$1.10 \times 10^{-6} \pm 1.4 \times 10^{-7}$	$9.12 \times 10^{-6} \pm 4.38 \times 10^{-6}$
Moles of Dex	$2.34 \times 10^{-9} \pm 3.0 \times 10^{-10}$	$1.93 \times 10^{-8} \pm 9.3 \times 10^{-9}$
% mass contributed by Dex	15	68

3.3.3.4 Electrochemical impedance spectroscopy (EIS)

EIS was used to investigate the stability of the polymer at –0.900 V vs SCE and at open-circuit potentials (OCP). These two potentials were selected so that an understanding of the properties of the polymer could be achieved at two stages; when it was first deposited and when the Dex^{2-} was released. The polymer was deposited, as described in Section 3.3.2.2, in two steps by constant potential. A potential of +0.900 V vs SCE was applied until a charge of 0.8 C cm^{-2} was reached and further growth occurred at a potential of +0.800 V vs SCE until a charge of 2.0 C cm^{-2} was reached. Representative impedance plots for PPyDex films under open-circuit conditions and at –0.900 V vs SCE are shown in Figure 3.20, in the complex plane and Bode formats. The modulus of the impedance, Z, and the phase angle presented as a function of the frequency gives the Bode plot, while the imaginary and real components of the impedance are plotted to give the complex plane. In all cases, the data were recorded as a function of the immersion period for a total of 8 h in 0.10 mol dm^{-3} NaCl. The first impedance profile was recorded following an initial 10 min polarisation period at the desired potential. Similar data were recorded for the bare Pt electrode, however these are not shown.

The impedance profile changes from a simple one-time constant model when the polymer is reduced to a two-time constant model when the polymer is maintained at OCP. From Figure 3.20B, it is clear that the impedance of the polymer at –0.900 V vs SCE is very different to that displayed by the PPyDex at OCP. As

mentioned previously, the polymer losses its conductivity after a reduction potential is applied for long periods of time[27]. The polymer under OCP is therefore more conductive and the impedance is lower. This phenomenon is commonly seen in conducting polymer electrodes due to the higher surface area and more efficient charge transfer of the polymer coating[33, 34].

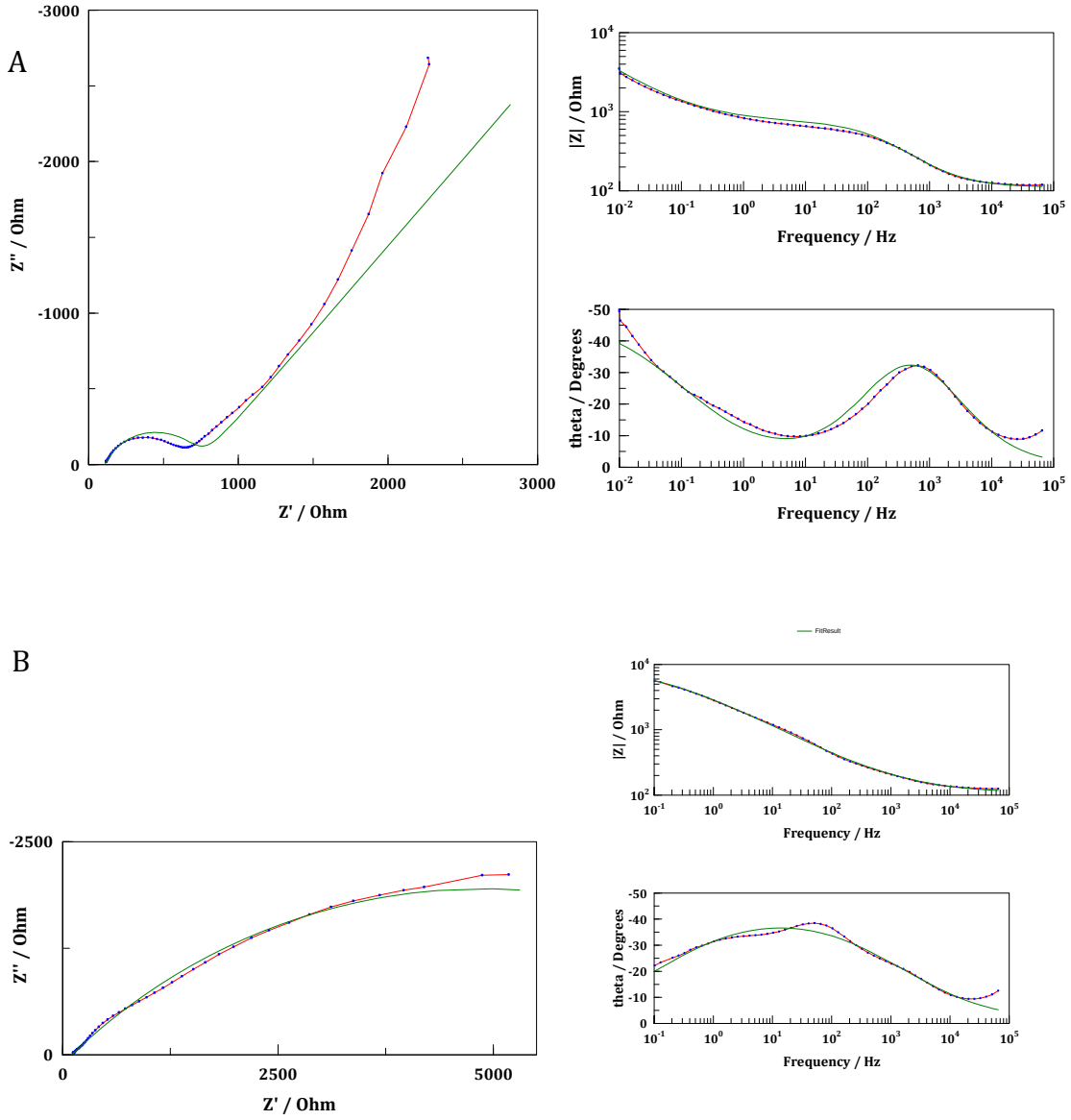

Figure 3.20: Complex plane plot and Bode plot recorded in 0.10 mol dm^{-3} NaCl using a sinusoidal excitation voltage of 10 mV, measured at **A** open-circuit potential and at **B** –0.900 V vs SCE for the PPyDex. Both the experimental data and the simulated fitted traces are shown. The PPyDex films were deposited on a Pt electrode to a charge of 2.8 C cm^{-2}. (Area = 0.125 cm^2). (Ohm refers to the unit of Ω).

These data were fitted to the equivalent circuits depicted in Figure 3.21 using a non-linear least squares fitting minimisation method in the ZView fitting programme. The circuit shown in Figure 3.21A was used to fit the experimental data when the PPyDex films were maintained at open-circuit potential, while a simple Randles cell, presented in Figure 3.21B, was used to model the data when the PPyDex was reduced. In these circuits, R1 represents the solution resistance; R2 represents the charge-transfer resistance, while CPE1 and CPE2 are constant phase elements. Constant phase elements were used to determine the capacitance of the interface and also diffusional processes and were used rather than capacitors to take into account the inhomogeneity of the surface of the electrode[35]. The impedance of the constant phase element is defined as $Z_{CPE} = T^{-1} (j\omega)^{-P}$, where P is a fractional exponent, having values between 0 and 1 and T is a frequency independent parameter. When the exponent is zero, P = 0, the CPE describes an ideal resistor; when P = 1, the CPE is equivalent to an ideal capacitor (T = C), while an exponent of 0.5, P = 0.5, corresponds to homogeneous semi-infinite diffusion.

There is good agreement, across the entire frequency range, between the experimental data and the fitted traces, as shown in Figure 3.20. Equally, the errors in each circuit element are low, as shown in Figure 3.22. In this figure an example of the fitting for the impedance of the PPyDex at –0.900 V vs SCE is shown. The % error in each circuit element is less than 2.4 %. Equally, the chi-squared value is low, indicating very good agreement between the experimental data and the equivalent circuit.

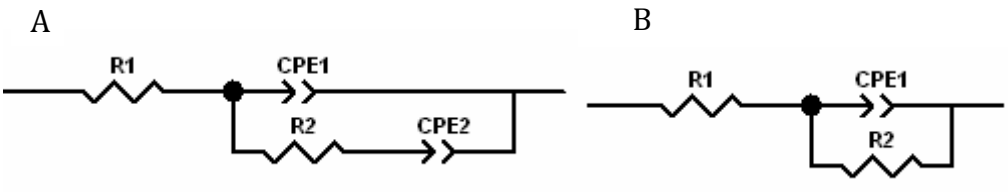

Figure 3.21: Equivalent circuits used to fit the data presented in Figure 3.20. **A** was used to fit all OCP data while **B** was fitted to all measurements at – 0.900 V vs SCE.

Element	Freedom	Value	Error	Error %
Rs	Free(+)	100.9	1.724	1.7086
CPE1-T	Free(+)	0.00013415	2.3356E-06	1.741
CPE1-P	Free(+)	0.46444	0.0034986	0.75329
Rct	Free(+)	11648	272.91	2.3434

Chi-Squared:	0.0050163
Weighted Sum of Squares:	0.69225
Data File:	C:\Documents and Settings\Eimear\My Documents\
Circuit Model File:	
Mode:	Run Fitting / Selected Points (0 - 70)
Maximum Iterations:	100
Optimization Iterations:	0
Type of Fitting:	Complex
Type of Weighting:	Calc-Modulus

Figure 3.22: Data fitting routine for circuit shown in Figure 3.21 B, circuit parameters, values and errors.

The steady-state conditions were probed by collecting the impedance spectra as a function of time and comparing the circuit parameters. The data recorded at this potential were fitted to the circuit model in Figure 3.21B and are shown in Table 3.2. This shows the magnitude of R1, R2 and CPE for PPyDex, at – 0.900 V vs SCE, for eight consecutive experiments. As stated earlier, when P has a value close to 0.5 it corresponds to a diffusional process[36] and coincides with a phase angle of 45°. Clearly in this case, the CPE represents a diffusional process and may be related to the ingress of Na^+ cations into the polymer matrix, as the film is reduced. The polymer was held at –0.900 V vs SCE for 10 min before the first impedance measurement was made. From the analysis, it is clear that after the first three measurements the circuit parameters remain nearly constant. This suggests good stability and the establishment of steady-state conditions after 180 min.

Table 3.2: Circuit parameters (derived from Figure 3.21B) for PPyDex, grown until a charge of 2.8 C cm^{-2} was reached, on a Pt electrode polarised at –0.900 V vs SCE in 0.10 mol dm^{-3} NaCl. Impedance data were recorded using a sinusoidal excitation voltage of 10 mV over 8 h. (Area = 0.125 cm^2).

PPyDex	R1 / Ω	T / Ω^{-1} s^P	P	R2 / Ω
Exp 1	75	1.6 x 10^{-4}	0.35	16243
Exp 2	103	1.6 x 10^{-4}	0.43	11066
Exp 3	102	1.5 x 10^{-4}	0.44	11240
Exp 4	101	1.5 x 10^{-4}	0.45	11692
Exp 5	101	1.4 x10^{-4}	0.46	11834
Exp 6	101	1.3 x 10^{-4}	0.46	11646
Exp 7	101	1.3 x 10^{-4}	0.47	12079
Exp 8	100	1.3 x 10^{-4}	0.47	12310

Figure 3.23 shows the R2, which is equivalent to the charge-transfer resistance, and the diffusional parameter, CPE1 (with P ≈ 0.5), measured at –0.900 V vs SCE for PPyDex as a function of time. Shown for comparison purposes are data recorded for bare Pt under the same experimental conditions. In this case, CPE1 corresponds to a capacitor, with P = 0.8. The same general pattern is observed for both electrodes with a slight increase in the resistance as a function of time, which indicates a loss in conductivity. Under these applied potential conditions, hydrogen adsorption occurs at the surface of the bare electrode. This slows down the electron kinetics and the adsorbed hydrogen acts like an insulation layer affecting the rate at which redox species are oxidised/reduced at the surface. However, a higher resistance is measured for the polymer. The reduction of PPyDex results in the formation of PPy^0 and Dex^{2-}. The presence of PPy^0 lowers the conductivity of the polymer and thus there is an increase in the charge transfer resistance on reduction of the polymer. The capacitance of the bare Pt electrode, about 40 μF cm^{-2}, is in good agreement with the double-layer capacitance of bare electrodes[37]. In the case of PPyDex, there is a gradual decrease in CPE1 from about 0 to 200 min, however the value remains essentially constant, for longer times. These data clearly show that the PPyDex is stable at these reduction potentials.

As shown in Figure 3.20, the impedance of PPyDex is very different at OCP. The complex plane plot shows the presence of a diffusion tail and the semicircle is much smaller indicating a highly conducting film. The impedance data were fitted to the circuit model shown in Figure 3.21A. In this case, CPE2 is equivalent to a capacitor with an exponent of approximately 0.8, while CPE1 represents the diffusional processes.

The charge-transfer resistances, R2, measured at OCP for both the bare Pt and PPyDex are plotted in Figure 3.24 as a function of time. The potential of the cell over the eight experiments was recorded at approximately +0.240 V vs SCE. The resistance of the PPyDex is much lower than that measured at the reduction potential. Indeed, the resistance, R2, is higher at the bare Pt than at the polymer. This is again due to the higher surface area and more efficient charge transfer of the polymer coating[33, 34]. The impedance of the polymer at OCP is relatively

constant over the 400 min period. This indicates that the polymer is stable and remains conducting over long periods of time under open-circuit conditions.

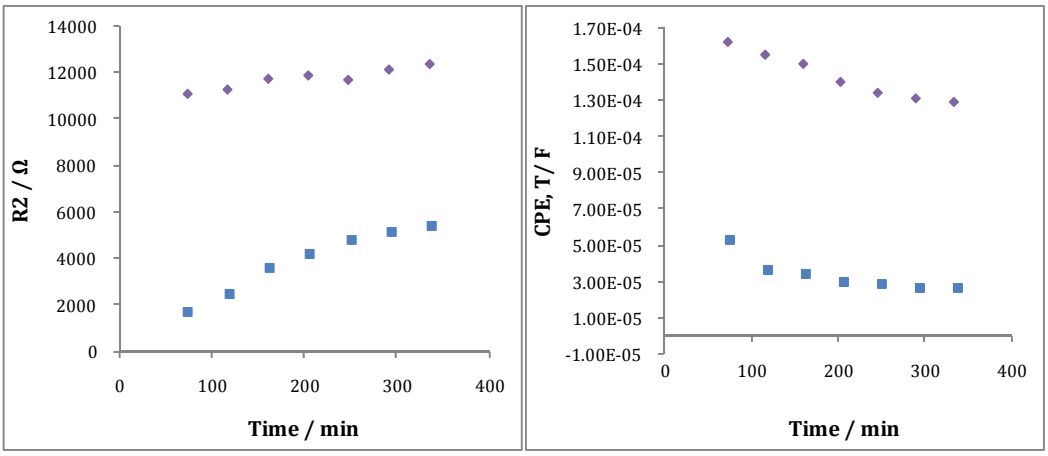

Figure 3.23: Resistance, R2, and constant phase element, CPE1, recorded at –0.900 V vs SCE in 0.10 mol dm^{-3} NaCl for ■ bare Pt and ♦ PPyDex. Impedance data were recorded using a sinusoidal excitation voltage of 10 mV. CPE1 corresponds to a diffusional process for PPyDex and to a capacitor for bare Pt.

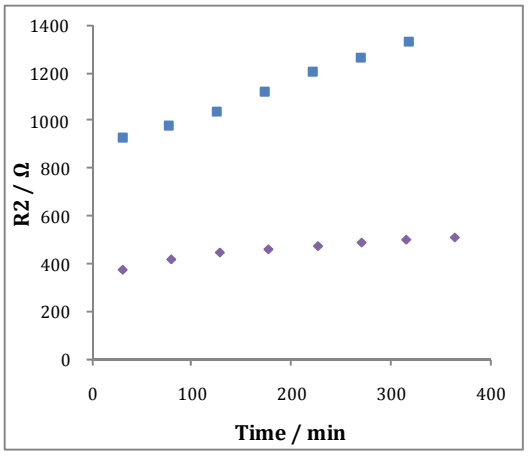

Figure 3.24: Resistance, R2, recorded for ■ bare Pt and ♦ PPyDex at OCP in 0.10 mol dm^{-3} NaCl. Impedance data were recorded using a sinusoidal excitation voltage of 10 mV.

3.3.3.5 Morphology

Optical imaging techniques were performed on the PPyDex film to obtain information on the morphology of the polymer. The films were firstly synthesised, washed thoroughly with distilled water to ensure the removal of any Dex^{2-} on the surface of the polymer and dried by exposure to a gentle air flow for 30 s. The polymer was grown to the optimum conditions, i.e., by applying a potential of

+0.900 V vs SCE until a charge of 0.8 C cm^{-2} was reached followed by a potential of +0.800 V vs SCE until a charge of 2.0 C cm^{-2} was reached. This meant the total charge of the polymer was 2.8 C cm^{-2}. Figure 3.25 shows the optical images recorded and a cauliflower, globular morphology is quite evident. In general, PPy films present a cauliflower-like morphology constituted by micro-spherical grains. It has been reported that such a particular structure is related to the dopant intercalation difficulty in the disordered polymeric chain[58, 59]. It is well documented that PPy films display a cauliflower-like morphology[59-63].

Figure 3.26 shows SEM micrographs of PPyDex grown under the same parameters as those previously described for the optical images. Again, the globular cauliflower morphology of PPy is quite evident. The cracks on the surface of the polymer are due to the polymer being dried. It is clear from both Figure 3.25 and Figure 3.26 that the cauliflower/globular shapes are not uniform in size. This could be a result of the controlled manner in which the polymer is grown with the rate of polymerisation being slowed down during the second part of growth. SEM micrographs of PPyCl grown to 2.8 C cm^{-2} in charge, from an electrolyte of 0.10 mol dm^{-3} NaCl and 0.20 mol dm^{-3} Py at +0.800 V vs SCE, are shown in Figure 3.27. The PPyCl film exhibits the same PPy morphology of globular shapes, but has a much rougher surface than the surface of the PPyDex. This could be due to the fact that this film polymerises easily and quickly at the surface of the electrode.

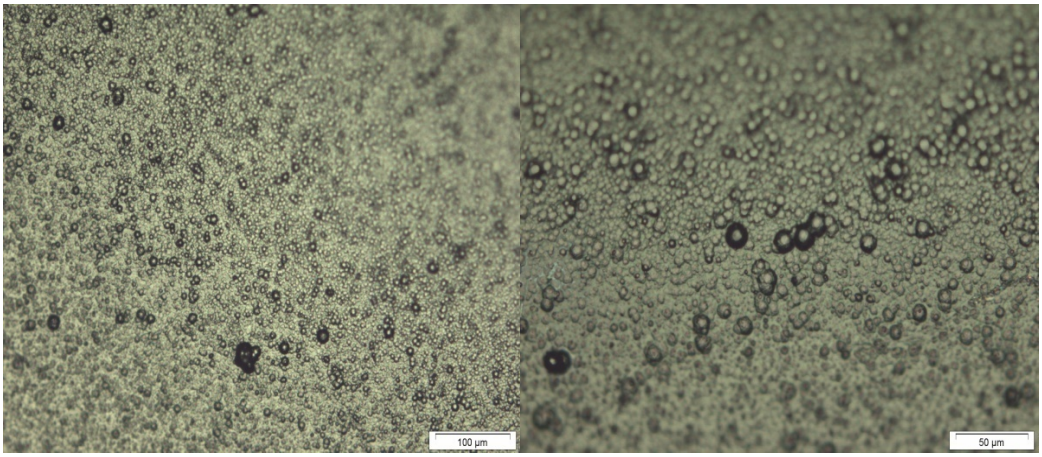

Figure 3.25: Optical images of PPyDex on a Pt disc. Polymers were electrochemically deposited in the presence of 0.05 mol dm^{-3} NaDex and 0.20 mol dm^{-3} Py at +0.900 V vs SCE

until 0.8 C cm^{-2} was reached before +0.800 V vs SCE was applied until a further 2.0 C cm^{-2} was reached giving a total charge of 2.8 C cm^{-2}.

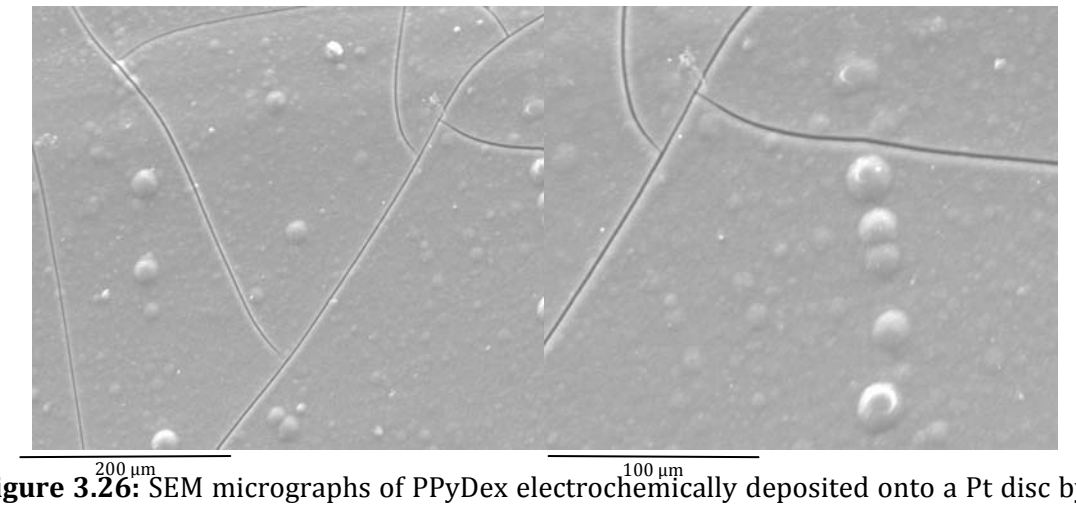

Figure 3.26: SEM micrographs of PPyDex electrochemically deposited onto a Pt disc by a constant potential of +0.900 V vs SCE until 0.8 C cm^{-2} was reached before +0.800 V vs SCE was applied until a further 2.0 C cm^{-2} was reached. This was done in the presence of 0.05 mol dm^{-3} NaDex and 0.20 mol dm^{-3} Py.

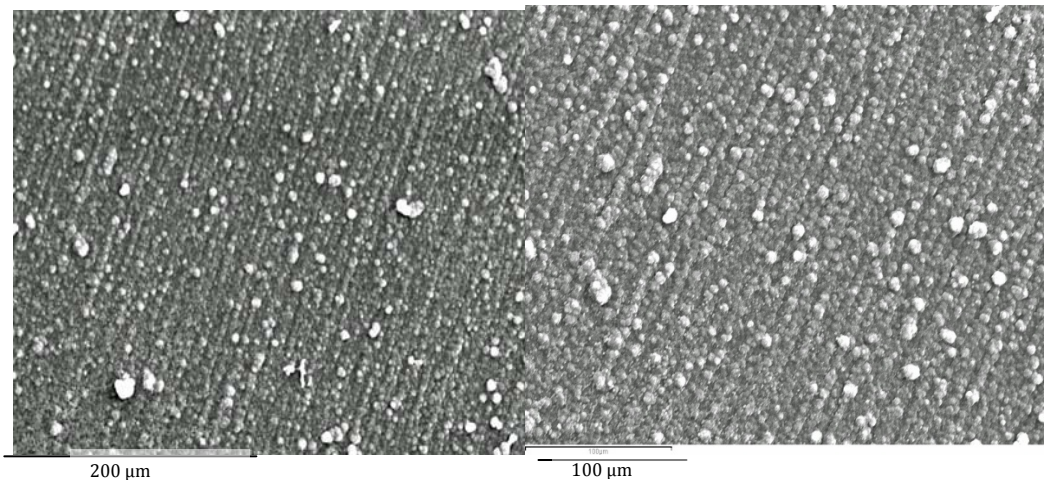

Figure 3.27: SEM micrographs of PPyCl electrochemically deposited onto a Pt disc by a constant potential of +0.800 V vs SCE to 2.8 C cm^{-2} in the presence of 0.10 mol dm^{-3} NaCl and 0.20 mol dm^{-3} Py.

3.3.4 Release studies

Before any of the release studies were carried out, the polymer was thoroughly rinsed with distilled H_2O, then immersed in distilled H_2O for 10 min and a potential of +0.500 V vs SCE was applied to ensure that any Dex^{2-} on the surface of the

polymer was washed away. In addition the 10 min immersion period was sufficient for any Dex^{2-} trapped within the porous polymer matrix to diffuse into the bulk H_2O.

3.3.4.1 Influence of PPyDex growth conditions on the release of Dex^{2-}

Release studies were carried out on the four polymer films, grown in the manner described in Section 3.3.2, to determine which method yielded the highest amount of Dex^{2-} release. A potential of –0.900 V vs SCE was applied to the PPyDex which was immersed in 0.10 mol dm^{-3} NaCl for 60 min and a sample of the solution was taken every 5 min and analysed to monitor the concentration of Dex^{2-}. The rate at which the Dex^{2-} is released from the polymer is measured by calculating the slope of the release profiles. For all four polymers, a similar trend in release profiles was observed, Figure 3.28, with an increase measured for the first 40 min before the release measurements reached a plateau, indicating a slower release from about 30 to 60 min. The lowest release was measured for the polymer deposited in two steps by applying +0.900 V vs SCE until 1.2 C cm^{-2} with the second step of CV scanning between –0.100 V and +0.800 V vs SCE at a scan rate of 50 mV s^{-1}. After 60 min, 15.81 µmol cm^{-2} of Dex^{2-} was measured from this polymer.

The largest Dex^{2-} release was measured from the polymer grown using the two step constant potential method described in Section 3.3.2.2, whereby a constant potential of +0.900 V vs SCE was applied until 0.8 C cm^{-2} of charge was consumed with further growth of the polymer at +0.800 V vs SCE until the total charge of the polymer reached 2.8 C cm^{-2}. At the end of the 60 min, 27 µmol cm^{-2} of Dex^{2-} was released from the polymer, however, in the first 5 min, 16 µmol cm^{-2} of Dex^{2-} was measured which meant the majority of the drug was released within 5 min of applying the reduction potential. The release rate of the first 5 min was 3.2 µmol cm^{-2} min^{-1} while the rate of release for the remainder of the hour was 0.18 µmol cm^{-2} min^{-1}. It is obvious that the rate of release slows considerably over the 60 min period. All further release studies were carried out on polymers grown in this manner. The second largest Dex^{2-} release was observed from the polymer grown in one step at constant potential. The PPyDex deposited at +0.900 V vs SCE

may be slightly over-oxidised, while deposition at +0.800 V vs SCE minimises the over-oxidation to give good release profiles.

It is not surprising that the PPyDex deposited onto PPyCl has a lower release of Dex^{2-}, as there is less Dex^{2-} in the composite film. It is difficult to compare the film deposited using the two step fixed potential followed by CV, as the charge consumed during the growth of the polymer is difficult to measure. Furthermore, as evident in Figure 3.11, the rate of electropolymerisation decreases with cycling, suggesting a loss in conductivity of the deposited polymer.

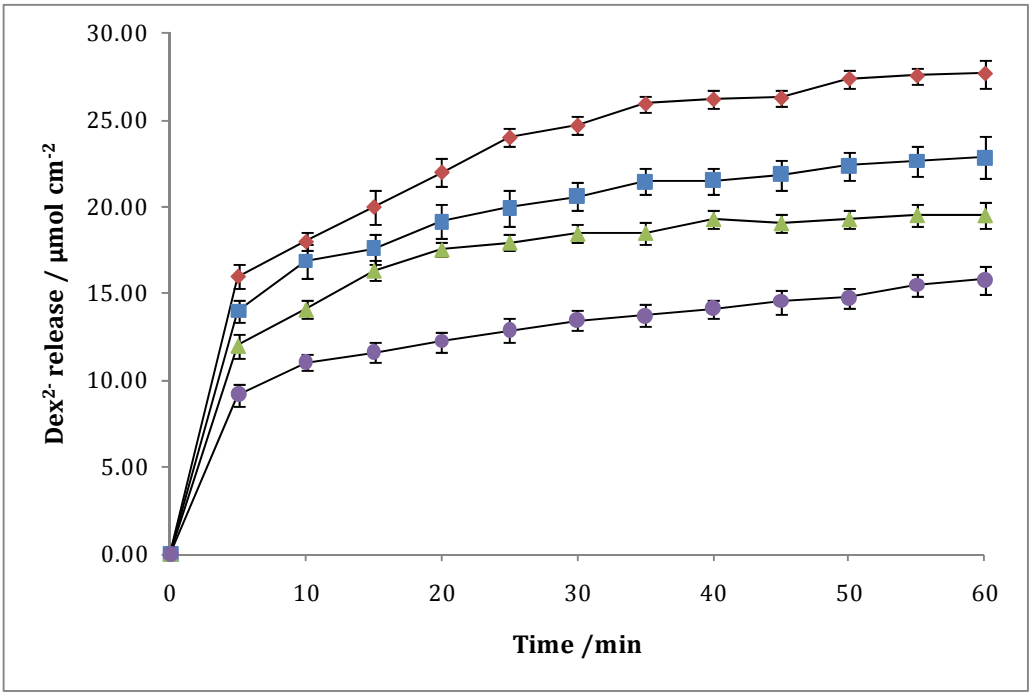

Figure 3.28: Amount of Dex^{2-} measured as a result of applying −0.900 V vs SCE to each polymer grown, in the presence of 0.05 mol dm^{-3} NaDex and 0.20 mol dm^{-3} Py, as follows: ♦ in two steps at a constant potential of +0.900 V vs SCE until 0.8 C cm^{-2} was reached with +0.800 V vs SCE applied until a further 2.0 C cm^{-2} was reached, ■ applying a constant potential of +0.900 V vs SCE to 2.8 C cm^{-2}, ▲ at a constant potential of +0.900 V vs SCE on a thin film of PPyCl and finally ● in two steps, first at a constant potential of +0.900 V vs SCE to a charge of 1.2 C cm^{-2} with the second step of CV scanning between −0.100 V and +0.800 V vs SCE at a scan rate of 50 mV s^{-1}. The amount of Dex^{2-} detected was measured by UV-vis spectroscopy in the presence of 0.10 mol dm^{-3} NaCl. (n=3)

3.3.4.2 Studies on the release potential

The release study was a straight-forward process in that the polymer was grown several times under the optimum parameters and then potentials ranging from +0.100 V vs SCE to –1.200 V vs SCE were applied for 60 min and the concentration of Dex^{2-} released from the polymer was determined using UV-vis spectroscopy. Samples were taken every 5 to 10 min. Samples were also taken from a release electrolyte in which the polymer was immersed under OCP. During the immersion period the OCP was measured to be approximately +0.200 V vs SCE. Figure 3.29 shows the release profiles at OCP, –0.400 V vs SCE and –0.900 V vs SCE and it is clear that the amount of Dex^{2-} being released is dependent on the potential applied and is not purely as a result of the drug diffusing across the polymer membrane. The rates at which the Dex^{2-} is released from the polymer at the different potentials are shown in Table 3.3. The rate of release at –0.900 V vs SCE for the first 5 min is 2.50 μmol cm^{-2} min^{-1}. This is significantly higher than the release rate measured at OCP or at –0.400 V vs SCE. However, as the release profile begins to plateau by 60 min, the rate of release slows down and is even slower than the rate of release at –0.400 V vs SCE.

At all potentials, quite a large proportion of Dex^{2-} is released in the first 5 min in relation to the amount of Dex^{2-} measured after 60 min. As discussed in Chapter 1, Section 1.4.4.5, the thickness of the polymer affects the rate and amount of drug released. The dissociation of the dopants from the polypyrrole chain may be an instant process, but the release of the anion is slow since it is driven by diffusion consisting of the movement of anions from the inner film to the surface and from the surface to the solution[27]. For thicker films like those studied in this work, the diffusion from the inner film to the surface is much slower, so the quick release is mainly from the surface and the bulk release may take hours. However, in the case of a thin polymer the entire film is reduced upon the application of a reduction potential and the drug release is instantaneous.

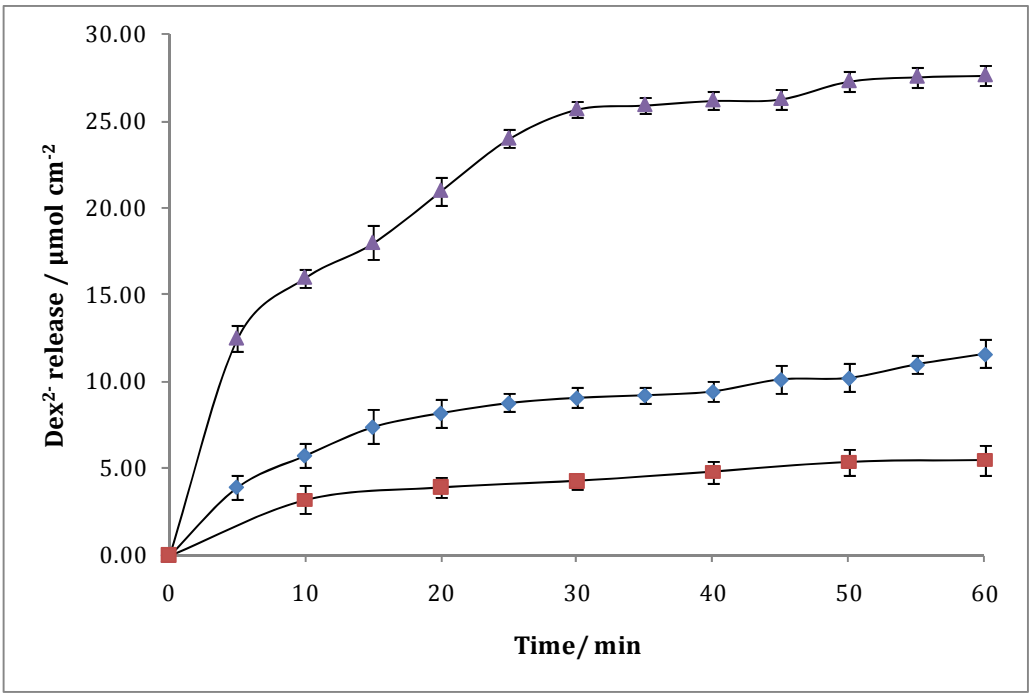

Figure 3.29: Release profiles for Dex^{2-} released at ■ OCP, ♦ –0.400 V vs SCE and ▲ – 0.900 V vs SCE. Polymerisation was achieved in two steps; applying +0.900 V vs SCE until 0.8 C cm^{-2} was reached with +0.800 V vs SCE applied until a further 2.0 C cm^{-2} was reached in the presence of 0.05 mol dm^{-3} NaDex and 0.20 mol dm^{-3} Py. (n=3).

Table 3.3: The rate of Dex^{2-} release at OCP, –0.400 V vs SCE and –0.900 V vs SCE.

Time range / min	Rate of release at OCP / µmol cm^{-2} min^{-1}	Rate of release at –0.400 V vs SCE / µmol cm^{-2} min^{-1}	Rate of release at –0.900 V vs SCE / µmol cm^{-2} min^{-1}
0-5	0.318	0.786	2.500
5-30	0.055	0.203	0.531
35-60	0.033	0.095	0.078

The amount of Dex^{2-} measured after 60 min at various different potentials is shown in Figure 3.30. In this 60 min time period, applying a potential of –0.900 V vs SCE yields the highest release of Dex^{2-} from the polymer, while applying more electropositive potentials, such as –0.200 V vs SCE, yield a much lower release. The amount of Dex^{2-} released at –1.000 V vs SCE is also very low as the polymer is fully reduced and side reactions such as H_2 evolution are predominant. Indeed, since all polymers contain the same concentration of Dex^{2-},

the best release profile for Dex^{2-} depends on the amount of Dex^{2-} desired in a defined time, i.e., if a slow release of Dex^{2-} over a long period of time is necessary, then the best potential range for release is between **–**0.200 V vs SCE and **–**0.600 V vs SCE. In contrast, if a fast release over a short time period is preferred then the best potential range is between **–**0.700 V vs SCE and –0.900 V vs SCE. From here, all release studies were carried out at **–**0.900 V vs SCE.

In the aforementioned reports[27-29] on the controlled release of Dex^{2-}, the amount of Dex^{2-} released was measured between 3 μg cm^{-2} to 80 μg cm^{-2}. In this study, 13.9 mg cm^{-2} is released after 60 min at –0.900 V vs SCE, which is considerably higher with an approximate 1000-fold increase on these literature values. In the previous reports, the PPy was either over-oxidised, or stimulated by connecting to a magnesium anode, or an alternative polymer material to PPy was examined, which may account for the lower release of Dex^{2-} reported. The release studies in this research can also be compared to the release of ATP^{-} from PPy[64, 65] as it is an anionic molecule of similar size. In these papers, the ATP^{-} was released by cyclic voltammetry or by applying a reduction potential. The highest amount of ATP^{-} was released at –0.700 V vs Ag|AgCl and approximately 600 nmol cm^{-2} was measured over a 50 min period. The rate of release was reported as 35 nmol cm^{-2} min^{-1}. Again, these release rates are much lower than the release rates observed in this study for Dex^{2-} from PPyDex.

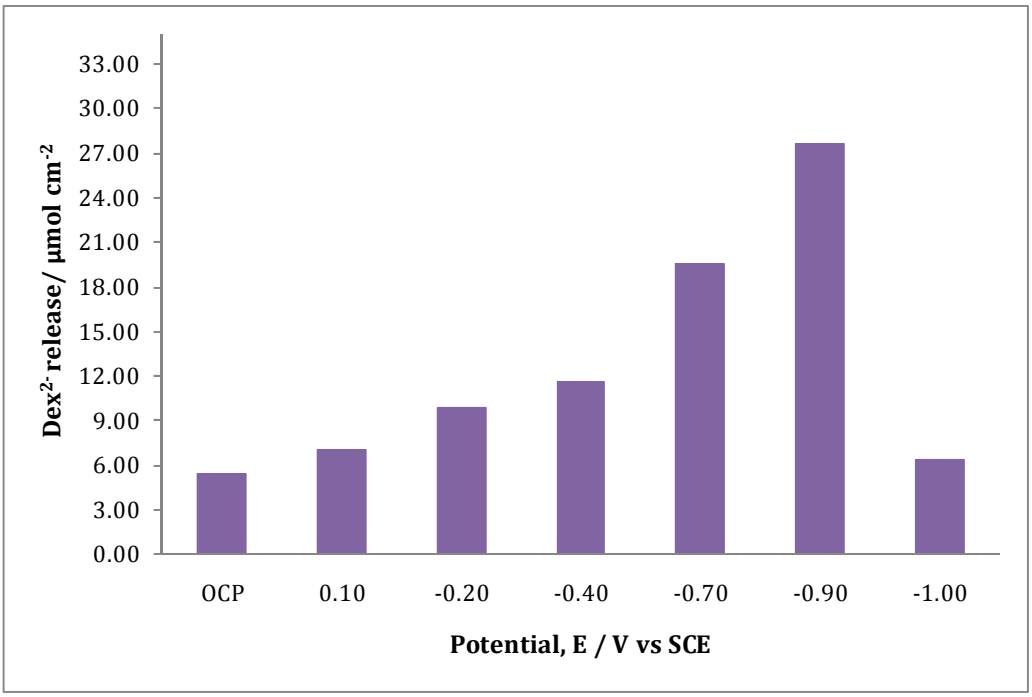

Figure 3.30: Amount of Dex^{2-} measured upon release from the polymer at varying potentials in the presence of 0.10 mol dm^{-3} NaCl over a period of 60 min. (n=3, %error = 3 %).

3.3.4.3 The amount of Dex^{2-} incorporated into the PPy

With the growth and release parameters optimised, the length of the release time was increased for two reasons; firstly to estimate how much drug was present in the polymer and secondly to find how long it would take to completely expel the drug from the polymer. Two sets of release studies were carried out over a period of 5 h, one at –0.900 V vs SCE and the other at OCP. The resulting release profiles are illustrated in Figure 3.31**.** The amount of Dex^{2-} released at –0.900 V vs SCE begins to plateau within the 1st hour and there is very little increase in Dex^{2-} release over the next four hours. This indicates that the majority of the drug is released within the first 40 min. The rate of release from 60 to 300 min was calculated as 0.012 µmol cm^{-2} min^{-1} which indicates that the rate of release has slowed down considerably.

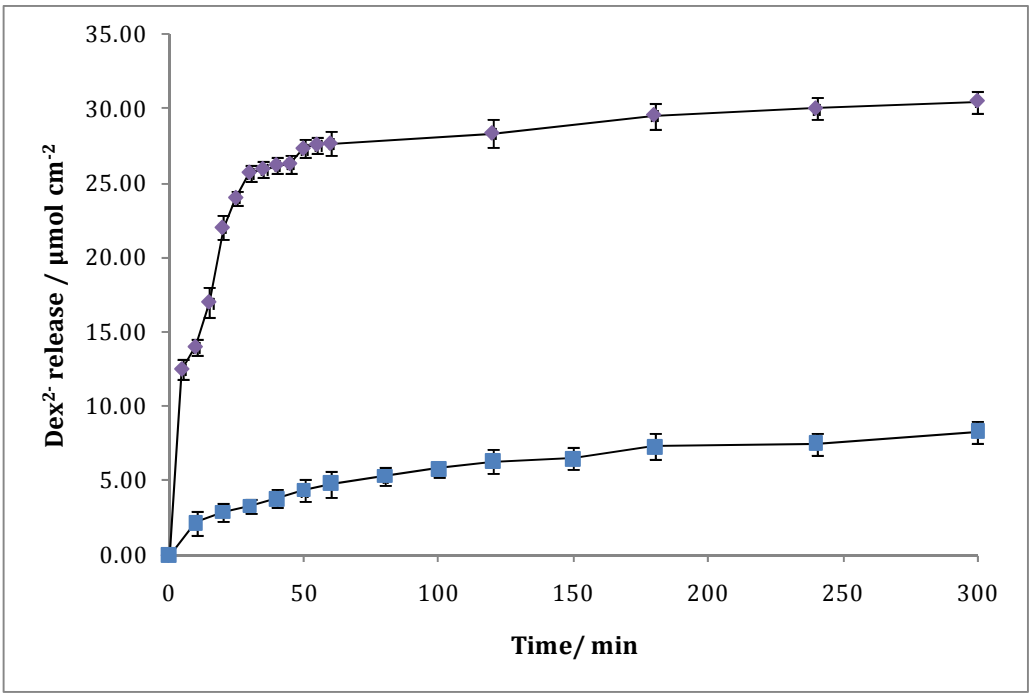

Figure 3.31: Amount of Dex released from the polymer at ♦ −0.900 V vs SCE and at ■ OCP over 5 h in the presence of 0.10 mol dm^{-3} NaCl. Polymerisation was carried out in two steps; applying +0.900 V vs SCE until 0.8 C cm^{-2} was reached with +0.800 V vs SCE applied until a further 2.0 C cm^{-2} was reached in the presence of 0.05 mol dm^{-3} NaDex and 0.20 mol dm^{-3} Py. (n=3).

The release profile for the OCP again shows the importance of applying a reduction potential to allow a larger amount of Dex^{2-} to be released. The rate of release for 60 to 300 min is calculated as 0.004 µmol cm^{-2} min^{-1}. This again suggests that the rate of release has slowed down over the 4 h. However, the fact that Dex^{2-} is still being released, although at a slow rate, indicates that eventually all Dex^{2-} will be released from the polymer but it will take a substantially longer time than when a reduction potential is applied.

In Section 3.3.3.4, the mass and doping levels of thin PPyDex polymers were examined and a maximum doping level of 0.30 was calculated for the bulk growth of the polymer on the quartz crystal. There are similarities between the slopes of the charge-time plots of both the EQCM and bulk polymers which indicate that the thin polymers grown by EQCM are similar to the bulk polymers and that perhaps there are also similar doping levels of 0.30 in the bulk polymer. However, the difference in charge between the bulk polymer and the thin polymer grown by

EQCM makes it extremely difficult to calculate the doping level and mass of the polymer accurately using Equation 3.9. Assuming that the majority of the Dex^{2-} incorporated into the polymer is expelled after 5 h, it can be estimated from these experiments that the amount of Dex^{2-} in the polymer is approximately 31 μmol cm^{-2}. The percentage of drug released from the polymer at the various potential ranges, discussed in Section 3.3.4.2, was calculated and the values are plotted in Figure 3.32. Based on these estimates, approximately 89% of the drug was released after 1 h at the optimum release potential of –0.900 V vs SCE, while approximately 17% was released at OCP.

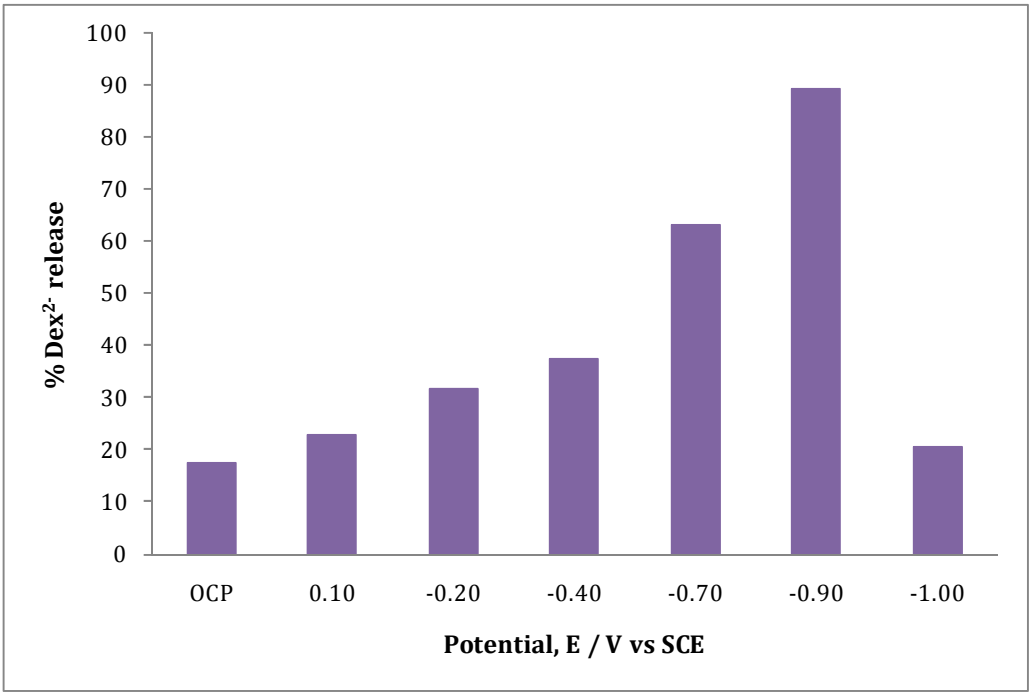

Figure 3.32: Estimated % of Dex^{2-} released at various potentials in the presence of 0.10 mol dm^{-3} NaCl.

Previous research has shown that dexamethasone is effective at a concentration range of 0.2 to 0.7 μmol dm^{-3} and at this local concentration pronounced reduced inflammatory tissue reaction is seen around the neural implant[16]. Based on histological studies, the reactive region indicated by enhanced glial fibrillary acidic protein (GFAP) activity around the neural electrode arrays has a radius of less than 500 μm[66]. Even though the neural implants have a significantly smaller surface area than the electrodes used in this study, these PPyDex films could be deposited

onto electrodes with diameters of about 500 μm. This in turn would reduce the amount of Dex^{2-} released. However the high release observed in this study suggests that these polymers (when deposited onto smaller surface areas) could release enough Dex^{2-} to effectively reduce inflamed tissue.

3.3.4.4 Investigations into the possibility of reusing the polymer

As discussed in Chapter 1, Section 1.4.3, reducing the PPy results in the release of the anionic drug which in this case is Dex^{2-}, shown in Equation 3.10, however, it was then investigated whether the reduced polymer, PPy^0, could be oxidised back to PPy^+ to incorporate more drug into the polymer matrix and control its release again.

$$PPy^{2+}Dex^{2-} + 2e^- \rightarrow PPy^0 + Dex^{2-} \qquad 3.10$$

These investigations were carried out as follows; the polymer was grown using the two step constant potential method and the drug was released at – 0.900 V vs SCE, the polymer was then placed in a solution of 0.06 mol dm^{-3} NaDex (a little higher than the concentration of NaDex used during polymerisation) and a potential of +0.900 V vs SCE was applied for 60 min in an attempt to incorporate the Dex^{2-} into the polymer. The drug was then released as before and samples were taken every 5 min over a 60 min period. The polymer was then replaced back into the NaDex solution for another 60 min and the incorporated Dex^{2-} was released as before. The four sets of release profiles are shown in Figure 3.33.

As expected there is a drop in the amount of Dex^{2-} released from the first to the second release, however, the amount of Dex^{2-} released thereafter increases with a significant rise in the amount of Dex^{2-} measured between the third and the fourth release experiment. This provides good evidence that the polymer can be reused several times for the same purpose. The rate of release from 30 to 60 min for the 1^{st}, 2^{nd}, 3^{rd} and 4^{th} release was determined as 0.08 μmol cm^{-2} min^{-1}, 0.04 μmol cm^{-2} min^{-1}, 0.06 μmol cm^{-2} min^{-1} and 0.03 μmol cm^{-2} min^{-1}, respectively. The initial drop in the amount of Dex^{2-} measured between the first and second release suggests that it is difficult to recover the conductivity of the PPy film after a

negative potential is applied for a long time[27] and it cannot be oxidised enough to incorporate large amounts of Dex^{2-} into the polymer. However, the increase in the concentration of released Dex^{2-} thereafter seems to suggest that once the polymer is initially oxidised, the re-oxidation of the polymer becomes easier and that each time the oxidation potential is applied more PPy is oxidised and this allows higher concentrations of Dex^{2-} to be incorporated.

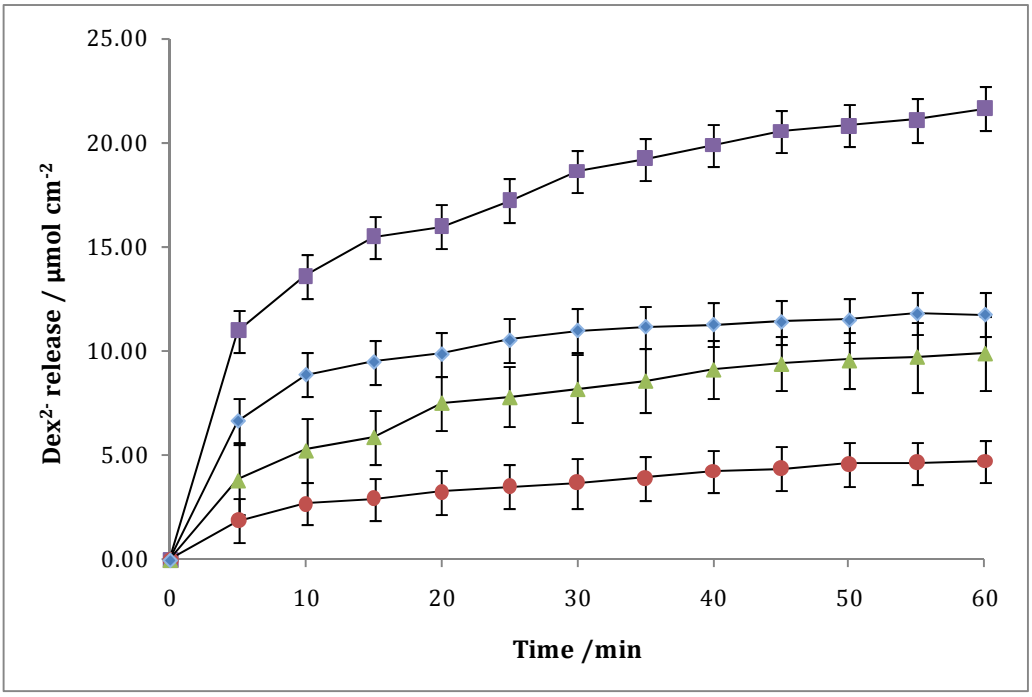

Figure 3.33: Amount of Dex^{2-} released from the polymer at –0.900 V vs SCE, in the presence of 0.10 mol dm^{-3} NaCl, over four 60 min periods; ■ 1st release, ● 2nd release after it was placed in 0.06 mol dm^{-3} NaDex for 60 min at a potential of +0.900 V vs SCE, ▲ 3rd release after it was placed in 0.06 mol dm^{-3} NaDex for 60 min at a potential of +0.900 V vs SCE for the second time and ♦ 4th release after it was placed in 0.06 mol dm^{-3} NaDex for 60 min at a potential of +0.900 V vs SCE for the third time. (n=3).

EQCM was then employed to monitor the change in mass of the polymer during the investigations into reusing the polymer. A polymer of 3.5 x 10^{-2} C in charge was deposited by applying a potential of +0.900 V vs Ag|AgCl. The Dex^{2-} was released from the polymer by applying a reduction potential of –0.900 V vs Ag|AgCl for 10 min in the presence of 0.10 mol dm^{-3} NaCl. The polymer was then placed in a monomer free solution of 0.06 mol dm^{-3} NaDex for 10 min while a potential of +0.900 V vs Ag|AgCl was again applied before the polymer was placed back into

the NaCl solution and a reduction potential of –0.900 V vs Ag|AgCl was applied for 10 min. The resulting mass-time plots are shown in Figure 3.34 starting with the growth of the polymer until the final release. The mass-time plot for the growth of the polymer is shown in Figure 3.34A, while its corresponding release can be seen in Figure 3.34B. The mass-time plot for the oxidation of the polymer is shown in Figure 3.34C, while the mass–time plot of the subsequent reduction of the polymer is shown in Figure 3.34D.

It is clear from Figure 3.34, that there is a general pattern whereby the application of an oxidation potential generally results in an increase of mass, while the reduction of the polymer proceeds with a decrease in mass. These changes in mass correspond to the release and incorporation of the Dex^{2-} from and into the PPy. The mass changes and the equivalent amounts of Dex^{2-} are shown in Table 3.4. From these data, it seems that a higher amount of Dex^{2-} is incorporated than is released during the first experiment and this leads to an increase in the amount of Dex^{2-} released during the second release experiment. Although these polymers are much thinner than those studied in Section 3.3.4.4, they provide some evidence as to why after the second release experiment there is an increase in the amount of Dex^{2-} measured upon release. It appears that more Dex^{2-} is incorporated after the initial release experiment when the oxidation potential is applied. This suggests that reduced PPy^{0} is readily oxidised back to PPy^{+} with the incorporation of Dex^{2-}. This pattern was observed on multiple occasions during the study of the bulk polymer.

Table 3.4: Mass change and equivalent amounts of Dex^{2-} as a result of the application of oxidation and reduction potentials to PPyDex.

Figure	Mass change	ΔM/ g	Amount of Dex/ moles
3.25 B	Decrease	3.75×10^{-7}	7.26×10^{-10}
3.25 C	Increase	8.14×10^{-7}	1.58×10^{-9}
3.25 D	Decrease	1.40×10^{-6}	2.70×10^{-9}

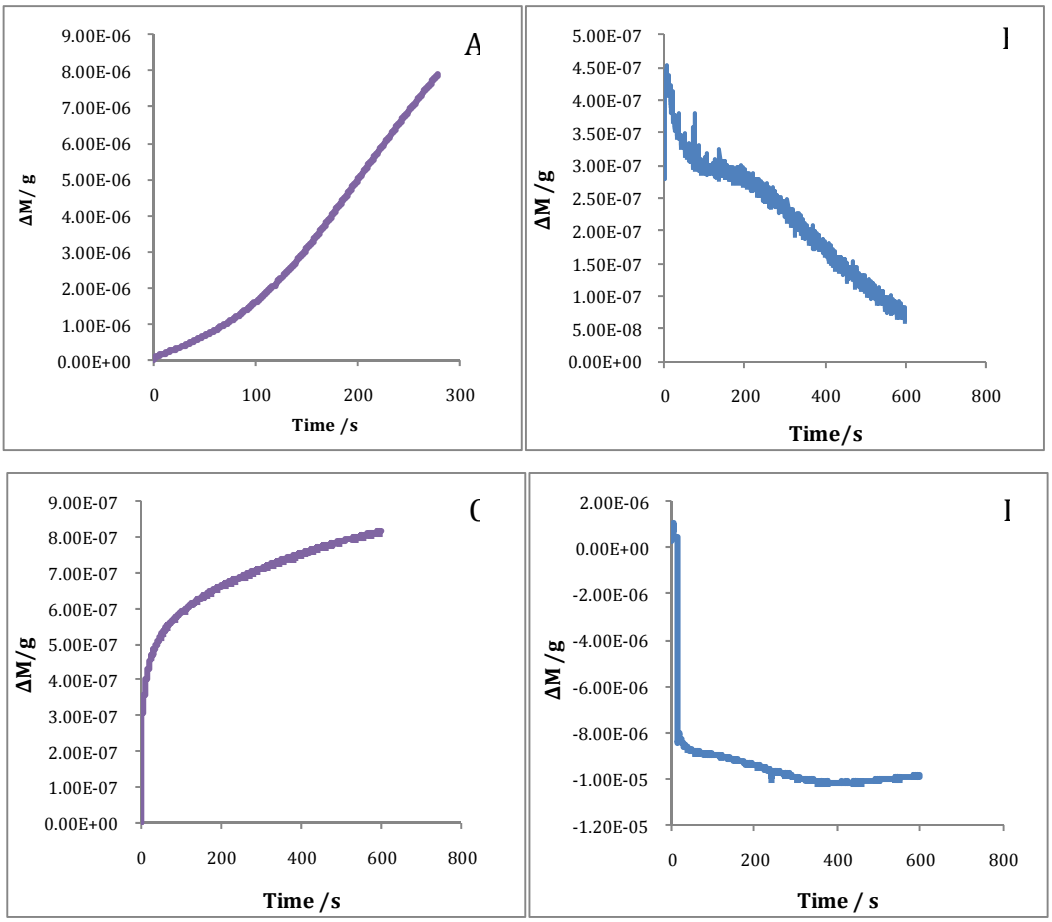

Figure 3.34: Mass-time plots recorded of the PPyDex film; **A** during deposition in the presence of 0.05 mol dm^{-3} NaDex and 0.20 mol dm^{-3} Py at +0.900 V vs SCE, **B** reduction of the polymer at –0.900 V vs SCE in the presence of 0.10 mol dm^{-3} NaCl, **C** oxidation of the polymer at +0.900 V vs SCE in 0.06 mol dm^{-3} NaDex and finally **D** reduction of the polymer again at –0.900 V vs SCE in the presence of 0.10 mol dm^{-3} NaCl.

3.3.4.5 Further controlling the release of the Dex^{2-}

As described in Chapter 1, Section 1.2, an ideal drug release device must fulfil two important requisites; firstly the ability to control the rate of release as a function of the applied potential and secondly the ability to switch 'on/off' the drug release[67]. It has already been demonstrated in Section 3.3.4.2 that the release of Dex^{2-} can be controlled by varying the applied potential. It was then investigated whether it was possible to stop and start the release of Dex^{2-} by applying oxidation and reduction potentials. To release the Dex^{2-}, a potential of –0.900 V vs SCE was applied, while a potential of +0.500 V vs SCE was applied with the aim of stopping the release. The release was switched on and off every 10 min for the 1st hour and every 20 min for the 2nd hour. Samples were taken every 5 min for the 1st hour and every 10 min for

the 2nd hour. The amount of Dex^{2-} measured over the 2 h period is shown in Figure 3.35. It is apparent that the release of Dex^{2-} is not completely stopped by applying an oxidation potential. Table 3.5 shows the amount of released Dex^{2-} measured during the switching 'on and off' periods. Although, drug release is not entirely prevented by the oxidation potential it is evident that the amount of Dex^{2-} released is considerably lower at the oxidation potential. The highest increase in release is obviously in the first 10 min followed by a small increase at the oxidation potential and a higher increase at the reduction potential. When the switching time is increased to 20 min, the amount of Dex^{2-} released at the reduction potential increases from 0.50 μmol cm^{-2} to 0.87 μmol cm^{-2}, while the amount of Dex^{2-} released on oxidation decreases from 0.40 μmol cm^{-2} to 0.26 μmol cm^{-2}.

Table 3.5: Increase in amount of Dex^{2-} measured when the release of Dex^{2-} is switched 'on and off' by applying reduction and oxidation potentials of –0.900 V vs SCE and +0.500 V vs SCE, respectively, in the presence of 0.10 mol dm^{-3} NaCl.

Time range/ min	Switched 'on/off'	Increase in Dex^{2-}release/μmol cm^{-2}
0-10	On	13.1
10-20	Off	0.20
20-30	On	0.59
30-40	Off	0.38
40-50	On	0.50
50-60	Off	0.40
60-80	On	0.87
80-100	Off	0.26
100-120	On	0.54

Lira *et al.*[67] reported the switching 'on/off' of Safranin release from a polyaniline-polyacrylamide (Pani/PAAM) composite in an acid solution and its effect on Safranin release was instant. This report suggests that conducting polymers on their own do not have the properties to ensure successful switching on and off of drug release and their ability to do so is due to the fact that the blend of hydrogels and conducting polymers changes the physical and chemical properties in the conducting polymer network. John and co-workers[68] also reported these effects in

a polypyrrole-polyacrylamide composite but found the kinetics of the redox switching processes to be much slower due to reduced ion mobility and/or decreased electronic conductivity within the blends. Nonetheless, the data reported here indicate that the switching 'on/off' of Dex^{2-} release from PPy can be achieved, to some degree, in that the release of the drug is slowed down substantially with the application of an oxidation potential.

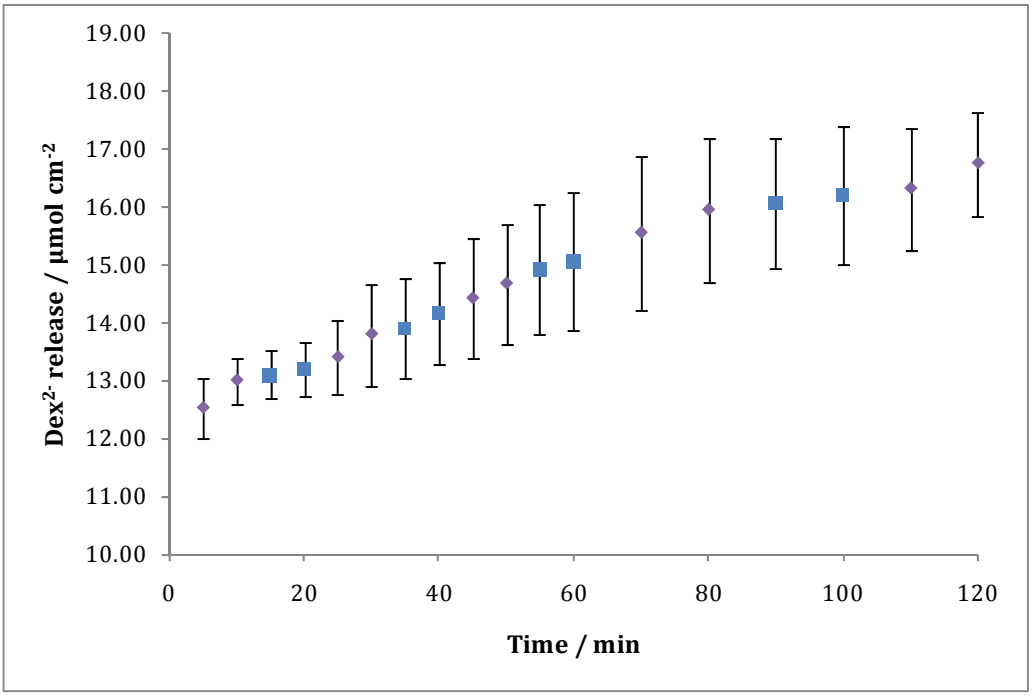

Figure 3.35: Amount of Dex^{2-} measured when the release was 'switched on' ♦ by applying a potential of –0.900 V vs SCE and 'switched off' ■ by applying a potential of +0.500 V vs SCE. It was switched on and off every 10 min for the 1st hour and every 20 min for the 2nd hour in the presence of 0.10 mol dm^{-3} NaCl. (n=2).

3.4 Summary of results

In this chapter, the successful incorporation and release of Dex^{2-} into and from a PPy membrane film and the characterisation of this film are presented and discussed. Four methods of depositing PPy doped with Dex^{2-} are discussed and in most cases the deposition of PPyDex was carried out in two steps. These methods involved a mixture of constant potential, cyclic voltammetry and depositing a pre-layer of PPyCl onto the electrode prior to deposition of PPyDex. The optimum method of polymerisation was found to be a two step-constant potential routine, whereby a constant potential of +0.900 V vs SCE was applied until 0.8 C cm^{-2} of

charge was consumed. This was then followed by further growth to 2.0 C cm^{-2} at +0.800 V vs SCE. The morphology of the PPyDex film was similar to PPyCl in that both exhibited the typical PPy characteristics of cauliflower-like and globular morphology although the surface of PPyCl was much rougher.

Using electrochemical impedance spectroscopy, it was found that upon formation, the PPyDex was stable and highly conducting, but lost conductivity when a reduction potential was applied. However, good stability was also observed under these reduction conditions. The redox properties were explored by CV and it was found that Dex^{2-} behaves like a medium-sized ion, which displays mixed ion exchange across the polymer film.

The amount of Dex^{2-} released was measured at several potentials from +0.100 V vs SCE to –1.200 V vs SCE over a period of 60 min. It was found that the rate of release was dependent on the potential applied. The fastest release occurred at an applied potential of –0.900 V vs SCE. It was calculated that approximately 89% of the drug was released after 1 h at this release potential, while approximately 17% was released at OCP.

Furthermore, it was possible to oxidise the reduced polymer so that further Dex^{2-} could be incorporated. These release/ incorporation experiments were carried out several times with the same polymer. EQCM measurements indicated that more Dex^{2-} was incorporated each time the oxidation potential was applied which implied that more PPy^{0} was oxidised back to PPy^{+}. Investigations into the possibility of switching 'on and off' the Dex^{2-} release, by applying oxidation and reduction potentials, were carried out. It was found that the rate of release was considerably mired with the application of an oxidation potential but the release of Dex^{2-} could not be completely prevented.

3.5 References

1. H. F. L. Meyer-Bahlburg, C. Dolezal, S. W. Baker, A. D. Carlson, J. S. Obeid, and M. I. New, *Journal of Clinical Endocrinology and Metabolism,* **89**:610 (2004).
2. Y.-X. Chen, Y. Wang, C.-C. Fu, F. Diao, L.-N. Song, Z.-B. Li, R. Yang, and J. Lu, *Endocrine- Related Cancer,* **17**:39 (2010).
3. N. Mayumi, T. Nobuyuki, M. Noriyuki, I. Takao, O. Hitoshi, and K. Mitsuhiro, *European Journal of Neuroscience,* **11**:1927 (1999).
4. K. L. Crossin, M.-H. Tai, L. A. Krushel, V. P. Mauro, and G. M. Edelman, *Proceedings of the National Academy of Sciences of the United States of America,* **94**:2687 (1997).
5. M. Luisa, N. Alessia, P. Elisabetta, G. Anita, P. Mauro, P. Luca, and L. Giulio, *British Journal of Pharmacology,* **126**:1307 (1999).
6. J. McCafferty, T. R. Brophy, J. D. Yelland, B. E. Cham, F. Bochner, and M. J. Eadie, *British Journal of Clinical Pharmacology,* **12**:434–436 (1981).
7. S. Tsuei, R. Moore, J. Ashley, and W. McBride, *Journal of Pharmacokinetics and Pharmacodynamics,* **7**:249 (1979).
8. M. F. D. Blake S. Wilson *Hearing Research* **242**:3–21 (2008).
9. R. T. Richardson, A. K. Wise, B. C. Thompson, B. O. Flynn, P. J. Atkinson, N. J. Fretwell, J. B. Fallon, G. G. Wallace, R. K. Shepherd, G. M. Clark, and S. J. O'Leary, *Biomaterials,* **30**:2614 (2009).
10. Laura Mora, Karin Y. Chumbimuni-Torres, Corbin Clawson, Lucas Hernandez, Liangfang Zhang, and J. Wang, *Journal of Controlled Release,* **140**:69 (2009).
11. A. Chang, H. Eastwood, D. Sly, D. James, R. Richardson, and S. O'Leary, *Hearing Research,* **255**:67 (2009).
12. W. Gstoettner, J. Kiefer, W.-D. Baumgartner, Stefan Pok, S. Peters, and O. Adunka, *Acta Otolaryngolica,* **124**:348 (2004).
13. C. Daron and B. Ronaldo, *The Laryngoscope,* **118**:1556 (2008).
14. A. N. Salt and S. K. R. Plontke, *Drug Discovery Today,* **10**:1299 (2005).
15. K. Takemura, M. Komeda, M. Yagi, C. Himeno, M. Izumikawa, T. Doi, H. Kuriyama, J. M. Miller, and T. Yamashita, *Hearing Research,* **196**:58 (2004).
16. W. Shain, L. Spataro, J. Dilgen, K. Haverstick, S. Retterer, M. Isaacson, M. Saltzman, and J. N. Turner, *Neural Systems and Rehabilitation Engineering, IEEE Transactions on,* **11**:186 (2003).
17. S. S. Lee, P. M. Hughes, and M. R. Robinson, *Current Opinion in Ophthalmology,* **20**:511 (2009).
18. J.-P. Sylvestre, R. H. Guy, and M. B. Delgado-Charro, *Physical Therapy,* **88**:1177 (2008).
19. M. Ni, J. Edelman, A. Gwon, and G. De Vries, *Invest. Ophthalmol. Vis. Sci.,* **46**:481 (2005).
20. S. Einmahl, M. Zignani, E. Varesio, J. Heller, J. L. Veuthey, C. Tabatabay, and R. Gurny, *International Journal of Pharmaceutics,* **185**:189 (1999).
21. R. N. Fedorak, B. Haeberlin, L. R. Empey, N. Cui, H. Nolen, L. D. Jewell, and D. R. Friend, *Gastroenterology,* **108**:1688 (1995).
22. G. Hochhaus, J. Barth, S. al-Fayoumi, S. Suarez, H. Derendorf, R. Hochhaus, and H. Mollmann, *Journal of Clinical Pharmacology,* **41**:425 (2001).

23. T. Loftsson, H. Sigurdsson, D. Hreinsdóttir, F. Konrádsdóttir, and E. Stefánsson, *Journal of Inclusion Phenomena and Macrocyclic Chemistry,* **57**:585 (2007).
24. T. N. Tozer, J. Rigod, A. D. McLeod, R. Gungon, M. K. Hoag, and D. R. Friend, *Pharmaceutical Research,* **8**:445 (1991).
25. M. Q. Zhou SY, Zhou J, Liu L, Li C, Zhao DH, *Acta Pharmaceutica Sinica,* **36**:325 (2001).
26. J. S. Kroin, R. B. Schaefer, and R. D. Penn, *Neurosurgery,* **46**:178 (2000).
27. R. Wadhwa, C. F. Lagenaur, and X. T. Cui, *Journal of Controlled Release,* **110**:531 (2005).
28. S. E. Moulton, M. D. Imisides, R. L. Shepherd, and G. G. Wallace, *Journal of Materials Chemistry,* **18**:3608 (2008).
29. G. Stevenson, S. E. Moulton, P. C. Innis, and G. G. Wallace, *Synthetic Metals,* **160**:1107 (2010).
30. M. Weise, *TA Instruments*.
31. http://www.sciencelab.com/msds.php?msdsId=9923684.
32. J. L. Anderson and I. Shain, *Analytical Chemistry,* **50**:163 (1978).
33. Y. Xiao, X. Cui, J. M. Hancock, M. Bouguettaya, J. R. Reynolds, and D. C. Martin, *Sensors and Actuators B: Chemical,* **99**:437 (2004).
34. X. Cui, J. F. Hetke, J. A. Wiler, D. J. Anderson, and D. C. Martin, *Sensors and Actuators A: Physical,* **93**:8 (2001).
35. E. Barsoukov and J. R. MacDonald, *Impedance Spectroscopy. Theory, Experiment and Applications.,*Wiley, 2005.
36. A. C. Fisher, *Electrode Dynamics* Oxford Science Publications 1996.
37. L. Formaro and S. Trasatti, *Analytical Chemistry,* **40**:1060 (1968).
38. S. Jing, T.-S. Jadranka, C. Shu Yi, L. Kwong Chi, and A. K. Paul, *Journal of Applied Polymer Science,* **111**:876 (2009).
39. J. Chengyou, Y. Fenglin, and Y. Weishen, *Journal of Applied Polymer Science,* **101**:2518 (2006).
40. P. M. M.R. Gandhi, G.M. Spinks, G.G. Wallace, *Synthetic Metals,* **73**:247 (1995).
41. C. Arbizzani, M. Mastragostino, L. Nevi, and L. Rambelli, *Electrochimica Acta,* **52**:3274 (2007).
42. P. L. Runnels, J. D. Joseph, M. J. Logman, and R. M. Wightman, *Analytical Chemistry,* **71**:2782 (1999).
43. T. Matencio, J. M. Pernaut, and EricVieil, *Journal of Brazilian Chemistry Society,* **14**:90 (2003).
44. I. Jureviciute, S. Bruckenstein, A. R. Hillman, and A. Jackson, *Physical Chemistry,* **2**:4193 (2000).
45. L. Sheng, Q. Yubing, and G. Xingpeng, *Journal of Applied Polymer Science,* **114**:2307 (2009).
46. B. D. Martin, J. Naciri, M. H. Moore, D. A. Lowy, M. A. Dinderman, E. C. Pehrsson, and B. Ratna, *Electrochemistry Communications,* **11**:169 (2009).
47. S. Brahim, D. Narinesingh, and A. Guisseppi-Elie, *Biosensors and Bioelectronics,* **17**:973 (2002).
48. V. Bavastrello, S. Carrara, M. K. Ram, and C. Nicolini, *Langmuir,* **20**:969 (2004).
49. S. M. Sayyah, S. S. A. El-Rehim, and M. M. El-Deeb, *Journal of Applied Polymer Science,* **90**:1783 (2003).

50. J. K. Pawel and A. C. James, *Electroanalysis,* **10**:73 (1998).
51. G. A. Snook and G. Z. Chen, *Journal of Electroanalytical Chemistry,* **612**:140 (2008).
52. G. Sauerbrey, *Zeitschrift für Physik,* **155**:206 (1959).
53. C. K. Baker and J. R. Reynolds, *Journal of Electroanalytical Chemistry,* **251**:307 (1988).
54. C. Debiemme-Chouvy, H. Cachet, and C. Deslouis, *Electrochimica Acta,* **51**:3622 (2006).
55. G. Maia, R. M. Torresi, E. A. Ticianelli, and F. C. Nart, *The Journal of Physical Chemistry,* **100**:15910 (1996).
56. E. Shouji, Y. Okamoto, F. Ozaki, and K. Naoi, *Polymers for Advanced Technologies,* **7**:177 (1996).
57. V. Syritski, A. Opik, and O. Forsen, *Electrochimica Acta,* **48**:1409 (2003).
58. M. Bazzaoui, L. Martins, E. A. Bazzaoui, and J. I. Martins, *Electrochimica Acta,* **47**:2953 (2002).
59. A. S. Liu and M. A. S. Oliveira, *Journal of Brazilian Chemistry Society,* **18**:143 (2007).
60. B. C. Thompson, S. E. Moulton, J. Ding, R. Richardson, A. Cameron, S. O'Leary, G. G. Wallace, and G. M. Clark, *Journal of Controlled Release,* **116**:285 (2006).
61. J. M. Ko, H. W. Rhee, S. M. Park, and C. Y. Kim, *J. Electrochem. Soc.,* **137** (1990).
62. N. C. T. Martins, T. M. e. Silva, M. F. Montemor, J. C. S. Fernandes, and M. G. S. Ferreira, *Electrochimica Acta,* **53**:4754 (2008).
63. A. F. Diaz, J. I. Castillo, J. A. Logan, and W.-Y. Lee, *Journal of Electroanalytical Chemistry,* **129**:115 (1981).
64. J.-M. Pernaut and J. R. Reynolds, *The Journal of Physical Chemistry B,* **104**:4080 (2000).
65. L. Li and C. Huang, *Journal of the American Society for Mass Spectrometry,* **18**:919 (2007).
66. D. H. Szarowski, M. D. Andersen, S. Retterer, A. J. Spence, M. Isaacson, H. G. Craighead, J. N. Turner, and W. Shain, *Brain Research,* **983**:23 (2003).
67. L. M. Lira and S. I. Córdoba de Torresi, *Electrochemistry Communications,* **7**:717 (2005).
68. B. C. Kim, G. M. Spinks, G. G. Wallace, and R. John, *Polymer,* **41**:1783 (2000).

Chapter 4

Incorporation and Controlled Release of a Medium Size Drug with Limited Solubility from Polypyrrole:

Diclofenac Sodium Salt

4.1 Introduction

Diclofenac belongs to the non-steroidal anti-inflammatory class of drugs (NSAID) and is one of the most effective of these in the treatment of musculoskeletal pain, such as arthritis and acute injury[1]. Trade names include Cataflam® and Difene®, which are supplied as potassium and sodium salts, respectively. In this chapter, the incorporation and controlled release of diclofenac sodium salt (NaDF), shown in Figure 4.1, is presented and discussed.

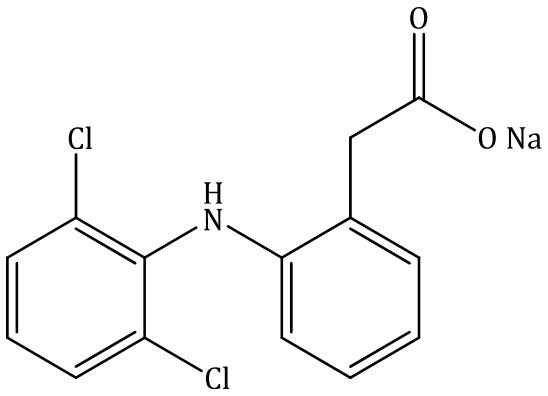

Figure 4.1: Diclofenac sodium salt (NaDF).

NaDF acts by inhibiting cyclooxygenase (COX), which is an enzyme that converts arachidonic acid into prostaglandins (PGs), thromboxanes and prostacyclins[2, 3]. The COX-1 isoenzyme is constitutively expressed in all tissues and its activation leads to the production of prostaglandins involved in maintenance of organ systems, such as, protection of the stomach wall or for kidney function[4]. The COX-2 is almost undetectable in most tissues under normal physiological conditions[5], but is induced when there is damage in the body, leading to the production of PGs. When pro-inflammatory cytokines are produced, COX-2 is expressed de novo in the inflamed tissue, resulting in PG formation, which mediates pain, fever and inflammation[6]. NSAID can inhibit both COX isoenzymes but NaDF demonstrates some selectivity towards COX-2 inhibition[6] and studies show that there is preferential uptake of the drug into inflamed tissue after a single oral dose[7]. It has also been shown that acidic NSAID preferentially accumulate in acidic compartments, such as the stomach, kidney and inflamed tissue. NaDF, with its carboxylic acid group, has a pKa of 4.0 and belongs to the class of weak acidic

drugs. It may show increased lipophilicity in acidic compartments, leading to higher concentrations in cell membranes[8].

The use of NSAID can also result in gastrointestinal toxicity in a large number of cases and is cited as a main side effect in the treatment of arthritis along with peptic ulcer and bleeding[9]. Although NaDF is one of the lesser toxic drugs in this class, these side effects emphasise the importance of the dose administered to the patient. NaDF is rapidly absorbed after oral administration, undergoes first-pass metabolism and the oral bioavailability of diclofenac ranges from 54-90 %[10]. It is also highly bound to serum protein, ≥ 99.5 %, and has a relatively low volume of distribution[10, 11] at 0.12 to 0.17 L kg^{-1}. Depending on the administered dose, studies on rats show that the maximum concentration, C_{max}, is reached within hours of ingestion and the half life ($t_{1/2}$) of the retention time is a couple of hours[12, 13], which is relatively short. Although it has a short $t_{1/2}$, NaDF is one of the more potent anti-inflammatory drugs and a dose as small as 1 mg kg^{-1} body weight is sufficient[14, 15].

From the literature, it is clear that the development of a device that could ensure the correct dose of NaDF to be delivered to a desired area of the body is imperative. For example, implanting such a device directly into the knee joint of an arthritis sufferer, would not only result in quick and effective pain relief, but would also circumvent the side effects mentioned above. Reports have documented that such drug delivery systems are being studied whereby NaDF can be encased in chitosan hydrogels[16], albumin microspheres[17] or agar beads[18]. However, in these systems the drug is not released in response to a trigger mechanism but at a steady rate over a given time. While time-dependent drug release may be suitable for some patients, it is not an ideal method to administer drugs and can lead to further issues with toxicity. Jain and co-workers[19] investigated the development of a transdermal delivery system for NaDF but again the same pitfalls exist for this type of delivery system.

In this work and chapter, it is demonstrated that the anionic DF^- can be incorporated within a polypyrrole (PPy) membrane film by way of doping and its release can be controlled electrochemically. These polymer films were

electrosynthesised and characterised using a number of techniques, including cyclic voltammetry (CV), electrochemical quartz crystal microbalance (EQCM), electrochemical impedance spectroscopy (EIS) and scanning electron microscopy (SEM). To the best of the author's knowledge, there are no reports in the literature of the electrochemical controlled release of DF^-.

4.2 Experimental

4.2.1 Materials

Diclofenac sodium salt (NaDF) was purchased from Sigma Aldrich and used as received. Pyrrole monomer (98%) was purchased from Aldrich and distilled prior to being used. All potentiostatic and CV experiments were carried out on a Solartron (Model SI 1285) potentiostat. All DF^- release studies were measured using a Varian Cary Series UV-vis spectrophotometer. EIS, EQCM and SEM were carried out using equipment described in Section 2.2.1.

4.2.1 Electrochemical experiments

The electrochemical cell was set up to use a platinum (Pt) wire as the auxiliary electrode. The PPy doped DF^- (PPyDF) films were formed in an aqueous electrolyte at 38 °C to increase the solubility of the DF^-. For these experiments a silver wire was used as the reference electrode, while for experiments at room temperature, a standard saturated calomel electrode (SCE) was used as a reference electrode. Unless otherwise stated, all other experiments were carried out at room temperature. Various substrates were tested as working electrodes including Pt, gold (Au) and glassy carbon (GC). During the release, all electrolytes were constantly stirred. As stated in Chapter 2, Section 2.5.1, a calibration curve for NaDF was obtained *via* UV-vis measurements and used to determine the amount of drug released. Diclofenac has a λmax of 276 nm. Techniques used in the characterisation of the polymer are described in Chapter 2, in Section 2.4.2.

4.3 Results and discussion

4.3.1 Properties of the drug

4.3.1.1 Stability

The electrochemical stability of the drug was investigated over a wide potential range, taking particular care to monitor any oxidation reaction, as carboxylic acids are well known to oxidise, but usually only at high anodic potentials[20]. CV was carried out on a bare Au electrode in 0.10 mol dm^{-3} NaDF and in phosphate buffer, pH 7.0, cycling between +0.000 V vs $Ag|Ag^+$ and +1.200 V vs $Ag|Ag^+$ at a scan rate of 50 mV s^{-1}. Similar data were recorded in a non-buffered 0.10 mol dm^{-3} NaCl. No supporting electrolyte was added to the NaDF solution so to avoid adsorption effects from the anions of the supporting electrolyte. The corresponding voltammograms are shown in Figure 4.2. In both cases there is redox activity at +0.700 V vs $Ag|Ag^+$ and +0.100 V vs $Ag|Ag^+$. This, however, is due to Au oxides and there is no evidence to suggest the oxidation of DF^-, even at the higher potentials of 1.200 V vs $Ag|Ag^+$.

The redox properties of Au in aqueous solutions are well documented[21, 22]. However, there is still some controversy over the exact events which occur during oxidation and the nature of the Au oxide, with AuO, $Au(OH)_2$ and Au_2O_3 all being proposed[23, 24]. An oxidation peak begins at approximately +0.700 V vs SCE which is initiated by adsorption of water and leads to the formation of AuOH, as can be seen in Equation 4.1. At more positive potentials, AuO, or chemisorbed AuO species, are formed in accordance with Equation 4.2. At this neutral pH, a reduction peak for AuO is commonly seen during the reverse sweep at +0.100 V vs SCE. These features are evident in Figure 4.2, indicating that the electrochemistry of Au is prevailing and the drug is stable and not susceptible to oxidation. Similar experiments were carried out at more negative potentials, between +0.700 to –1.200 V vs $Ag|Ag^+$. Again, the NaDF remained stable.

$$Au(H_2O) \rightarrow AuOH + e^- + H^+ \qquad 4.1$$

$$AuOH \rightarrow AuO + e^- + H^+ \quad 4.2$$

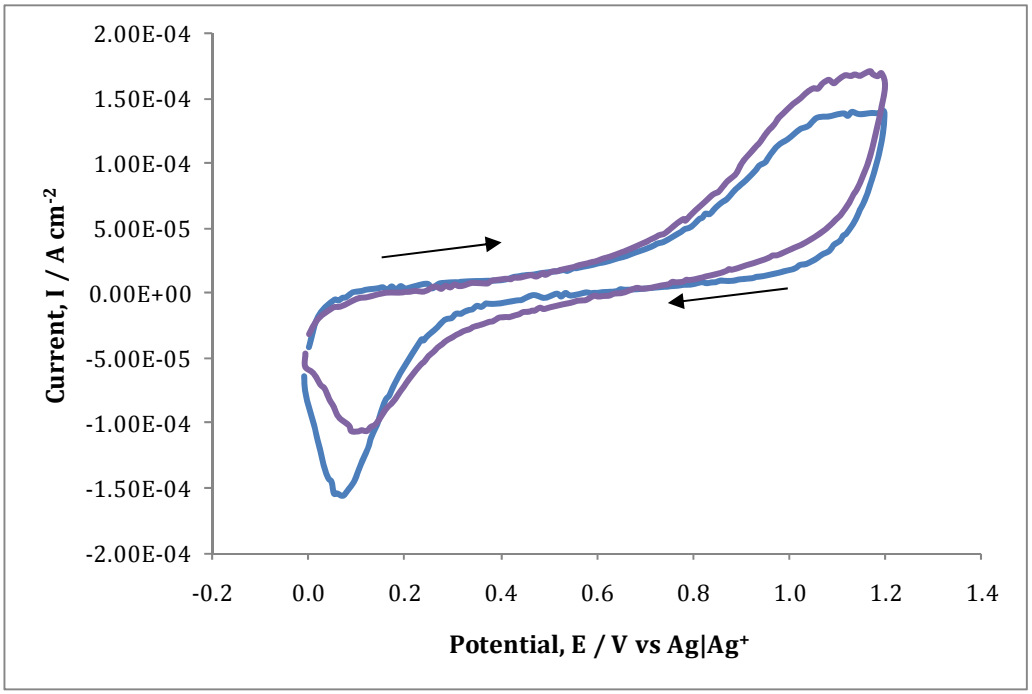

Figure 4.2: Cyclic voltammograms recorded for bare Au electrode in — 0.10 mol dm^{-3} NaDF and — phosphate buffer, pH 7.0, at 38 °C. The potential was swept between +0.000 V vs $Ag|Ag^+$ and 1.200 V vs $Ag|Ag^+$ at a scan rate of 50 mV s^{-1}.

4.3.1.2 Solubility

The solubility of NaDF in water is 1113 mg L^{-1} at room temperature [25]. As the anion is necessary to dope the PPy, the experimental conditions were chosen to give high concentrations of the anion. Furthermore, the anionic DF^- species is more soluble in water than the HDF species. The well-known Henderson Hasselbalch Equation was used to compute the % of anions in solution. NaDF is a strong salt and will be fully ionised in water, Equation 4.3. However, in the presence of H^+ the anionic DF^- is protonated and equilibrium between the neutral acid form, HDF, and the anionic DF^- exists, as shown in Equation 4.4. The dissociation of the neutral HDF molecule to the anionic form, DF^-, is described in Equation 4.5 and using this together with Equations 4.6, 4.7 and 4.8, the % of anionic DF^- can be found.

$$DF^-Na^+ \rightarrow DF^- + Na^+ \quad 4.3$$

$$DF^- + H^+ \rightleftharpoons HDF \quad 4.4$$

$$K = \frac{[DF^-][H^+]}{[HDF]} \quad 4.5$$

$$pH = pKa + \lg\frac{[DF^-]}{[HDF]} \quad 4.6$$

In this analysis, α is used to represent the degree of dissociation, where [HDF] = (1-α) and [DF^-] = [H^+] = α. Then Equation 4.6 can be rearranged to give Equations 4.7 and 4.8.

$$10^{pKa-pH} = \frac{1}{\alpha} - 1 \quad 4.7$$

$$\%[DF^-] = \frac{100}{1 + 10^{pKa-pH}} \quad 4.8$$

The influence of pH on the % of anions in solution is highlighted in Figure 4.3, where various pH values were substituted into Equation 4.8 and the % of anions was plotted as a function of pH. From Figure 4.3 it can be seen that HDF is predominantly neutral at low pH values but becomes more anionic in nature as the pH of the solution is increased. The pH of the NaDF-containing pyrrole (Py) solution is 7.4. At this pH, the % of DF^- anions in solution is 99 % and the equilibrium favours the anionic form of DF and no further adjustments to the pH were necessary.

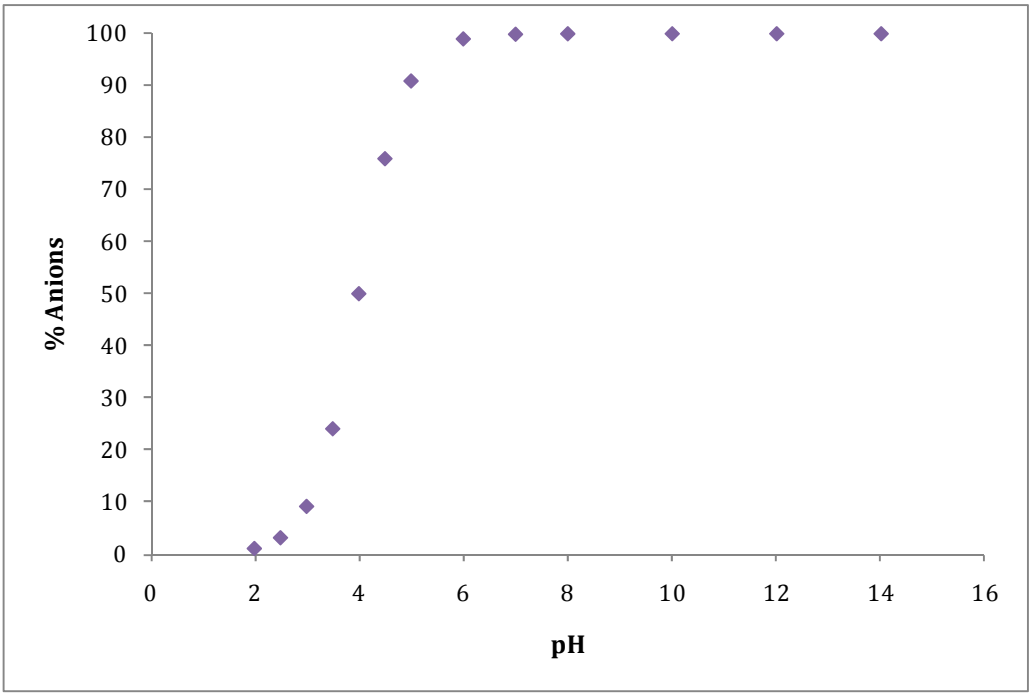

Figure 4.3: The percentage of anions as a function of pH of NaDF. The % of anions for the given pH was calculated by substituting various pH values into Equation 4.8.

4.3.2 Electrodeposition of the polymer

4.3.2.1 Initial attempts following the optimum conditions for PPyDex

As described in Chapter 3, a film of PPy doped with Dex^{2-} can be deposited by applying a constant potential in the presence of 0.05 mol dm^{-3} NaDex and 0.20 mol dm^{-3} Py using Pt as the working electrode. Under the same conditions, constant potentials of +0.700 V vs SCE, +0.800 V vs SCE and +0.900 V vs SCE were applied in an attempt to electrosynthesise PPy doped with DF^- anions. Figure 4.4 shows the resulting potentiostatic plots, with both the recorded current and charge plotted as a function of the electropolymerisation period. Upon application of the potential, there is an initial charging current, which arises from the charging of the double layer. This charging current decays rapidly. After 10 s there is an increase in current but within 100 s it begins to decrease and continues to drop reaching approximately 4.6 x 10^{-5} A cm^{-2} at 900 s. Although the initial increase in current suggests oxidation of the monomer and deposition of the polymer, the decrease in current thereafter indicates that further polymerisation does not occur. The applied potential seems to have little influence on the rate of electropolymerisation. Indeed, the charge is slightly lower at the higher potential

of +0.900 V vs SCE. This is somewhat unusual as the applied potential is well known to influence the rate of electropolymerisation and this has been well documented in the literature[26-28].

From visual inspection of the electrode it appeared that the polymer had deposited on some areas of the electrode but growth was not uniform over the whole electrode surface. A number of parameters were varied in an attempt to deposit a uniform and adherent PPyDF film. These are described in Sections 4.3.2.2, 4.3.2.3 and 4.3.2.4.

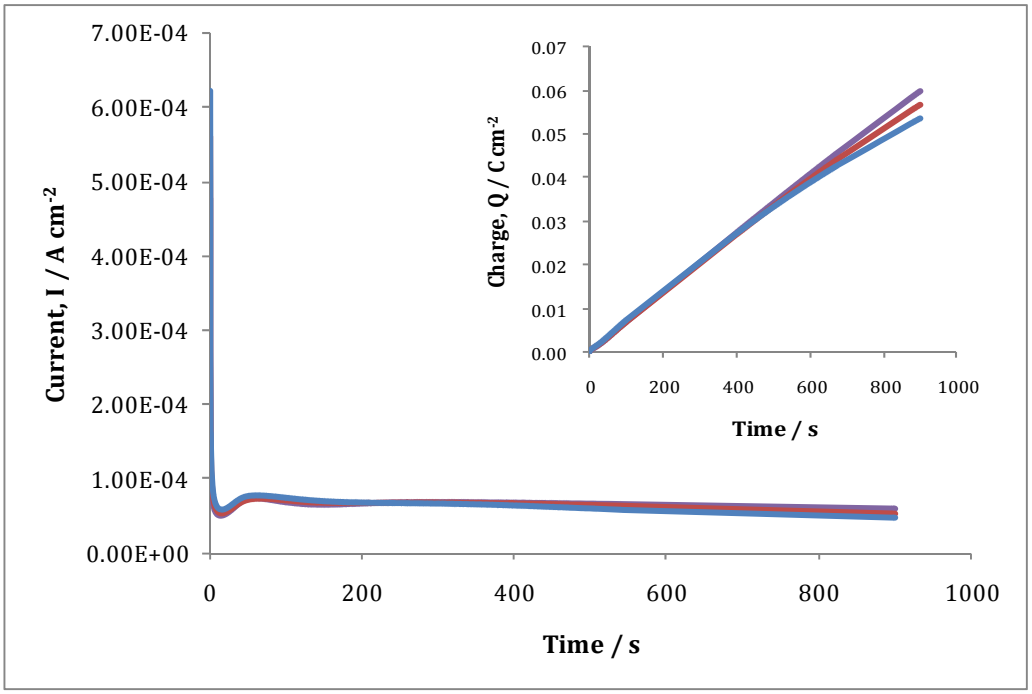

Figure 4.4: Current-time plots recorded at Pt in the presence of 0.05 mol dm^{-3} NaDF and 0.20 mol dm^{-3} Py, at — +0.700 V vs SCE, — +0.800 V vs SCE and — +0.900 V vs SCE. Inset: Corresponding charge-time plots. Experiments were carried out at room temperature (RT).

4.3.2.2 Influence of concentration of NaDF on the growth of the polymer

The concentration of NaDF was increased to 0.10 mol dm^{-3}, however, at this concentration the solubility limit of DF^{-} in water at room temperature was exceeded. The solution was heated to 50 °C in a water bath to increase the solubility of DF^{-}. At 50 °C, the DF^{-} was sufficiently soluble to give a 0.10 mol dm^{-3} solution. The conductivity of the electrolyte was measured and compared to that of

0.10 mol dm^{-3} NaCl to ensure it was a suitable electrolyte. A conductivity measurement of 4.40 mS was established for 0.10 mol dm^{-3} NaDF, while the conductivity of 0.10 mol dm^{-3} NaCl was found to be 8.76 mS. This indicates that the NaDF electrolyte is indeed appropriate for electrochemistry and sufficiently conducting. This is in good agreement with the calculated percentage of DF^- anions (99 %) in solution at a pH of 7.4, Section 4.3.1.2. At temperatures of 50 °C, a SCE reference electrode is not suitable and for this reason Ag wire was used as the reference electrode for all further polymerisation experiments.

The potentiostatic current-time and charge-time plots for the formation of PPyDF at the Pt electrode at various concentrations of NaDF; 0.10 mol dm^{-3}, 0.15 mol dm^{-3} and 0.20 mol dm^{-3} is shown in Figure 4.5. A constant potential of +0.900 V vs $Ag|Ag^+$ was applied and the solution temperature was maintained at 50 °C. At all three concentrations, similar currents are reached by 400 s, approximately 1.6 x 10^{-4} A cm^{-2}, which suggests that similar levels of polymerisation takes place.

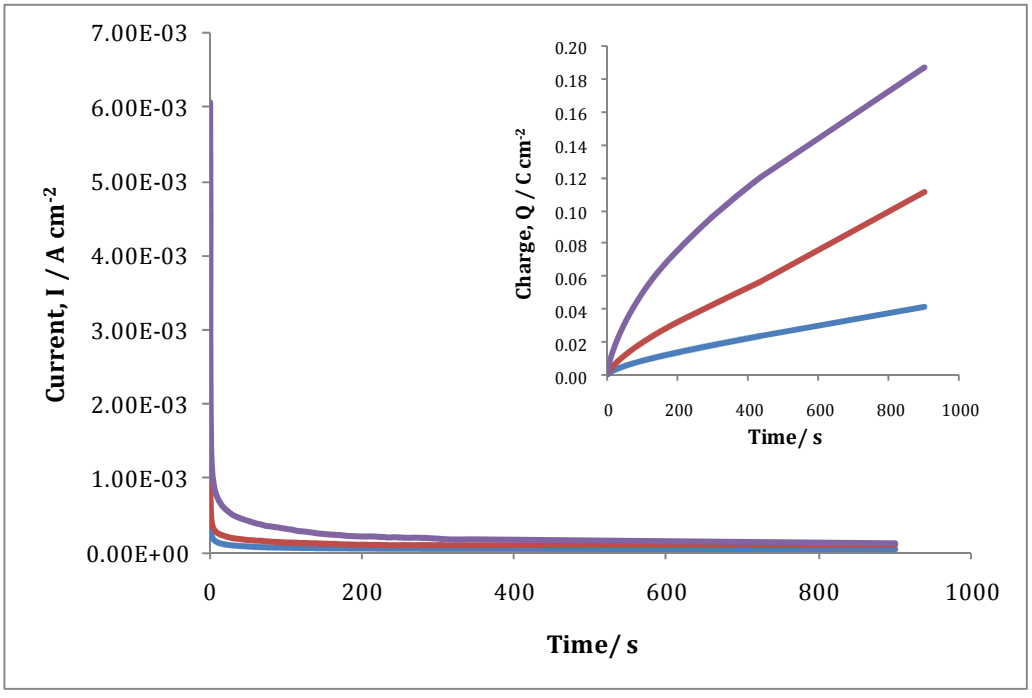

Figure 4.5: Potentiostatic plots recorded during the formation of PPyDF at +0.900 V vs $Ag|Ag^+$ in — 0.10 mol dm^{-3}, — 0.15 mol dm^{-3} and — 0.20 mol dm^{-3} NaDF in the presence of 0.20 mol dm^{-3} Py. Inset: Corresponding charge-time plots. Experiments were carried out at 50 °C.

From the charge-time plot shown in the inset of Figure 4.5, it appears that at the lowest NaDF concentration the PPyDF reaches the highest charge. Again, this is somewhat different to the majority of reports which show an increase in the rate of electropolymerisation with increasing concentrations of dopant[29, 30]. However, the data in Figure 4.5 may be related to the solubility of the drug. At the higher concentrations, the solubility limit of the drug at the polymer-solution interface is easier to exceed, leading to the precipitation of the drug at the polymer interface and a decrease in the rate of polymer growth.

It is clear from a comparison of Figure 4.4 and Figure 4.5 that there is an increase in the rate of polymerisation at the higher temperature. Although the currents seen in Figure 4.5 are higher than those in Figure 4.4, the electrode was not fully covered with polymer. Since increasing the concentration did not result in adequate polymerisation, attention was turned to the nature of the working electrode.

4.3.2.3 Influence of the nature of the working electrode

Polymerisation at Au and GC electrodes was then attempted by applying +0.700 V vs $Ag|Ag^{+}$ in the presence of 0.10 mol dm^{-3} NaDF and 0.20 mol dm^{-3} Py at 50 °C and the potentiostatic plots recorded are shown in Figure 4.6. The same pattern is seen in all three plots in that there is an increase in the current, between about 50 and 400 s, which indicates polymerisation, followed by a sharp decrease before the currents plateau. The GC showed the best promise for successful polymerisation; however, it was very difficult to measure visually how much polymer was present and whether it was deposited evenly across the polymer. For that reason, the Au electrode was chosen as the working electrode in all further experiments.

It should be noted that a decrease in redox properties of PPy is observed as the temperature increases[31]. Although the rate of the electropolymerisation reaction is increased with increasing temperatures, the PPy that is deposited on the electrode is more likely to become over-oxidised and this has an insulating effect which hinders the further growth the PPy. Therefore, 50 °C is not an ideal temperature

for executing electrochemical experiments and the temperature of the solution was lowered. The lowest temperature that could be reached before DF^- fell out of the bulk solution was 38 °C and all further polymerisation experiments were carried out at this temperature.

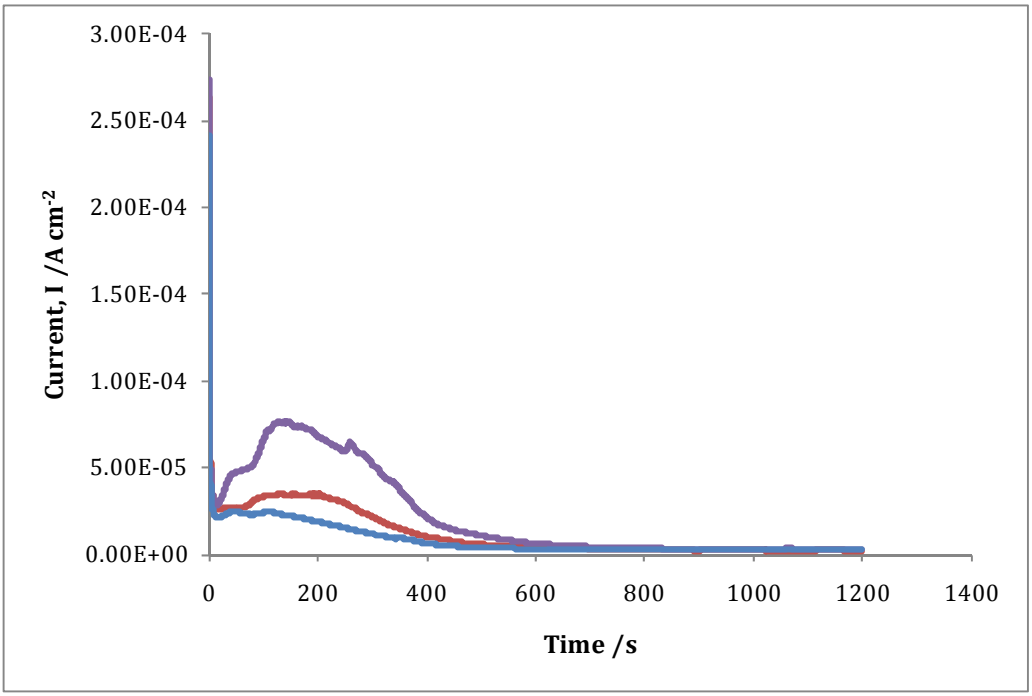

Figure 4.6: Potentiostatic plot of the growth of PPyDF at +0.700 V vs SCE in the presence of 0.10 mol dm^{-3} NaDF and 0.20 mol dm^{-3} Py using working electrodes of — GC, — Au and — Pt. Experiments were carried out at 50 °C.

4.3.2.4 Two-step polymerisation-PPyCl film and constant potential

In view of the fact that very little polymer was deposited on the bare electrode, a method that was employed during the electrosynthesis of PPyDex was used. This method is described in Section 3.3.2.4 and involves the electrodeposition of a film of PPy doped with Cl^-, at +0.700 V vs SCE in the presence of 0.10 mol dm^{-3} NaCl and 0.20 mol dm^{-3} Py, prior to the deposition of the PPy doped with Dex^{2-}. In this case, the PPy doped with Cl^- (PPyCl) was deposited to a charge of 0.70 C cm^{-2} and the PPy doped with DF^- was deposited by applying a constant potential for 20 min. Longer polymerisation times were not used as this could lead to the over-oxidation of the deposited polymer.

Figure 4.7 shows the current-time plots and the corresponding charge-time plots recorded when the PPyDF film was deposited on a PPyCl film by applying potentials of +0.800 V vs $Ag|Ag^+$ and +0.900 V vs $Ag|Ag^+$ in the presence of 0.10 mol dm^{-3} NaDF and 0.20 mol dm^{-3} Py. The currents for the polymerisation at +0.800 V vs $Ag|Ag^+$ are slightly higher. It is also clear from the charge-time plots that the polymer formed at +0.800 V vs $Ag|Ag^+$ has a charge twice as high as that grown at +0.900 V vs $Ag|Ag^+$. This indicates that more polymer is deposited at +0.800 V vs $Ag|Ag^+$. All further polymerisation experiments were carried out at +0.800 V vs SCE. The charge-time plots, shown in Figure 4.7B, are not typical of the growth behaviour seen for PPy deposited from simple electrolytes[32-34]. For the initial growth of the polymer, the rate of polymerisation is constant, at 2.5 x 10^{-4} C cm^{-2} s^{-1}, but it then begins to deviate away from this constant rate which suggests the rate of polymerisation decreases. This type of growth pattern is seen in insulating polymers[35, 36] and suggests changes in the conductivity of the deposited polymer with continued electropolymerisation. It is also evident that the loss in conductivity is greater at the higher potential of +0.900 V vs $Ag|Ag^+$.

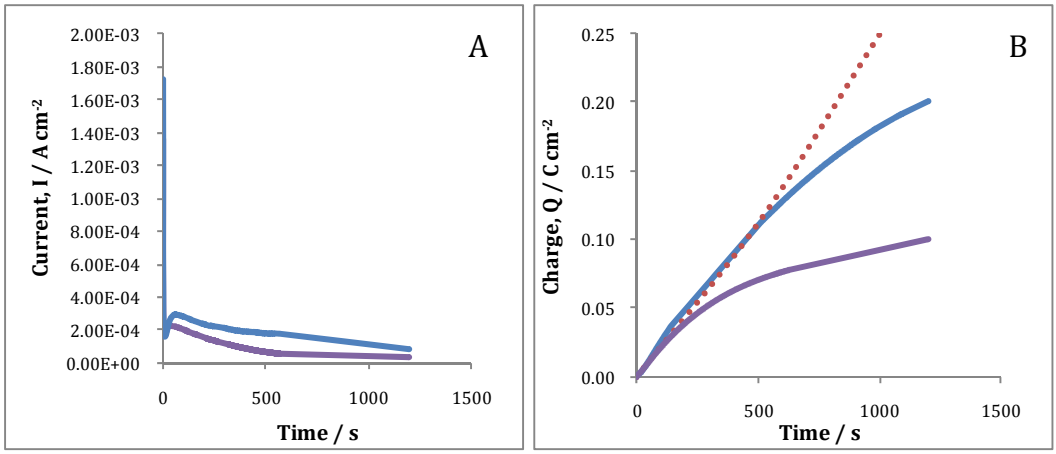

Figure 4.7: A Current-time plots and **B** charge-time plots recorded in the presence of 0.10 mol dm^{-3} NaDF and 0.20 mol dm^{-3} Py at — +0.800 V vs $Ag|Ag^+$ and — +0.900 V vs $Ag|Ag^+$. The charge-time growth profiles deviate away from the initial rate of polymerisation (▪▪▪). The PPyDF was deposited onto a film of PPyCl deposited to a charge of 0.70 C cm^{-2} on a Au electrode at +0.700 V vs SCE. Deposition of PPyDF was carried out at 38 °C.

4.3.3 Characterisation of the polymer

4.3.3.1 Redox properties of the PPy doped with DF determined by CV

The redox properties of the PPy doped with DF^- were probed using cyclic voltammetry (CV). As discussed in Section 3.3.3.2, a slow scan rate and low pH provide auspicious conditions under which CVs can be carried out[37-39]. The potential was swept between –1.200 V vs SCE and +0.700 V vs SCE at a scan rate of 25 mV s^{-1} in the presence of 0.10 mol dm^{-3} NaCl at pH ~ 3.0. Figure 4.8 shows the resulting cyclic voltammograms recorded over 20 cycles. There is a broad reduction peak extending between –0.400 V vs SCE and –1.000 V vs SCE and there is also evidence of an oxidation peak at similar potentials on the forward cycle. The polymer remains reasonably stable over the 20 cycles with little change in the voltammograms with continuous cycling.

CV was carried out at different scan rates on the PPyCl film on which the PPyDF film was deposited and typical voltammograms are shown in Figure 4.9. This PPyCl film deposited on the Au electrode is similar to the PPyCl film polymerised on Pt electrode discussed in Section 3.3.3.2 and shows distinct oxidation and reduction peaks at about +0.100 V vs SCE and –0.070 V vs SCE, respectively. By comparing Figure 4.8 and Figure 4.9, it is obvious that the presence of PPyDF is inhibiting the electrochemistry of the polymer. This is probably related to the crystal-like structures on the surface of the polymer, which form an insulating layer.

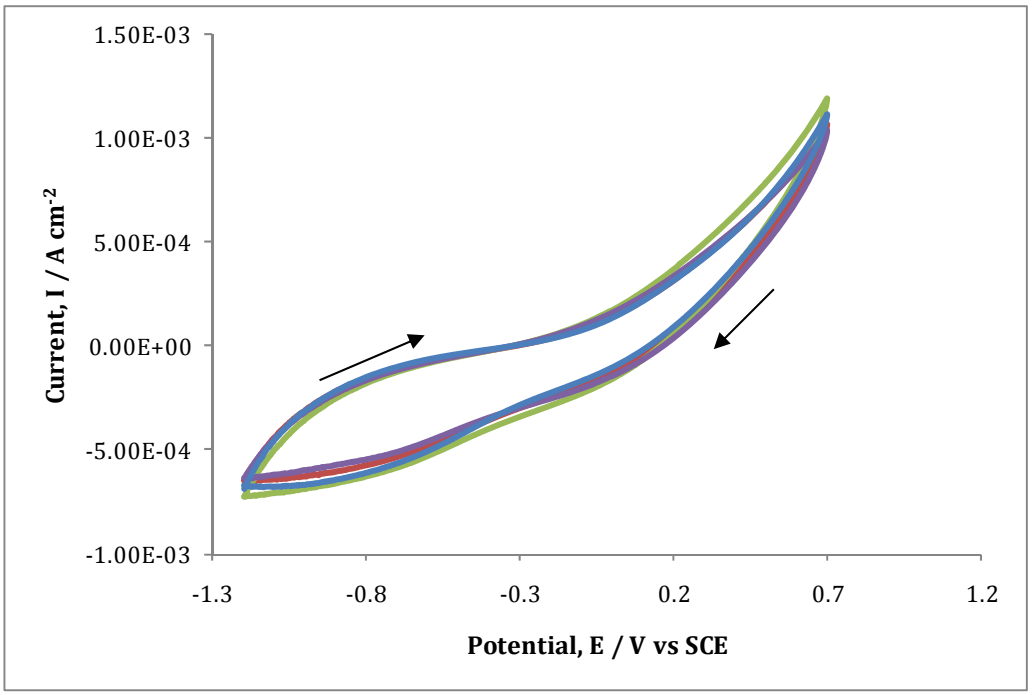

Figure 4.8: Cyclic voltammograms recorded for PPyDF in 0.10 mol dm^{-3} NaCl, pH~3.0. The potential was swept between –1.200 V vs SCE and +0.700 V vs SCE at 25 mV s^{-1} for 20 cycles; — cycle 5, — cycle 10, — cycle 15 and — cycle 20. The PPyDF was deposited on a thin film of PPyCl on an Au electrode in 0.10 mol dm^{-3} NaDF and 0.20 mol dm^{-3} Py at 38 °C.

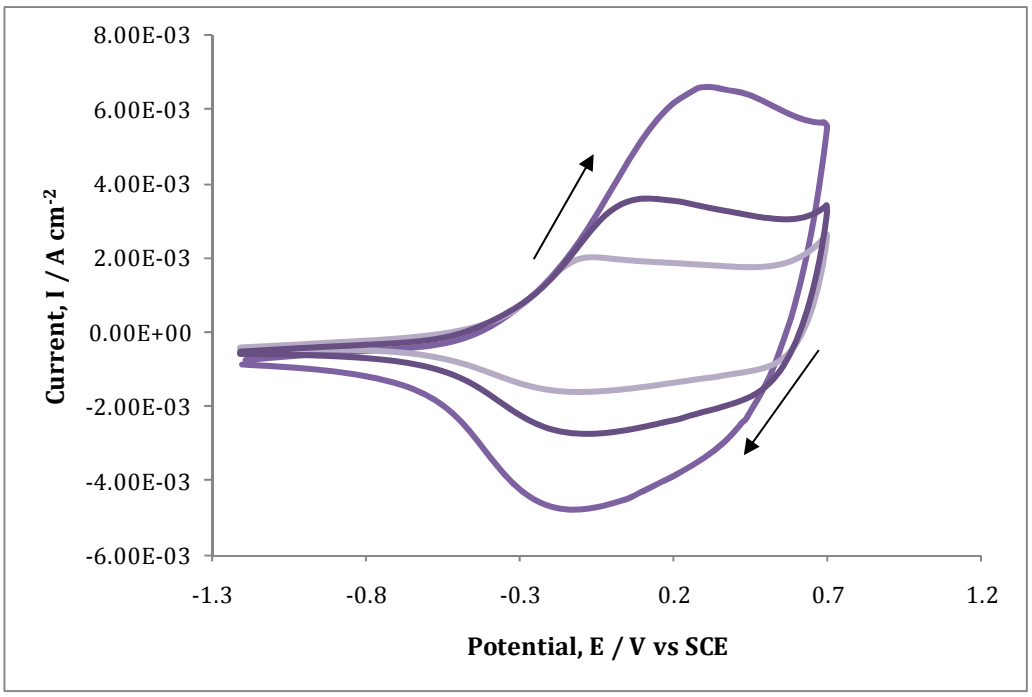

Figure 4.9: Cyclic voltammograms, 20th cycle, of PPyCl in the presence of 0.10 mol dm^{-3} NaCl, pH~3.0. The potential was swept between –1.200 V vs SCE and +0.700 V vs SCE at —

25 mV s^{-1}, — 50 mV s^{-1} and — 100 mV s^{-1}. The PPyCl was deposited at +0.700 V vs SCE to a charge of 0.70 C cm^{-2} at RT.

4.3.3.2 Redox properties of PPyDF explored by EQCM

EQCM measurements were then utilised to examine the change in mass during the switching of the polymer in 0.10 mol dm^{-3} NaCl. It should be noted that for these experiments, the electrolyte could not be kept at a constant temperature of 38 °C but was heated to a temperature of 50 °C before it was transferred into the EQCM cell. As the polymerisation took less than 5 min to occur, the drug remained in solution while the polymer was being deposited. The PPyDF polymer was deposited directly onto the Au on the quartz crystal as the presence of the PPyCl polymer resulted in the film being too thick and accordingly deviations from the Sauerbrey equation, Equation 2.2, were seen.

It has been demonstrated that viscoelasticity effects become dominant and lead to changes in the resulting frequency of the crystal when a conducting polymer film exceeds a thickness of about 500 nm[40]. In order to apply the Saurbrey equation the film must exhibit rigidity and perfect elasticity. These approximations are valid provided the film thickness is small compared to the thickness of the crystal. Accordingly, in these studies, the PPyDF was deposited directly onto the Au quartz crystal electrode until a charge of 1.20 x 10^{-2} C was consumed. The equation used to calculate the theoretical mass does not take into account solvent participation and it also assumes the current efficiency for the electropolymerisation of the monomer is 100 % [41].

Both the cyclic voltammogram recorded at 4.0 mV s^{-1}, cycle 3, and the corresponding mass changes are shown in Figure 4.10. The redox properties of the polymer are more apparent in Figure 4.10 than in Figure 4.8. A clear oxidation peak can be seen at +0.400 V vs $Ag|Ag^{+}$ and the reduction peak is evident at – 0.500 V vs $Ag|Ag^{+}$. The lower scan rate of 4.0 mV s^{-1} is responsible for this shift in redox properties[37]. In addition, the currents shown in Figure 4.10 are lower, indicating different quantities of deposited polymer, which in turn will affect the ease of oxidation and reduction of the deposited PPyDF film. Indeed, the reduction

peak of the PPyDF film deposited to higher charges, Figure 4.8, extends over a much wider potential range, from about –0.400 V vs SCE and –1.200 V vs SCE, compared to that observed for the thinner PPyDF film in Figure 4.10. Furthermore, as discussed earlier, the insoluble shards of drug dispersed throughout the thicker polymer film reduces the electrochemical activity of the film considerably.

The current as well as the mass change were recorded simultaneously, while the potential was swept from –1.000 V vs Ag|AgCl to +0.800 V vs Ag|AgCl. It is evident that there is an increase in mass during the oxidation of the polymer which corresponds to the uptake of anions. The increase in mass is observed at –0.100 V vs Ag|AgCl and continues until +0.800 V vs Ag|AgCl. It is also apparent that during the reduction scan there is a decrease in mass. This corresponds to the loss of the DF^- from the polymer. The decrease in mass is witnessed at –0.200 V vs Ag|AgCl and continues until the end of the reduction cycle, at –1.000 V vs Ag|AgCl. This decrease in mass corresponds to an estimated 1.73×10^{-9} moles of DF^-. There is also a decrease in mass during the forward oxidation scan from –1.000 V vs Ag|AgCl to +0.000 V vs Ag|AgCl as the polymer is still in the reduced state from the previous cycle. It can be seen that the rate of mass increase is lower than the rate of mass decrease which highlights the fact that the reduction process is faster than the oxidation process. This, in turn, gives rise to an overall loss, of about 0.6 μg, in the total mass of the film during one cycle.

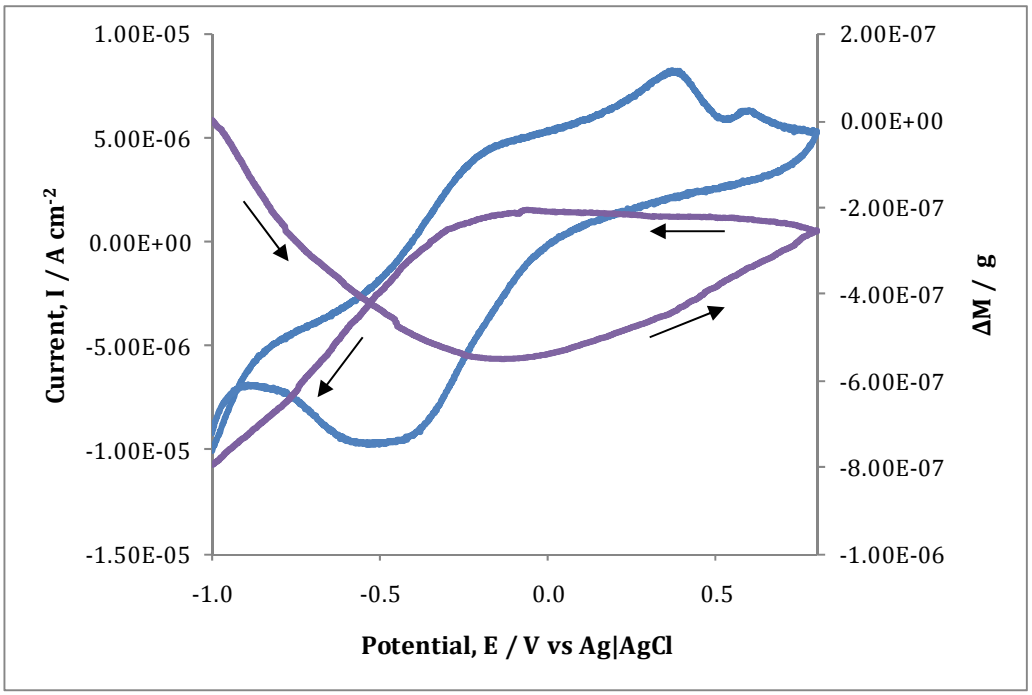

Figure 4.10: CV data (cycle 3) recorded for — the current and — the mass change as a function of potential obtained for a PPyDF film cycled in 0.10 mol dm^{-3} NaCl. The potential was swept from –1.000 V to +0.800 vs Ag|AgCl at a scan rate of 4.0 mV s^{-1}. (Area = 0.125 cm^2).

4.3.3.3 Morphology of the polymer

In order to obtain information on the morphology of the PPyDF film, optical imaging techniques were performed. The films were first synthesised, washed thoroughly with distilled water to ensure the removal of any DF^- on the surface of the polymer and dried by exposure to a gentle air flow for 30 s. When the polymer was dry, it was noted that it was no longer black but was greyish in appearance. Figure 4.11 shows the optical images recorded and it is apparent that there are crystal-like shards on the surface of the polymer. This was thought to be simply due to drug crystals lying on the surface of the polymer as a result of the polymer not being washed sufficiently. More care was taken in rinsing the polymer thoroughly and SEM micrographs were obtained of both the PPyCl film on which the PPyDF was deposited and the PPyDF film itself. The micrograph of PPyCl is shown in Figure 4.12 and is very similar to PPyDex and PPy morphology in general with the cauliflower-like surface[42-44]. However, the micrograph of PPyDF, seen in Figure 4.13 shows a distinctly different morphology. The crystal-like shards, which

were seen under the microscope and were presumed to be due to insufficient washing, are actually part of the morphology of the polymer. Micrographs taken at higher magnification display how the polymer grows in between the crystals. The cauliflower-like morphology of PPy is still evident between crystals, but the surface morphology is dominated by the crystals. These crystal-like shards and splints have not been reported in the literature in relation to the morphology of PPy.

SEM micrographs taken after a reduction potential was applied for 60 min show that these crystals have been removed. This can be seen in Figure 4.14. In previous studies, the cauliflower morphology of PPyDex was still present after the reduction potential was applied; however, it seems that in the presence of the reduction potential the PPyDF polymer surface is modified considerably. It seems that these crystals are large insoluble forms of the drug that are entrapped within the polymer matrix and give rise to the greyish colour of the polymer. Indeed, this may also explain the difficulty encountered during polymerisation and the unusual potentiostatic plots that were recorded, showing a decrease in the rate of electropolymerisation with increasing concentrations of DF^- and increasing applied potentials. The presence of these crystals in the polymer and on its surface decreases the conductivity of the film and thus affects the rate of polymerisation. The appearance of the polymer is very different after a reduction potential is applied as these crystal drug molecules are dissolved and released from the surface.

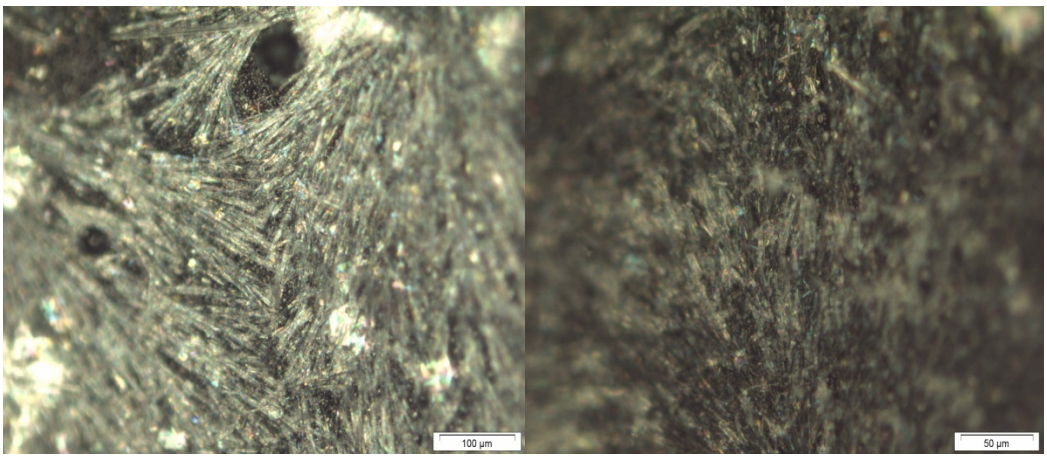

Figure 4.11: Optical images of PPyDF on a Au disc electrode. Polymers were electrochemically deposited in the presence of 0.10 mol dm^{-3} NaDF and 0.20 mol dm^{-3} Py at +0.800 V vs SCE for 20 min at 38 °C. The PPyDF was deposited on a PPyCl film which was 0.70 C cm^{-2} in charge.

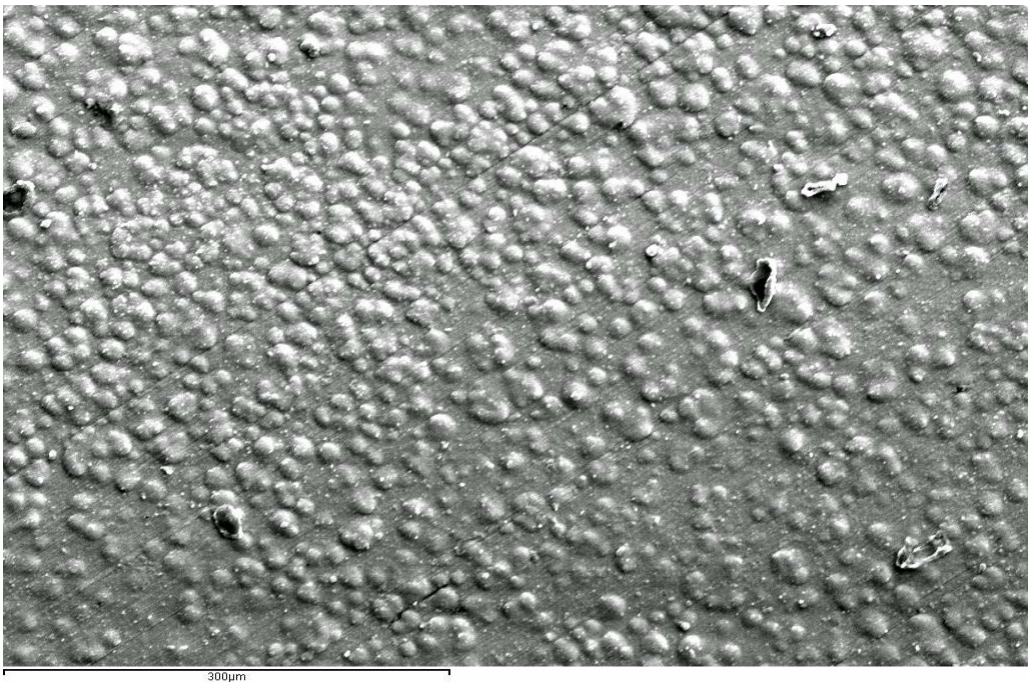

Figure 4.12: SEM micrograph of PPyCl on Au disc electrode. The film was electrodeposited in the presence of 0.10 mol dm^{-3} NaCl and 0.20 mol dm^{-3} Py at RT. A potential of +0.700 V vs SCE was applied until a charge of 0.70 C cm^{-2} was consumed.

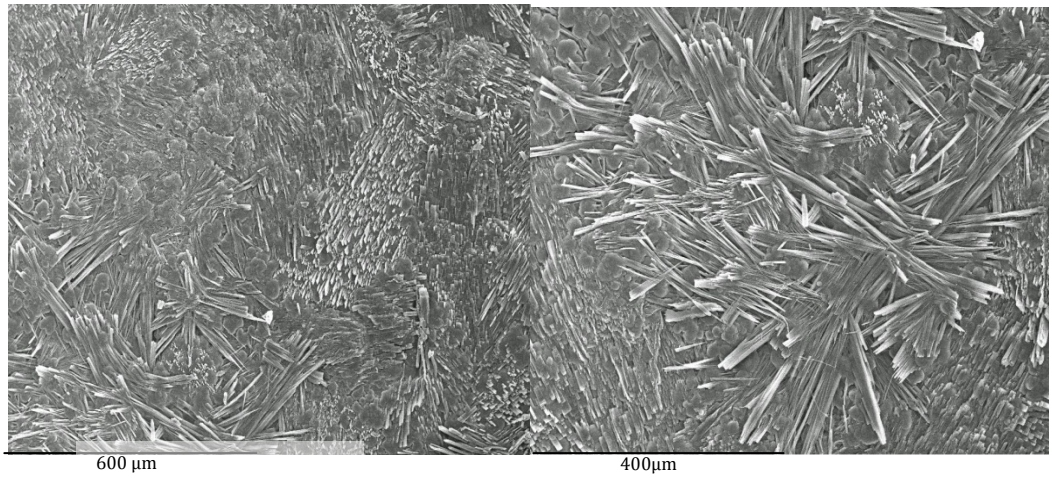

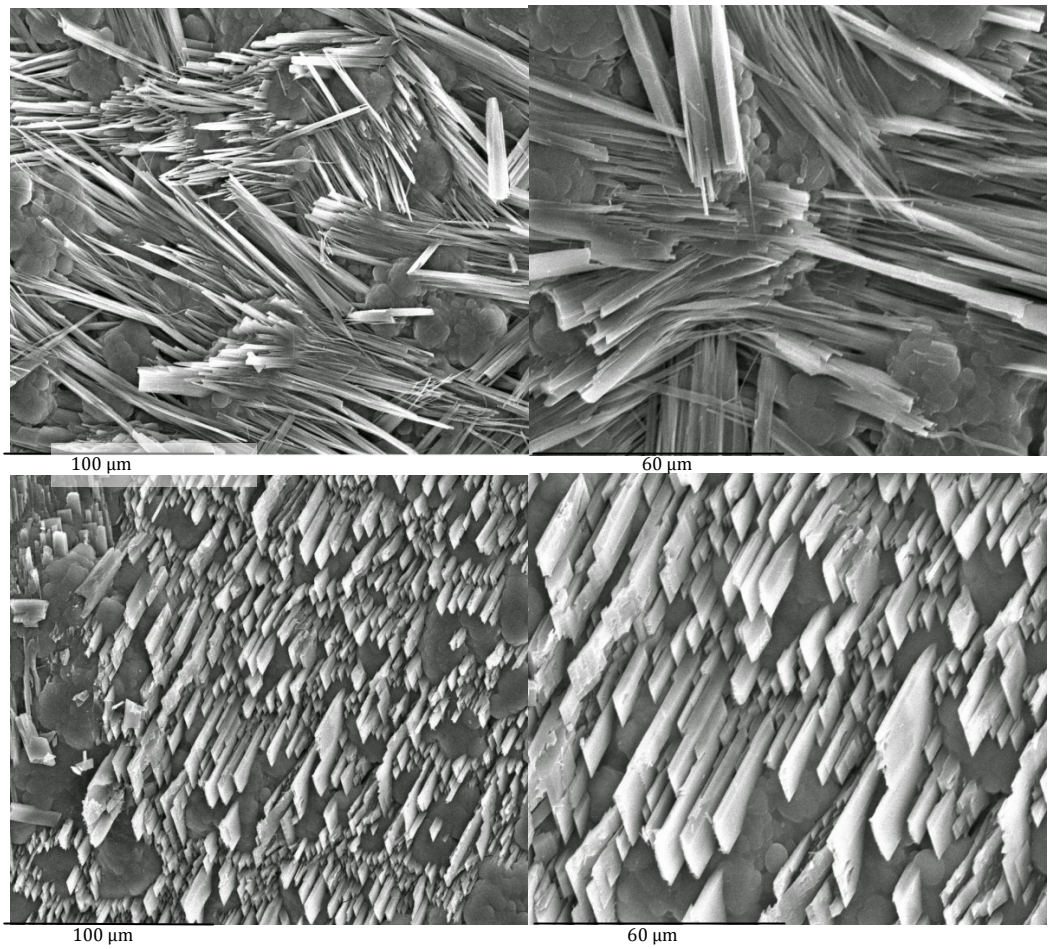

Figure 4.13: SEM micrographs of PPyDF electrodeposited onto a film of PPyCl on a Au disc electrode. PPyDF was electrosynthesised in the presence of 0.10 mol dm^{-3} NaDF and 0.20 mol dm^{-3} Py at 38 °C. A potential of +0.800 V vs $Ag|Ag^{+}$ was applied for 20 min at 38 °C.

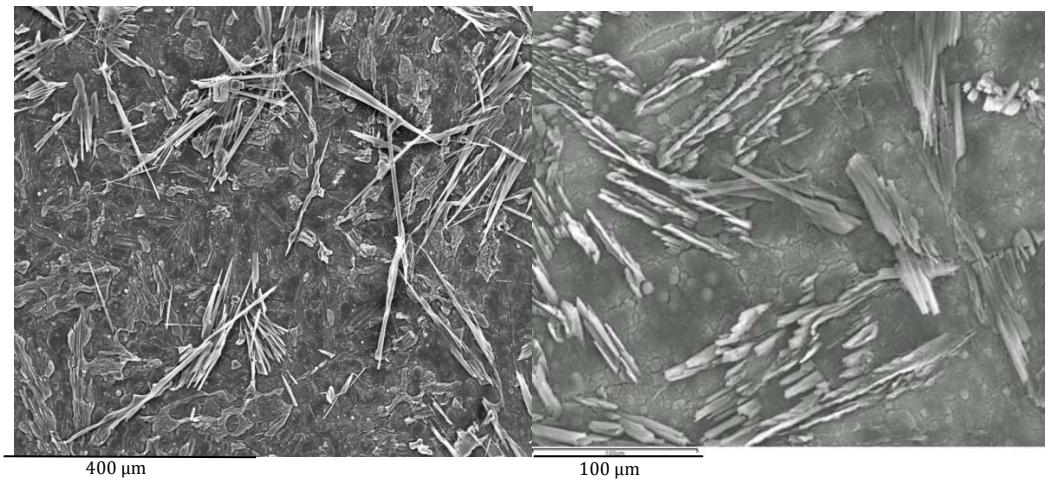

Figure 4.14: SEM micrographs of PPyDF after a potential of –0.700 V vs SCE was applied for 60 min in the presence of 0.10 mol dm^{-3} NaCl at RT.

4.3.3.4 Polymer characterisation by EIS

The polymer was grown as previously described on a film of PPyCl (0.70 C cm^{-2} in charge) on a Au electrode at a constant potential of +0.800 V vs SCE for 20 min. EIS was carried out at –0.900 V vs SCE and at open-circuit potentials (OCP). By undertaking impedance measurements at these potentials, the properties of the polymer could be investigated under conditions used to release DF^-. The data were recorded as a function of time over a 6 h period in 0.10 mol dm^{-3} NaCl. The initial impedance profile was recorded following a 10 min polarisation period at the desired potential. Representative impedance plots recorded for the PPyDF films under open-circuit conditions and at –0.900 V vs SCE are shown in **Error! Not a valid bookmark self-reference.** in the complex plane and Bode formats. Impedance data were also recorded for a bare Au electrode immersed in 0.10 mol dm^{-3} NaCl under similar experimental conditions.

The impedance measured for the PPyDF film at –0.900 V vs SCE is similar in magnitude to the impedance of the polymer at OCP, as shown from a comparison of both the Complex and Bode plots in **Error! Not a valid bookmark self-reference.**. This is very different to the PPyDex system, which displayed lower impedance at OCP. In general, the polymer at OCP is more conductive since the polymer is oxidised and there is a larger surface area which allows more efficient charge transfer[45, 46].

All data were fitted to the equivalent circuits depicted in Figure 4.16. The circuit shown in Figure 4.16A was used to fit the experimental data when the bare Au electrode was held at OCP. This corresponds to a two-time constant model. A simple Randles cell, presented in Figure 4.16B, was used to model the data when PPyDF films were reduced and maintained at OCP. In these circuits, R1 represents the solution resistance; R2 represents the charge-transfer resistance while CPE1 and CPE2 are constant phase elements. Constant phase elements were used to determine the capacitance of the polymer interface rather than pure capacitors; this allows for the inhomogeneity of the surface to be taken into account[47]. Equation 4.9 defines the impedance of a constant phase element, where T

represents the magnitude of the capacitance, ω is the angular frequency (2πf), f is the frequency of the signal and P is an exponent. When P exhibits a value of 1.0 the constant phase element corresponds to a true ideal capacitor, when the value is between 0.8 and 1.0 it is regarded as a non-ideal capacitor and when it has a value of 0.5 it corresponds to a diffusional process[48].

$$Z = \frac{1}{T\sqrt{(-1\omega)^P}} \qquad 4.9$$

As shown in **Error! Not a valid bookmark self-reference.** the level of agreement between the experimental data and the simulated data is good. Moreover, the errors in the circuit elements were less than 3.0%. The steady-state conditions were probed by collecting the impedance spectra over eight consecutive experiments and comparing the circuit parameters. Figure 4.17 shows the R2, which is equivalent to the charge-transfer resistance, and capacitance (P ≈ 0.8) measured at OCP for both the bare Au electrode and PPyDF as a function of time. The potential of the cell over the eight experiments was recorded at approximately +0.120 V vs SCE for the PPyDF. The capacitance of the polymer is relatively constant which indicates that the polymer is stable as a function of time. However, the capacitance is low, about 8 μF compared to the typical values of mF recorded for conducting polymers, when maintained in the oxidised state[49]. The R2 values are also relatively constant. In contrast, it takes approximately 200 min before the bare gold substrate reaches steady-state conditions.

A

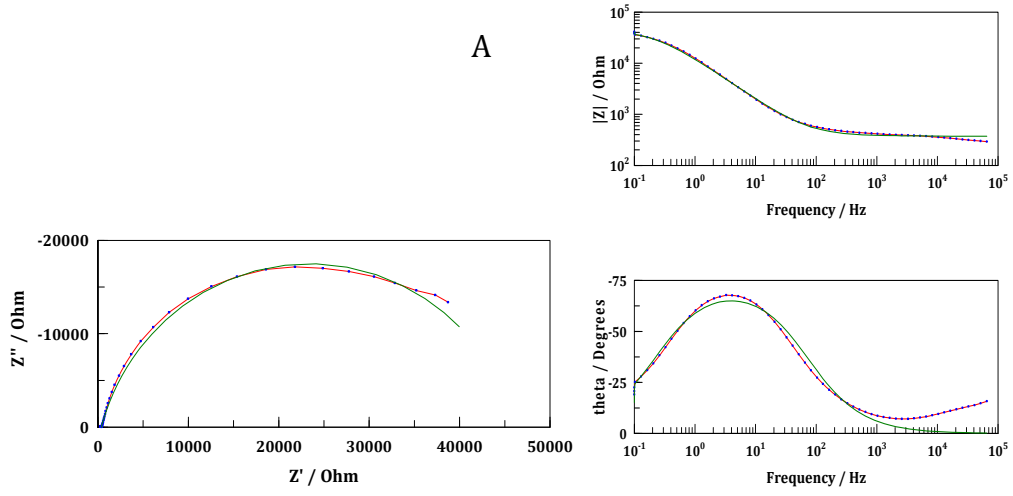

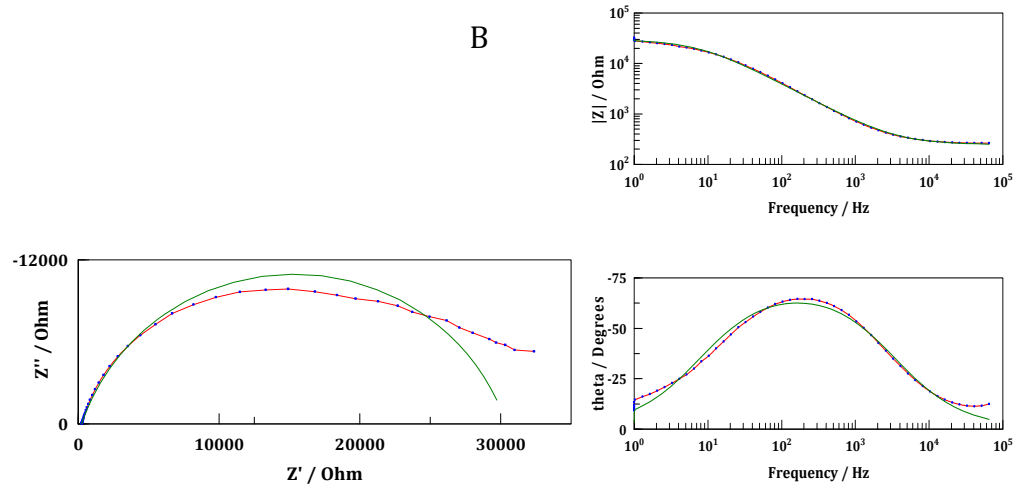

Figure 4.15: Complex Plane plots and Bode plot recorded for PPyDF in 0.10 mol dm^{-3} NaCl using a sinusoidal excitation voltage of 10 mV, measured **A** at open-circuit potential and **B** at –0.900 V vs SCE. Data recorded and simulated data fit. (Area = 0.125 cm^2).

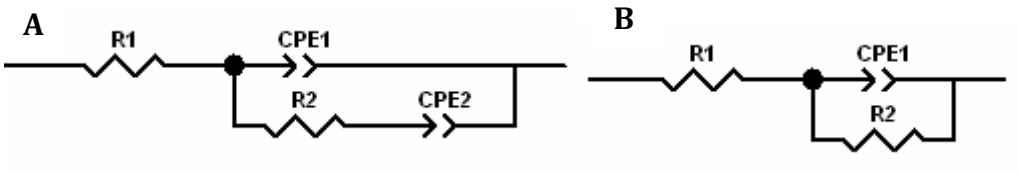

Figure 4.16: Equivalent circuits used to fit the data recorded for PPyDF and bare Au at OCP and –0.900 V vs SCE.

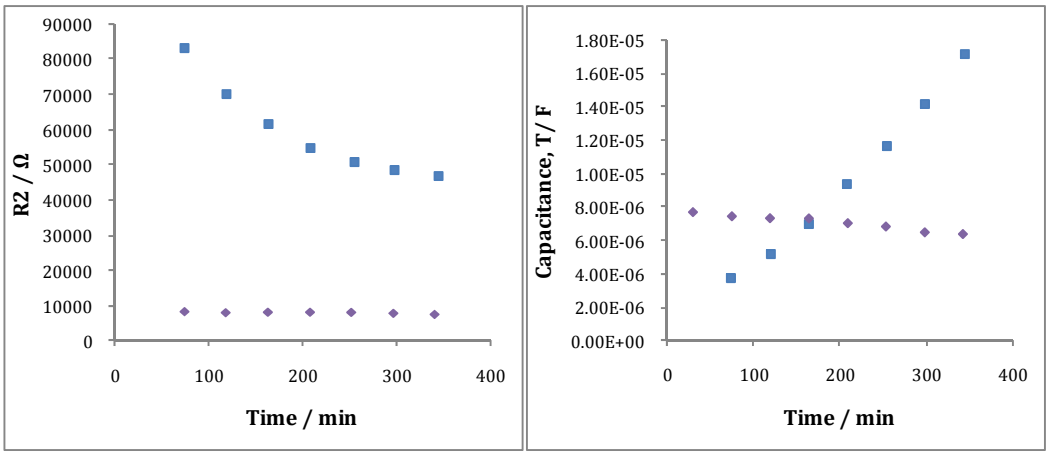

Figure 4.17: Resistance and capacitance, T with P ≈ 0.8, data recorded for ■ bare Au and ♦ PPyDF at OCP in 0.10 mol dm^{-3} NaCl. Impedance data were recorded using a sinusoidal excitation voltage of 10 mV. (Area = 0.125 cm^2).

The R2 and capacitance (T with P ≈ 0.8) measured at – 0.900 V vs SCE for both the bare Au electrode and PPyDF are presented in Figure 4.18. At the bare electrode, it can be seen that there is an increase in resistance and a slight decrease in

capacitance which indicates a loss in conductivity. At these reduction potentials, hydroxide adsorption occurs at the surface of the bare electrode which results in the decline of electron kinetics at the surface[50]. The reduction of the PPyDF results in the formation of PPy^0 and DF^-. The presence of the PPy^0 lowers the conductivity of the polymer which is consistent with an increase in resistance observed at 200 min and an overall decrease in the capacitance from 8 to 1 μF.

In conclusion, the data from the growth plots, redox properties and the impedance spectroscopy corroborate that the PPyDF film is less conducting than most PPy films. This insulating effect is likely to be due to the presence of the crystal-like structures which are clearly evident in Figure 4.13.

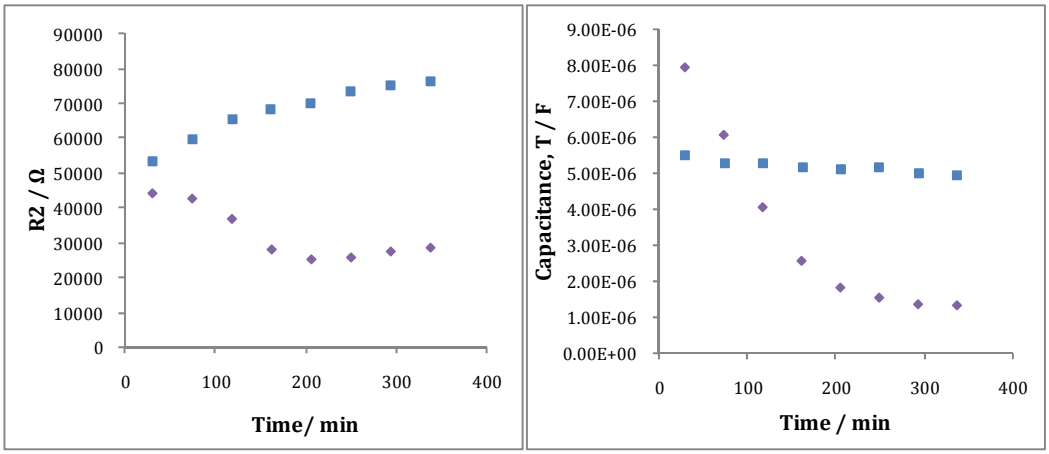

Figure 4.18: Resistance and capacitance, T with P ≈ 0.8, data recorded for ■ bare Au and ♦ PPyDF at –0.900 V vs SCE in 0.10 mol dm^{-3} NaCl. Impedance data were recorded using a sinusoidal excitation voltage of 10 mV. (Area = 0.125 cm^2).

4.3.3.5 The mass and doping levels of PPy doped with DF^-

As in Section 3.3.3.4, EQCM was employed to estimate the mass of the polymer and the doping level of DF^- within the PPyDF. Using the Sauerbrey equation, Equation 2.3, the shift in the resonant frequency of the crystal was then used to calculate the mass of the polymer. This equation assumes the current efficiency for the electropolymerisation of pyrrole is 100% and that no water is incorporated into the film[41]. The PPyDF polymer was deposited directly onto the Au on the quartz crystal as the presence of the PPyCl polymer resulted in the film being too thick and subsequently deviations from the Sauerbrey equation, Equation 2.3, were

observed. Accordingly, in these studies, the PPyDF was deposited directly onto the Au quartz crystal electrode until a charge of 1.20 x 10^{-2} C was consumed.

The changes in frequency of the crystal and the corresponding mass changes as the PPyDF film is deposited are shown in Figure 4.19. This growth profile can be divided into three segments, an initial period of about 30 s, where very small quantities of polymer are deposited. This corresponds to the initial nucleation of the polymer at the gold surface. This is then followed by a period where the polymer is deposited at a much higher rate. Finally, after approximately 150 s, the rate of deposition decreases again. Representative mass-charge and charge-time plots are shown in Figure 4.20 and again show a very clear nucleation period, where the mass-to-charge ratio is lower. During the next phase, which is equivalent to the higher rates of polymer deposition, there is a linear increase in charge with time, Figure 4.20B, in agreement with the data recorded at the macro-electrode, Figure 4.7. The slope of this linear segment was calculated as 3.9 x 10^{-5} C s^{-1} for the thin polymer deposited by EQCM. There is also a linear relationship between the charge consumed and the mass of the polymer during this phase.

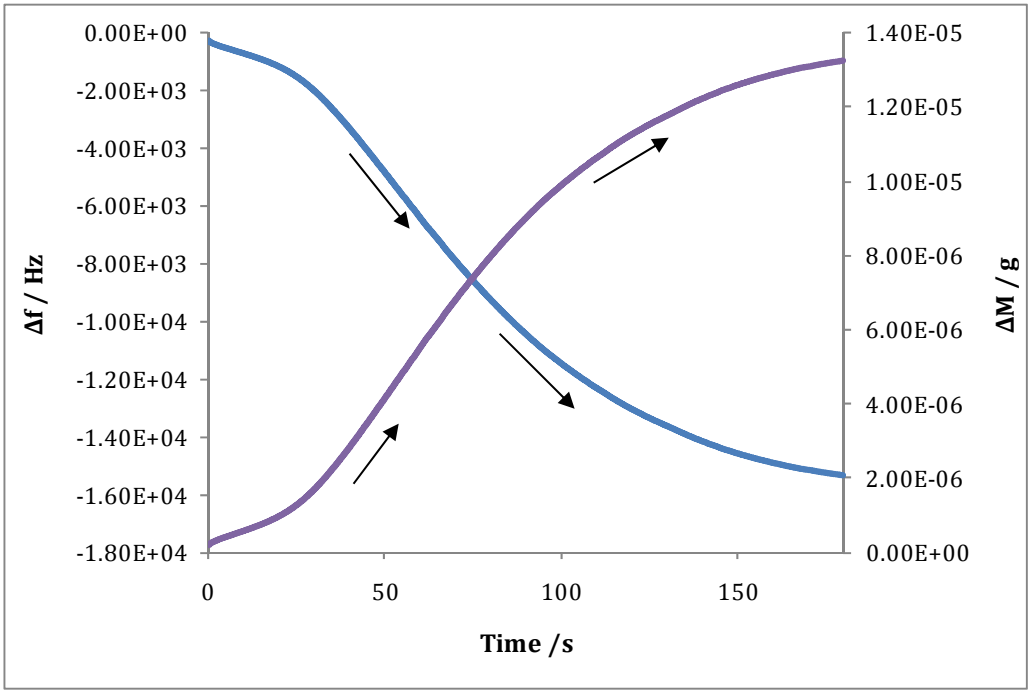

Figure 4.19: Frequency (—) and mass (—) recorded during the formation of PPyDF in the presence of 0.10 mol dm^{-3} NaDF and 0.20 mol dm^{-3} Py at a potential of +0.800 V vs Ag|AgCl until a charge of 9.6 x 10^{-3} C was consumed. (Area = 0.208 cm^2).

The doping level of DF^- in the polymer can be calculated using a derivation of Faraday's law, Equation 2.5, as outlined for the PPyDex system in Chapter 3, Section 3.3.3.4. Using the average mass-charge ratio of 2.0 x 10^{-5} g C^{-1} for the PPyDF, the doping level was calculated between 0.30 and 0.33 which is the typical doping level found for polypyrrole[32, 51, 52]. Taking these doping levels, the mass of DF^- in the polymer was calculated as 5.0 x 10^{-6} g which corresponds to 1.69 x 10^{-8} moles of DF^-. Consequently, the mass % of DF^- in the PPyDF film is approximately 58%.

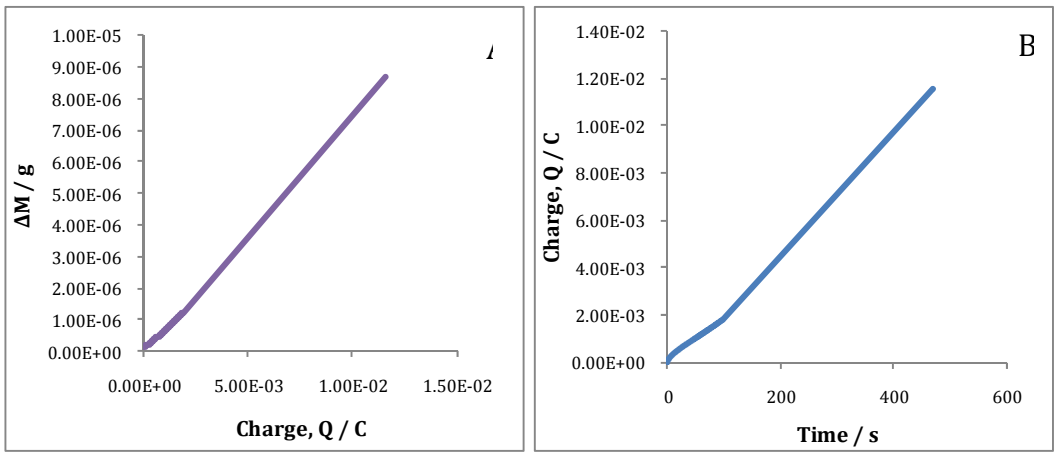

Figure 4.20: A Mass-charge plot and **B** charge-time plot recorded during the deposition of the PPyDF film on Au quartz crystal electrode in the presence of 0.10 mol dm^{-3} NaDF and 0.20 mol dm^{-3} Py. (Area of quartz crystal = 0.208 cm^2).

4.3.4 Release studies

Before any of the release studies were carried out the polymer was thoroughly rinsed in distilled H_2O, then immersed in distilled H_2O for 10 min and a potential of +0.500 V vs SCE was applied to ensure that any DF^- on the surface of the polymer was removed. This potential was chosen as it would not cause oxidation or reduction of the polymer that might affect the drug release studies. In addition the

10 min immersion period was sufficient for any DF^- trapped within the porous polymer matrix to diffuse into the bulk H_2O.

4.3.4.1 Verifying optimum growth potential

Two polymers were deposited as described in Section 4.3.2.4 and a potential of – 0.900 V vs SCE was applied in the presence of 0.10 mol dm^{-3} NaCl. Samples were taken every 5 min and the amount of DF^- present was measured by UV-vis spectroscopy at a λ_{max} of 276 nm. The amount of DF^- measured from the two polymer films is shown in Figure 4.21 and it is clear that the polymer electrosynthesised at +0.800 V vs $Ag|Ag^+$ resulted in a higher release of DF^- than the polymer deposited at +0.900 V vs $Ag|Ag^+$. This is connected with the greater ease of polymerisation at +0.800 V vs $Ag|Ag^+$, as evidenced in Figure 4.7. Unlike the release profiles seen with Dex^{2-}, the amount of DF^- released does not plateau within the first 60 min. Instead, there is a gradual increase in the amount of DF^- released over the 60 min period. The amount of Dex^{2-} released was much larger than that of DF^- but this may be due to the difference in the charge of the polymers and consequently the thickness of the polymer. As stated earlier, the thickness of the PPyDF is limited by the insulating nature of the surface, and these films are considerably thinner than the PPyDex films.

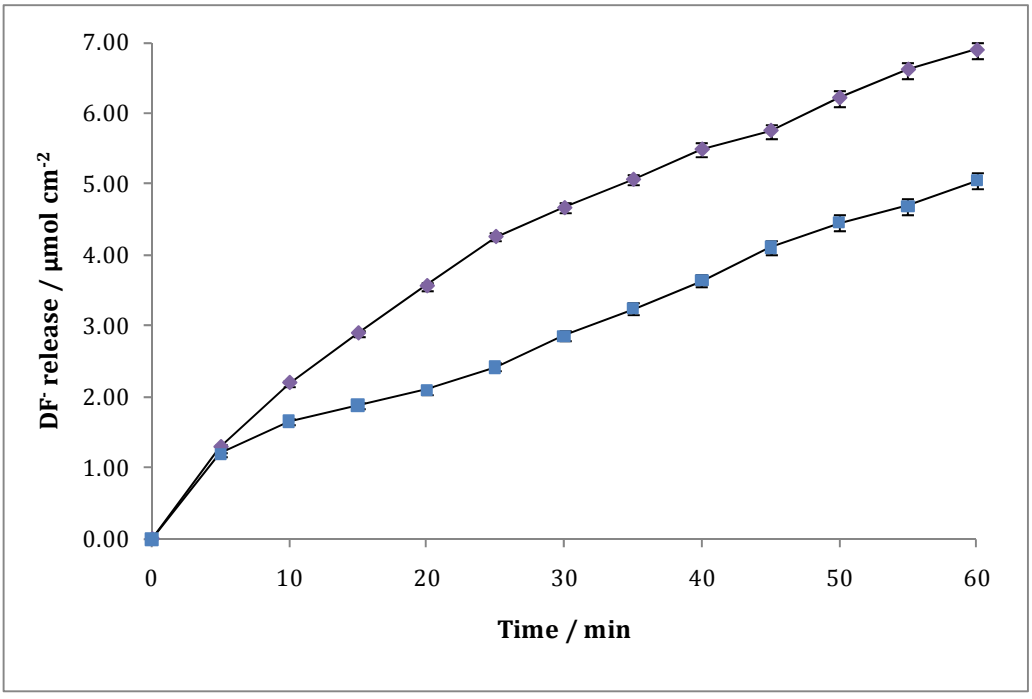

Figure 4.21: Amount of DF^- released at –0.900 V vs SCE, in the presence of 0.10 mol dm^{-3} NaCl from two polymer films grown at ♦ +0.800 V vs $Ag|Ag^+$ and ■ +0.900 V vs $Ag|Ag^+$ in 0.10 mol dm^{-3} NaDF and 0.20 mol dm^{-3} Py. The PPyDF films were grown on a PPyCl film, 0.70 C cm^{-2} in charge at a Au working electrode. Polymerisation was carried out at 38 °C. (n=2).

4.3.4.2 Effect of growth time

As discussed previously in Section 4.3.2.4, the potentiostatic plots show a peak in the current within approximately 200 s and then the current decreases until the oxidation potential is stopped at 20 min. The decrease in current indicates that very little polymerisation occurs after this point. To investigate whether this had any effect on the amount of DF^- incorporated and released, three polymers were grown to different time points along the peak at 100 s, 150 s and 200 s. A fourth polymer was grown for 60 min to facilitate a comparison with the films deposited for a 20 min period. The charges to which the four polymers reached are shown in Table 4.1. Regardless of the current profile, there is an increase in the charge as the polymerisation period is increased. However, it is apparent how slow the rate of polymerisation is with the polymer only reaching a charge of 0.32 C cm^{-2} after a potential of +0.800 V vs $Ag|Ag^+$ was applied for 60 min.

Release studies were carried out on these polymers and the amount of DF^- released as a function of time is shown in Figure 4.22. It can be seen that the polymer grown for 100 s yields a higher DF^- release than those grown for 150 or 200 s. Also the amount of DF^- released from the polymer grown for 60 min is less than the amount measured previously from the polymer grown for 20 min, Figure 4.21. This is more than likely due to the presence of the insoluble HDF crystals which slow down the rate of polymerisation. This makes it increasingly more difficult to incorporate and release DF^- from the polymer membrane. Even though the polymer deposited at +0.800 V vs $Ag|Ag^+$ for 100 s only reaches a charge of 0.01 C cm^{-2}, it releases less than half the amount of DF^- released from the polymers grown for 20 min. This shows that there is a poor relationship between the charge consumed during the deposition of the PPyDF and the concentration of DF^- released. This, in all probability, is due to the entrapment of insoluble drug crystals even at this early

stage of polymerisation. Indeed, the charge-time plot depicted in Figure 4.7 shows evidence for the deposition of the drug crystals after about 120 s, as the charge-time curve begins to deviate from the linear profile.

Table 4.1: Charge consumed during the formation of PPyDF at +0.800 V vs $Ag|Ag^{+}$ in 0.10 mol dm^{-3} NaDF and 0.20 mol dm^{-3} Py as a function of the electropolymerisation period.

Time / s	Charge, Q / C cm^{-2}
100	0.013
150	0.019
200	0.023
3600	0.325

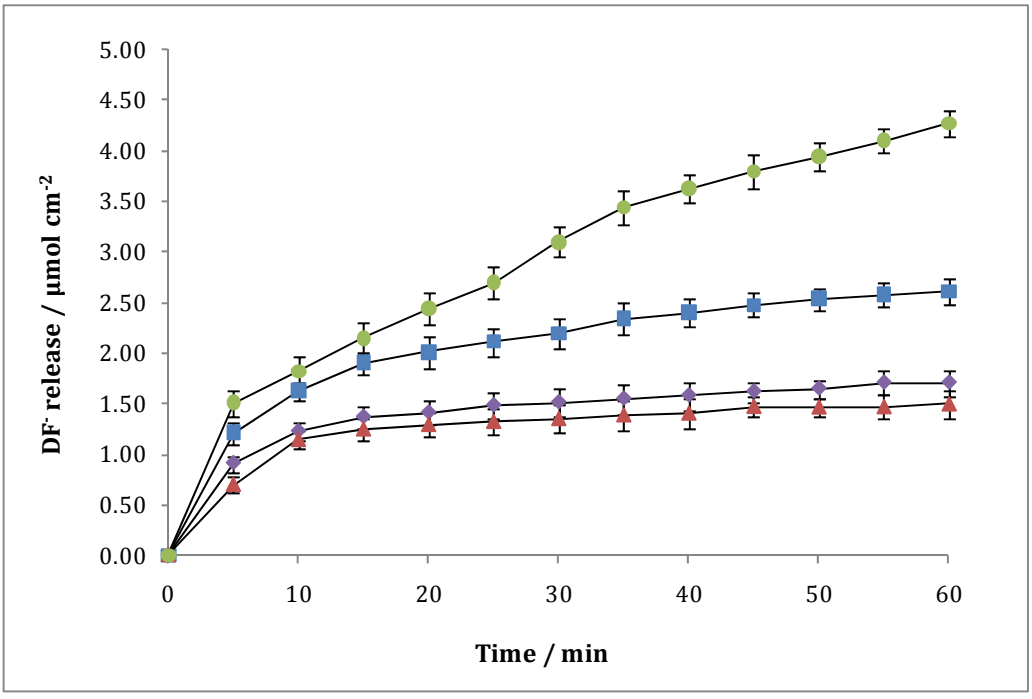

Figure 4.22: Amount of DF^{-} released in the presence of 0.10 mol dm^{-3} NaCl at –0.700 V vs SCE. The PPyDF was deposited onto a film of PPyCl in the presence of 0.10 mol dm^{-3} NaDF and 0.20 mol dm^{-3} Py at +0.800 V vs $Ag|Ag^{+}$ for ■ 100 s, ♦ 150 s, ▲ 200 s and ● 60 min. (n=2).

4.3.4.3 Finding the most effective release potential

In these studies, all PPyDF films were deposited by applying a constant potential of +0.800 V vs $Ag|Ag^+$ for 20 min in the presence of 0.10 mol dm^{-3} NaDF and 0.20 mol dm^{-3} Py at 38 ^oC. The potential at which the largest DF^- release occurs was then investigated. Several reduction potentials were applied and release profiles were also measured at the open-circuit potential (OCP). The potential in the cell under OCP conditions was found to be +0.160 V vs SCE and was steady over the course of the 60 min. The release profiles at OCP, –0.500 V vs SCE and –0.700 V vs SCE are shown Figure 4.23. The rate of release measured at these three potentials is shown in Table 4.2. As seen with Dex^{2-}, it is again clear that the amount of drug released is dependent on the potential applied and is not as a result of the drug diffusing from the polymer film, or simply the dissolution of the drug crystals.

Table 4.2: Rate of DF^- release measured at OCP, –0.500 V vs SCE and –0.700 V vs SCE. The PPyDF was deposited onto a film of PPyCl in the presence of 0.10 mol dm^{-3} NaDF and 0.20 mol dm^{-3} Py at +0.800 V vs $Ag|Ag^+$ at 38 °C for 20 min.

Time range / min	**At OCP / µmol cm^{-2} min^{-1}**	**At –0.500 V vs SCE / µmol cm^{-2} min^{-1}**	**At –0.700 V vs SCE / µmol cm^{-2} min^{-1}**
0-10	0.121	0.161	0.306
15-60	0.021	0.026	0.073

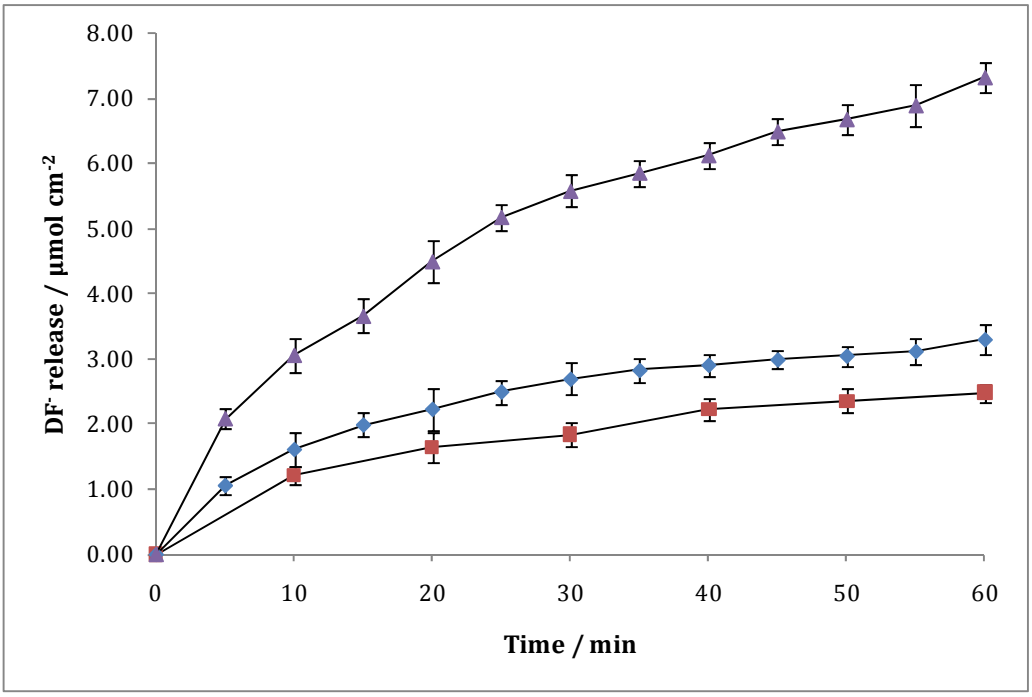

Figure 4.23: Release profiles of DF^- at ■ OCP, ♦ –0.500 V vs SCE and ▲ –0.700 V vs SCE. The PPyDF was deposited onto a film of PPyCl in the presence of 0.10 mol dm^{-3} NaDF and 0.20 mol dm^{-3} Py at +0.800 V vs $Ag|Ag^+$ at 38 ^oC for 20 min. (n=3).

The amount of DF^- measured at the various potentials is shown in Figure 4.24. The highest amount of DF^- was measured at –0.700 V vs SCE, while at the oxidation potential of +0.500 V vs SCE a slightly lower amount of DF^- was released than at OCP. The highest release occurs at potentials between –0.700 V vs SCE and –0.900 V vs SCE which is slightly different to that observed with the PPyDex system. As shown in Figure 4.8, the reduction of the PPyDF film extends from –0.400 V vs SCE to about –1.000 V vs SCE. Accordingly, the optimum release potentials are close to the potential where the PPyDF is reduced.

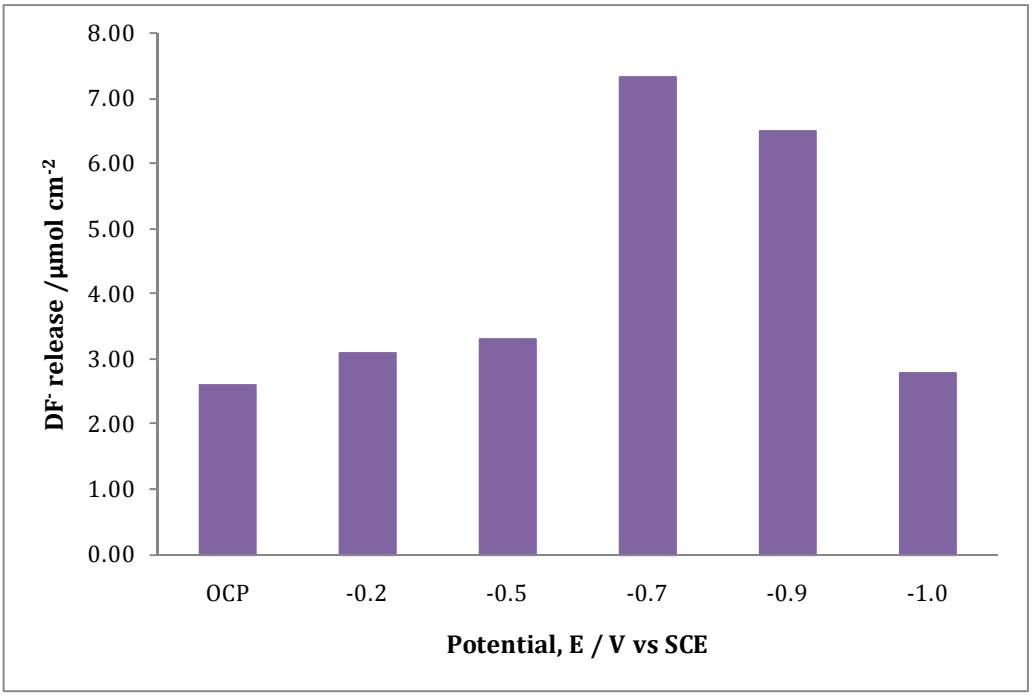

Figure 4.24: Amount of DF^- measured after 60 min at various release potentials in the presence of 0.10 mol dm^{-3} NaCl. The PPyDF was deposited onto a film of PPyCl in the presence of 0.10 mol dm^{-3} NaDF and 0.20 mol dm^{-3} Py at +0.800 V vs $Ag|Ag^+$ at 38 ^oC for 20 min. (n=3 and % error is less than 6%).

A release study was carried out under the optimum conditions for 5 h in an effort to estimate how much DF^- was doped in the polymer. A 5 h release study was also carried out at OCP as a comparative study. Figure 4.25 shows the amount of DF^- measured during both release studies and it is apparent that the majority of the drug is released within the first hour and the release profile begins to plateau after 2 h. After 5 h of applied release, the amount of DF^- measured is approximately 9.0 µmol cm^{-2} which is an increase of approximately 2.0 µmol cm^{-2} from the first to the fifth hour. This means the rate of release decreases from 0.073 µmol cm^{-2} min^{-1} in the first hour to 0.009 µmol cm^{-2} min^{-1} in the last 4 h period. Likewise, at OCP there is a decrease in the rate of release which was measured as 0.003 µmol cm^{-2} min^{-1} from the first to the fifth hour. After 5 h at OCP, the amount of DF^- measured is 3.06 µmol cm^{-2}. From this, it is estimated that the amount of DF^- in the polymer is approximately 9.0 µmol cm^{-2} which is less than the amount of Dex^{2-} calculated to be doped within the PPyDex polymer.

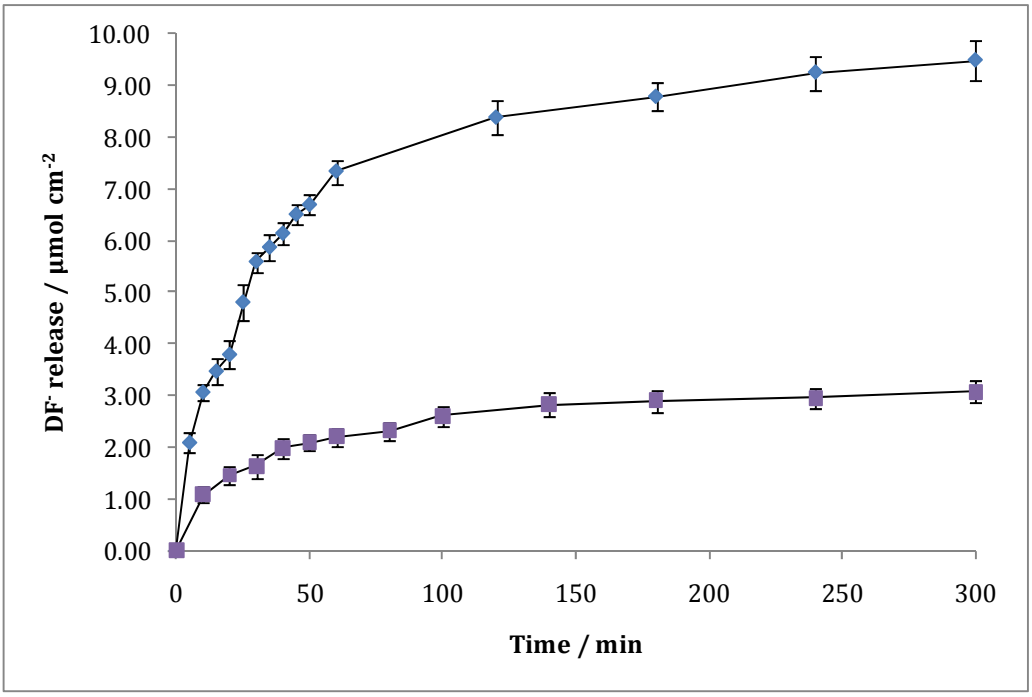

Figure 4.25: Amount of DF^- released from PPyDF at ♦ –0.700 V vs SCE and at ■ OCP over a period of 5 h in the presence of 0.10 mol dm^{-3} NaCl. The PPyDF was deposited onto a film of PPyCl in the presence of 0.10 mol dm^{-3} NaDF and 0.20 mol dm^{-3} Py at +0.800 V vs $Ag|Ag^+$ at 38 °C for 20 min. (n=3).

As mentioned in Section 4.1, there are no reports in the literature of the electrochemical controlled release of DF^-. Studies have been carried out using time-controlled releases and the amount of drug released from these systems varied. Hincal and co-workers[17] reported a 40 % - 50 % NaDF release from albumin microspheres which had a diameter of approximately 15 µm made up from a composition of 125 mg albumin and 12.5 mg NaDF. Manjunatha *et al.*[18] documented a yield of over 65 % for the release of NaDF from beads that were prepared based on dispersing the drug in solutions of ionic polysaccharides, such as chitosan and sodium alginate. The highest yield in this paper was reported when the ratio of drug to polymer was 1:1, although it is not clearly stated how much drug was in the beads initially. Finally, the transdermal release of NaDF described by Vyas *et al.*[19] had a release rate of 0.188 mg cm^{-2} h^{-1}. This is significantly lower than the rate of release reported in this chapter, which is 1.29 mg cm^{-2} h^{-1}.

4.3.4.4 The amount of DF^- doped within the polymer

In order to calculate how much DF^- was doped within the PPyDF, the bulk system was related to the EQCM system by examining the rate of polymerisation in both systems from the charge-time plots. For the thin polymer deposited during EQCM studies, the slope was calculated as 3.9×10^{-5} C s^{-1} (which is equivalent to 1.8×10^{-4} C cm^{-2} s^{-1}). The slope of the bulk polymer was found to be 2.5×10^{-4} C cm^{-2} s^{-1}, during the early stages of deposition. This indicates that the polymers in both systems grow in a similar manner, at least during the early deposition of the polymer and until the shards and crystals accumulate at the surface. The doping levels calculated for the EQCM polymer can then be used together with the charge consumed during the growth of the bulk polymer to calculate the mass of the bulk polymer, using Equation 2.4. Taking the doping levels as either 0.30 or 0.33, the amount of DF^- in the bulk polymer was calculated between 2.7×10^{-7} mol and 2.94×10^{-7} mol. However, this is much lower than the amount of DF^- that is actually being measured during the release studies of the polymer, particularly the release study carried out over 5 h, Figure 4.25, where 9.0×10^{-6} mol of DF^- was released.

However, this can be explained easily by considering the crystal-like structures seen encased in the polymer in Section 4.3.3.1. These insoluble forms of the drug give rise to pockets of drug crystals in the polymer. During the reduction of the polymer these crystals are dissolved giving higher concentrations of DF^-. This may also explain why there is very little difference in the amount of DF^- released at OCP and at –0.500 V vs SCE, as shown in Figure 4.23, as the majority of released DF^- is contributed by the insoluble crystals on the polymer surface, which slowly dissolve.

In order to gain more information on the maximum amount of DF^- that can be released without the complications from the insoluble crystals, thin PPyDF films were studied using EQCM. The PPyDF film was electrodeposited on the quartz crystal, as described in Section 4.3.3.5, and was rinsed thoroughly with distilled H_20 before being placed in an electrolyte of 0.10 mol dm^{-3} NaCl. A reduction

potential of –0.700 V vs Ag|AgCl was applied for 600 s and the frequency recorded and the related calculated mass are shown in Figure 4.26. There is a sharp decrease in mass over the entire 600 s period, which is consistent with the loss of DF^- from the film. The mass of this polymer upon polymerisation was 1.31 x 10^{-5} g and the loss in mass at the reduction potential is approximately 3.6 x 10^{-6} g which is a drop of 27 % in mass and corresponds to the release of 1.14 x 10^{-8} moles of DF^-. Although there is a further decrease in the mass beyond 600 s, additional studies showed that the further loss in mass was small, reaching no more than 4.0 x 10^{-6} g in total.

For these thin PPyDF films there is a much better correlation between the amount of DF^- incorporated within the PPyDF film and the amount released at –0.700 V vs Ag|AgCl. This is related to the absence of large amounts of the insoluble crystals, which are deposited with continued electropolymerisation.

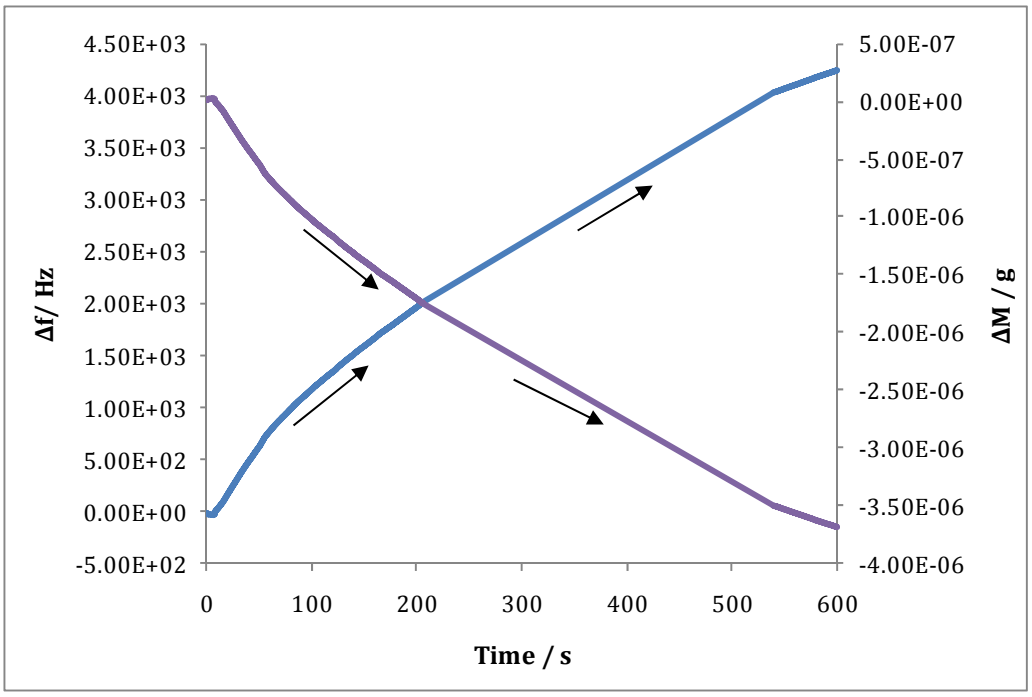

Figure 4.26: Frequency (—) recorded and mass (—) calculated in the presence of a reduction potential of –0.700 V vs Ag|AgCl in 0.10 mol dm^{-3} NaCl. Film was prepared from a 0.10 mol dm^{-3} NaDF and 0.20 mol dm^{-3} solution at +0.800 V vs Ag|AgCl until a charge of 9.6 x 10^{-3} C was consumed. (Area = 0.208 cm^2).

4.3.4.5 Reusing the polymer to release DF^-

As seen in Section 3.3.3.4, it was found that it was possible to oxidise the reduced PPy^0 back to PPy^+ so that Dex^{2-} could be incorporated into the polymer. Similar studies were then carried out with the PPyDF system and Equation 4.10 outlines the basic principle behind this. The polymer was electrodeposited and the drug was released at – 0.700 V vs SCE for 60 min. The polymer was then rinsed and placed into an electrolyte of 0.12 mol dm^{-3} NaDF (slightly higher than the concentration of NaDF in the polymerisation electrolyte) and a potential of +0.800 V vs $Ag|Ag^+$ was applied for 60 min in an attempt to incorporate the DF^- into the polymer, Equation 4.11. The temperature of the NaDF solution was 42 °C which was higher than the original polymerisation temperature to ensure all the NaDF stayed in solution. The polymer was washed and release studies were carried out as before. It was then rinsed and replaced in the NaDF only electrolyte and the process was repeated again.

$$PPy^+DF^- + e^- \rightleftharpoons PPy^0 + DF^- \qquad 4.10$$

$$PPy^0 + DF^- \rightleftharpoons PPy^+DF^- + e^- \qquad 4.11$$

As with the PPyDex, it was found that the polymer could be successfully 'redoped' with the drug however the pattern witnessed for PPyDF was quite different as can be seen in Figure 4.27. The amount of drug released on the second occasion is almost triple that of the first release. The amount of drug released decreases with each release with the fourth release still yielding a slightly higher amount than the first. Although the trend is different to what was seen for PPyDex, the increase in drug release from the first to the second release indicates that PPy^0 is oxidised back to PPy^+ and this enables more DF^- to be doped on the polymer. The SEM micrographs taken after the reduction potential was applied, Figure 4.14, show that the polymer that encased the drug crystals has collapsed. This leads to a more porous outer polymer layer and the possible exposure of the PPyCl film. This means that the insulating effect of the PPyDF has been removed and the polymer film left has an increased conductivity.

During the application of the reduction potential, it is probable that some chloride is released from the polymer and it is likely it is this polymer film, the underlying PPyCl, that becomes doped with DF^- in the presence of the oxidation potential in 0.12 mol dm^{-3} NaDF. This may explain the large increase in DF^- release from the first to the second release. The decrease in release thereafter, however, correlates with the belief that the polymer loses conductivity the longer the reduction potential is applied and it is more difficult to oxidise the polymer again to ensure the same levels of DF^- are incorporated and released.

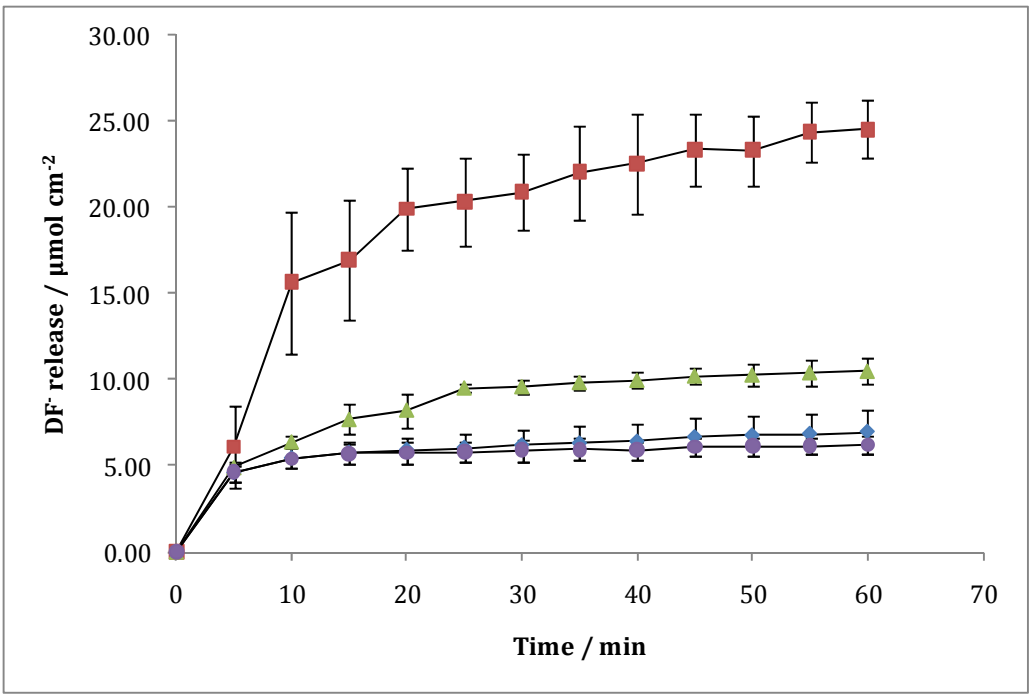

Figure 4.27: The amount of DF^- measured in the presence of 0.10 mol dm^{-3} NaCl from PPyDF at −0.700 V vs SCE. The polymer was then placed in a solution of 0.12 mol dm^{-3} NaDF and a potential of +0.800 V vs $Ag|Ag^+$ was applied before the DF^- was released again. The polymer was then placed back into the NaDF solution and the process was repeated. 1st release ♦; 2nd release ■; 3rd release ▲ and 4th release ●. (n=3).

4.3.4.6 Comparison of the release of DF^- and Dex^{2-}

As mentioned previously, the amount of DF^- is much lower than the amount of Dex^{2-} released, but this is due to the difference in the charge of the polymer films. To accurately compare the two release systems, the polymers need to be of equal charge or thickness. As discussed in Chapter 3, the PPyDex polymer had a charge of

2.8 C cm^{-2} and to deposit the PPyDF film to the same charge would take a significant length of time considering it reached a charge of 0.2 C cm^{-2} in 20 min. For this reason, the PPyDex was deposited to a charge of 0.2 C cm^{-2} directly onto the Pt electrode while PPyDF was deposited in the usual manner onto the PPyCl film on the Au electrode. Applied release potentials of –0.700 V vs SCE and –0.900 V vs SCE were used to stimulate the release of DF^- and Dex^{2-}, respectively. In Figure 4.28 the amount of each drug measured over 60 min is compared and it can be seen that more DF^- is released than Dex^{2-}. This indicates that more DF^- is immobilised into the PPy than Dex^{2-} which is likely since the DF^- is smaller in size than the Dex^{2-} anion. However, as pointed out earlier, the insoluble drug crystals also contribute to the concentration of DF^- measured in the release electrolyte.

Again, both release profiles show that the amount of drug released increases consistently over the 60 min. As discussed in Section 3.3.4.2, the dissociation of the dopants from the PPy chain may be an instantaneous process, but the release of the anion is driven by diffusion, consisting of the movement of anions from the inner film to the surface and from the surface to the solution[53], which can be quite a slow process. Unlike the release profiles seen in Figure 4.28, the release profiles for Dex^{2-} from the thicker polymer plateaus after ~ 35 min and this is related to the quick release from the surface followed by the slower release of the bulk which takes time to diffuse from the inner film to the surface. However, for thinner films, like those discussed in this chapter, the diffusion from the inner film to the surface is faster, so there is no delay in releasing the drug in the bulk polymer after the drug at the surface is released. This may explain why the release profiles for the thin and thick PPyDex films are very different.

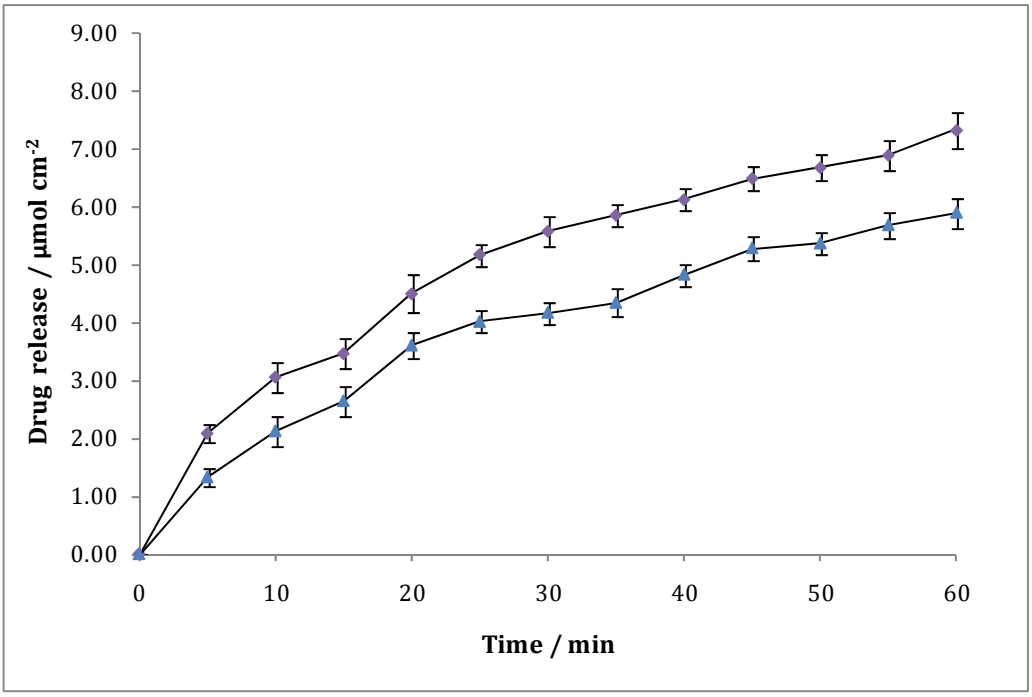

Figure 4.28: Amount of ♦ DF^- measured at –0.700 V vs SCE compared to the amount of ▲ Dex^{2-} measured at –0.900 V vs SCE over 60 min, in the presence of 0.10 mol dm^{-3} NaCl.

4.3.4.7 Formation of drug crystals on the surface of the polymer

As discussed in Section 4.3.1.2, the pH of the NaDF-containing Py solution is 7.4 and the % of anions calculated at this pH is 99%. It is also clear from Figure 4.3 that the pH influences the % of anions in solution and at low pH values the equilibrium is shifted towards the insoluble HDF, as seen in Equation 4.4. In Chapter 1, Section 1.4.1, the electropolymerisation of Py is described using the mechanism proposed by Diaz *et al.*[54]. It is proposed that the initial step is the generation of the radical cation. The coupling of two Py radicals results in the formation of a bond between the two α positions to give a radical dication. The loss of two protons generates a neutral dimer which is then oxidised to form a radical dimer, as can be seen in Figure 4.29. This can couple with a radical monomer to form a trimer and the polymerisation progresses in this fashion to completion. The increase in protons during the polymerisation causes a local acidity at the interface of the electrode. This shifts the equilibrium of some of the DF^- anions in solution towards HDF. Depending on the rate of electropolymerisation, significant local pH changes can occur. For example, Rajeshwar and co-workers[55] used a micro-pH electrode to monitor the changes in pH during the formation of PPyCl and recorded

pH values as low as 3.0 compared to the bulk pH of 5.6. However, there are still enough DF^- anions in solution to allow the progression of the polymer deposition and these insoluble drug crystals become entrapped within the polymer as it is deposited on the electrode.

The rate of polymerisation is hindered by the presence of these crystals on the surface of the electrode as seen in the potentiostatic current-time plots and charge-time plots in Figure 4.7. The presence of the drug crystals on the surface of the polymer also increases the amount of DF^- measured during the release studies which is discussed in Sections 4.3.4.2 – 4.3.4.5.

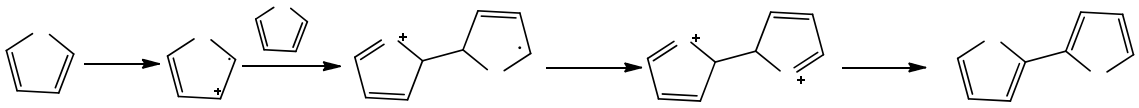

Figure 4.29: Mechanism for the formation of PPy dimer and the generation of H^+.

4.4 Summary of results

In this chapter, the incorporation and release of diclofenac, DF^-, into and from a PPy membrane film is described. At concentrations of 0.10 mol dm^{-3} and higher, the NaDF is insoluble in water and the deposition of PPy doped with DF^- is only possible under heated conditions. Direct electrodeposition of the polymer onto the bare Au electrode proved difficult and therefore it was deposited upon a thin film of PPyCl.

As evidenced from the charge-time plots the rate of polymerisation decreases within 500 s of the oxidation potential being applied. The morphology of the polymer was found to be very different to any morphology previously documented for PPy. Crystal-like shards were observed on the surface and embedded within the PPy. Further characterisation of the polymer using cyclic voltammetry and electrochemical impedance spectroscopy were used to measure electrochemical activity of the polymer and its conductivity. It was found that the PPyDF was not highly conductive due to the crystal-like shards in the polymer. These crystal-like

shards are insoluble forms of the drug encased in the polymer and their presence at the surface limits the growth of the PPyDF film.

Release studies for DF^- were carried out and the highest amount of DF^- released was measured at –0.700 V vs SCE. The total amount released over a 60 min period was about 7.0 μmol cm^{-2} yet only a slightly higher amount, 9.0 μmol cm^{-2}, was measured over a period of 5 h. However, this is not thought to be an accurate reflection of the amount of DF^- being doped onto the polymer as the release of the insoluble forms of the drug increased the amount of drug being measured on release. SEM micrographs taken of the polymer after the release studies showed that the majority of the insoluble DF^- crystals were removed from the polymer and this will contribute to the final concentration of DF^- in the release electrolyte. It was found that after the release of these crystals, higher amounts of DF^- could be doped onto the polymer and this meant the successful release of larger amounts of DF^- was possible. This was attributed to the exposure of a more porous polymer structure, the underlying PPyCl, which became doped with DF^- in the presence of the oxidation potential and this resulted in higher uptake and doping by the DF^- anions.

4.5 References

1. D. L. Gardner, *Journal of Anatomy,* **184**:465 (1994).
2. J. A. Mitchell and T. D. Warner, *British Journal of Pharmacology* **128**:1121 (1999).
3. J. R. Vane and R. M. Botting, *Scandinavian Journal of Rheumatology,* **25**:9 (1996).
4. T. Hla and K. Neilson, *Proceedings of the National Academy of Sciences U S A,* **89**:7384 (1992).
5. E. A. Meade, W. L. Smith, and D. L. DeWitt, *Journal of Biological Chemistry,* **268**:6610 (1993).
6. T. D. Warner, F. Giuliano, I. Vojnovic, A. Bukasa, J. A. Mitchell, and J. R. Vane, *Proceedings of the National Academy of Sciences U S A,* **96**:7563 (1999).
7. A. Schweitzer, N. Hasler-Nguyen, and J. Zijlstra, *BioMed Central Pharmacology,* (2009).
8. C. S. Bruner, *Product Genesis Inc.,* (2004).
9. V. Dhikav, S. Singh, S. Pande, A. Chawla, and K. S. Anand, *Journal, Indian Academy of Clinical Medicine,* **4**:315 (2003).
10. N. Davies and K. Anderson, *Clinical Pharmacokinetics,* **33**:184 (1997).
11. P. Todd and E. Sorkin, *Drugs* **35**:244 (1988).

12. T. Khazaeinia and F. Jamali, *Journal of Pharmacy and Pharmaceutical Sciences,* **6**:352 (2003).
13. M. R. León-Reyes, G. Castañeda-Hernández, and M. I. Ortiz, *Journal of Pharmacy and Pharmaceutical Sciences,* **11**:68 (2008).
14. R. Menasse, P. R. Hedwall, J. Kraetz, C. Pericin, L. Riesterer, A. Sallmann, R. Ziel, and R. Jaques, *Scandinavian Journal of Rheumatology,* **22**:5 (1978).
15. M. Aktaruzzaman, J.Alam, A. Rahman, and M. M. Hossain., *Bangladesh Journal of Veterinary Medicine,* **6**:99 (2008).
16. S. Dreve, I. Kacso, I. Bratu, and E. Indrea, *Journal of Physics: Conference Series* **182** (2009).
17. M. Tuncay, S. Calis, H.S. Kas, M.T. Ercan, I. Peksoy, and A. A. Hincal, *Journal of Microencapsulation* **17**:145 (2000).
18. K. Manjunatha, M. Ramana, and D. Satyanarayana, *Indian Journal of Pharmaceutical Sciences,* **69**:384 (2007).
19. S. P. Vyas, P. J. Gogoi, and S. K. Jain, *Drug Development and Industrial Pharmacy,* **17**:1041 (1991).
20. P. Canizares, J. García-Gómez, J. Lobato, and M. A. Rodrigo, *Industrial & Engineering Chemistry Research,* **42**:956 (2003).
21. K. Ogura, S. Haruyama, and K. Nagasaki, *Journal of The Electrochemical Society,* **118**:531 (1971).
22. N. Parviz, G. Mohammad Reza, A. Taher, and D. Parandis, *Electroanalysis,* **18**:947 (2006).
23. K. Juodkazis, J. Juodkazyte, T. Juodiene, V. Sukiene, and I. Savickaja, *Electrochimica Acta,* **51**:6159 (2006).
24. S. J. Xia and V. I. Birss, *Journal of Electroanalytical Chemistry,* **500**:562 (2001).
25. F. Adamo, L. Michele, O. Isabella, and Z. Vittorio, *Journal of Pharmaceutical Sciences,* **75**:23 (1986).
26. S. Asavapiriyanont, G. K. Chandler, G. A. Gunawardena, and D. Pletcher, *Journal of Electroanalytical Chemistry,* **177**:245 (1984).
27. G. Zotti, S. Cattarin, and N. Comisso, *Journal of Electroanalytical Chemistry,* **235**:259 (1987).
28. S. B. Saidman and J. B. Bessone, *Journal of Electroanalytical Chemistry,* **521**:87 (2002).
29. Y. Li and J. Yang, *Journal of Applied Polymer Science,* **65**:2739 (1997).
30. A. S. Liu and M. A. S. Oliveira, *Journal of Brazilian Chemistry Society,* **18**:143 (2007).
31. S. Sadki, P. Schottland, N. Brodie, and G. Sabourand, *Royal Society of Chemistry,* **29**:283 (2000).
32. A. F. Diaz, J. I. Castillo, J. A. Logan, and W.-Y. Lee, *Journal of Electroanalytical Chemistry,* **129**:115 (1981).
33. A. M. Fenelon and C. B. Breslin, *Corrosion Science,* **45**:2837 (2003).
34. J. M. Ko, H. W. Rhee, S. M. Park, and C. Y. Kim, *Journal of Electrochemistry Society,* **137** (1990).
35. Cosimino Malitesta, Francesco Palmisano, Luisa Torsi, and P. G. Zambonin, *Analytical Chemistry,* **62**:2735 (1990).
36. J. M. Elliott, L. M. Cabuché, and P. N. Bartlett, *Analytical Chemistry,* **73**:2855 (2001).

37. I. Jureviciute, S. Bruckenstein, A. R. Hillman, and A. Jackson, *Physical Chemistry,* **2**:4193 (2000).
38. T. Matencio, J. M. Pernaut, and EricVieil, *Journal of Brazilian Chemistry Society,* **14**:90 (2003).
39. P. L. Runnels, J. D. Joseph, M. J. Logman, and R. M. Wightman, *Analytical Chemistry,* **71**:2782 (1999).
40. C. K. Baker and J. R. Reynolds, *Journal of Electroanalytical Chemistry,* **251**:307 (1988).
41. C. Debiemme-Chouvy, H. Cachet, and C. Deslouis, *Electrochimica Acta,* **51**:3622 (2006).
42. M. Bazzaoui, L. Martins, E. A. Bazzaoui, and J. I. Martins, *Electrochimica Acta,* **47**:2953 (2002).
43. N. C. T. Martins, T. M. e. Silva, M. F. Montemor, J. C. S. Fernandes, and M. G. S. Ferreira, *Electrochimica Acta,* **53**:4754 (2008).
44. B. C. Thompson, S. E. Moulton, J. Ding, R. Richardson, A. Cameron, S. O'Leary, G. G. Wallace, and G. M. Clark, *Journal of Controlled Release,* **116**:285 (2006).
45. X. Cui, J. F. Hetke, J. A. Wiler, D. J. Anderson, and D. C. Martin, *Sensors and Actuators A: Physical,* **93**:8 (2001).
46. Y. Xiao, X. Cui, J. M. Hancock, M. Bouguettaya, J. R. Reynolds, and D. C. Martin, *Sensors and Actuators B: Chemical,* **99**:437 (2004).
47. E. Barsoukov and J. R. MacDonald, *Impedance Spectroscopy. Theory, Experiment and Applications.,*Wiley, 2005.
48. A. C. Fisher, *Electrode Dynamics* Oxford Science Publications 1996.
49. X. Ren and P. G. Pickup, *The Journal of Physical Chemistry,* **97**:3941 (1993).
50. O. Antoine, Y. Bultel, and R. Durand, *Journal of Electroanalytical Chemistry,* **499**:85 (2001).
51. A. O. V. Syritski, O. Forsen, *Electrochimica Acta* **48**:1409 (2003).
52. Q. Xie, S. Kuwabata, and H. Yoneyama, *Journal of Electroanalytical Chemistry,* **420**:219 (1997).
53. R. Wadhwa, C. F. Lagenaur, and X. T. Cui, *Journal of Controlled Release,* **110**:531 (2005).
54. E. M. Genies, G. Bidan, and A. F. Diaz, *Journal of Electroanalytical Chemistry,* **149**:101 (1983).
55. C. S. C. Bose, S. Basak, and K. Rajeshwar, *The Journal of Physical Chemistry,* **96**:9899 (1992).

Chapter 5

Development of an Organic System for the Inclusion of two Water-Insoluble Drugs into Polypyrrole and their Subsequent Release:

Indomethacin Sodium Salt and Sulindac Sodium Salt

5.1 Introduction

Indomethacin and sulindac are both non-steroidal anti-inflammatory drugs (NSAID) and are used in the treatment of fever, pain and inflammation. Indomethacin (Indo) was first approved by the FDA in 1965 and its brand name is Indocin®. Sulindac (Sul) was FDA approved in 1978 and its tradename is Clinoril®. As these two drugs are in the same drug class as diclofenac sodium, their mechanism is almost identical. They act by inhibiting both cyclooxygenases (COX-1 and COX-2), which are enzymes that convert arachidonic acid into prostaglandins (PGs), thromboxanes and prostacyclins[1, 2]. The COX-1 isoenzyme is expressed in all tissues and its activation leads to the production of PGs involved in the maintenance of organ systems such as protection of the stomach wall or for kidney function[3]. The COX-2 is almost undetectable in most tissues under normal physiological conditions[4] but when there is damage in the body, proinflammatory cytokines are produced. This leads to COX-2 expression in the inflamed tissue resulting in PG formation, which mediates pain, fever and inflammation[5].

In this research, indomethacin sodium salt (NaIndo) and sulindac sodium salt (NaSul), shown in Figure 5.1, were studied. The carboxyl group on the Indo gives rise to a pKa of 4.5[6]. Indo is one of the most potent NSAID and is second only to diclofenac sodium ahead of naproxen and ibuprofen[7]. As can be seen in Figure 5.1, the nitrogen in the indole ring of NaIndo has been replaced in NaSul by a double bond, a so-called indene isostere which has the same electronic character as the lone pair of the indole nitrogen[8]. Because of the double bond, the aracyl substituent lies permanently in the cis configuration, ensuring good receptor fit. The electron withdrawing p-methylsulfoxide increases potency and the solubility of the drug. The pKa of Sul is 4.7[9].

Sul is a pro-drug metabolised by the liver and intestinal flora to a sulfone, which has no anti-inflammatory activity, and a sulfide, which is the active anti-inflammatory metabolite[10, 11], as shown in Figure 5.2. Regular use of NSAID has been associated with reduced risk of breast cancer. Sulindac and its metabolites

have been identified as possible candidates in the prevention of tumors and breast cancer[10, 12].

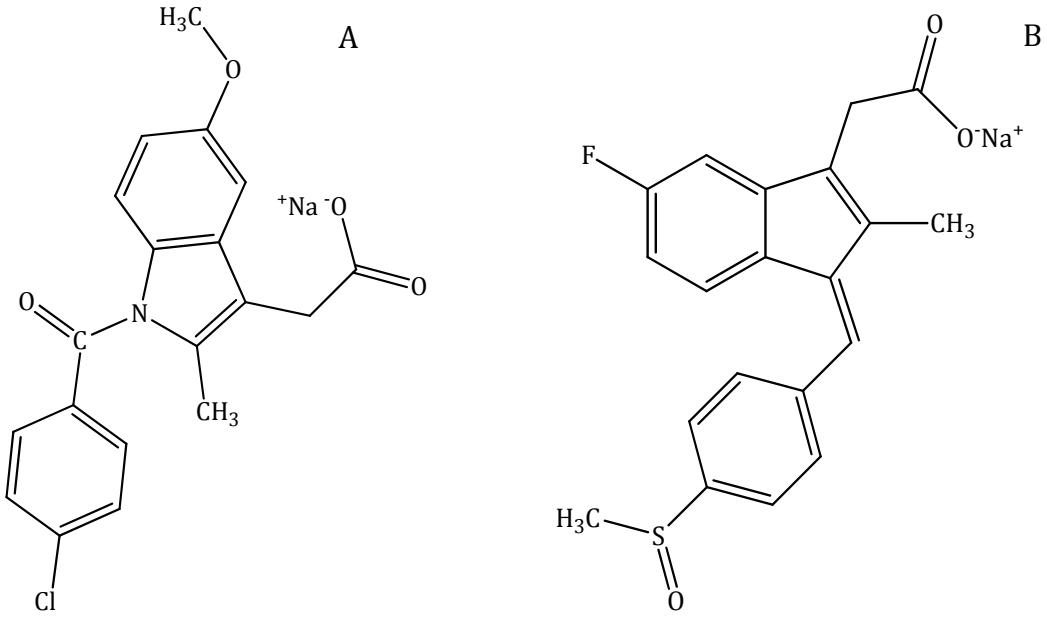

Figure 5.1: A Indomethacin sodium salt (NaIndo) and **B** Sulindac Sodium Salt (NaSul).

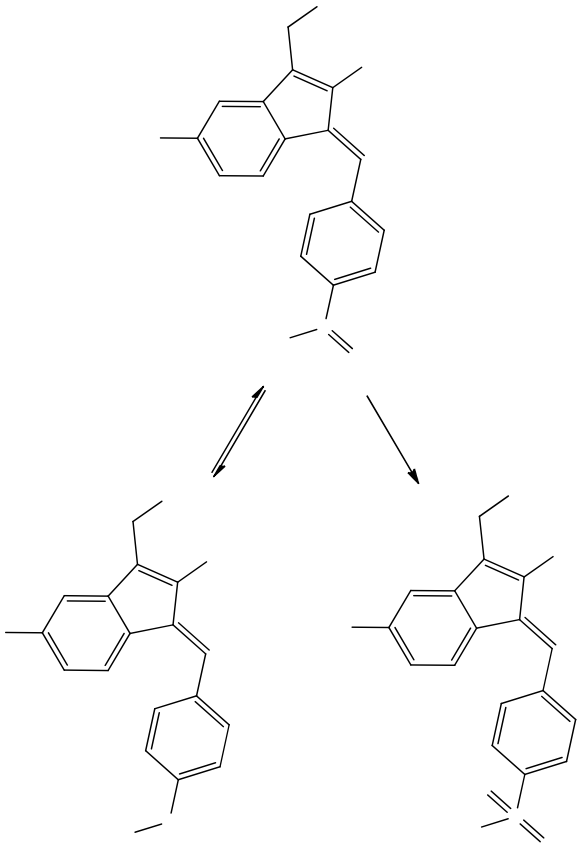

Figure 5.2: Sulindac and its major metabolites.

Although Indo and Sul have similar chemical structures, they have very different interactions with other drugs that patients receiving Indo or Sul may also be prescribed[13, 14]. Indo is eliminated *via* renal excretion, metabolism and biliary excretion. The therapeutic regimen ranges between 25 mg for a standard dose to 100 mg for slow release tablets and suppositories[15]. The half-life ($t_{1/2}$) varies between 2.6 and 11.2 h. The volume of distribution ranges from 0.34 to 1.57 L kg^{-1} and the plasma clearance ranges from 0.044 to 0.109 L kg^{-1} h^{-1} [16]. Sul, which is not as potent as Indo, is available in 150 mg and 200 mg tablets for oral administration[13, 14]. The pro-drug sulindac form of the drug is active, and has a $t_{1/2}$ of 7-8 h. It is reversibly converted to the corresponding sulfide form, which has even greater activity and a $t_{1/2}$ of 16.8 h[17]. The parent drug is also irreversibly converted to the sulfone analogue, which is inactive and excreted. Thus, sulindac has a long overall half life, and can be dosed less frequently[8].

As previously mentioned, both of these drugs have been on the market since the late sixties/early seventies and can be used in a variety of treatments. As a result, over the last number of years interest in the development of drug delivery systems (DDS) for the controlled release of these drugs has grown. Since both drugs can be described as hydrophobic, this complicates matters and conventional DDS, such as hydrogels, are not suitable. The controlled release of Indo has been documented using polymeric micelles[18-21]. Hydrophobic drugs can be physically encapsulated inside the hydrophobic core of the micelles formed from amphiphilic block co-polymers and the entrapped drug can be slowly released from the micelles[19]. The controlled release of Indo transdermally and from co-polymeric nanostructures has also been reported[22, 23]. While the controlled release of Sul from triblock co-polymers and polymeric microcarriers has been published[24, 25], to the best of the author's knowledge, there are no reports in the literature of the electrochemical controlled release of either $Indo^-$ or Sul^-.

In this chapter, polypyrrole (PPy) membrane films are electrodeposited onto a Pt electrode with either $Indo^-$ or Sul^- incorporated into the polymer by way of doping. An organic medium was required to increase the solubility of the drugs. The formation of PPy in the presence of acetonitrile (ACN) has been well

documented[26-33]. However, the formation of PPy doped with either $Indo^-$ or Sul^- was not possible in the presence of ACN and so ethanol (EtOH) was then chosen as the solvent. There are very few reports in the literature of the electrochemical oxidation of pyrrole (Py) to form a polymer film in the presence of EtOH[34, 35]. This is more than likely due to the poor conductivity of EtOH and the low solubility of simple salts, such as KCl or NaCl, in EtOH. However, with the addition of tetrabutylammonium perchlorate (TBAP), the conductivity of the EtOH was increased sufficiently to allow the formation of PPy doped with either $Indo^-$ or Sul^-.

5.2 Experimental

5.2.1 Materials

Indomethacin sodium salt (NaIndo) and sulindac sodium salt (NaSul) were both purchased from Sigma Aldrich and used as received. Pyrrole monomer (98%) was purchased from Aldrich and distilled prior to being used. All potentiostatic and cyclic voltammetry (CV) experiments were carried out on a Solartron (Model SI 1285) potentiostat. All release studies were carried out using a Varian Cary Series UV-vis spectrophotometer. Electrochemical impedance spectroscopy (EIS), electrochemical quartz crystal microbalance (EQCM) measurements, differential scanning calorimetry (DSC) and scanning electron microscopy (SEM) were carried out using the equipment described in Section 2.2.1.

5.2.2 Electrochemical experiments

The electrochemical cell was set up to use a Pt wire as the auxiliary electrode and a Pt electrode as the working electrode. PPy doped with $Indo^-$ (PPyIndo film) was formed at 36 °C and PPy doped with Sul^- (PPySul film) was deposited at 40 °C. The elevated temperatures were used to increase the solubility of $Indo^-$ and Sul^- in EtOH. For these experiments, a silver wire was used as a pseudo-reference electrode, while for all other experiments a standard saturated calomel electrode (SCE) was used as a reference electrode. During the release studies, all electrolytes were constantly stirred. As stated in the Chapter 2, Section 2.5.1, calibration curves for NaIndo and NaSul were obtained using UV-vis spectroscopy and used to determine the amount of drug released. The λ_{max} values of NaIndo and NaSul were

measured at 320 nm and 330 nm, respectively. Techniques including CV, EIS, EQCM and SEM were used in the characterisation of the polymers and are described in Chapter 2 in Section 2.4.

5.3 Results and discussion

5.3.1 Stability of the drugs and conductivity of the electrolytes

DSC was performed on the dry NaIndo and NaSul powders and the resulting thermograms are shown in Figure 5.3. The samples were held at 50 °C for 5 min before they were heated to 300 °C at a rate of 10 °C min^{-1}. The experiments were carried out under N_2 atmosphere to prevent oxidation phenomena. Two sharp endothermic peaks are seen at 162 °C and 187.5 °C which correspond to the melting of Indo and Sul, respectively[36-38]. The peaks thereafter correspond to the decomposition of the drugs.

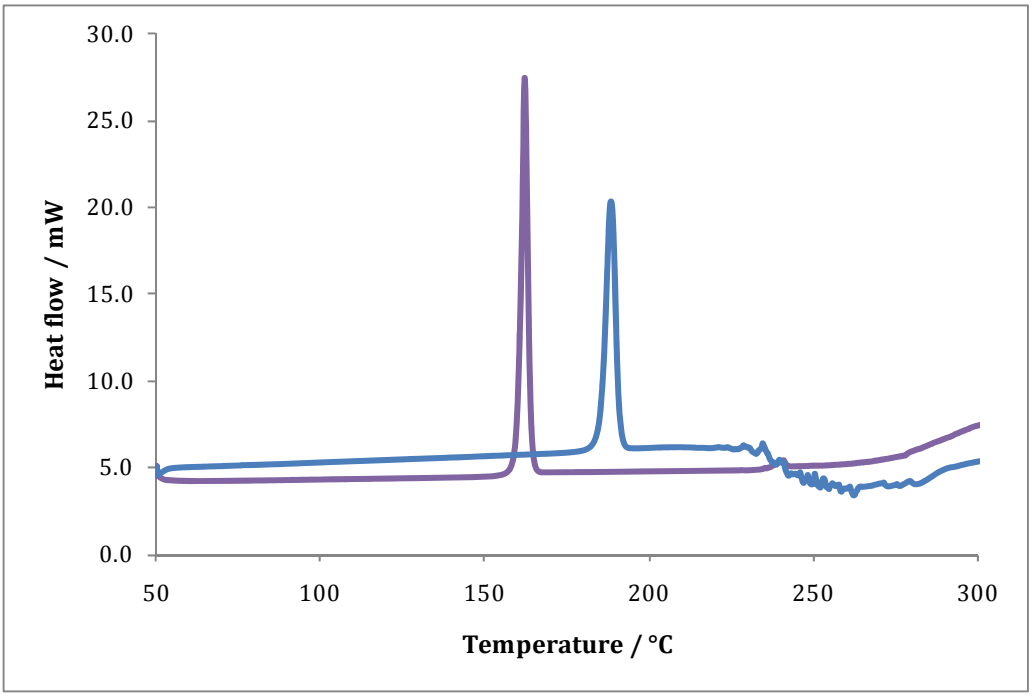

Figure 5.3: DSC thermogram of 3.0 mg samples of NaIndo and NaSul, isothermal pretreatment at 50 °C for 5 min. The temperature was scanned from 50 °C to 300 °C at a rate of 10 °C min^{-1}.

To verify that EtOH with TBAP is a suitable electrolyte for the polymerisation of Py, conductivity measurements were obtained at varying concentrations of TBAP in

the drug-EtOH solution. A concentration of 0.20 mol dm^{-3} of NaIndo was chosen. NaIndo was dissolved in EtOH at 60 °C but the temperature of the solution was lowered to 36 °C before the Py was added and the electropolymerisation reaction was carried out. The concentration of TBAP was varied and the resulting conductivity measurements are shown in Table 5.1.

NaSul is less soluble in EtOH and at a concentration of 0.20 mol dm^{-3}, a temperature of 70 °C was required to ensure the solubility of NaSul in EtOH. At 50 °C the drug reached its limit of solubility and precipitated from the EtOH solution. As previously described in Chapter 4, Section 4.3.2.3, at high temperatures there is a decrease in the redox activity of PPy[39]. Although the rate of the electropolymerisation reaction is increased with increasing temperatures, the PPy deposited on the electrode is more likely to become over-oxidised, promoting an insulating effect, which obstructs further growth of the PPy. For this reason, the concentration of the NaSul was lowered to 0.12 mol dm^{-3}. At this concentration the NaSul remained soluble at 40 °C and this temperature was chosen for the electropolymerisation reactions. The influence of TBAP on the conductivity of the NaSul-EtOH solution is shown in Table 5.1.

The low conductivity of the drug-EtOH solutions is clearly evident from Table 5.1, varying from 5 to 8 μS. However, there is a significant increase in the conductivity on addition of TBAP. For the drug-EtOH solutions, the conductivity has a near-linear relationship with the concentration of the TBAP, as shown in Figure 5.4. The R^2 values calculated are 0.988 and 0.976 for the NaIndo-EtOH and NaSul-EtOH, respectively. A linear correlation between the concentration and conductivity of an electrolyte is an indication of a strong electrolyte[40]. Figure 5.5 shows the molar conductivity as a function of the square root of the TBAP concentration for both drug-EtOH solutions. For a strong electrolyte a linear plot between the molar conductivity and the square root of concentration should satisfy the relationship, $\Lambda = \Lambda^\circ - \kappa\sqrt{C}$, (where Λ° is the molar conductivity at infinite dilution and κ is the Kohlrausch coefficient which depends on the nature of the specific salt in solution). This was not observed for the addition of TBAP as shown in Figure 5.5. However, a near-linear relationship is observed as the limiting molar conductivity is

approached, as opposed to the exponential relationship which is typical of weak electrolytes. These data show clearly that on addition of TBAP to the drug-EtOH solutions, suitable electrolytes with high conductivity are obtained.

The concentration of the TBAP is very important in relation to the concentration of the drug. The ClO_4^- anion of the TBAP is a small and mobile dopant that is a source of competition during the oxidation of Py and subsequent doping of the polymer. An increase in the concentration of the TBAP would mean a corresponding increase in the concentration of the drug to prevent the preferential doping of the PPy by the ClO_4^- over the drug. However, as the concentrations of the drug were limited by the solubility of the drug, the concentration of TBAP was set to give a drug/TBAP ratio $\geq$ 1.0. Therefore, a concentration of 0.20 mol dm^{-3} TBAP was chosen for the Indo system and a concentration of 0.08 mol dm^{-3} TBAP was chosen for the Sul system, which resulted in good conductivities of 2.03 mS and 1.63 mS for the two respective systems.

Table 5.1: Influence of TBAP on the conductivity of Indo-EtOH and Sul-EtOH solutions. Concentration of NaIndo was 0.20 mol dm^{-3}, while the concentration of NaSul was 0.12 mol dm^{-3}.

Concentration of TBAP / mol dm^{-3}	**Conductivity of NaIndo-EtOH solution / mS**	**Conductivity of NaSul-EtOH solution / mS**
0.00	0.008	0.005
0.04	0.062	1.080
0.08	1.074	1.632
0.12	1.426	2.180
0.16	1.780	2.620
0.20	2.030	3.030
0.24	2.450	3.380

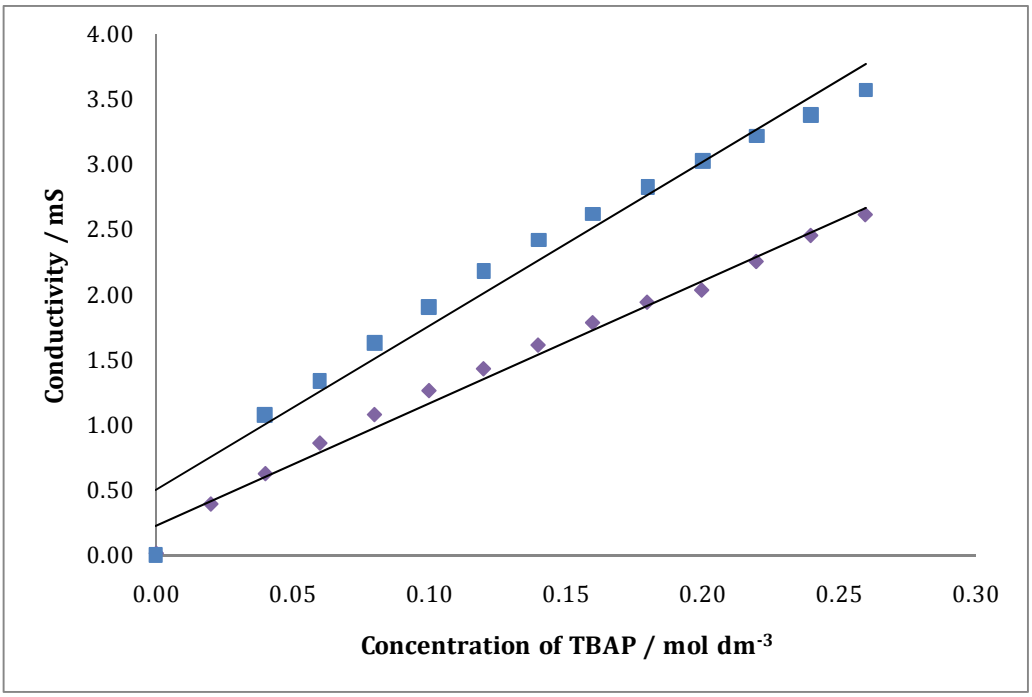

Figure 5.4: Conductivity of TBAP in ♦ NaIndo-EtOH and ■ NaSul-EtOH measured at 40 °C as a function of the concentration of TBAP. Concentration of NaIndo was 0.20 mol dm^{-3}, while the concentration of NaSul was 0.12 mol dm^{-3}.

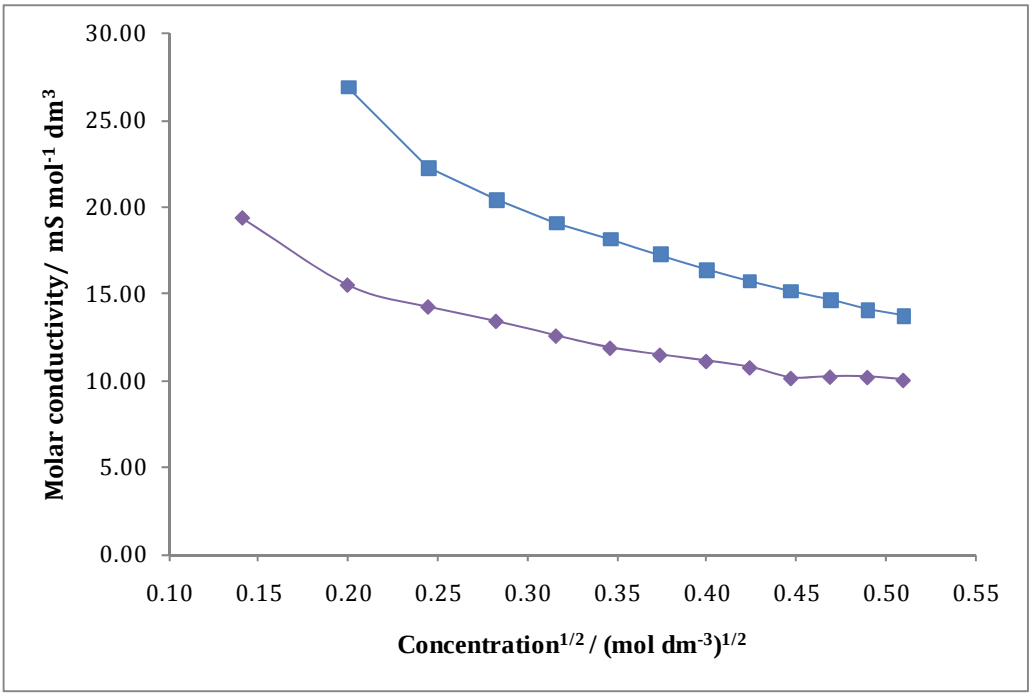

Figure 5.5: Molar conductivity of TBAP in ♦ NaIndo-EtOH and ■ NaSul-EtOH as a function of the square-root of the concentration of TBAP. Concentration of NaIndo was 0.20 mol dm^{-3}, while the concentration of NaSul was 0.12 mol dm^{-3}.

CV was then carried out to investigate the effect of TBAP on the electrochemistry of the system and to monitor the stability of the drug over a wide potential window. CV was performed at the bare Pt electrode at 25 mV s^{-1} and the potential was swept between -1.200 V vs $Ag|Ag^+$ and +0.700 V vs $Ag|Ag^+$ in the presence of four electrolytes; drug only in EtOH, TBAP only in EtOH, drug and TBAP in EtOH and an aqueous 0.10 mol dm^{-3} NaCl electrolyte, free from drug, EtOH and TBAP. Previous reports have documented the redox properties of Indo by CV[41, 42]. In these cases the Indo was dissolved in castor oil and CVs were performed in the presence of a phosphate buffer or Britton-Robinson buffer. The oxidation and reduction of Indo were observed at +0.600 V vs Ag|AgCl and +0.00 V vs Ag|AgCl, respectively[41]. From Figure 5.6, it is clear that the same redox properties for Indo are not observed in EtOH. The currents measured in the NaIndo-only containing EtOH solution are very low and the inset shows the recorded voltammogram more clearly. It is apparent that the CV is dominated by H_2 evolution at potentials more electronegative than –0.700 V vs $Ag|Ag^+$. However, the conductivity of this drug-EtOH solution is very low. Nevertheless, on addition of TBAP to the solution, similar CVs are recorded, although the currents are now much higher, due to the enhanced conductivity of the solution. Again, the CV is dominated by H_2 evolution at approximately –0.700 V vs $Ag|Ag^+$. This solution is now sufficiently conducting to observe the redox reactions of Indo, however no redox activity is observed.

All three CVs recorded in EtOH are very different to that recorded in the aqueous NaCl solution, as shown in Figure 5.6. The plot recorded in this aqueous solution is dominated by the electrochemistry of platinum and hydrogen adsorption/desorption. Interestingly, the CV recorded in the TBAP-EtOH solution displays some redox properties with broad waves centred at +0.100 V vs $Ag|Ag^+$ and at –0.700 V vs $Ag|Ag^+$. The broad oxidation wave observed in the TBAP-EtOH solution is similar to that seen with the aqueous NaCl solution and can be attributed to the formation of platinum oxides/hydroxides. The EtOH solutions contain a sufficient amount of water to facilitate these reactions at the platinum surface.

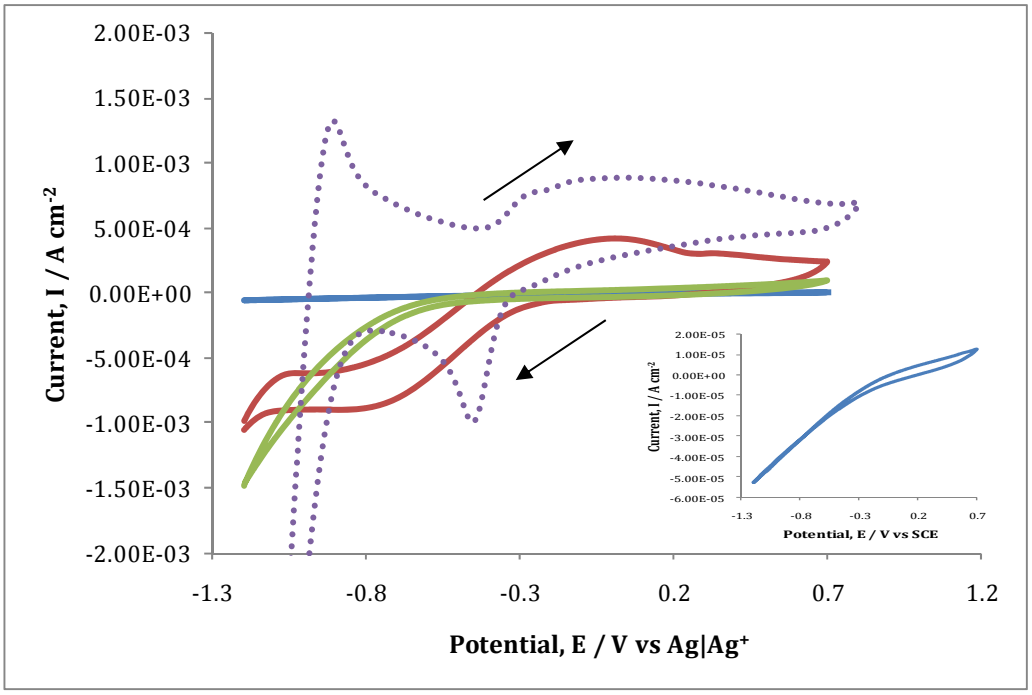

Figure 5.6: Cyclic voltammograms recorded at the bare Pt electrode at 25 mV s^{-1} in the presence of — 0.20 mol dm^{-3} NaIndo in EtOH (36 °C), — 0.20 mol dm^{-3} TBAP in EtOH (36 °C), — 0.20 mol dm^{-3} NaIndo and 0.20 mol dm^{-3} TBAP in EtOH (36 °C) and finally ▪▪▪ 0.10 mol dm^{-3} NaCl (at RT). The potential was swept between –1.200 V vs $Ag|Ag^+$ and +0.700 V vs $Ag|Ag^+$. Inset: in 0.20 mol dm^{-3} NaIndo in EtOH (36 °C).

Figure 5.7 shows the cyclic voltammograms recorded for the NaSul system. As seen with the NaIndo system, the currents measured in the NaSul-only containing EtOH are very low and the inset shows the resulting voltammogram more clearly. Again, H_2 evolution is a prevailing feature of the recorded CV. On addition of TBAP to the NaSul-EtOH solution, a significant increase in the current is observed. An oxidation peak is observed at about –0.500 V vs $Ag|Ag^+$, however this is close to the broad redox wave observed in the TBAP-EtOH solution and is unlikely to be due to the redox activity of NaSul. On comparing Figure 5.6 and Figure 5.7 some differences in the CVs are evident. For the NaSul system, similar oxidation currents are measured for the TBAP with and without the drug, but with the NaIndo system the presence of the NaIndo with the TBAP decreases the currents significantly. This suggests that the NaSul system allows electrochemistry to occur more easily than the NaIndo system. Both Figure 5.6 and Figure 5.7 indicate that the drugs are stable.

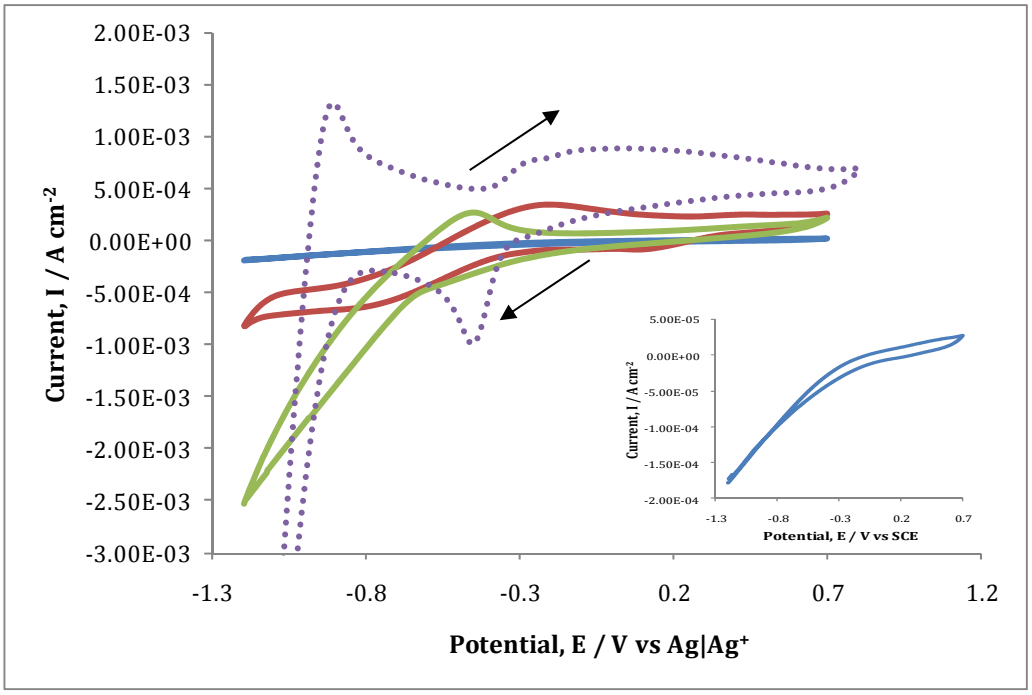

Figure 5.7: Cyclic voltammograms recorded at the bare Pt electrode at 25 mV s^{-1} in the presence of — 0.12 mol dm^{-3} NaSul in EtOH (40 °C), — 0.08 mol dm^{-3} TBAP in EtOH (40 °C), — 0.12 mol dm^{-3} NaSul and 0.08 mol dm^{-3} TBAP in EtOH (40 °C) and finally ▪▪▪ 0.10 mol dm^{-3} NaCl (at RT). The potential was swept between –1.200 V vs $Ag|Ag^+$ and +0.700 V vs $Ag|Ag^+$. Inset: in 0.20 mol dm^{-3} NaSul in EtOH (40 °C).

5.3.2 Electrodeposition of the polymers

5.3.2.1 Electrodeposition of PPyIndo

With parameters such as concentration of the drug, supporting salt and temperature optimised, attention was turned to the formation of PPy doped with $Indo^-$. Deposition of the polymer was achieved by applying a constant potential for 20 min. Potentials of +0.700 V vs $Ag|Ag^+$, +0.800 V vs $Ag|Ag^+$ and +0.900 V vs $Ag|Ag^+$ were applied and the resulting potentiostatic plots are shown in Figure 5.8. Adherent PPy films doped with $Indo^-$ were formed at each potential, but it is clear from both the current-time and the charge-time plots that the highest rate of polymer growth occurred at +0.900 V vs $Ag|Ag^+$. In order to ensure that a similar polymer was formed every time, which is important for the release studies, the polymer was grown to a set charge of 2.8 C cm^{-2}. Good reproducibility was achieved. This is clearly shown in Figure 5.9, where several charge-time plots

recorded under the same experimental conditions are shown. The average rate of polymerisation at +0.900 V vs Ag|Ag$^+$ was calculated as 2.38 x 10^{-3} C cm^{-2} s^{-1}.

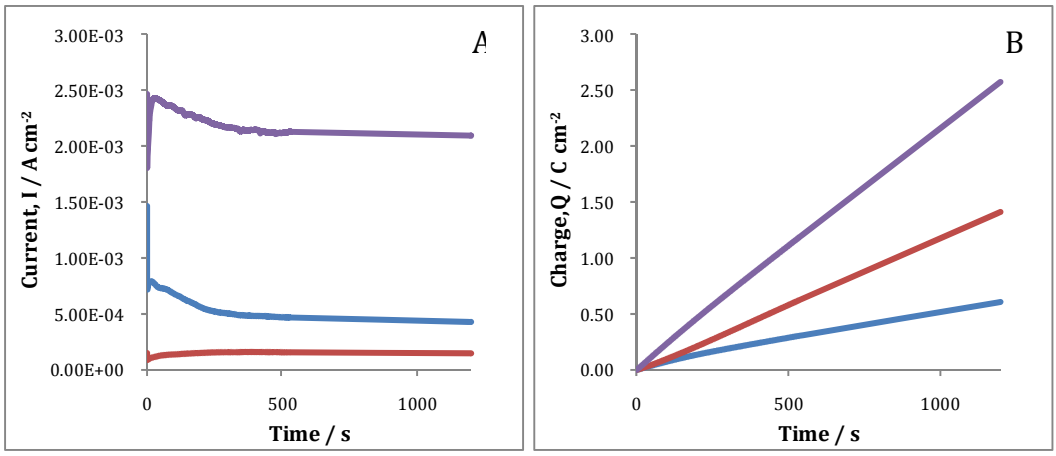

Figure 5.8: A Potentiostatic current-time plots and **B** charge-time plots for the formation of PPy doped with Indo$^-$ at 36 °C at — +0.700 V vs Ag|Ag$^+$, — +0.800 V vs Ag|Ag$^+$ and — +0.900 V vs Ag|Ag$^+$ from a solution of of 0.20 mol dm^{-3} NaIndo, 0.20 mol dm^{-3} TBAP and 0.20 mol dm^{-3} Py dissolved in EtOH.

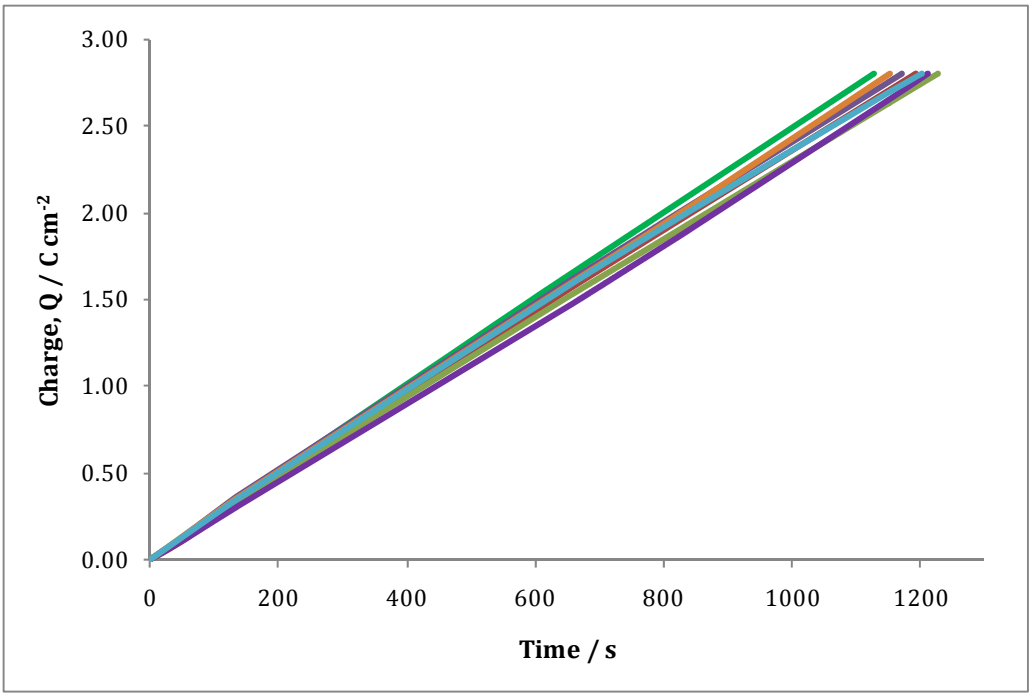

Figure 5.9: Charge-time plots for the electrodeposition of PPyIndo, deposited until a charge of 2.8 C cm^{-2} was reached, at +0.900 V vs Ag|Ag$^+$ in the presence of 0.20 mol dm^{-3} NaIndo, 0.20 mol dm^{-3} TBAP and 0.20 mol dm^{-3} Py in EtOH at 36 °C.

5.3.2.2 Formation of PPy doped with Sul⁻

As discussed in Section 5.3.1, a concentration of 0.12 mol dm^{-3} NaSul was chosen for the deposition of PPySul in EtOH and 0.08 mol dm^{-3} TBAP was added to increase the conductivity of the EtOH electrolyte to 1.63 mS. Polymerisation was carried out at 40 °C by applying a constant potential. Potentials of +0.800 V vs $Ag|Ag^+$ and +0.900 V vs $Ag|Ag^+$ were applied for 20 min and typical potentiostatic current-time and charge-time plots are shown in Figure 5.10. As with PPyIndo, the highest rate of electropolymerisation was observed at +0.900 V vs $Ag|Ag^+$ and for the release studies the PPySul was grown to a set charge of 2.8 C cm^{-2} to ensure reproducibility. The rate of polymerisation at +0.900 V vs $Ag|Ag^+$ was calculated as 2.0 x 10^{-3} C cm^{-2} s^{-1}, which is similar to the rate of polymerisation of PPyIndo.

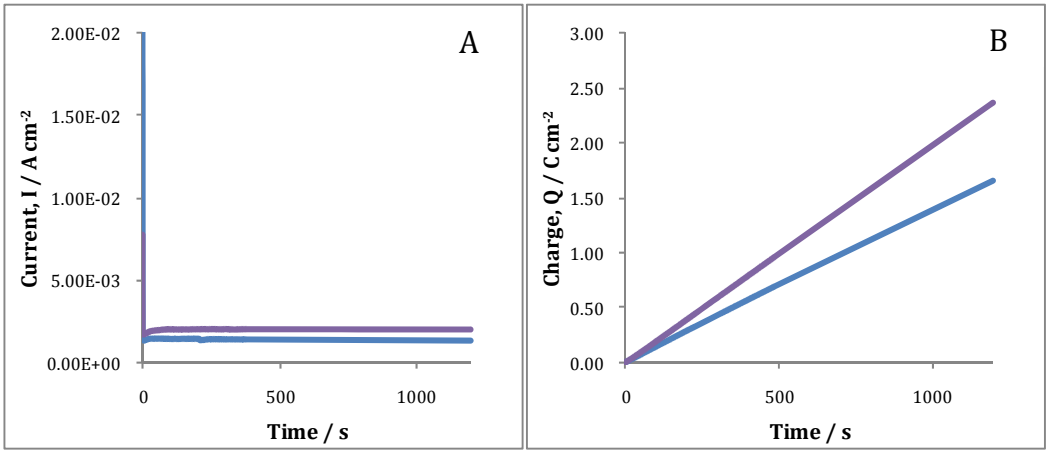

Figure 5.10: A Potentiostatic current-time plots and **B** charge-time plots for the formation of PPy doped with Sul^-, deposited until a charge of 2.8 C cm^{-2} was consumed, at — +0.800 V vs $Ag|Ag^+$ and — +0.900 V vs $Ag|Ag^+$ in the presence of 0.12 mol dm^{-3} NaSul, 0.08 mol dm^{-3} TBAP and 0.20 mol dm^{-3} Py in EtOH. Experiments were carried out at 40 °C.

In Section 3.3.2.2, the rate of polymerisation for the bulk PPyDex was calculated between 3.3 x 10^{-3} and 4.8 x 10^{-3} C cm^{-2} s^{-1}. Taking into account the concentration of the NaDex, 0.05 mol dm^{-3}, the rate of polymerisation in the aqueous system is higher than that measured here for the organic system. As discussed in Chapter 1, Section 1.4.1, the initial step in the mechanism of electropolymerisation of Py, proposed by Diaz *et al.*[43], is the generation of the radical cation. The coupling of

two Py radicals results in the formation of a bond between the two α positions to give a radical dication. There is a certain amount of electrostatic repulsion between the two radical cations which may be influenced by local polarity effects. Several studies have been carried out comparing the polymerisation of Py in the presence of water, ACN and mixtures of both water and ACN[26, 44-46]. These studies show that the presence of water has a positive effect on the electropolymerisation of Py and this is believed to be due to its higher dielectric constant (80 compared to 37 for ACN) which reduces the Coulombic repulsions between the radical cations and consequently facilitates the radical-radical coupling. Furthermore, the dielectric constant of EtOH is 24 at 25 °C which is lower than that of ACN and the dielectric constant is known to decrease with an increase in temperature[47]. With the polymerisation in EtOH carried out between 36 °C and 40 °C, this is the most likely explanation for the difference in the rates of polymerisation between the aqueous and organic systems.

5.3.2.3 Influence of temperature on rate of polymerisation

The temperature of the electropolymerisation solution was varied to monitor its effect on the rate of polymer growth. The PPyIndo was deposited by applying a potential of +0.900 V vs $Ag|Ag^+$ for 60 min at 40 °C, 45 °C, 50 °C, 55 °C and 60 °C. The charge-time plots recorded and the charges reached are shown in Figure 5.11. It is clear from Figure 5.11 that the temperature influences the rate of polymerisation. At 45 °C, the largest charge was consumed and the rate was calculated as 3.8×10^{-3} C cm^{-2} s^{-1} with the slowest rate of polymerisation of 1.9×10^{-4} C cm^{-2} s^{-1} calculated at the higher temperatures of 50 °C, 55 °C and 60 °C. The rate of deposition at 45 °C is slightly higher than that measured at 36 °C.

Similar patterns were also seen in the rate of polymerisation of PPySul. Studies were carried out at 45 °C, 50 °C, 55 °C and 60 °C to investigate what effect increasing the temperature would have on the rate of polymer deposition. A constant potential of +0.900 V vs $Ag|Ag^+$ was applied for 60 min and the charge-time plots recorded along with the charges consumed in that time are shown in Figure 5.12. Again, it is evident in Figure 5.12 that the rate of polymerisation decreases as the temperature increases. At 45 °C the rate of polymerisation is

4.0 x 10^{-4} C cm^{-2} s^{-1}, which is a factor of 10 slower than the rate of polymerisation measured in Section 5.3.2.2 for the deposition of PPySul at 40 °C.

From these studies, it was apparent that a lower temperature provides more suitable conditions for polymerisation. As previously stated, the rate of the electropolymerisation reaction may be increased as the temperatures are elevated but the PPy deposited on the electrode is more likely to become over-oxidised, causing an insulating effect, which hinders further growth of the PPy. Furthermore, the dielectric constant of the electrolyte decreases as the temperature increases and this also affects the rate at which polymerisation can occur. For all further studies, the electrolytes were kept at the lowest temperature that ensured the solubility of the drug, i.e., 36 °C for the Indo system and 40 °C for the Sul system.

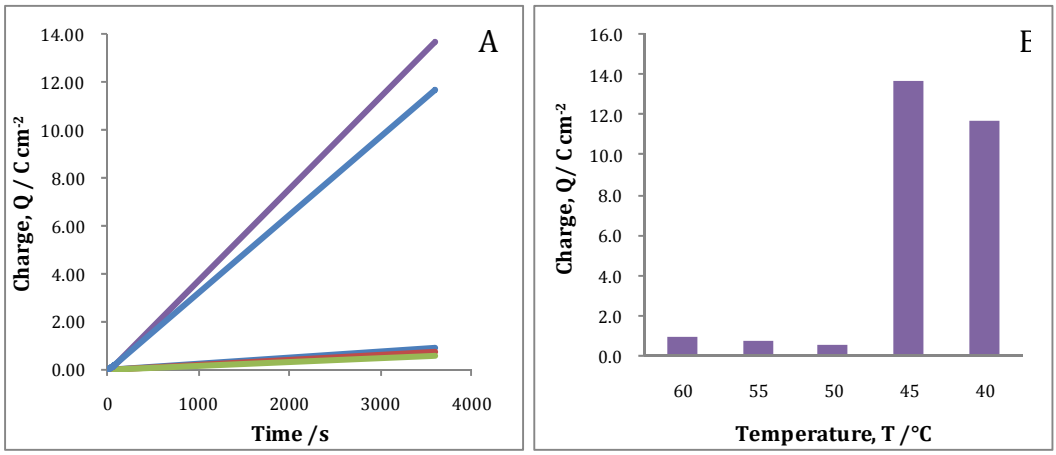

Figure 5.11: A Charge-time plots and **B** amount of charge consumed in 60 min as a function of temperature in the presence of 0.20 mol dm^{-3} NaIndo, 0.20 mol dm^{-3} TBAP and 0.20 mol dm^{-3} Py in EtOH. A constant potential of +0.900 V vs $Ag|Ag^{+}$ was applied for 60 min at 40 °C, 45 °C, 50 °C, 55 °C and 60 °C.

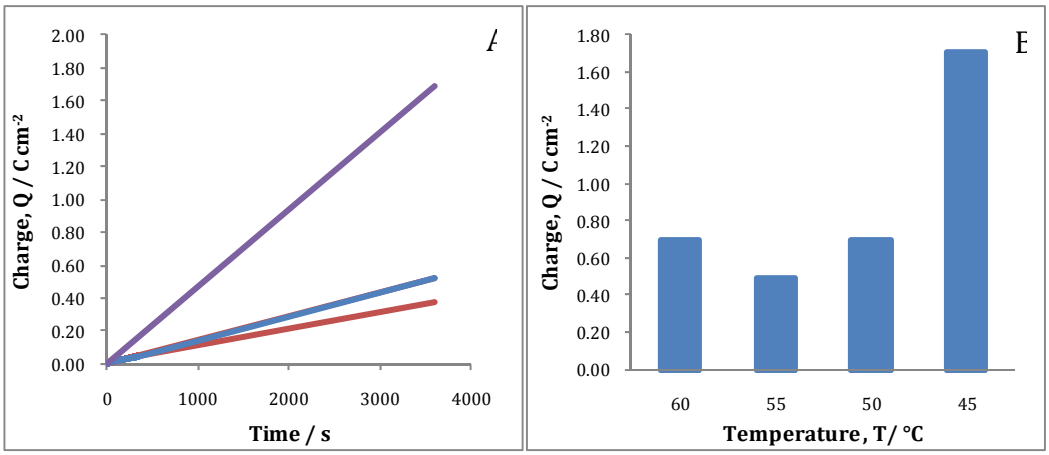

Figure 5.12: A Charge-time plots and **B** amount of charge consumed in 60 min as a function of temperature in the presence of 0.12 mol dm^{-3} NaSul, 0.08 mol dm^{-3} TBAP and 0.20 mol dm^{-3} Py in EtOH. A constant potential of +0.900 V vs $Ag|Ag^{+}$ was applied for 60 min at 45 °C, 50 °C, 55 °C and 60 °C.

5.3.3 Characterisation of the polymers

5.3.3.1 Redox properties of the polymers

Cyclic voltammetry (CV) was employed to investigate the redox properties of the polymers. As discussed in Section 3.3.3.2, a slow scan rate and low pH provide favourable conditions under which CV can be performed[48-50]. The polymers were deposited, as described in Sections 5.3.2.1 and 5.3.2.2. Both polymers were grown until a charge of 2.8 C cm^{-2} was consumed. The potential was swept between –1.200 V vs SCE and +0.700 V vs SCE at a scan rate of 25 mV s^{-1} in the presence of 0.10 mol dm^{-3} NaCl at pH ~ 3.0. The cyclic voltammograms recorded are compared to a CV of PPyCl performed under the same conditions in Figure 5.13. In all cases the redox properties observed are due to the expulsion and incorporation of the anion across the polymer membrane. The redox properties of the PPyCl are clearly evident at approximately +0.200 V vs SCE and –0.200 V vs SCE. The redox waves are broad consistent with the relatively slow expulsion of Cl anions as the film is reduced and the incorporation of Cl^{-} as the oxidation process proceeds.

For PPySul, a reduction peak can be seen at +0.200 V vs SCE with a broad oxidation wave extending from about –0.300 V to +0.700 V vs SCE. Again, the peaks are broad. Reduction of the PPySul film occurs in the same potential window as the

PPyCl film, however, the oxidation wave appears at slightly higher potentials. In contrast, the cyclic voltammogram recorded for PPyIndo is very different. The currents recorded for the PPyIndo film are very low compared to those seen for both PPyCl and PPySul. A small but distinct reduction peak can be seen at – 0.600 V vs SCE for PPyIndo along with a small oxidation wave at approximately +0.100 V vs SCE. This variation in current between the PPySul and the PPyIndo films suggests that PPyIndo is not as electrochemically active as the PPySul.

In order to probe these properties, further investigations were carried out on both polymer films using electrochemical impedance spectroscopy (EIS).

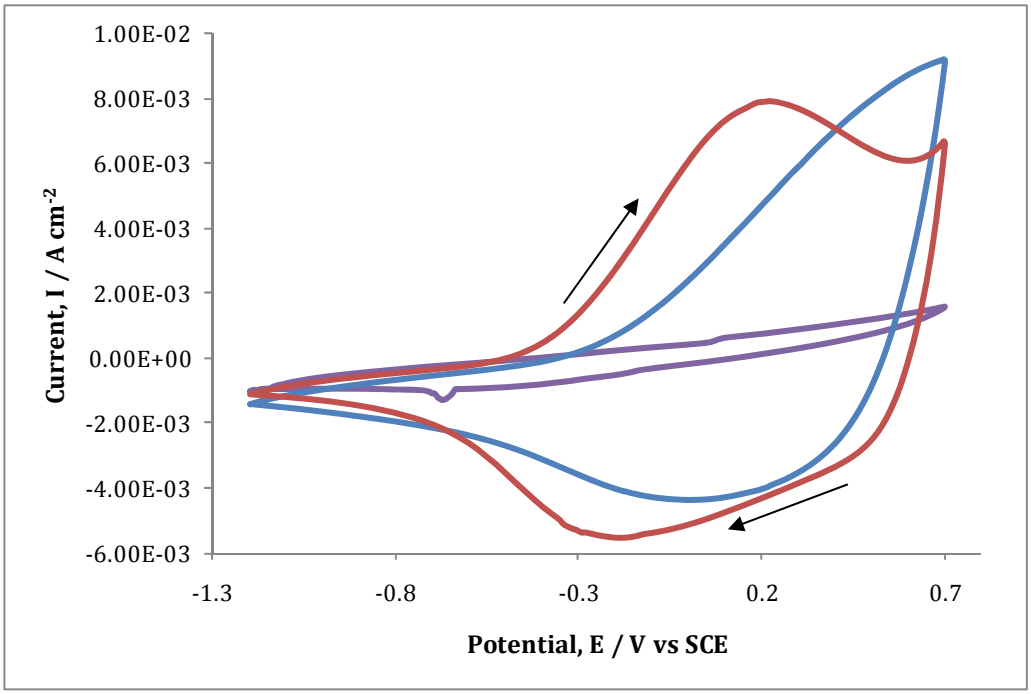

Figure 5.13: Cyclic voltammograms, 20th cycle, recorded in the presence of 0.10 mol dm^{-3} NaCl (pH 3) for — PPyIndo, — PPySul and — PPyCl. Potentials were swept between – 1.200 V vs SCE and +0.700 V vs SCE at a scan rate of 25 mV s^{-1}.

5.3.3.2 Characterisation of the polymers by EIS

PPyIndo and PPySul were deposited as before by applying a potential of +0.900 V vs $Ag|Ag^{+}$ until a charge of 2.8 C cm^{-2} was consumed in the appropriate electrolytes. PPyIndo and PPySul were formed at 36 °C and 40 °C, respectively. All impedance measurements were carried out at room temperature and were

employed to investigate the stability of the polymer at – 0.900 V vs SCE and at open-circuit potentials (OCP). As in previous studies, the two potentials were chosen so that an understanding of the properties of the polymer could be achieved at two stages; when it was first deposited and when the drugs were released.

Representative impedance plots for PPyIndo and PPySul films are shown in Figure 5.14 and Figure 5.15, respectively, in the complex plane and Bode formats. The modulus of the impedance, Z, and the phase angle presented as a function of the frequency gives the Bode plot, while the imaginary and real components of the impedance are plotted to give the complex plane. In all cases, the data were recorded as a function of the immersion period for a total of 8 h in 0.10 mol dm^{-3} NaCl. The first impedance profile was recorded following an initial 10 min polarisation period at the desired potential. Similar data were recorded for the bare Pt electrode, however these are not shown.

All data were fitted to the equivalent circuits depicted in Figure 5.16. The circuit shown in Figure 5.16A was used to fit the experimental data when the bare Pt electrode and PPySul were held at OCP. This corresponds to a two-time constant model. A simple Randles cell, presented in Figure 5.16B, was used to model the data when PPyIndo was held at OCP and when the bare Pt, PPySul and PPyIndo were all maintained at –0.900 V vs SCE. In these circuits, R1 represents the solution resistance; R2 represents the charge-transfer resistance, while CPE1 and CPE2 are constant phase elements. Constant phase elements were used to determine the capacitance of the polymer interface rather than pure capacitors; this allows for the inhomogeneity of the surface to be taken into account[51]. As described in Chapter 2, Section 2.4.7, the CPE has a T component and a P component, where T is the magnitude of the impedance and P is the exponent. When P exhibits a value of 1.0 the constant phase element corresponds to a true ideal capacitor, when the value is between 0.8 and 1.0 it is regarded as a non-ideal capacitor and when it has a value of 0.5 it corresponds to a diffusional process[52]. As shown from a comparison of the experimental and fitted data in both Figure 5.14 and Figure 5.15, very good agreement between the experimental measurements

and simulated data was obtained. Clearly, there is a significant difference between the two polymer systems under open-circuit conditions. The PPyIndo is characterised by a large and depressed semicircle consistent with a high charge transfer resistance, while the PPySul system exhibits a diffusion tail and much lower impedance values across the entire frequency range. These data are in good agreement with the CV measurements, presented in Figure 5.13.

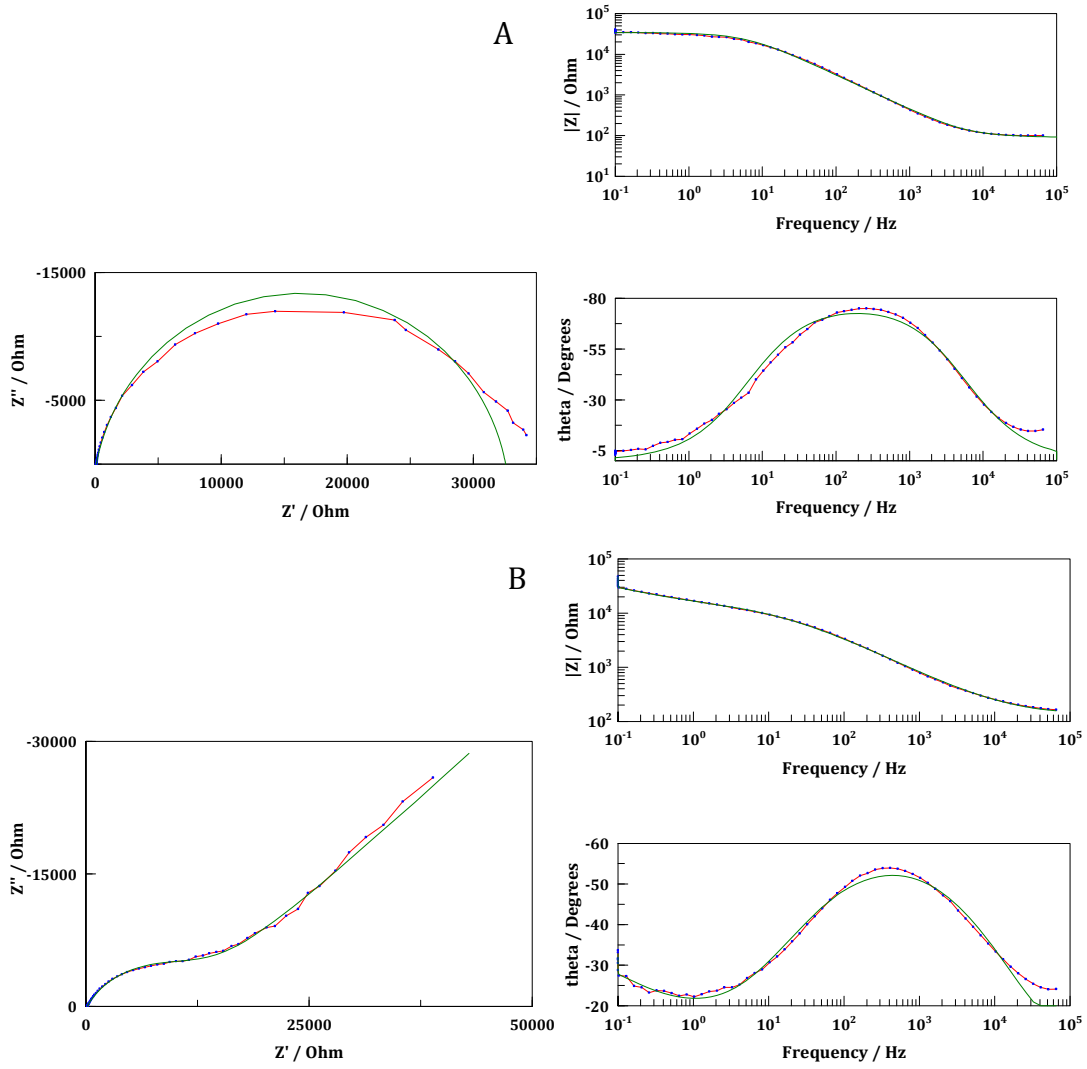

Figure 5.14: Complex Plane plot and Bode plot recorded in 0.10 mol dm^{-3} NaCl using a sinusoidal excitation voltage of 10 mV, measured at **A** open-circuit potential and at **B** –0.900 V vs SCE for the PPyIndo. Both the experimental data and the simulated fitted traces are shown. The PPyIndo films were deposited on a Pt electrode to a charge of 2.8 C cm^{-2} at 36 °C. (Area = 0.125 cm^2). (Ohm refers to the unit of Ω).

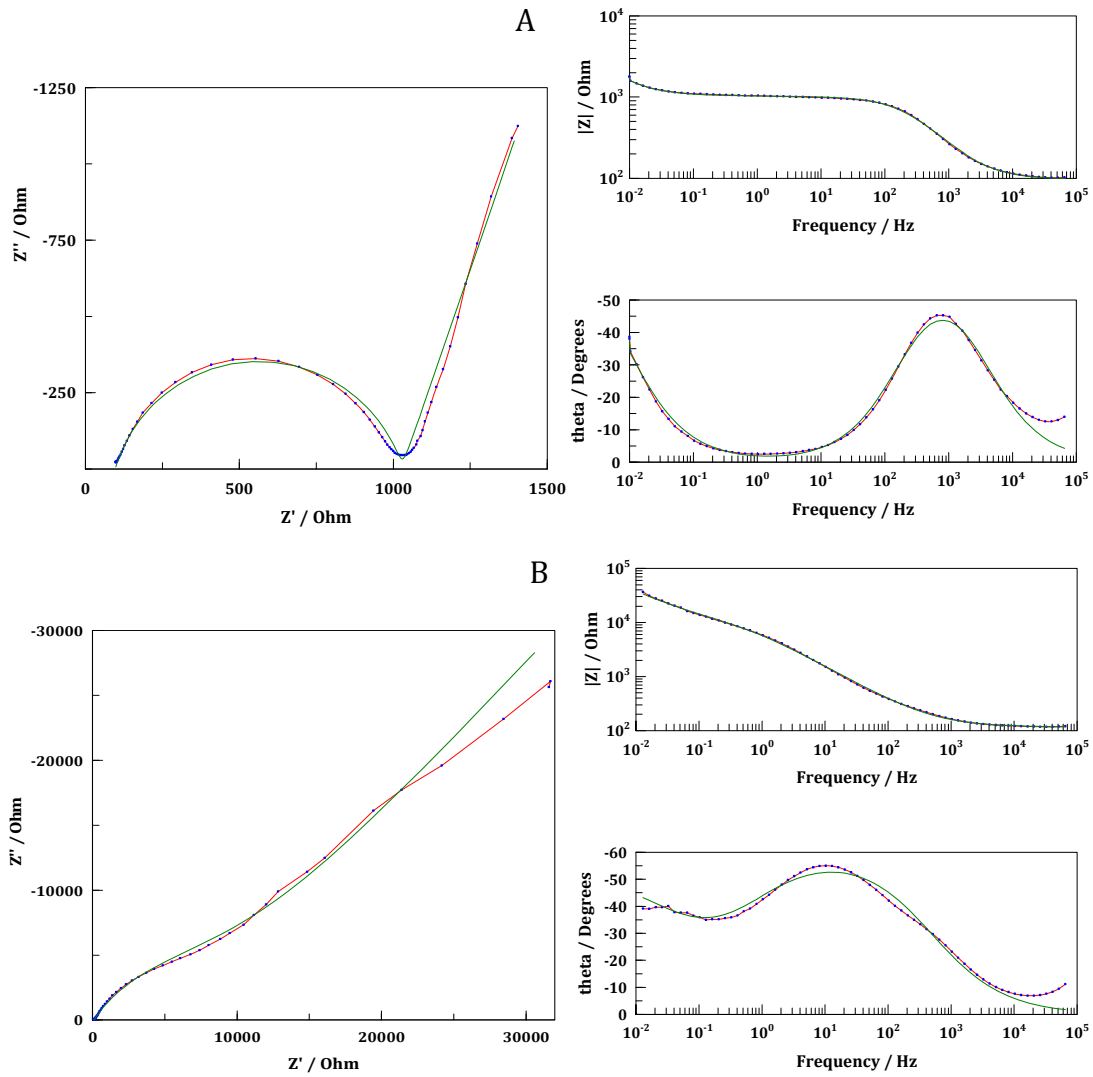

Figure 5.15: Complex Plane plot and Bode plot recorded in 0.10 mol dm^{-3} NaCl using a sinusoidal excitation voltage of 10 mV, measured at **A** open-circuit potential and at **B** –0.900 V vs SCE for the PPySul. Both the experimental data and the simulated fitted traces are shown. The PPySul films were deposited on a Pt electrode to a charge of 2.8 C cm^{-2} at 40 °C. (Area = 0.125 cm^2). (Ohm refers to the unit of Ω).

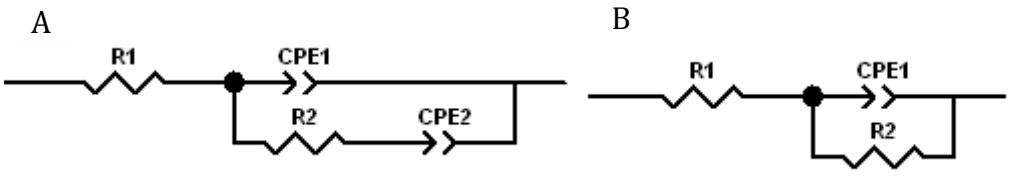

Figure 5.16: Equivalent circuits used to fit the data recorded for PPyIndo and PPySul and bare Pt electrode at OCP and –0.900 V vs SCE.

The steady-state conditions were probed by collecting the impedance spectra over eight consecutive experiments and comparing the circuit parameters. Figure 5.17 shows the R2, which is equivalent to the charge-transfer resistance, and capacitance (P ≈ 0.8) measured at OCP for both the bare Pt electrode and PPyIndo as a function of time. The potential of the cell recorded over the eight experiments was approximately +0.350 V vs SCE for the PPyIndo. Under these conditions, the PPyIndo is oxidised and the R2 reaches values close to 30 kΩ. PPy is known to have high electronic conductivity in the oxidised or even slightly oxidised states[53, 54]. Therefore, the electronic resistance of the film is negligible under these conditions. Instead, this high resistance denotes the resistance to ion transfer at the polymer solution interface, the electron transfer resistance at the platinum polymer boundary and the intrinsic charge transfer resistance. The R2 values recorded at the PPyIndo increase as a function of the immersion time. These increasing values may be related to conformational changes, solvent and/or electrolyte movement within the film.

On the other hand, the capacitance of the polymer is relatively constant as a function of time. However, as seen with PPyDF the capacitance is low at about 3 μF compared to the typical values of mF recorded for conducting polymers, when maintained in the oxidised state[55, 56].

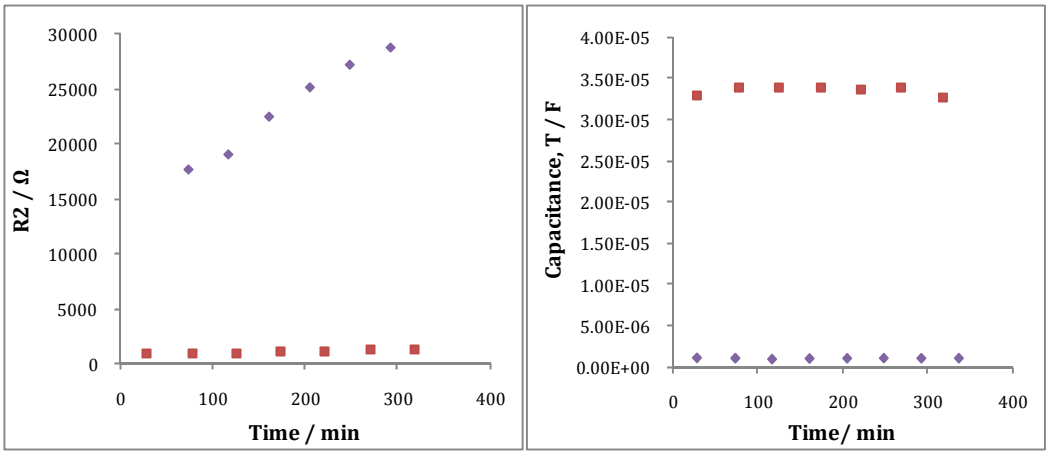

Figure 5.17: Resistance, R2, and capacitance, T with P ≈ 0.8, recorded at OCP in 0.10 mol dm^{-3} NaCl for ■ bare Pt and ♦ PPyIndo. Impedance data were recorded using a sinusoidal excitation voltage of 10 mV. (Area = 0.125 cm^2).

The R2 and CPE1 measured at –0.900 V vs SCE for both the bare Pt and PPyIndo are presented in Figure 5.18. CPE1 corresponds to a diffusional process for PPyIndo and a capacitor for bare Pt. At the bare electrode, it can be seen that there is a slight increase in resistance and a decrease in capacitance as a function of time, which indicates a loss in conductivity. At these reduction potentials, hydrogen adsorption occurs at the surface of the bare electrode which results in the decrease of electron kinetics at the surface[57]. The reduction of the PPyIndo results in the formation of PPy^0 and $Indo^-$. The presence of the PPy^0 lowers the electronic conductivity of the polymer, which is consistent with an increase in resistance. The resistance and capacitance measured at the higher time periods is relatively constant, which indicates the polymer is relatively stable when it is reduced.

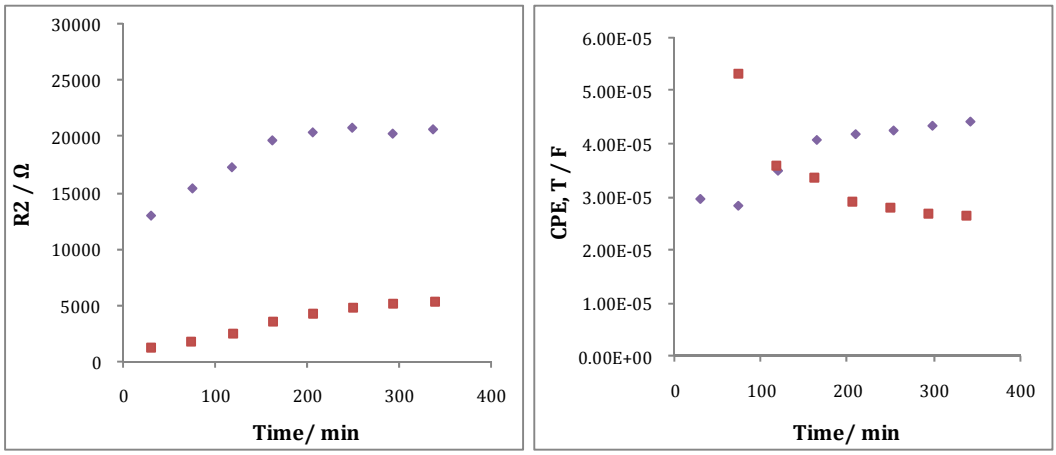

Figure 5.18: Resistance, R2, and constant phase element, CPE, recorded at –0.900 V vs SCE in 0.10 mol dm^{-3} NaCl for ■ bare Pt and ♦ PPyIndo. Impedance data were recorded using a sinusoidal excitation voltage of 10 mV. CPE1 corresponds to a diffusional process for PPyIndo and a capacitor for bare Pt. (Area = 0.125 cm^2).

Figure 5.19 shows the R2, which is equivalent to the charge-transfer resistance, and capacitance (P ≈ 0.8) measured at OCP for both the bare Pt electrode and PPySul as a function of time. For the PPySul, the potential of the cell recorded over the eight experiments was approximately +0.270 V vs SCE. The R2 values recorded for PPySul are considerably lower than those recorded for PPyIndo. As seen with PPyDex, the resistance, R2, is higher at the bare Pt than at the polymer. This is due to the higher surface area and more efficient charge transfer of the conducting polymer coating[53, 58]. The R2 values at OCP vary from 200 to 1000 Ω over the 400

min period. This suggests that the polymer is relatively stable and remains highly conducting over long periods of time under open-circuit conditions. Again the capacitance is lower than what is typically recorded for conducting polymers.

Figure 5.20 shows the R2 and capacitance recorded for both the Pt electrode and the PPySul at a reduction potential of –0.900 V vs SCE. As seen with the previous polymers discussed in Chapters 3 and 4 and with PPyIndo, the polymer has a higher R2 than seen at the bare electrode. This is due to a loss in the electronic conductivity as a result of the formation of PPy^0 and Sul^-, which in turn increases the resistance. Interestingly, the R2 values are similar for the PPySul and PPyIndo when the polymers are reduced.

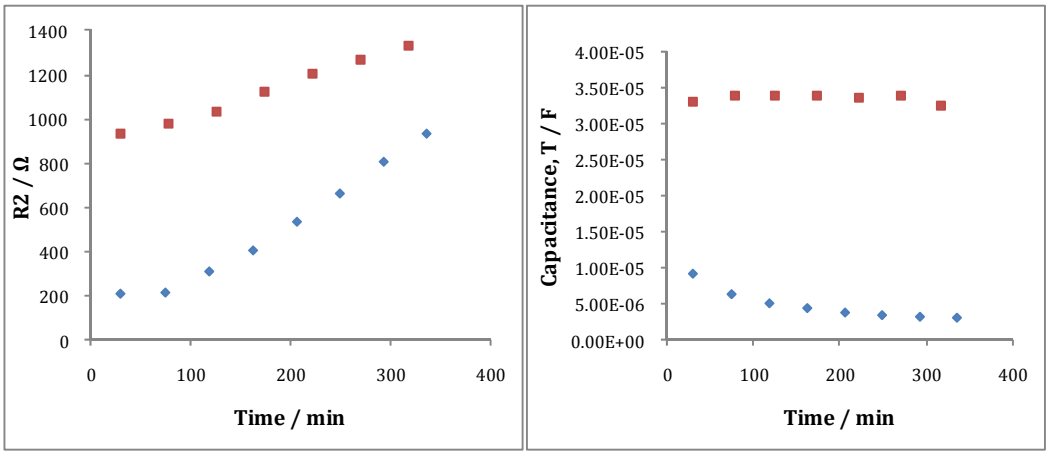

Figure 5.19: Resistance and capacitance, T with P ≈ 0.8, data recorded for ■ bare Pt and ♦ PPySul at OCP in 0.10 mol dm^{-3} NaCl. Impedance data were recorded using a sinusoidal excitation voltage of 10 mV. (Area = 0.125 cm^2).

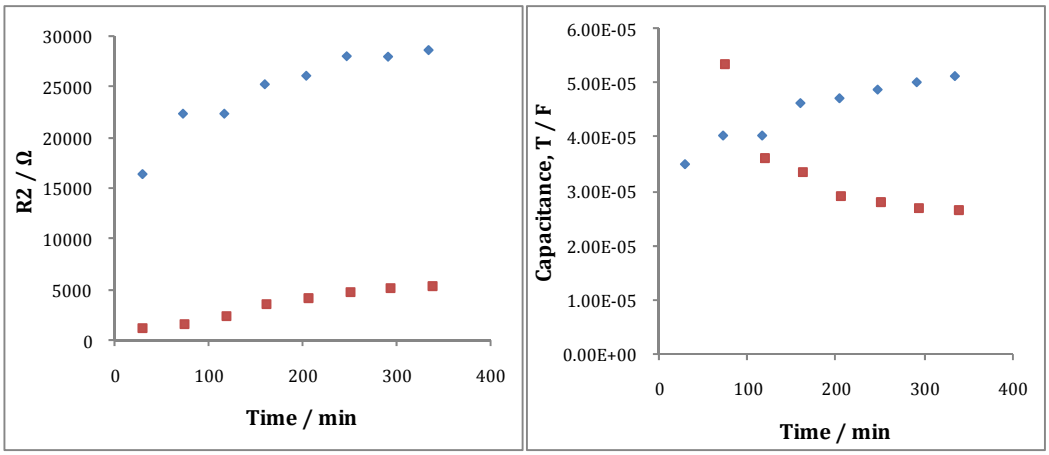

Figure 5.20: Resistance, R2, and capacitance, CPE1, T with P ≈ 0.8, recorded at -0.900 V vs SCE in 0.10 mol dm^{-3} NaCl for ■ bare Pt and ♦ PPySul. Impedance data were recorded using a sinusoidal excitation voltage of 10 mV. (Area = 0.125 cm^2).

The capacitances measured in this study of PPyIndo and PPySul are lower than the CPE measured for PPyDex and indeed lower than the typical capacitance recorded for polypyrrole[56]. Kim and co-workers[59] studied the electrochemical properties of PPy films prepared in water and ACN and found that the polymers prepared in aqueous media show larger capacitance values. This suggests that the PPy films prepared in water have higher porosities and are capable of storing more charge than those prepared in ACN. This may also be the case for polymers prepared in EtOH.

5.3.3.3 Mass and doping levels of the polymers

EQCM measurements were carried out in order to estimate the mass and doping levels of the polymers. Similar to the EQCM studies of PPyDF, described in Section 4.3.3.5, the electrodeposition of the PPyIndo and PPySul could not be carried out under the heated conditions used for the growth of the bulk polymer. The electrolytes could not be sustained at constant temperatures in the EQCM cell and were therefore heated to 70 °C before they were transferred into the EQCM cell. This was sufficient to allow the drugs to remain soluble in solution during the entire polymerisation time, between 100 and 300 s.

The Sauerbrey equation, Equation 2.2, relates the frequency shift of the crystal to the change in mass of the polymer. This equation is only applicable under certain

conditions[60]; the polymer film must behave as a rigid and perfectly elastic layer. The rigid film approximation is valid if the polymer thickness is small compared to the thickness of the crystal and if the overall mass loading results in a change in frequency that is small with respect to the resonant frequency of the unloaded crystal. Accordingly, the analysis was confined to thin PPyIndo and PPySul films. In these studies, the polymers were grown to a charge of 2.0 x 10^{-2} C by applying a constant potential of +0.900 V vs Ag|AgCl. It should also be noted that this equation assumes the current efficiency for the electropolymerisation of Py is 100% and that no solvent is incorporated into the film[61]. Furthermore, even though it is likely that some ClO_4^- is also doped within the polymer, its contribution to the polymer is not taken into account in this section. The doping levels are calculated on the assumption that the drug under investigation is the sole dopant even though it is probable that some ClO_4^- is also doped within the polymer. The amount of ClO_4^- incorporated in the PPy films is investigated later in this chapter in Section 5.3.4.2.

The mass-charge plots and charge-time plots for the PPy films doped with $Indo^-$ are shown in Figure 5.21. The data from three separate experiments are plotted, showing good reproducibility in the nucleation and growth of the PPyIndo films. The linear charge-time plot, seen in Figure 5.21B, suggests that the rate of polymerisation is constant at approximately 1.25 x 10^{-4} C s^{-1}. However, in Figure 5.21A, it is apparent that the mass-to-charge ratio is not constant and there seems to be three stages of polymer growth. At low charges only a very small amount of polymer is deposited. This is followed by a rapid increase in mass and the deposition of larger quantities of the polymer, to give a mass-to-charge ratio of about 1.2 x 10^{-3} g C^{-1}. Finally, the mass-to-charge ratio decreases to about 9.0 x 10^{-4} g C^{-1}.

Using Equation 2.4, a derivation of Faraday's law, and the charge consumed during deposition, the average final mass and doping levels of the polymer were calculated and are shown in Table 5.2. The average doping level was calculated as 0.24 which indicates a ratio of 4:1 for monomer-to-dopant which has been reported for PPy doped with camphorsulfonate (CS^-)[62]. The percentage of total mass contributed by the $Indo^-$ was 54 %. This is lower than the percentage of Dex^{2-}

and similar to that of the DF^-. This seems reasonable considering the molecular weights of the dopants and the higher doping levels calculated for Dex^{2-} and DF^-.

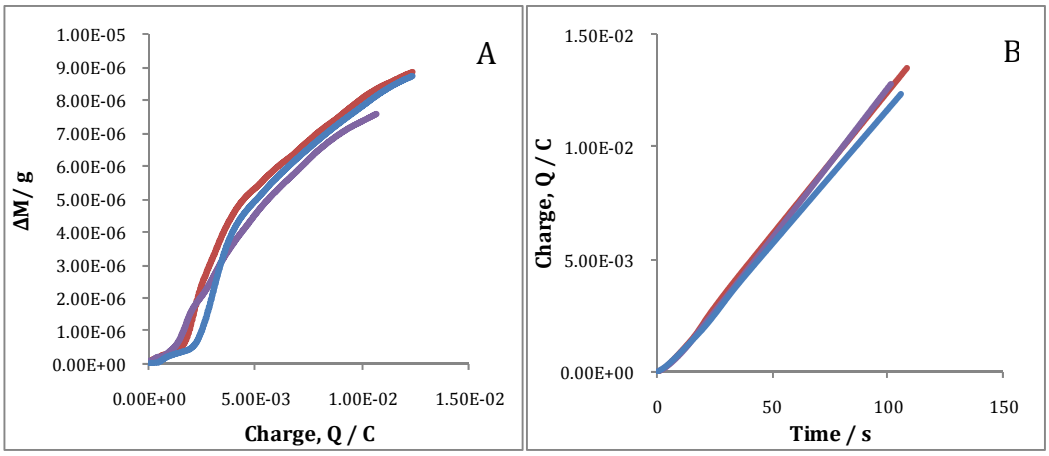

Figure 5.21: A Mass-charge plot and **B** charge-time plot recorded during the deposition of the PPyIndo film at different occasions on Au quartz crystal electrode in the presence of 0.20 mol dm^{-3} NaIndo, 0.20 mol dm^{-3} TBAP and 0.20 mol dm^{-3} Py in EtOH. (Area of quartz crystal = 0.208 cm^2).

Table 5.2: Data values calculated for the profile of PPyIndo polymers grown by EQCM.

Parameter	Average value
Charge, Q / C	$1.21 \times 10^{-2} \pm 4 \times 10^{-4}$
Mass of the polymer / g	$8.35 \times 10^{-6} \pm 5 \times 10^{-7}$
Doping level, x	0.24 ± 0.02
Mass contributed by $Indo^-$/ g	$4.52 \times 10^{-6} \pm 2.9 \times 10^{-7}$
Amount of $Indo^-$ / moles	$1.35 \times 10^{-8} \pm 8 \times 10^{-10}$
% mass contributed by $Indo^-$	54

Figure 5.22 shows the mass-charge plots and the charge-time plots recorded for PPySul. Again, good reproducibility is observed during the early stages of polymer growth, as evident by the overlapping traces. A linear relationship can be seen in Figure 5.22B between the charge and time. A deposition rate of 6.4×10^{-5} C s^{-1} was calculated while a mass-to-charge ratio of 3.98×10^{-4} g C^{-1} was calculated from the plots seen in Figure 5.22A. It is obvious from a comparison of these data with the corresponding data for the PPyIndo films, that for these thin polymers the PPyIndo

is deposited at a faster rate than the PPySul. It is also very clear from a comparison of the mass-charge curves that the early stages of polymer nucleation are very different. There is a clear induction period for the PPyIndo system. However, the PPySul film appears to nucleate more readily giving a constant mass-to-charge ratio up to a charge of about 1.0 x 10^{-2} C.

Taking Equation 2.4, the average mass and doping levels of the PPySul polymers were calculated and are shown in Table 5.3. A doping level of 0.075 was calculated for the PPySul, which is considerably lower than the doping levels calculated for PPyIndo and a reason for this may be associated with the lower concentration of dopant in this system compared to the Indo system. As a result the percentage of the total mass attributed to the Sul^- is only 28 %. Indeed, a doping level this low is unusual for PPy, with even polymers of low electrical conductivity having doping levels of 0.25–0.28[62, 63]. Doping levels as low as 0.14 and 0.15 have only been documented for pyrrole derivatives of poly(N-butylpyrrole) and poly(2-cyanoethyl)pyrrole[64].

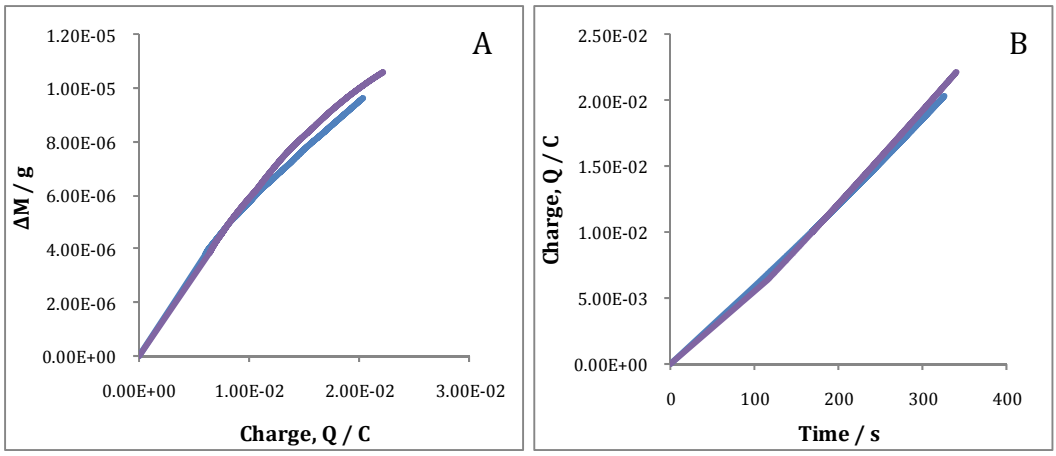

Figure 5.22: A Mass-charge plot and **B** charge-time plot recorded during the deposition of the PPySul film on Au quartz crystal electrode in the presence of 0.12 mol dm^{-3} NaSul, 0.08 mol dm^{-3} TBAP and 0.20 mol dm^{-3} Py. The quartz crystal has a surface area of 0.208 cm^2.

Table 5.3: Data values calculated for the profile of PPySul polymers grown by EQCM.

Parameter	Average value
Charge, Q / C	$2.13 \times 10^{-2} \pm 9.0 \times 10^{-4}$
Mass of the polymer / g	$1.01 \times 10^{-5} \pm 4.7 \times 10^{-7}$
Doping level, x	0.075 ± 0.005
Mass contributed by Sul^- / g	$2.81 \times 10^{-6} \pm 1.2 \times 10^{-7}$
Amount of Sul^- / moles	$8.40 \times 10^{-9} \pm 3.6 \times 10^{-10}$
% mass contributed by Sul^-	28

5.3.3.4 Morphology

Scanning electron microscopy (SEM) was performed on PPyIndo and PPySul to obtain information on the morphology of the polymers. The films were firstly synthesised, washed thoroughly with acetone and distilled water to ensure the removal of any $Indo^-$ or Sul^- on the surface of the polymers and dried by exposure to a gentle air flow for 30 s. The polymers were grown under the optimum conditions outlined in Sections 5.3.2.1 and 5.3.2.2 at +0.900 V vs SCE to a charge of 2.8 C cm^{-2}. SEM micrographs of PPyIndo and PPySul are shown in Figure 5.23 and Figure 5.24, respectively. In general, PPy films present a cauliflower-like morphology constituted by micro-spherical grains. It has been reported that such a particular structure is related to the dopant intercalation difficulty in the disordered polymeric chain[30, 65]. It is well documented that PPy films exhibit a cauliflower-like morphology[59, 65-67].

The cauliflower-like morphologies seen in Figure 5.23 and Figure 5.24 are more globular than those seen in Section 3.3.3.5 for PPyDex and PPyCl. This could be due to the organic media in which the PPyIndo and PPySul were prepared. The SEM micrographs shown here resemble morphologies observed in previous studies of PPy prepared in ACN and water mixtures[68, 69].

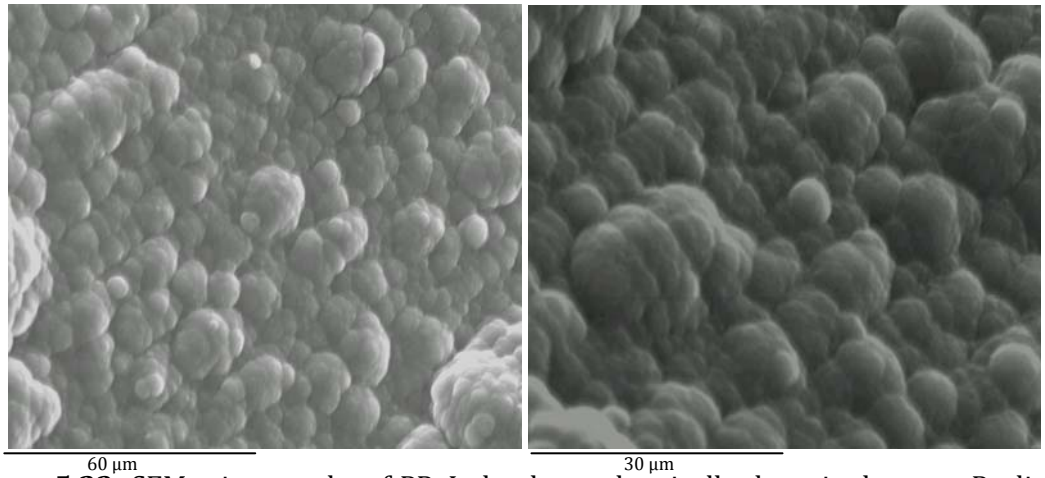

Figure 5.23: SEM micrographs of PPyIndo electrochemically deposited onto a Pt disc at 36 °C by a constant potential of +0.900 V vs $Ag|Ag^+$ to 2.8 C cm^{-2} in the presence of 0.20 mol dm^{-3} Indo, 0.20 mol dm^{-3} TBAP and 0.20 mol dm^{-3} Py in EtOH.

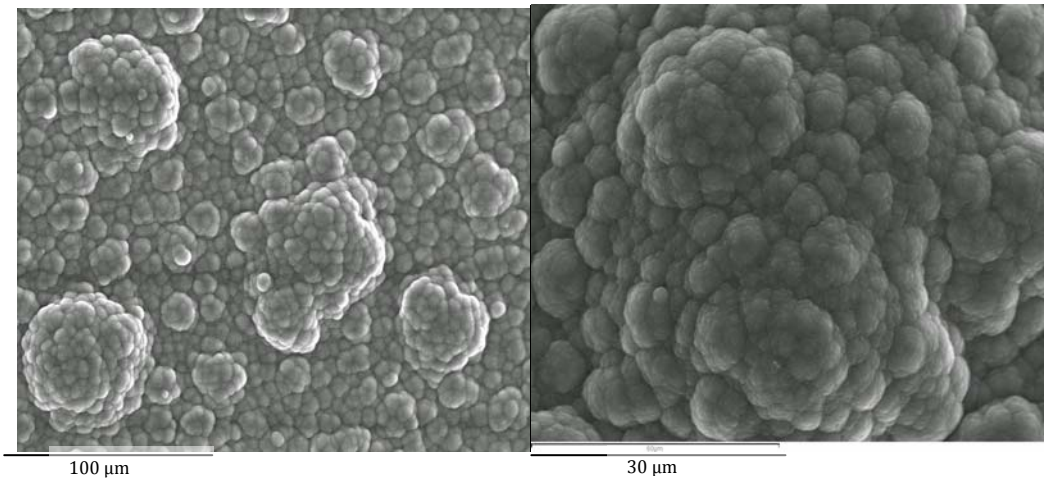

Figure 5.24: SEM micrographs of PPySul electrochemically deposited onto a Pt disc at 40 °C by a constant potential of +0.900 V vs $Ag|Ag^+$ to 2.8 C cm^{-2} in the presence of 0.12 mol dm^{-3} Sul, 0.08 mol dm^{-3} TBAP and 0.20 mol dm^{-3} Py in EtOH.

5.3.4 Release studies

Before any of the release studies were carried out, the polymer was thoroughly rinsed in acetone, then immersed in distilled H_2O for 10 min and a potential of +0.500 V vs SCE was applied to ensure that any $Indo^-$ or Sul^- on the surface of the polymer was washed away. In addition the 10 min immersion period was sufficient for any $Indo^-$ or Sul^- trapped within the porous polymer matrix to diffuse into the bulk H_2O.

5.3.4.1 Optimum release potentials

With the growth parameters optimised and the polymers characterised, the focus was then moved to the release studies. As with release studies discussed in Chapters 3 and 4, the polymer was deposited onto the electrode under the optimum conditions and various potentials, both cathodic and anodic, were applied in the presence of 0.10 mol dm^{-3} NaCl. Samples from the release solution were taken every 5 or 10 min over a 60 min period. Release studies were also performed under OCP conditions to measure the concentration of drug released by diffusion across the PPy membrane.

The rates of release of both $Indo^-$ and Sul^- were dependent on the potentials applied. Figure 5.25 shows the release profiles of $Indo^-$ at OCP, –0.200 V vs SCE and –0.800 V vs SCE and quite a large amount of drug is measured at all potentials. The potential measured in the cell at OCP was +0.300 V vs SCE. After the 60 min period at OCP, approximately 48 μmol cm^{-2} of $Indo^-$ was measured which is more than the amount of Dex^{2-} released after 5 h at its optimum release potential. However, at –0.800 V vs SCE approximately 215 μmol cm^{-2} of $Indo^-$ was released over the 60 min period. This is a significant rate of release and is much higher than that observed with any of the other drugs in this work and is more than likely related to the concentration of drug in the electrolyte during polymerisation. Unlike the release profiles seen for the release of Dex^{2-}, the release of $Indo^-$ at –0.800 V vs SCE increases consistently and only begins to plateau at about 50-55 min. The rates of release at all potentials were calculated for the first 10 min and for the 10-60 min period and are shown in Table 5.4. It is clear from the data shown in Table 5.4 that the rates of release decrease significantly after the first 10 min with a rate of 8.32 μmol cm^{-2} min^{-1} calculated for the first 10 min at –0.800 V vs SCE and a rate of 2.70 μmol cm^{-2} min^{-1} calculated for the next 50 min.

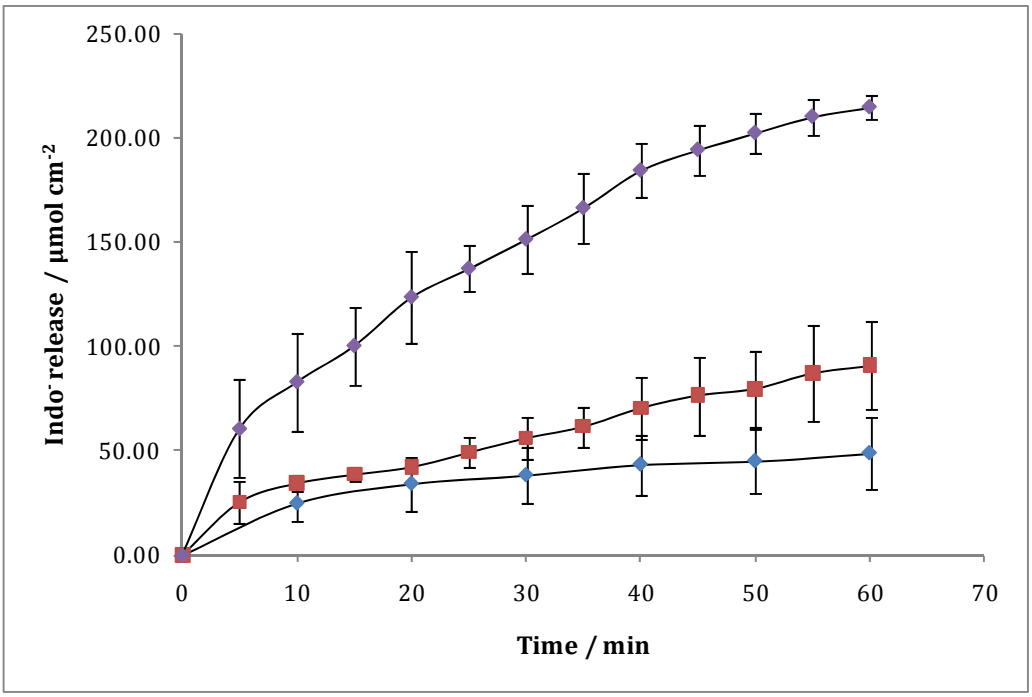

Figure 5.25: Release profiles for Indo⁻ released at ♦ OCP, ■ –0.200 V vs SCE and ♦ –0.800 V vs SCE. Polymerisation was achieved by applying +0.900 V vs Ag|Ag⁺ until a charge of 2.8 C cm^{-2} was reached in the presence of 0.20 mol dm^{-3} NaIndo, 0.20 mol dm^{-3} TBAP and 0.20 mol dm^{-3} Py in EtOH. (n=3).

Table 5.4: The average rate of Indo⁻ release at OCP, –0.200 V vs SCE and –0.800 V vs SCE.

Time period/ min	Rate of release at OCP/ µmol cm^{-2} min^{-1}	Rate of release at – 0.200 V vs SCE/ µmol cm^{-2} min^{-1}	Rate of release at – 0.800 V vs SCE/ µmol cm^{-2} min^{-1}
0-10	2.50	3.46	8.32
10-60	0.45	1.20	2.70

The release profiles of Sul⁻ at OCP, –0.200 V vs SCE and –0.900 V vs SCE are shown in Figure 5.26. At –0.900 V vs SCE, 54 µmol cm^{-2} was measured after 60 min while approximately 6 µmol cm^{-2} was released after 60 min at OCP. The potential of the cell at OCP was measured as +0.280 V vs SCE. This highlights the importance of the applied potential on the amount of Sul⁻ release. In contrast to the release profile of Indo⁻ at the optimum release potential, the release profile of Sul⁻ at –0.900 V vs SCE begins to plateau within the first 20 min. This is evident from the rates of release calculated at these three potentials, presented in Table 5.5. For the

first 10 min, the average rate of release at –0.900 V vs SCE is 4.18 μmol cm^{-2} min^{-1} but for the rest of the hour the rate of release is reduced to 0.25 μmol cm^{-2} min^{-1}.

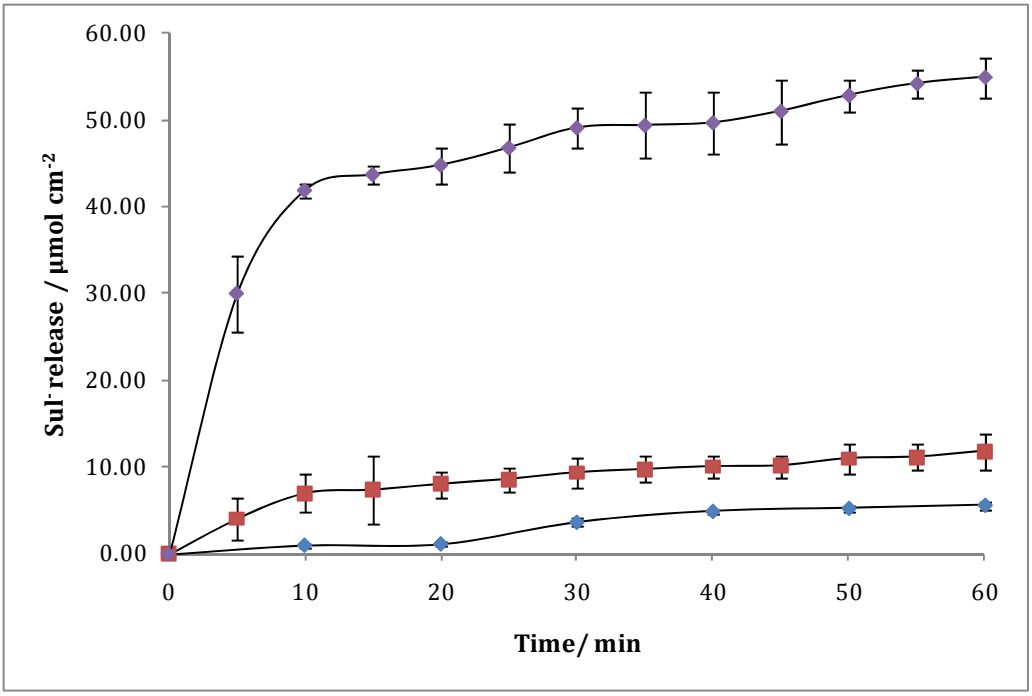

Figure 5.26: Release profiles for Sul^- released at ♦ OCP, ■ –0.200 V vs SCE and ♦ –0.900 V vs SCE. Polymerisation was achieved by applying +0.900 V vs $Ag|Ag^+$ until a charge of 2.8 C cm^{-2} was reached in the presence of 0.12 mol dm^{-3} NaSul, 0.08 mol dm^{-3} TBAP and 0.20 mol dm^{-3} Py in EtOH. (n=3).

Table 5.5: The average rate of Sul^- release at OCP, –0.200 V vs SCE and –0.900 V vs SCE.

Time period/ min	Rate of release at OCP/ μmol cm^{-2} min^{-1}	Rate of release at – 0.200 V vs SCE/ μmol cm^{-2} min^{-1}	Rate of release at – 0.900 V vs SCE/ μmol cm^{-2} min^{-1}
0-10	0.10	0.70	4.18
10-60	0.04	0.09	0.25

The amount of $Indo^-$ and Sul^- released at the end of the 60 min period at various potentials is shown in Figure 5.27. There is a similar trend in the release of both drugs with an increase in drug release observed as the polymer is further reduced. The highest drug release is seen at –0.800 V vs SCE and –0.900 V vs SCE for the $Indo^-$ and Sul^-, respectively. At more electronegative potentials, the amount of drug

released decreases as the polymer is fully reduced and side reactions such as H_2 evolution prevail. The amount of drug released at +0.100 V vs SCE is slightly higher than that at OCP which is reasonable considering the potential in the cell was measured between +0.280 V and +0.300 V vs SCE.

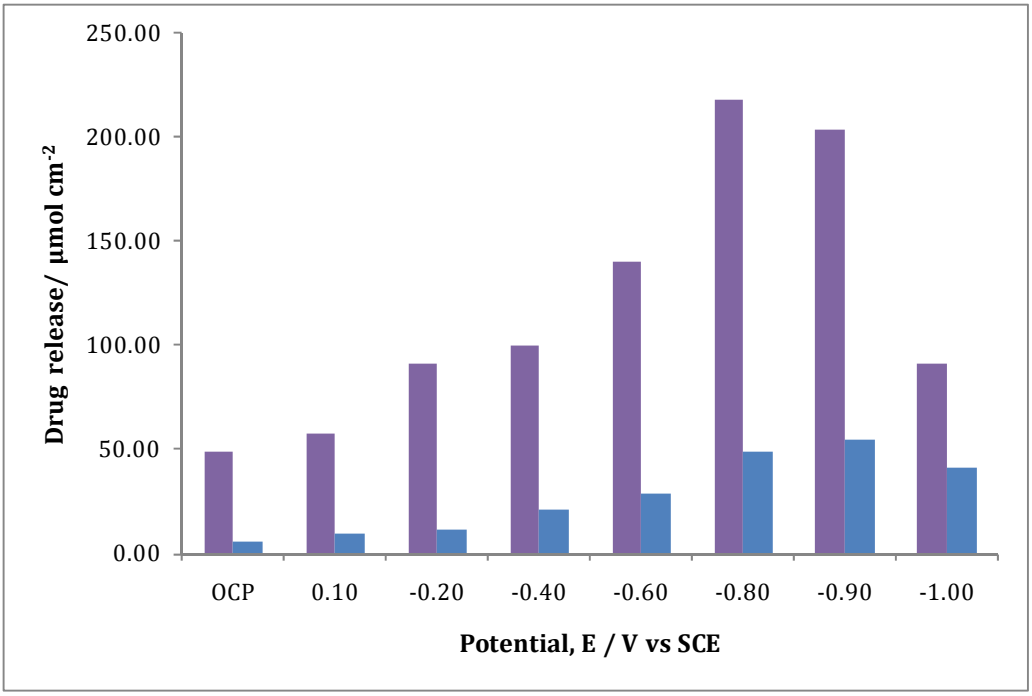

Figure 5.27: Amount of ■ $Indo^-$ and ■ Sul^- measured upon release from the polymer at varying potentials in the presence of 0.10 mol dm^{-3} NaCl over a period of 60 min. (n=3, %error = 4.2%).

In order to estimate how much drug was doped within the polymer, release studies were carried out over a 5 h period at the optimum release potentials for each drug. These release profiles for both $Indo^-$ and Sul^- can be seen in Figure 5.28. It is clear that the release of Sul^- begins to plateau very early and the amount of Sul^- being released increases very slowly over the last 4 hours. The rate of release between the 1st and 5th hour is 0.02 µmol cm^{-2} min^{-1} which is a 10-fold decrease in the rate measured within the 1st hour. This suggests that most of the drug incorporated within the polymer is released and from this it can be estimated that approximately 60 µmol cm^{-2} of Sul^- is doped within the polymer upon electrodeposition. This implies that at –0.900 V vs SCE, 90 % of the Sul^- is released within 60 min. Benson and co-workers[25] reported the release of 7 mg Sul from

polymer mircocarriers over a 20 h period and this equated to 90 % of the drug entrapped within the polymer. This is much lower than the amount of Sul^- incorporated and released from PPy in this work, which is approximately 20 mg.

From the release profile of $Indo^-$ at –0.800 V vs SCE, shown in Figure 5.28, it is obvious that the rate of release does not begin to plateau until the 2nd hour and the rate of release decreases significantly from the 2.70 μmol cm^{-2} min^{-1} measured in the 1st hour to 0.17 μmol cm^{-2} min^{-1} over the last 4 hours. The amount of $Indo^-$ incorporated into the polymer can then be estimated as approximately 260 μmol cm^{-2}. This suggests that at –0.800 V vs SCE, approximately 82 % of $Indo^-$ is released within 60 min.

Lee *et al.*[23] reported the release of Indo transdermally across skin that was pretreated with an erbium:YAG laser and observed an average rate of release of 27.53 μg cm^{-2} h^{-1}. Taking the rate of release of $Indo^-$ in this work to be 2.70 μmol cm^{-2} min^{-1}, this corresponds to 54.1 mg cm^{-2} h^{-1} which is higher than that of the transdermal release. Kim *et al.*[21, 22] reported a 42 % release of Indo from micelles and nanospheres but it is not clear how much Indo was initially entrapped, while Liu *et al.*[19], who also reported the release of Indo from micelles, calculated the encapsulation of approximately 9 to 10 drug molecules per micelle.

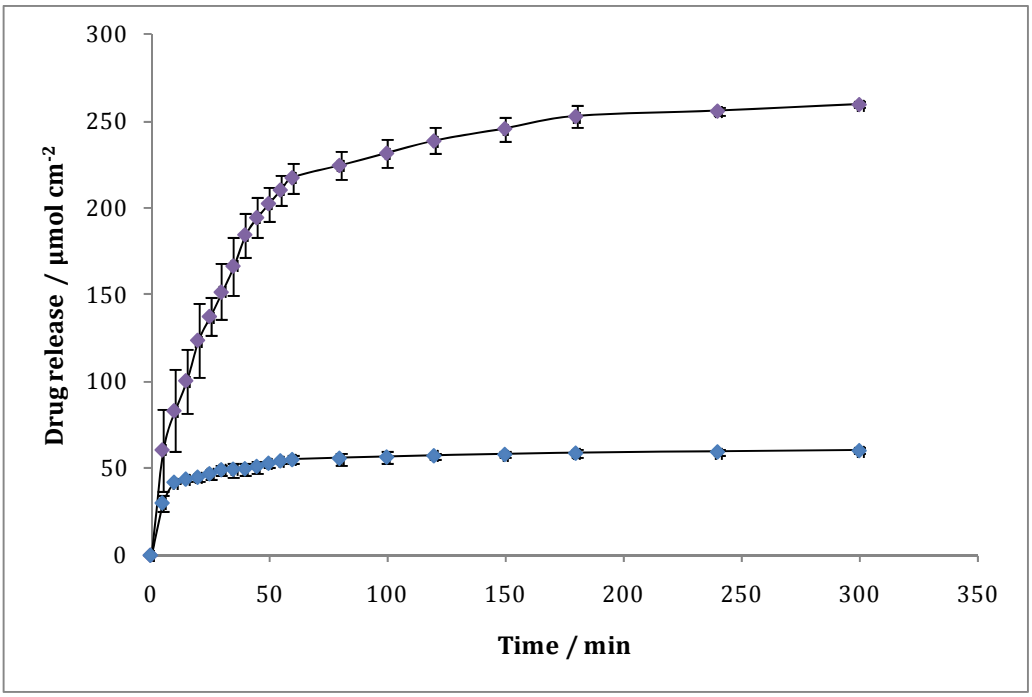

Figure 5.28: Amount of ♦ $Indo^-$ released from PPyIndo at –0.800 V vs SCE and ♦ Sul^- released from PPySul at –0.900 V vs SCE. Both polymers were deposited at +0.900 V vs $Ag|Ag^+$ to a charge of 2.8 C cm^{-2} from an EtOH solution. (n=3).

5.3.4.2 Amount of ClO_4^- doped within the polymer

As discussed in Section 5.3.1, TBAP was added to the electrolytes to increase the conductivity of EtOH. From the release studies presented in Section 5.3.4.1, it is clearly evident that the drugs are doped within the polymer during the electrosynthesis, but it is also likely that some perchlorate, ClO_4^-, is incorporated into the polymer during deposition. ClO_4^- is a small and mobile dopant that can be easily incorporated and released from the polymer[70, 71]. Therefore, the simplest way to detect if ClO_4^- is doped within the polymer is to measure its release from the polymer. Typical absorbance spectra of NaIndo, NaSul and TBAP are shown in Figure 5.29A. The λ_{max} of $Indo^-$ is 320 nm, while λ_{max} of Sul^- is 330 nm. It is clear from the spectra seen in Figure 5.29A that if any ClO_4^- is released from the polymer that its absorbance would be masked by the absorbance of the drugs.

In order to determine the concentration of ClO_4^- released during the drug release studies, a spectrophotometric method, used by Ensafi *et al.*[72] was adapted and used. Ensafi *et al.*[72] reported the detection of trace amounts of ClO_4^- by adding

excess of a cationic dye, brilliant cresyl blue (BCB). BCB forms an insoluble ion pair with ClO_4^-, which can then be extracted into methyl isobutyl ketone. In Figure 5.29B, the absorbance of the ClO_4^--BCB^+ ion pair can be seen. A concentration of 5.0 x 10^{-3} mol dm^{-3} BCB was used and at concentrations this high two peaks are seen for the BCB which correspond to the absorbance of the monomer and dimer of BCB in solution[73]. By monitoring the absorbance of the ion pair at 625 nm, the concentration of ClO_4^- in a sample can then be determined. A calibration curve was obtained for various concentrations of ClO_4^- and a representative calibration curve is shown in Figure 5.30. A linear regression of 0.999 was achieved and the slope of this line was then used to determine the amount of ClO_4^- released from the polymer. The polymers were deposited in the usual manner and release studies were carried out at the optimum conditions for 60 min. At the end of this 60 min period, the concentration of ClO_4^- in the sample was measured. It can be assumed that the majority of the ClO_4^- anions are released in this time interval as it is such a small dopant. The amount of ClO_4^- released from PPyIndo and PPySul was approximately 2.19 x 10^{-6} mol cm^{-2} and 2.04 x 10^{-6} mol cm^{-2}, respectively. This is quite small in comparison to the amount of $Indo^-$ and Sul^- doped within the polymers. However, this does mean that the doping levels calculated for the $Indo^-$ and Sul^- are slightly lower than those reported in Section 5.3.3.3.

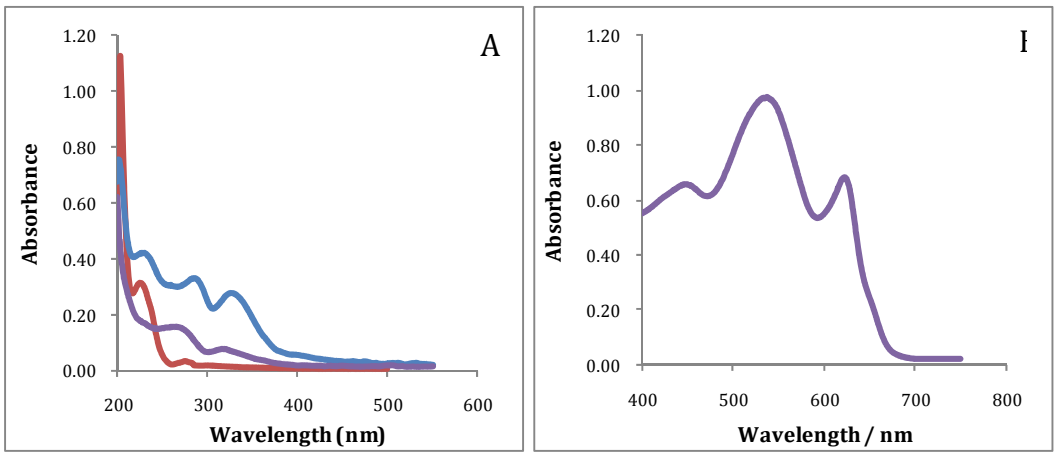

Figure 5.29: A Absorbance spectra of — NaIndo (1.80 x 10^{-4} mol dm^{-3}), — NaSul (2.40 x 10^{-4} mol dm^{-3}) and — TBAP (1.0 x 10^{-3} mol dm^{-3}) and **B** Absorbance spectra of ClO_4^-—BCB^+ ion pair (concentrations 5.60 x 10^{-6} mol dm^{-3} ClO_4^- and 5.0 x 10^{-3} mol dm^{-3} BCB).

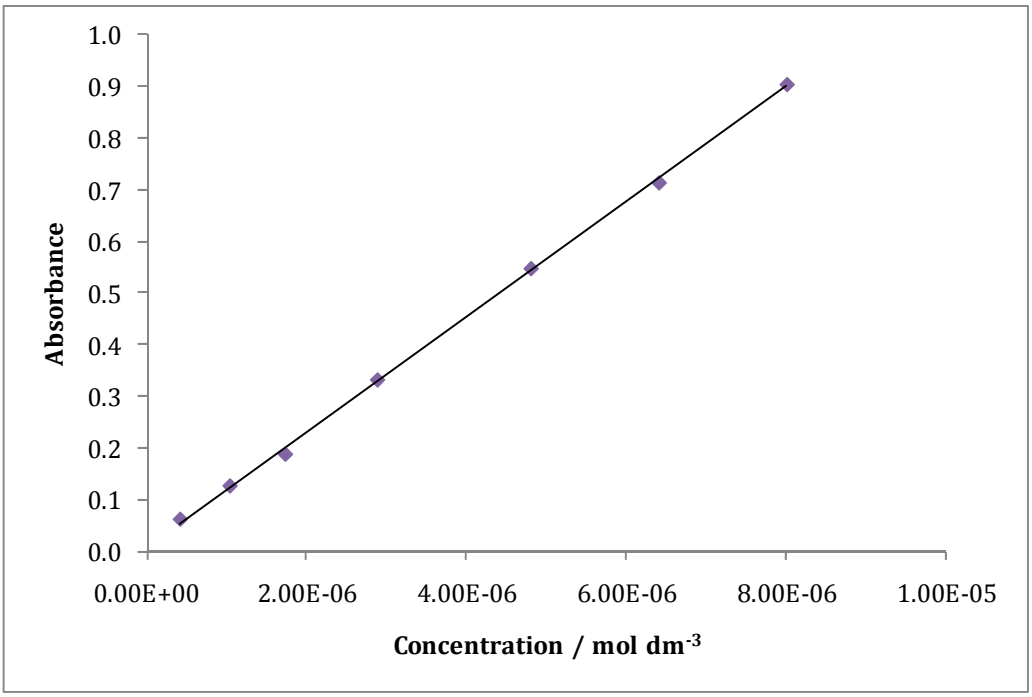

Figure 5.30: Calibration curve of ClO_4^--BCB^+ ion pair. The absorbance was read at 625 nm, the concentration of ClO_4^- was varied between 4.17 x 10^{-7} and 8.00 x 10^{-6} mol dm^{-3} with a constant concentration of 5.0 x 10^{-3} mol dm^{-3} of BCB.

5.3.4.3 Investigations into the possibility of reusing the polymer

In previous release studies discussed in Chapters 3 and 4, it was shown that after the release of the drug the PPy^0 could be oxidised back to PPy^+ to allow further drug incorporation and release to occur, as shown in Equation 5.1. The polymers were electrodeposited as before and the drugs were released at their optimum release potential over 60 min. The polymers were then rinsed and placed into a drug-only electrolyte and an oxidation potential was applied in order to dope the polymer with the drug in question.

$$PPy^+Drug^- + e^- \rightleftharpoons PPy^0 + Drug^- \qquad 5.1$$

For the PPyIndo system, the drug-only electrolyte had a concentration of 0.30 mol dm^{-3} NaIndo and a potential of +0.900 V vs $Ag|Ag^+$ was applied for 60 min in an attempt to incorporate the $Indo^-$ into the polymer. The temperature of the NaIndo solution was maintained at 65 °C which was higher than the original polymerisation temperature to ensure all the NaIndo remained soluble in solution.

The polymer was washed thoroughly and the $Indo^-$ release was carried out as before. The polymer was then rinsed and replaced in the NaIndo only electrolyte and the process was repeated again. The resulting release profiles are shown in Figure 5.31. It is clear that the polymer can be successfully reused to incorporate and release $Indo^-$ more than once. The amount of $Indo^-$ released decreases with further release studies which is consistent with reports that the polymer loses conductivity the longer a reduction potential is applied[46]. It is then more difficult to oxidise the polymer again to ensure the same levels of $Indo^-$ are incorporated and released. However, even after the polymer is oxidised for a third time over 100 μmol cm^{-2} of $Indo^-$ is released from the polymer. This is still a high rate of drug release.

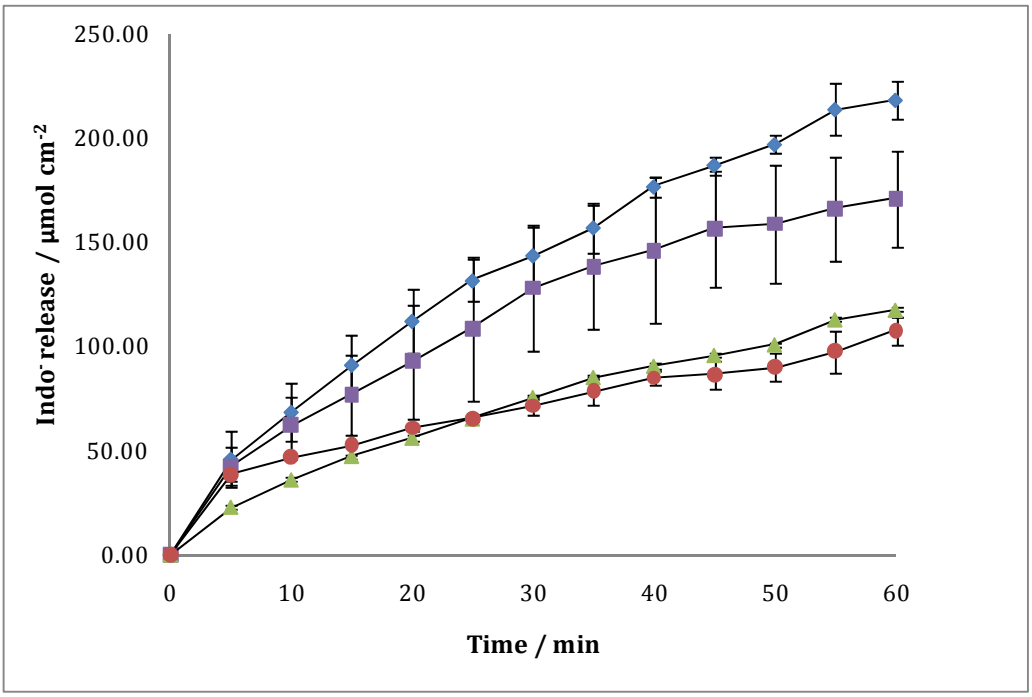

Figure 5.31: Amount of $Indo^-$ released from the polymer at −0.800 V vs SCE, in the presence of 0.10 mol dm^{-3} NaCl, over four 60 min periods; ♦ 1st release, ■ 2nd release after it was placed in 0.30 mol dm^{-3} NaIndo for 60 min at a potential of +0.900 V vs $Ag|Ag^+$ at 65 °C, ▲ 3rd release after it was placed in 0.30 mol dm^{-3} NaIndo for 60 min at a potential of +0.900 V vs $Ag|Ag^+$ at 65 °C for the second time and ● 4th release after it was placed in 0.30 mol dm^{-3} NaIndo for 60 min at a potential of +0.900 V vs $Ag|Ag^+$ at 65 °C for the third time. (n=3).

Similar results were seen for the Sul^- release, as shown in Figure 5.32. For the PPySul system, the drug-only electrolyte had a concentration of 0.20 mol dm^{-3} NaSul and was kept at a temperature of 70 °C which was higher than the original polymerisation temperature to ensure all the NaSul remained soluble in solution. A potential of +0.900 V vs $Ag|Ag^+$ was applied for 60 min in an attempt to incorporate the drug into the polymer. The highest amount of Sul^- release was measured for the first release and similar amounts of Sul^- was measured during the second and third release studies when a reduction potential of –0.900 V vs SCE was applied with approximately 47 µmol cm^{-2} of Sul^- released. For all three releases, the profiles begin to plateau within the first 10-20 min.

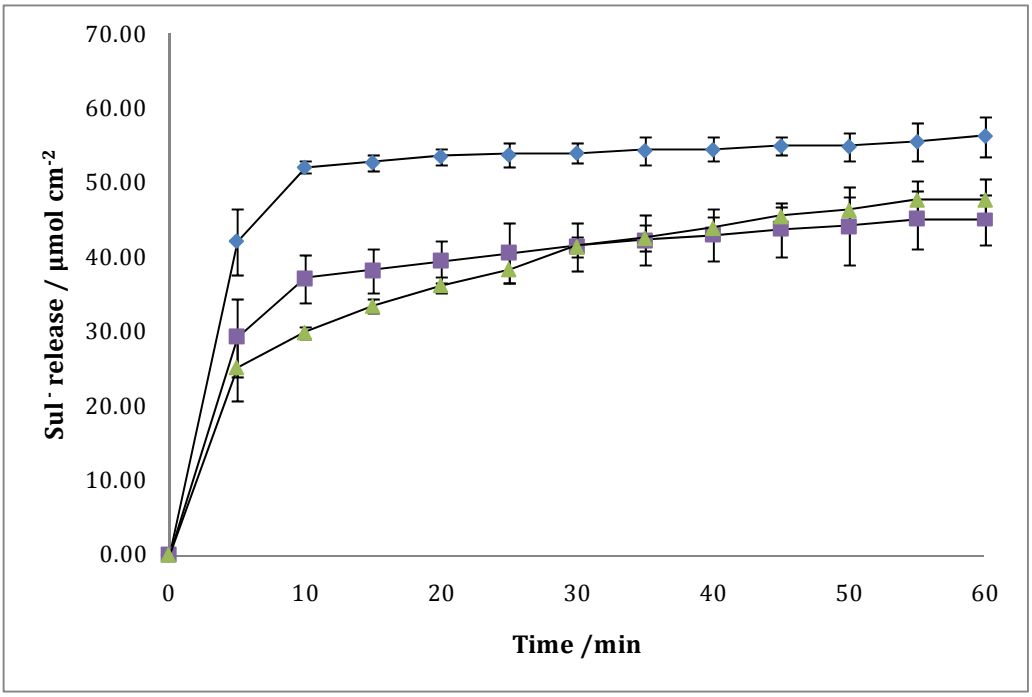

Figure 5.32: The amount of Sul^- measured in the presence of 0.10 mol dm^{-3} NaCl from PPySul at –0.900 V vs SCE. The polymer was then placed in a solution of 0.12 mol dm^{-3} NaSul and a potential of +0.900 V vs $Ag|Ag^+$ was applied before the Sul^- was released again. The polymer was then placed back into the NaSul solution and the process was repeated. 1st release ♦; 2nd release ■; 3rd release ▲. (n=3).

The release profiles seen for reusing the polymers of PPyIndo and PPySul are both different to those seen for PPyDex or PPyDF. PPyDF displays different release profiles due to the presence of the drug crystals on the surface of the polymer

during the 1st release study. In Section 3.3.4.4, it was found that once the PPyDex is oxidised it becomes easier for re-oxidation to take place and there is an increase in the amount of Dex^{2-} release from the 2nd to 3rd release study. However, PPy films prepared at high temperatures or in the presence of EtOH are less conductive than those prepared in aqueous conditions at room temperature[39]. It may be that the PPyIndo and PPySul are not sufficiently conducting to allow higher amounts of drug to be incorporated upon re-oxidation. It should be noted that no TBAP is present in the drug-only electrolyte in which the re-oxidation of the polymer takes place as it is only required to enable the initial deposition of the polymer. This means that no ClO_4^- is doped within the polymer once the 1st set of release studies are complete and during all further release studies only the $Indo^-$ or Sul^- are released. The fact that there is not a notable decrease in drug release from the 1st to 2nd release study means that, if desired, a reduction potential could first be applied to remove any ClO_4^- from the polymer and then the polymer could be re-oxidised to give high release rates for $Indo^-$ or Sul^-.

5.3.4.4 Switching 'on and off' the drug release

As discussed in Chapter 1, Section 1.2, an ideal drug release device must fulfil two important stipulations; firstly the ability to control the rate of release as a function of the applied potential and secondly the ability to switch 'on/off' the drug release[74]. In Section 3.3.4.5, the possibility of switching 'on/off' the Dex^{2-} release was investigated and it was found that although the release could not be completely stopped, the rate of release was considerably slowed down by applying an oxidation potential. The possibility of controlling the release of $Indo^-$ and Sul^- was then investigated. Potentials of –0.800 V vs SCE or –0.900 V vs SCE were applied to release $Indo^-$ and Sul^-, respectively, while a potential of +0.500 V vs SCE was applied with the objective of stopping the release of the drugs. The release was switched on and off every 20 min over a 2 h period. Samples were taken every 5 min during the 1st hour and every 10 min during the 2nd hour in the presence of 0.10 mol dm^{-3} NaCl.

The release profiles, recorded under these conditions, of both $Indo^-$ and Sul^- are shown in Figure 5.33 and Figure 5.34, respectively, and the increase in $Indo^-$ and Sul^- release at the different potentials is shown in Table 5.6. In comparison to the release profiles of both drugs presented in Section 5.3.4.1, it is clear that less drug is released when an oxidation potential is applied. After 40 min of switching the polymer, approximately 130 μmol cm^{-2} of $Indo^-$ is released, however, when a constant potential of –0.800 V vs SCE is applied for 40 min approximately 184 μmol cm^{-2} of $Indo^-$ is measured. Indeed, more $Indo^-$ is released in 60 min at a constant potential of –0.800 V vs SCE than after 2 hours of switching 'on/off' the release of $Indo^-$. In the case of PPySul, after 60 min of switching 'on/off' approximately 44 μmol cm^{-2} of Sul^- is released from the polymer but at a constant potential of –0.900 V vs SCE, over 50 μmol cm^{-2} of Sul^- is released. Although the application of an oxidation potential does not completely stop the release of either $Indo^-$ or Sul^-, it is clear from both Figure 5.33 and Figure 5.34 that the rate of release is significantly decreased when the polymers are oxidised.

Table 5.6: Increase in amount of $Indo^-$ and Sul^- measured when the release of drug is switched 'on and off' by applying reduction potentials (–0.800 V vs SCE for the PPyIndo film and –0.900 V vs SCE for the PPySul film) and an oxidation potential (+0.500 V vs SCE) in the presence of 0.10 mol dm^{-3} NaCl.

Time range/ min	Switched 'on/off'	Increase in $Indo^-$ release/μmol cm^{-2}	Increase in Sul^- release/μmol cm^{-2}
0-20	On	93.16	38.20
20-40	Off	36.59	3.98
40-60	On	17.08	1.83
60-80	Off	16.79	1.72
80-100	On	10.38	6.45
100-120	Off	6.00	0.69

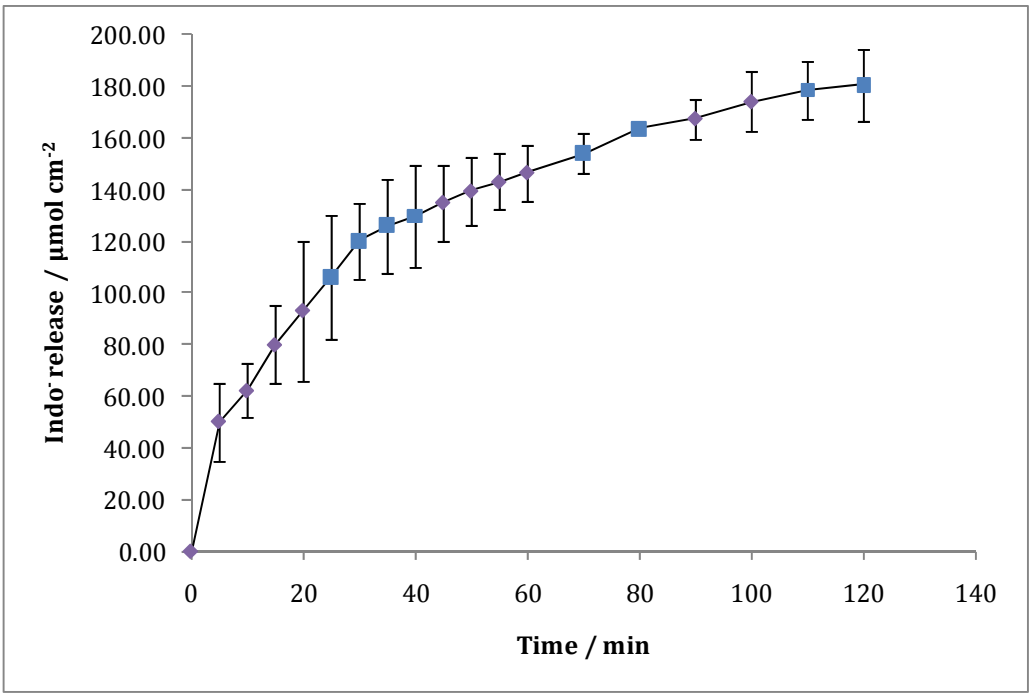

Figure 5.33: Amount of $Indo^-$ measured when the release was 'switched on' ♦ by applying a potential of –0.800 V vs SCE and 'switched off' ■ by applying a potential of +0.500 V vs SCE. It was switched on and off every 20 min over 2 h in the presence of 0.10 mol dm^{-3} NaCl. (n=3).

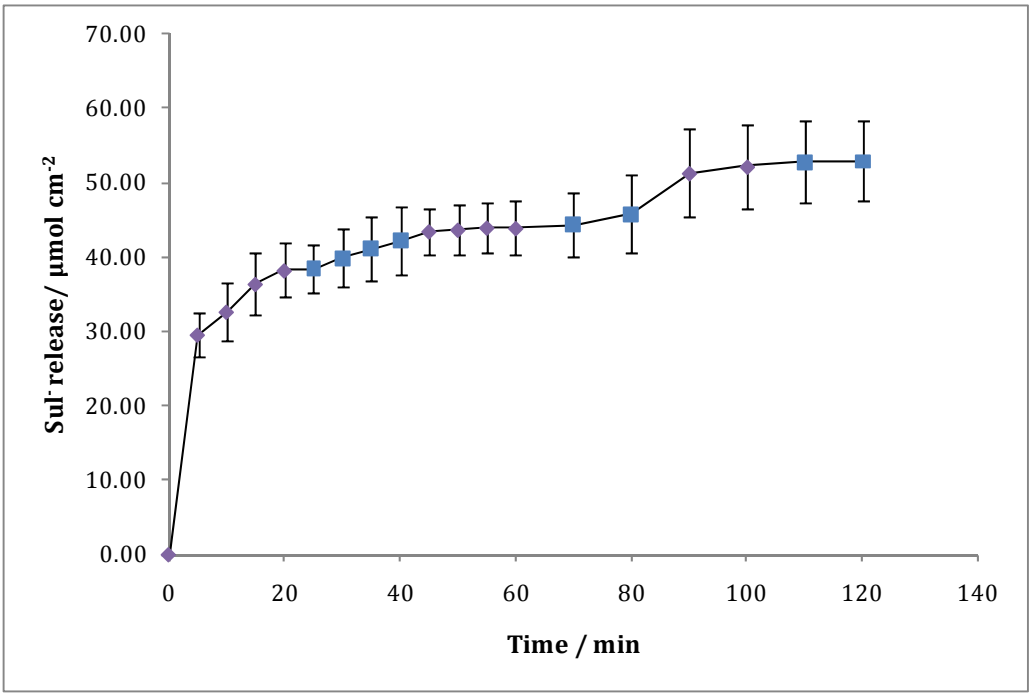

Figure 5.34: Amount of Sul^- measured when the release was 'switched on' ♦ by applying a potential of –0.900 V vs SCE and 'switched off' ■ by applying a potential of +0.500 V vs SCE. It was switched on and off every 20 min over 2 h in the presence of 0.10 mol dm^{-3} NaCl. (n=3).

5.4 Summary of results

In this chapter, the successful electrodeposition of polypyrrole membrane films doped with either indomethacin or sulindac in the presence of EtOH is described. Tetrabutylammonium perchlorate (TBAP) was added to the EtOH to increase the conductivity of the electropolymerisation solution. The polypyrrole films were deposited under heated conditions to ensure the solubility of the drugs in the EtOH solution. The concentration of the TBAP was kept to a minimum so that the anionic ClO_4^- would not be preferentially doped within the polymer over the drugs. All polymers were deposited at a constant potential to a charge of 2.8 C cm^{-2} and it was found that the rate of polymerisation was dependent on the temperature at which deposition occurred.

Electrochemical impedance spectroscopy (EIS) and electrochemical quartz crystal measurements (EQCM) were both employed to characterise the polymer films. It was found that PPy films deposited in EtOH are less conductive than those electrosynthesised under aqueous conditions. In particular, the PPyIndo film exhibits poor conducting properties, as evidenced from both cyclic voltammetry data and EIS. The morphology of the polymers was found to be typical of PPy electrodeposited in the presence of an organic media, such as ACN.

During the release studies it was found that approximately 260 μmol cm^{-2} of $Indo^-$ was doped within the polymer at optimum conditions and after 60 min at –0.800 V vs SCE, 82 % of the $Indo^-$ was released. While at –0.900 V vs SCE, 54 μmol cm^{-2} of Sul^- was released from PPySul after 60 min which is equivalent to 90 % of the total amount of Sul^- estimated to be doped within the polymer. It was calculated that between 2.04 x 10^{-6} mol cm^{-2} and 2.19 x 10^{-6} mol cm^{-2} of ClO_4^- was also incorporated into the polymers during deposition. However, this ClO_4^- can be released with the application of a reduction potential and the polymer can be re-oxidised to allow the release of large amounts of $Indo^-$ or Sul^-. Furthermore, the rate of drug release can be controlled with the application of an oxidation potential.

5.5 References

1. J. A. Mitchell and T. D. Warner, *British Journal of Pharmacology* **128**:1121 (1999).
2. J. R. Vane and R. M. Botting, *Scandinavian Journal of Rheumatology,* **25**:9 (1996).
3. T. Hla and K. Neilson, *Proceedings of the National Academy of Sciences of the United States of America* **89**:7384 (1992).
4. E. A. Meade, W. L. Smith, and D. L. DeWitt, *Journal of Biological Chemistry,* **268**:6610 (1993).
5. T. D. Warner, F. Giuliano, I. Vojnovic, A. Bukasa, J. A. Mitchell, and J. R. Vane, *Proceedings of the National Academy of Sciences of the United States of America* **96**:7563 (1999).
6. A. Nokhodchi, Y. Javadzadeh, M. R. Siahi-Shadbad, and M. Barzegar-Jalali, *Journal of Pharmacy and Pharmaceutical Science,* **8**:18 (2005).
7. R. Menasse, P. R. Hedwall, J. Kraetz, C. Pericin, L. Riesterer, A. Sallmann, R. Ziel, and R. Jaques, *Scandinavian Journal of Rheumatology,* **22**:5 (1978).
8. D. E. Duggan, *Drug Metabolism Reviews,* **12**:325 (1981).
9. U. Bolder, N. V. Trang, L. R. Hagey, C. D. Schteingart, H.-t. Ton-nu, C. Cerrè, R. P. J. Oude Elferink, and A. F. Hofmann, *Gastroenterology,* **117**:962 (1999).
10. N. N. Mahmoud, S. K. Boolbol, A. J. Dannenberg, J. R. Mestre, R. T. Bilinski, C. Martucci, H. L. Newmark, A. Chadburn, and M. M. Bertagnolli, *Carcinogenesis,* **19**:87 (1998).
11. S. S. Fan and T. Y. Shen, *Journal of Medicinal Chemistry,* **24**:1197 (1981).
12. P. A. Thompson, C.-H. Hsu, S. Green, A. T. Stopeck, K. Johnson, D. S. Alberts, and H. H. S. Chow, *Cancer Prevention Research,* **3**:101 (2010).
13. P. P. Koopmans, W. G. P. M. Kateman, Y. Tan, C. A. M. van Ginneken, and F. W. J. Gribnau, *Clinical Pharmacology and Therapeutics,* **37**:625 (1985).
14. P. P. Koopmans, T. Thien, C. M. Thomas, R. J. V. d. Berg, and F. W. Gribnau, *British Journal of Clinical Pharmacology,* **21**:417 (1986).
15. Adams KR, Halliday LD, Sibeon RG, Baber N, Littler T, and O. ML., *British Journal of Clinical Pharmacology* **14**:286 (1982).
16. G. Alván, M. Orme, L. Bertilsson, R. Ekstrand, and L. Palmér, *Clinical Pharmacology and Therapeutics* **18**:364 (1975).
17. Duggan DE, Hare LE, Ditzler CA, Lei BW, and K. KC, *Clinical Pharmacology and Therapeutics,* **21**:326 (1977).
18. J. M. J. Fréchet, *Proceedings of the National Academy of Sciences of the United States of America,* **99**:4782 (2002).
19. M. Liu, K. Kono, and J. M. J. Fréchet, *Journal of Controlled Release,* **65**:121 (2000).
20. C. J. F. Rijcken, O. Soga, W. E. Hennink, and C. F. v. Nostrum, *Journal of Controlled Release,* **120**:131 (2007).
21. S. Y. Kim, I. L. G. Shin, Y. M. Lee, C. S. Cho, and Y. K. Sung, *Journal of Controlled Release,* **51**:13 (1998).
22. S. Y. Kim, Y. M. Lee, H. J. Shin, and J. S. Kang, *Biomaterials,* **22**:2049 (2001).
23. W.-R. Lee, S.-C. Shen, H.-H. Lai, C.-H. Hu, and J.-Y. Fang, *Journal of Controlled Release,* **75**:155 (2001).
24. S. K. Agrawal, N. Sanabria-DeLong, J. M. Coburn, G. N. Tew, and S. R. Bhatia, *Journal of Controlled Release,* **112**:64 (2006).

25. W. Landgraf, N.-H. Li, and J. R. Benson, *Drug Delivery Technology* **3**(2003).
26. F. Beck, M. Oberst, and R. Jansen, *Electrochimica Acta,* **35**:1841 (1990).
27. F. Fusalba and D. Belanger, *Journal of Physical Chemistry,* **103**:9044 (1999).
28. X. Hu, G. Wang, and T. K. S. Wong, *Synthetic Metals,* **106**:145 (1999).
29. M. Zhou and J. Heinze, *Electrochimica Acta,* **44**:1733 (1999).
30. M. Bazzaoui, E. A. Bazzaoui, L. Martins, and J. I. Martins, *Synthetic Metals,* **130**:73 (2002).
31. S. Carquigny, O. Segut, B. Lakard, F. Lallemand, and P. Fievet, *Synthetic Metals,* **158**:453 (2008).
32. M. Zhou, M. Pagels, B. Geschke, and J. Heinze, *The Journal of Physical Chemistry B,* **106**:10065 (2002).
33. K. Imanishi, M. Satoh, Y. Yasuda, R. Tsushima, and S. Aoki, *Journal of Electroanalytical Chemistry,* **242**:203 (1988).
34. E. Brillas, J. Carrasco, R. Oliver, F. Estrany, J. Vilar, and J. M. Morlans, *Electrochimica Acta,* **45**:4049 (2000).
35. K. Kawai, N. Mihara, S. Kuwabata, and H. Yoneyama, *Journal of The Electrochemical Society,* **137**:1793 (1990).
36. X. Pan, T. Julian, and L. Augsburger, *AAPS PharmSciTech,* **7**:E72 (2006).
37. L. G. Adam and J. M. Adam, *Journal of Pharmaceutical Sciences,* **96**:2978 (2007).
38. M. C. Tros de Llarduya, C. MartÃ-n, M. M. GoÃ±i, and M. C. MartÃ-nez-OhÃ¡rriz, *Drug Development and Industrial Pharmacy,* **24**:295 (1998).
39. S. Sadki, P. Schottland, N. Brodie, and G. Sabourand, *Royal Society of Chemistry,* **29**:283 (2000).
40. R. G. Compton and G. H. W. Sanders, *Electrode Potentials,*Oxford Science Publications, 1996.
41. A. Radi, *Electroanalysis,* **10**:103 (1998).
42. I. S. Shehatta and M. S. Ibrahim, *Canadian Journal of Chemistry* **79**:1431 (2001).
43. A. F. Diaz and K. K. Kanazawa, *Journal of Chemistry Society Chemical Communication*:635 (1979).
44. F. Beck, *Electrochimica Acta,* **33**:839 (1988).
45. F. Beck and M. Oberst, *Synthetic Metals,* **28**:C43 (1989).
46. J. Heinze, *Topics in Current Chemistry,* **152**:2 (1990).
47. G. Akerlof, *Journal of the American Chemical Society,* **54**:4125 (1932).
48. S. B. Irena Jureviciute, A. Robert Hillman and Angela Jackson, *Physical Chemistry,* **2**:4193 (2000).
49. T. Matencio, J. M. Pernaut, and EricVieil, *Journal of Brazilian Chemistry Society,* **14**:90 (2003).
50. P. L. Runnels, J. D. Joseph, M. J. Logman, and R. M. Wightman, *Analytical Chemistry,* **71**:2782 (1999).
51. E. Barsoukov and J. R. MacDonald, *Impedance Spectroscopy. Theory, Experiment and Applications.,*Wiley, 2005.
52. A. C. Fisher, *Electrode Dynamics,*Oxford Science Publications 1996.
53. X. Cui, J. F. Hetke, J. A. Wiler, D. J. Anderson, and D. C. Martin, *Sensors and Actuators A: Physical,* **93**:8 (2001).
54. A. Hallik, A. Alumaa, J. Tamm, V. Sammelselg, M. Väärtnõu, A. Jänes, and E. Lust, *Synthetic Metals,* **156**:488 (2006).

55. M. Hughes, G. Z. Chen, M. S. P. Shaffer, D. J. Fray, and A. H. Windle, *Chemistry of Materials,* **14**:1610 (2002).
56. X. Ren and P. G. Pickup, *The Journal of Physical Chemistry,* **97**:3941 (1993).
57. O. Antoine, Y. Bultel, and R. Durand, *Journal of Electroanalytical Chemistry,* **499**:85 (2001).
58. Y. Xiao, X. Cui, J. M. Hancock, M. Bouguettaya, J. R. Reynolds, and D. C. Martin, *Sensors and Actuators B: Chemical,* **99**:437 (2004).
59. J. M. Ko, H. W. Rhee, S. M. Park, and C. Y. Kim, *Journal of Electrochemical Society,* **137** (1990).
60. C. K. Baker and J. R. Reynolds, *Journal of Electroanalytical Chemistry,* **251**:307 (1988).
61. C. Debiemme-Chouvy, H. Cachet, and C. Deslouis, *Electrochimica Acta,* **51**:3622 (2006).
62. V. Syritski, A. Öpik, and O. Forsén, *Electrochimica Acta,* **48**:1409 (2003).
63. M. C. Pedro, C. Milagros, O. Estibalitz, C. Elena, and A. P. José, *Surface and Interface Analysis,* **39**:26 (2007).
64. Z. Deng, D. C. Stone, and M. Thompson, *Analyst,* **122**:1129 (1997).
65. A. S. Liu and M. A. S. Oliveira, *Journal of Brazilian Chemistry Society,* **18**:143 (2007).
66. A. F. Diaz, J. I. Castillo, J. A. Logan, and W.-Y. Lee, *Journal of Electroanalytical Chemistry,* **129**:115 (1981).
67. S. Jing, T.-S. Jadranka, C. Shu Yi, L. Kwong Chi, and A. K. Paul, *Journal of Applied Polymer Science,* **111**:876 (2009).
68. A. F. Diaz and B. Hall, *IBM Journal of Research and Development,* **27**:342 (1983).
69. T. Hernandez-Perez, M. Morales, N. Batina, and M. Salmon, *Journal of The Electrochemical Society,* **148**:C369 (2001).
70. M. D. Levi, C. Lopez, E. Vieil, and M. A. Vorotyntsev, *Electrochimica Acta,* **42**:757 (1997).
71. E. Abbas, K. Maryam, O. Abdollah, and A. R. Abbas, *Journal of Applied Polymer Science,* **117**:3107 (2009).
72. A. A. Ensafi and B. Rezaei, *Analytical Letters,* **31**:167 (1998).
73. Q.-F. Zhang, Z.-T. Jiang, Y.-X. Guo, and R. Li, *Spectrochimica Acta Part A: Molecular and Biomolecular Spectroscopy,* **69**:65 (2008).
74. L. M. Lira and S. I. Córdoba de Torresi, *Electrochemistry Communications,* **7**:717 (2005).

Chapter 6

Immobilisation of a Small Anionic Drug into Polypyrrole:

Valproic Acid Sodium Salt

6.1 Introduction

Valproic acid (also known as dipropylacetic acid, 2-propyl-pentanoic acid or 2-propylvaleric acid) was first synthesised in 1881 by Burton[1]. In the 1960s, the anticonvulsant property of valproic acid (VPA) was recognised and throughout the 60s and 70s there were several reports of its clinical effects[2-5]. There is a general agreement that it is effective in the treatment of primary generalised epilepsy and myoclonic epilepsy[6]. However, in recent times it has received interest for the treatment of bipolar disorders[7, 8]. Valproic acid sodium salt (NaVPA), shown in Figure 6.1, has a medium molecular weight (166.2 g mol^{-1}) and its structure is unrelated to other antiepileptic drugs on the market. It is hygroscopic, soluble in water, methanol and ethanol and is insoluble in acetone, chloroform, ethyl ether and benzene. It also has a pK_a of 4.95. Typical therapeutic doses[9] range from 50-100 μg ml^{-1} or 347-693 μmol L^{-1}.

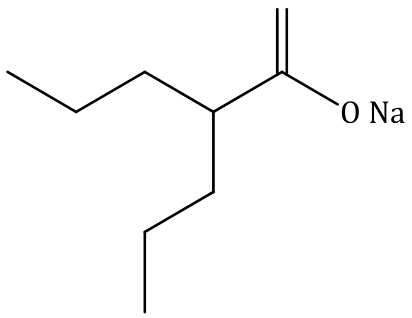

Figure 6.1: Valproic acid sodium salt (NaVPA).

VPA is available in several oral forms such as solutions, tablets, enteric-coated capsules and slow-release preparations. It is not fully understood how VPA works as an anticonvulsant. It has been suggested that it interacts with voltage-sensitive sodium channels with its presence inhibiting repetitive firing of the neuron at high frequency. VPA also increases the levels of whole brain gamma-aminobutyric acid (GABA) content and these elevations have been shown to correlate well against seizures[10]. *In vitro* studies have shown that VPA inhibits GABA transaminase, an enzyme that speeds the degradation of GABA[10, 11]. VPA is highly bound (90 %) to proteins in the blood. This means that only 10 % is free or unbound and able to enter the brain. However, with multiple doses the proportion of VPA that is free

and therefore available in the brain can rise substantially[12]. More than 95 % of VPA is broken down in the liver by several different metabolic pathways. Numerous metabolites contribute to its pharmacological and toxic actions. Some of the side effects related to VPA are liver damage, impaired beta oxidation and disruption of the urea cycle[12, 13]. This can lead to hyperammonemia and is more frequent when VPA is used in conjunction with other antiepileptic medications such as phenobarbital and phenytoin[12-14].

Within the literature, the half life ($t_{1/2}$) of VPA can vary somewhat but all agree that prolonged half lives have been observed in children and the elderly and this is thought to be due to a decrease in plasma protein binding and a reduction of drug metabolising capacity resulting in a decrease in the clearance of the free drug by the liver[13, 15, 16]. The absorption half-life ($t_{1/2abs}$) has been documented to be in a range of 30 min to 4 h. At therapeutic doses, VPA half life varies from 10 to 20 h in adults with an elimination half life ($t_{1/2el}$) varying from 5 to 24 h[7, 13, 15-17]. The $t_{1/2el}$ is longer in studies with multiple oral doses compared to those employing single oral doses of VPA. The volume of distribution is relatively small in adults, 0.10 to 0.47 L kg^{-1}, due to high plasma protein binding. The steady state plasma concentration is reached after 4 days of daily doses[7, 13, 15-17]. VPA has an insufficient response to a UV-vis detector and therefore serum or plasma samples are tested using HPLC, GC-MS and immunoassays[18-22].

Epilepsy is one such illness that would benefit greatly from the development of a controlled drug release system that could prevent or control epileptic seizures. A seizure is a sudden surge of electrical activity in the brain that usually affects how a person feels or acts for a short time. This electrical activity could trigger the release of the necessary drug. The controlled release of VPA and phenytoin (another antiepileptic drug) has been reported from sol-gel titania ceramic devices and it was found that at higher loadings of the drug the initial release is considerably lower than at lower loadings[23, 24]. The use of conducting polymers in controlled drug release studies can be restricted somewhat due to the limitation in the choice of dopant and the molecular weight of the delivered drug, however, with a molecular weight of 166.2 g mol^{-1} and a negative charge due to the sodium salt,

NaVPA is the smallest of all the drugs studied in this work and seems like an ideal dopant.

As discussed in Chapter 1, Section 1.3, polypyrrole (PPy) can be doped using various electrochemical techniques and traditional methods such as potentiostatic, galvanostatic and cyclic voltammetry (CV) have easily demonstrated this[25]. However, from the literature only one report of PPy doped with VPA^- has been found. Sabah *et al.*[26] reported the preparation of a PPy film doped with VPA^- using pulsed galvanostatic technique, however, they did not show any data to prove that this polymer was formed. They described how the polymer film was prepared on a platinum (Pt) electrode in the presence of 0.10 mol dm^{-3} NaVPA and 0.10 mol dm^{-3} pyrrole (Py). Optimum growth occurred with the application of five pulses, each 200 s, at 0.10 mA cm^{-2} with a rest of 60 s between each pulse. This experiment was repeated and the results are reported in Section 6.3.2.1. It was found that with each pulse applied the potential increased and the VPA^- was no longer stable. Therefore, it is highly unlikely that PPy doped with VPA^- was prepared in the manner described in that paper.

In this work, several attempts were made to dope PPy with VPA^- electrochemically. Vapour phase polymerisation was also investigated as an alternative method to incorporate the VPA^- into the PPy membrane film. In this chapter, it is experimentally demonstrated that even though this drug has the properties to ensure it is a successful dopant, it is not as straightforward a process as expected.

6.2 Experimental

6.2.1 Materials

Valproic acid sodium salt (NaVPA) was purchased from Sigma Aldrich and used as received. Pyrrole monomer (98%) was purchased from Aldrich and distilled prior to being used. The majority of the electrochemical techniques employed were carried out with an EDAQ potentiostat with the remainder performed using a Solartron (Model SI 1285) potentiostat.

6.2.2 Electrochemical experiments

An electrochemical cell was set up to include Pt mesh as the auxiliary electrode and for the majority of the experiments a Ag|AgCl electrode was used as the reference electrode with a standard saturated calomel electrode (SCE) employed for the rest. Polymerisation was attempted using different substrates as the working electrodes. These included gold mylar, Pt, glassy carbon (GC) and indium tin oxide (ITO) glass. Several electrochemical techniques were employed in an attempt to electrodeposit PPy doped with VPA^- including; pulsed galvanostatic technique, constant potential and CV. Vapour phase polymerisation was also employed as an alternative technique to electrochemistry. These techniques are all described in Chapter 2, Section 2.4.

All release studies were carried out in triplicate in 10 ml of artificial cerebral spinal fluid (aCSF) with a sample of 300 µl taken at certain time intervals. The volume of the release electrolyte was maintained at 10 ml for the entire length of release. The dilution factor was taken into account when the data were analysed. The amount of drug in the release samples was measured using a valproic acid assay in conjunction with a Beckman Coultar Synchron Clinical System, model Unicel DxC600. In Section 6.3.6, the amount of pTS^- and VPA^- in the release samples was measured using UV-vis spectroscopy. Calibration curves for NapTS and NaVPA were obtained and used to determine the amount of pTS^- and VPA^- in the sample, as described in Section 2.5.1.

6.3 Results and discussion

6.3.1 Conductivity measurements and redox properties of NaVPA

The conductivity of the NaVPA in an aqueous solution was measured in order to determine if it was a suitable electrolyte for the polymerisation of pyrrole (Py). Figure 6.2 shows that the conductivity increases linearly with increasing concentration with an R^2 of 0.989. These conductivity values are sufficiently high to carry out electrochemistry in the absence of a supporting electrolyte, e.g., tetrabutylammonium perchlorate (TBAP), to enhance its conductivity.

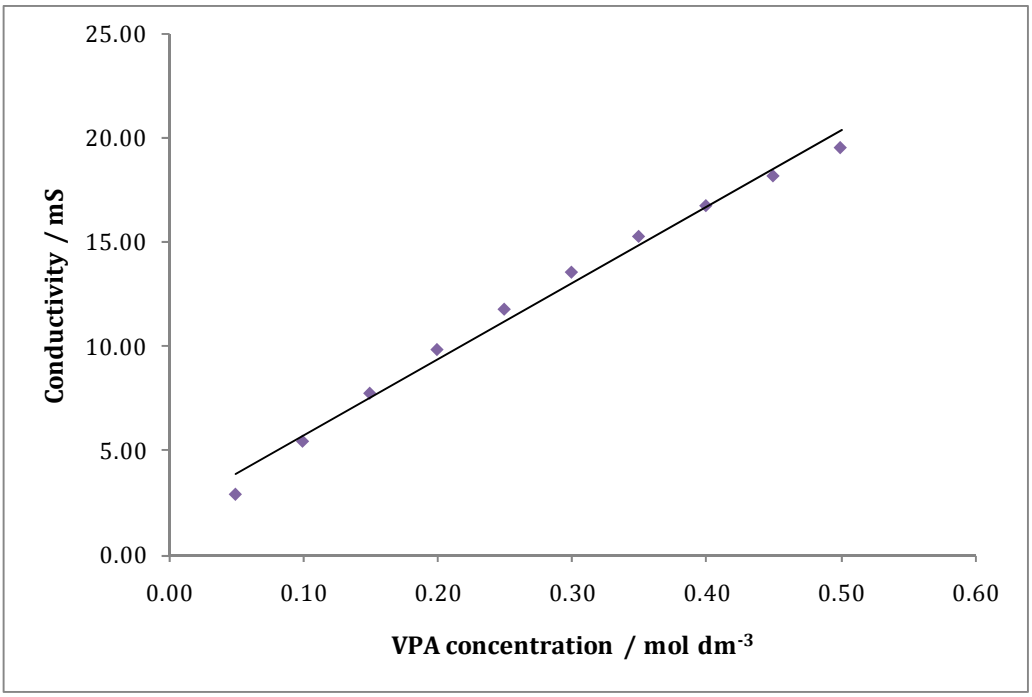

Figure 6.2: Conductivity of NaVPA measured as a function of concentration.

Using gold mylar as the working electrode, the redox properties of NaVPA were probed using CV. It was found that the redox properties of NaVPA were similar to those of acetic acid, as shown in Figure 6.3, which was expected since they are both aliphatic carboxylic acids. Oxidation and reduction peaks were observed for both NaVPA and acetic acid at +1.400 V vs Ag|AgCl and +0.200 V vs Ag|AgCl, respectively. The oxidation of the NaVPA begins to occur at +1.200 V vs Ag|AgCl which suggests that the drug is stable to oxidation between – 0.500 V vs Ag|AgCl and +1.200 V vs Ag|AgCl. These are typical oxidation values for carboxylic acids which are well known to oxidise at high anodic potentials[27]. The peak potential is close to the water decomposition and is often overlapped with oxygen evolution.

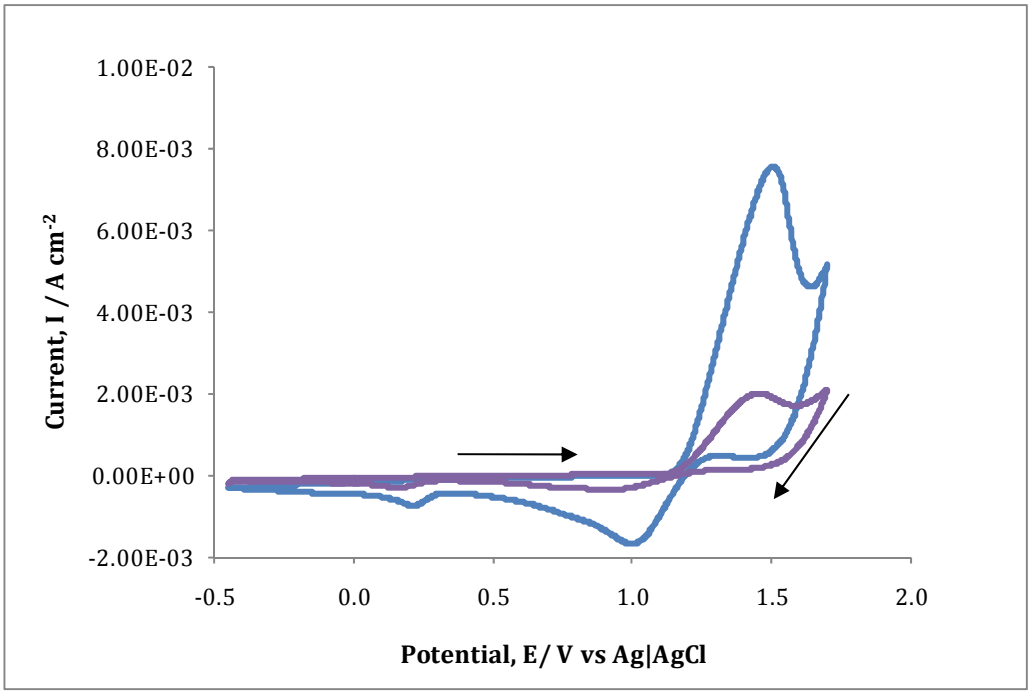

Figure 6.3: Redox properties of — 0.05 mol dm^{-3} NaVPA and — 0.05 mol dm^{-3} acetic acid recorded by CV scanning between – 0.450 V vs Ag|AgCl and +1.700 V vs Ag|AgCl at a scan rate of 25 mV s^{-1} using gold mylar as the working electrode.

6.3.2 Electrochemical polymerisation

6.3.2.1 Pulsed galvanostatic technique

The formation of VPA$^-$ doped PPy was first attempted using pulsed galvanostatic technique as reported by Sabah *et al.*[26] and the parameters are described in Section 6.1. Extremely high potentials were reached during each pulse, as shown in Figure 6.4, which resulted in no polymer growth. The potential increased from +1.700 V vs Ag|AgCl at pulse 1 to an initial potential of 3.500 V vs Ag|AgCl at pulse 5 which then settled at +1.900 V vs Ag|AgCl. At these high potentials, the VPA$^-$ is no longer stable and becomes oxidised, as shown in Figure 6.3. Also, at these electropositive potentials oxygen evolution occurs due to the oxidation of H_2O, Equation 6.1. Furthermore, the PPy also becomes over-oxidised at high potentials. These oxidation reactions will prevent the electrodeposition of PPy at the electrode surface.

$$2H_2O \rightarrow O_2 + 4e^- + 4H^+ \qquad 6.1$$

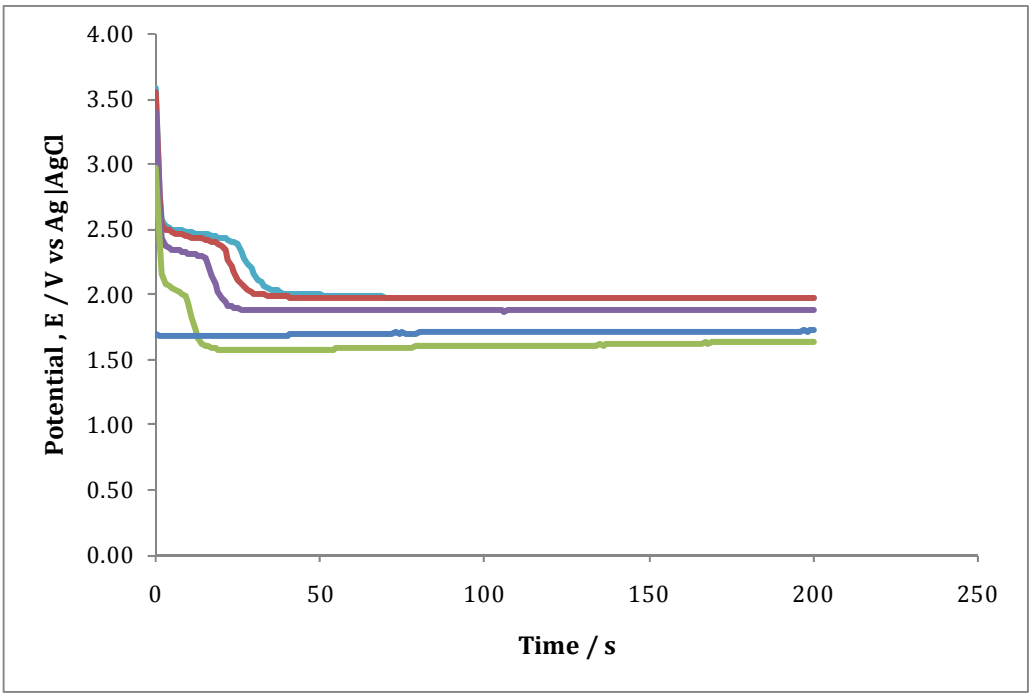

Figure 6.4: Galvanostatic plot recorded during the application of 5 pulses, — pulse 1, — pulse 2, — pulse 3, — pulse 4 and — pulse 5, of 0.10 mA cm^{-2} in the presence of 0.10 mol dm^{-3} NaVPA and 0.10 mol dm^{-3} Py at a Pt electrode. Each pulse was applied for 200 s with a rest of 60 s in between each pulse.

6.3.2.2 Constant potential

In an attempt to control the potential of the electrode and maintain it below the oxidation potential of VPA^-, constant potential measurements were carried out to form the PPyVPA. Figure 6.5 shows the charge-time plots recorded during the first 150 s of the application of a constant potential, +0.900 V vs Ag|AgCl, in the presence of 0.10 mol dm^{-3} NaVPA and 0.20 mol dm^{-3} Py. This constant potential of +0.900 V vs Ag|AgCl was also applied for 50 min but no electropolymerisation occurred on the surface of the electrode. In Chapter 4, the successful deposition of PPyDF was achieved by the deposition of a thin film of PPy doped with Cl^- (PPyCl) onto the electrode surface prior to the deposition of PPyDF. The PPyCl film provided a rougher surface on which the PPyDF could grow. In this work, a thin film of PPyCl was formed on the gold mylar and deposition of PPy doped with VPA^- was attempted. Whilst this resulted in an increase in the charge in the first 150 s, as seen in Figure 6.5B, there was no evidence of deposited PPyVPA on the surface of the electrode even after 50 min.

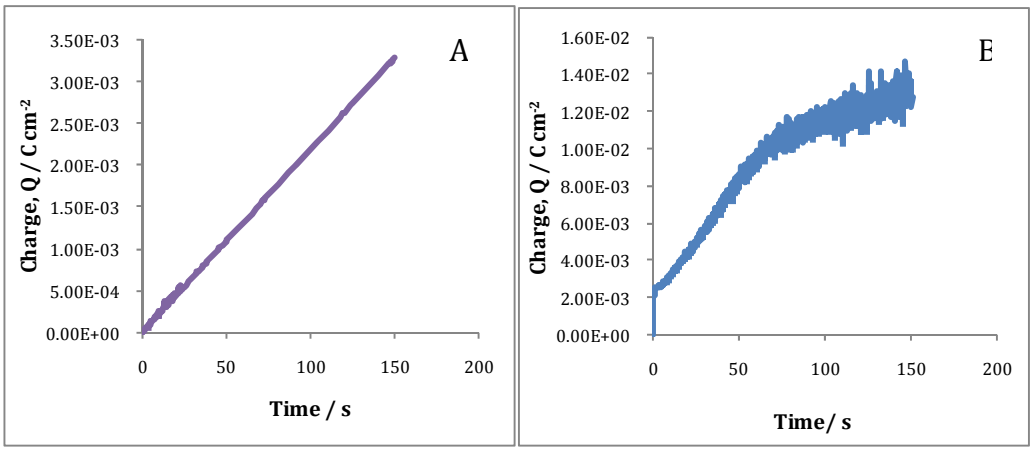

Figure 6.5: Charge-time plots of the first 150 s of the attempted formation of VPA^- doped PPy by constant potential. A constant potential of +0.900 V vs Ag|AgCl was applied for polymerisation of Py on; **A** the bare gold mylar electrode and **B** a thin layer of PPyCl, in the presence of 0.10 mol dm^{-3} NaVPA and 0.20 mol dm^{-3} Py.

Although no polymer was visible on the electrode surface, it is clear from Figure 6.5 that some oxidation of the monomer takes place. As discussed in Chapter 1, Section 1.4.1, the initial step in the mechanism of the electropolymerisation of Py, proposed by Diaz *et al.*[28], is the generation of the radical cation. The coupling of two Py radicals results in the formation of a bond between the two α positions to give a radical dication. The loss of two protons generates a neutral dimer which is then oxidised to form a radical dimer. This can couple with a radical monomer to form a trimer and the polymerisation progresses in this fashion to completion. It may be that with the application of a constant potential these dimers and trimers form but the presence of the VPA^- prevents the further progression of the polymerisation.

6.3.2.3 Studies on the use of a pre-layer

As stated in the Chapter 2, Section 2.3, three different pre-layers were studied with the aim of depositing PPy doped with VPA^- on top of them. Pre-layers have been known to support polymerisation as they can provide a rough surface on which growth is more favourable and they can lower the potential at which the polymer can be deposited[29]. All pre-layers were grown galvanostatically at a current density of 0.50 mA cm^{-2} and comprised of either para-toluene sulfonate (pTS^-) doped PPy, 4,5-dihydroxy-1,3-benzene disulfonic acid (Tiron) doped PPy or

perchlorate (ClO_4^-) doped polyterthiophene (PTTh). The concentrations of the dopants and monomers used are listed in Table 6.1. On each of these pre-layers, electrodeposition of VPA^- doped PPy was attempted by CV from a solution electrolyte of 0.50 mol dm^{-3} NaVPA and 0.20 mol dm^{-3} Py. The pre-layers were deposited onto Pt wire to charges of 0.075 C cm^{-2}, 0.150 C cm^{-2} and 1.000 C cm^{-2} for PPy doped with pTS^-, PPy doped with Tiron and PTTh doped with ClO_4^-, respectively. Representative data are shown in Figure 6.6. A similar pattern was observed for all three pre-layers, as shown in Figure 6.6B. With each cycle the currents decrease which implies that further polymerisation does not occur.

Table 6.1: Summary of electrolytes used for the deposition of PPy and PPTh pre-layers.

Dopant	Concentration/mol dm^{-3}	Monomer	Concentration/ mol dm^{-3}
NapTS	0.05	Pyrrole	0.20
Tiron	0.10	Pyrrole	0.20
TBAP	0.10	Terthiophene	0.01

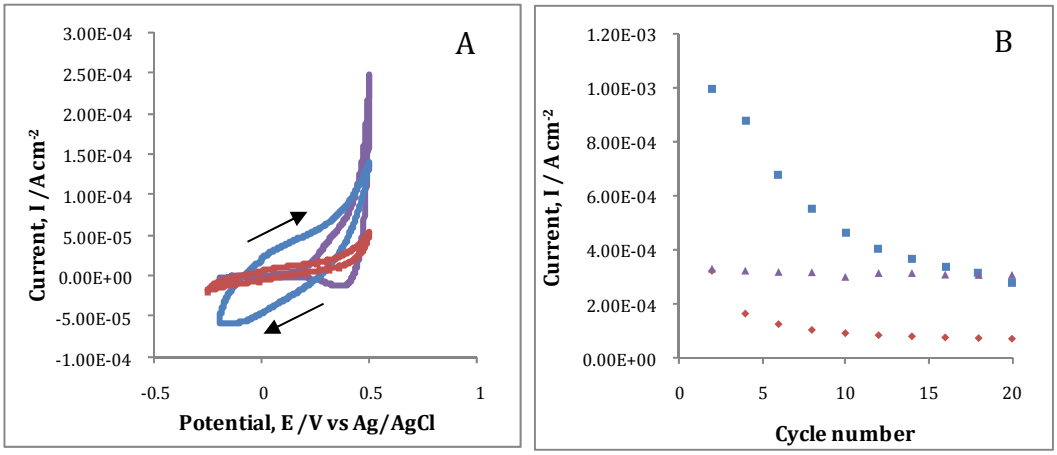

Figure 6.6: **A** CV plots of attempted growth of PPyVPA, in the presence of 0.50 mol dm^{-3} NaVPA and 0.20 mol dm^{-3} Py, on three different pre-layers; — $PTThClO_4$, — PPypTS and — PPyTiron, scanning between –0.250 V vs Ag|AgCl and +0.500 V vs Ag|AgCl at a scan rate of 25 mV s^{-1}. All are cycle 13 of 20. **B** shows the decrease in current measured at +0.500 V vs Ag|AgCl with increasing cycle number for ▲ $PTThClO_4$, ■ PPypTS and ♦ PPyTiron.

6.3.2.4 Cyclic voltammetry (CV)

Several CV experiments were carried out over a range of potentials and the concentration of NaVPA was varied. Figure 6.7 shows two sets of cyclic voltammograms scanning between –0.250 V vs Ag|AgCl and +0.950 V vs Ag|AgCl at 25 mV s^{-1} in the presence of; A: 0.25 mol dm^{-3} NaVPA and 0.20 mol dm^{-3} Py and B: 0.50 mol dm^{-3} NaVPA and 0.20 mol dm^{-3} Py. Three different substrates were used; gold mylar, GC and Pt wire. In the case where Pt wire was employed as the working electrode, the CVs indicate that the oxidation of Py occurs at +0.500 V vs Ag|AgCl. This suggests that some polymerisation of the monomer takes place, but the corresponding currents are extremely low. This is further evidence that the VPA^- is preventing the further polymerisation of Py. Since Pt was clearly the most promising electrode material, all further CV experiments in this section were carried out with Pt as the working electrode.

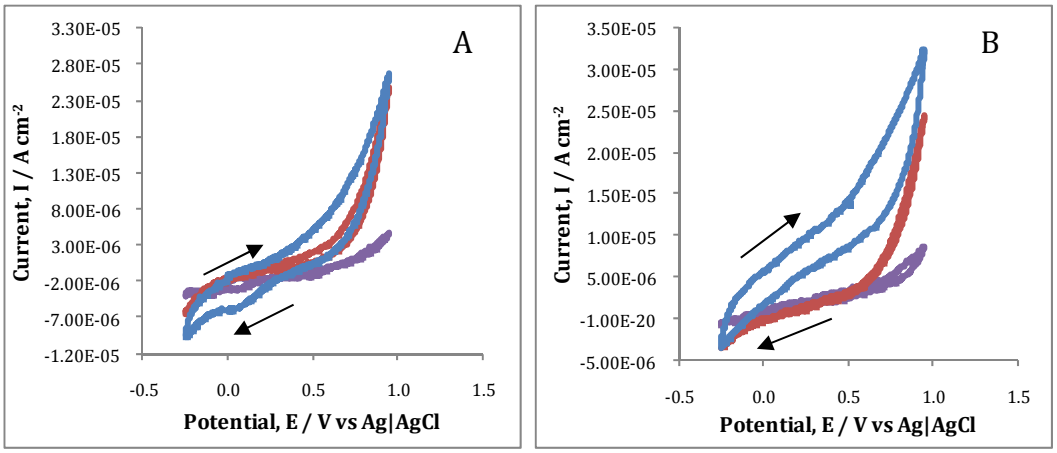

Figure 6.7: Cyclic voltammograms recorded in **A** 0.25 mol dm^{-3} NaVPA and **B** 0.50 mol dm^{-3} NaVPA in the presence of 0.20 mol dm^{-3} Py scanning between – 0.250 V vs Ag|AgCl and +0.950 V vs Ag|AgCl at 25 mV s^{-1} using a working electrode of — Pt wire, — gold mylar and — GC.

It could also be that, in the presence of the VPA^-, an oxide layer forms on the surface of the electrode. This layer may act as an insulator, blocking the electron transfer and therefore preventing polymer formation and deposition, as happens in the case of aluminium and its alloys[30]. Electron transfer mediation is a well reported technique for overcoming kinetic limitations of electron transfer at metal electrodes. Bierwagen and co-workers[30] reported using catalytic amounts of Tiron

as a mediator to allow direct electrodeposition of PPy onto an aluminium surface. CV was performed in the presence of 0.10 mol dm^{-3} Tiron and 0.20 mol dm^{-3} Py, scanning between –0.250 V vs Ag|AgCl and +0.900 V vs Ag|AgCl at a scan rate of 25 mV s^{-1}. Electrodeposition of PPyTiron took place quite easily. A second experiment was then performed with the addition of 2.0 ml of 0.30 mol dm^{-3} NaVPA (0.06 mol dm^{-3}) to the electrolyte solution and CV was repeated under the same conditions. Again, electrodepositon failed to occur in the presence of VPA^-. As shown in Figure 6.8, the oxidation of Py monomer occurs at +0.500 V vs Ag|AgCl similar to that seen in Figure 6.7 however the currents are significantly lower. It is evident from this that the VPA^- again somehow inhibits the polymerisation of the Py monomer.

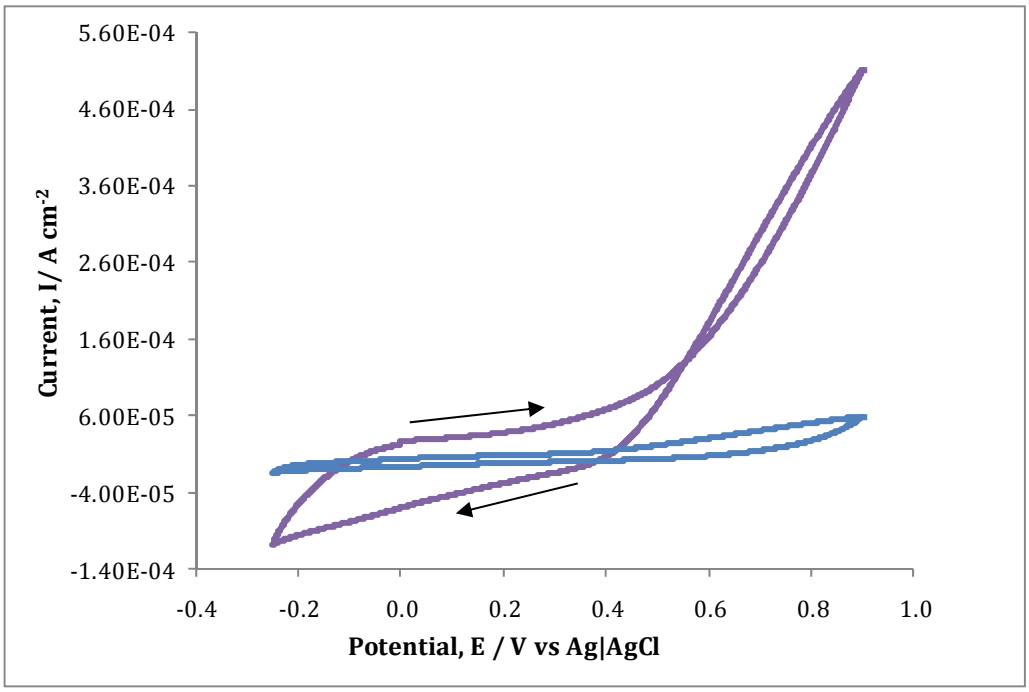

Figure 6.8: Cyclic voltammograms recorded at 25 mV s^{-1}, the potential was swept between – 0.250 V vs Ag|AgCl and +0.900 V vs Ag|AgCl in the presence of — 0.10 mol dm^{-3} Tiron and 0.20 mol dm^{-3} Py with — 2.0 ml of 0.30 mol dm^{-3} (0.06 mol dm^{-3}) of NaVPA added. A Pt wire was used as the working electrode.

Phosphate buffer saline (PBS) was used as a supporting electrolyte to investigate if its presence would facilitate the electrodeposition of PPyVPA. The electropolymerisation of Py was achieved by CV, scanning between –0.250 V vs Ag|AgCl and +0.900 V vs Ag|AgCl, in the presence of PBS and 0.20 mol dm^{-3} Py, at a scan rate of 25 mV s^{-1}. As before, approximately 0.20 ml of

0.30 mol dm^{-3} NaVPA (0.06 mol dm^{-3}) was then added to the electrolyte to test if polymerisation would still occur in its presence. There was no visible polymerisation on the surface of the electrode in the presence of the VPA^-. Figure 6.9 shows the cyclic voltammograms recorded for the growth of PPy in the absence and presence of the VPA^-. These plots are quite similar and indicate that oxidation of the monomer occurs but there is a decrease in current in the presence of the VPA^- which prevents the formation of the polymer film at the electrode.

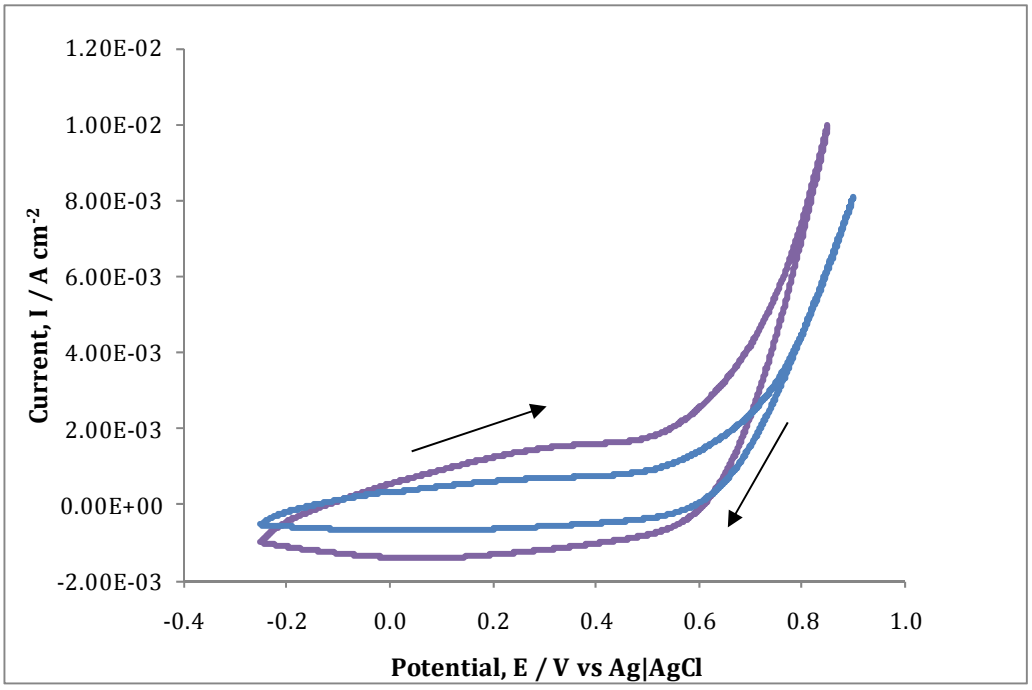

Figure 6.9: CV plots recorded at a scan rate of 25 mV s^{-1} between - 0.250 V vs Ag|AgCl and +0.900 V vs Ag|AgCl. The electrolyte consisted of — PBS and 0.20 mol dm^{-3} Py with — 2.0 ml of 0.30 mol dm^{-3} (0.06 mol dm^{-3}) NaVPA. A Pt wire was used as the working electrode.

The pH of the electrolyte was varied in an attempt to electrosynthesise the PPyVPA directly onto the Pt wire. The pH of the NaVPA-Py electrolyte was measured at 7.5. This was lowered to 6.2 and 5.6 using HCl. The pH could not be lowered any further than this as the addition of the acid shifted the equilibrium to the undissociated HVPA acid which is insoluble in water, Equation 6.2.

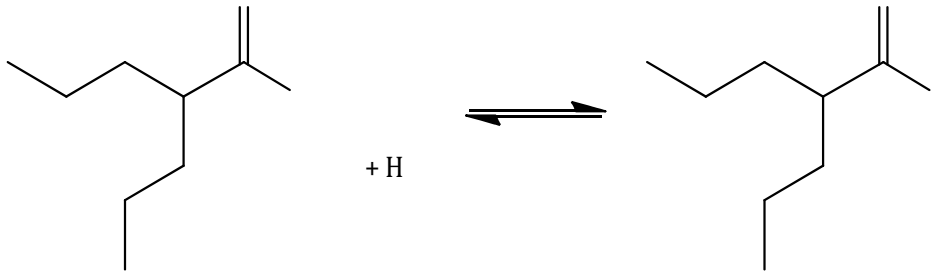

6.2

In order to shift the equilibrium further towards the soluble form of the VPA, the pH was increased with the addition of 5 x 10^{-4} mol dm^{-3} histamine (HA). HA has two centres that can be protonated, the aliphatic amino group, pKa ~ 9.4, and the proton free nitrogen of the imidazole ring, pKa ~ 5.8[31]. The aliphatic amino group is readily protonated and in the presence of the HA, the VPA exists as the anionic species, Equation 6.3.

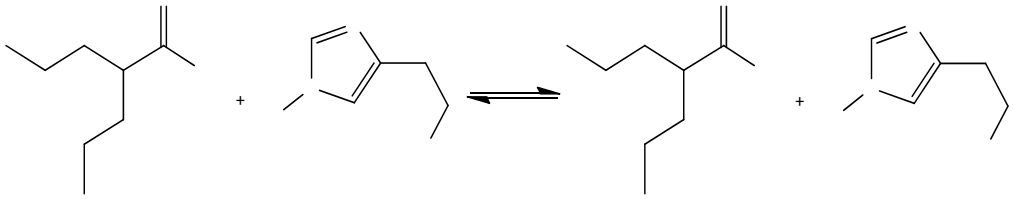

6.3

The pH was then increased to 8.2 and 9.3 with HA. NaOH could also have been used for this purpose but the HA removes protons from the electrolyte while increasing the pH. Electropolymerisation was attempted at all five of these pH values by sweeping the potential between –0.200 V vs SCE and +1.200 V vs SCE at a scan rate of 25 mV s^{-1}. The cyclic voltammograms recorded are shown in Figure 6.10. With increasing pH, the corresponding currents decrease. This is not surprising as polymerisation of Py at pH > 8.0 is difficult[32-34] but the fact that VPA^- is insoluble at pH values lower than 5.6 may be the reason that doping PPy with this drug is not possible.

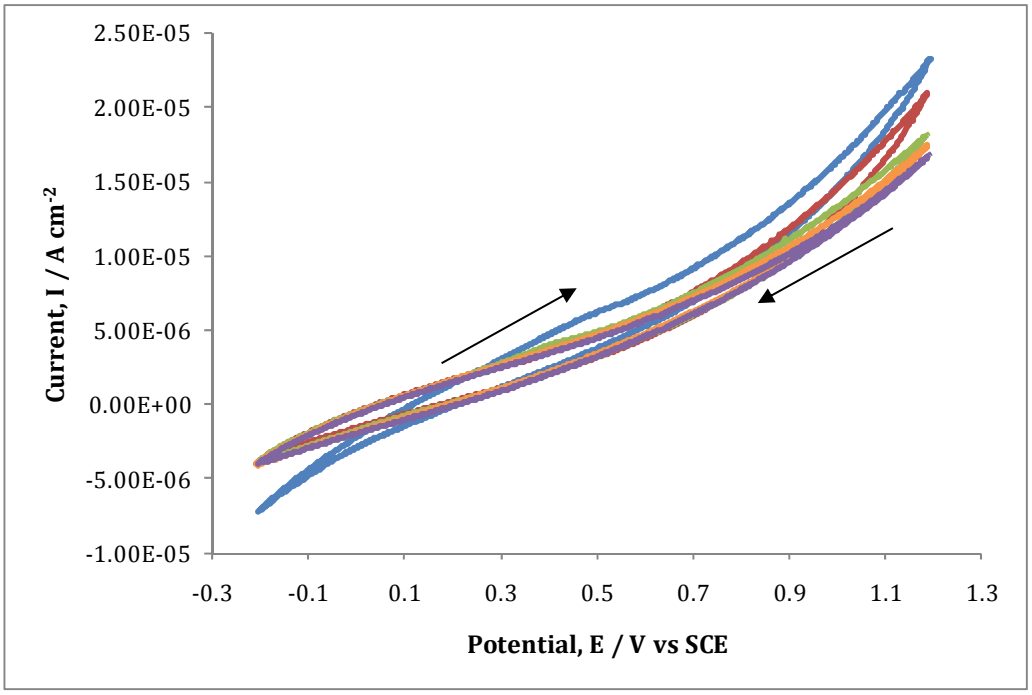

Figure 6.10: CV plots of attempted growth of VPA^- doped PPy from 0.10 mol dm^{-3} NaVPA and 0.20 mol dm^{-3} Py, scanning between –0.200 V vs SCE and +1.200 V vs SCE at a scan rate of 25 mV s^{-1}. The pH of the electrolyte was varied; — 5.6, — 6.2, — 7.5, — 8.2 and — 9.3.

As discussed in Section 4.3.1.2, the well known Henderson Hasselbalch Equation, Equation 6.4, can be used to determine the % of anions in solution. The influence of pH on the % of anions in solution is evident in Figure 6.11, where various pH values were substituted into Equation 6.4 and the % of anions was plotted as a function of pH. At pH 7.5, the % of VPA anions in solution is 99 % and the equilibrium favours the anionic form of VPA, however, at pH 5.0 the % of VPA anions in solution is 52 %.

$$\% [VPA^-] = \frac{100}{1 + 10^{pKa-pH}} \qquad 6.4$$

As seen in Chapter 4, the rate of deposition of PPy doped with DF^- was hindered due to the presence of insoluble drug crystals at the surface of the electrode. VPA has a higher pKa than DF and its equilibrium is shifted towards its insoluble form at higher pH values than those seen for the formation of HDF. It is likely that the local pH changes that affect the deposition of PPyDF have an even greater effect on

the formation of PPyVPA. In the case of the PPyDF, some deposition of the polymer occurs prior to the formation of the insoluble drug crystals but, in this case, it seems that during the initial oxidation of the monomer the equilibrium shifts towards acidic conditions and causes insoluble HVPA to form at the electrode, Equation 6.2, and this prevents the deposition of any PPyVPA. This seems like the most reasonable and likely explanation as to why the direct electrodeposition of PPy doped with VPA^- does not occur.

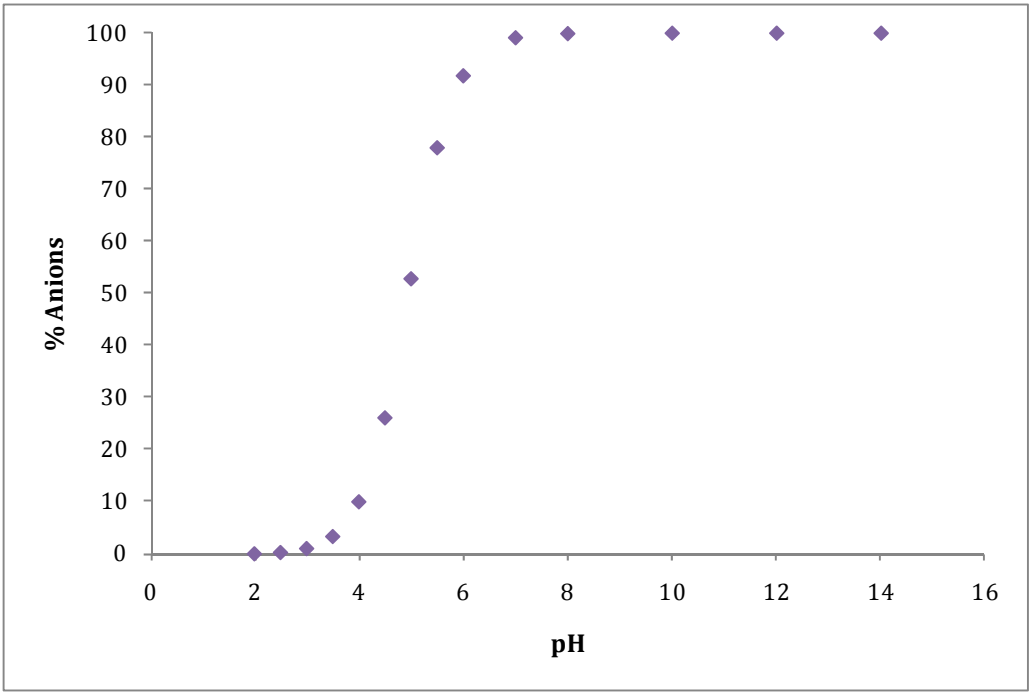

Figure 6.11: The percentage of anions as a function of pH of NaVPA. The % of anions for the given pH was calculated by substituting various pH values into Equation 6.4.

6.3.3 Post-doping PPy with VPA^-

Having tried and tested numerous electrochemical methods to dope the PPy with VPA^-, the possibility of 'post-doping' an already formed PPy film with VPA^- was investigated. A film of PPypTS was prepared on gold mylar galvanostatically by applying a current density of 0.50 mA cm^{-2} for 5 min. It was then cycled in 0.10 mol dm^{-3} $NaNO_3$ before 2.0 ml of NaVPA was added to the electrolyte. The change in currents caused by the addition of the NaVPA was monitored by comparing the characterisation cyclic voltammograms before and after the addition of NaVPA. The concentrations of the NaVPA were varied; 0.30 mol dm^{-3}, 0.50 mol dm^{-3} and 0.70 mol dm^{-3} which when added to the electrolyte gave final

concentrations of 0.06 mol dm^{-3}, 0.10 mol dm^{-3} and 0.14 mol dm^{-3}, respectively. From Figure 6.12, it can be seen that with increasing concentrations of NaVPA there is a decrease in the corresponding currents which implies that the VPA^- is somehow having a negative effect on the conductivity of the previously formed polymer of PPypTS.

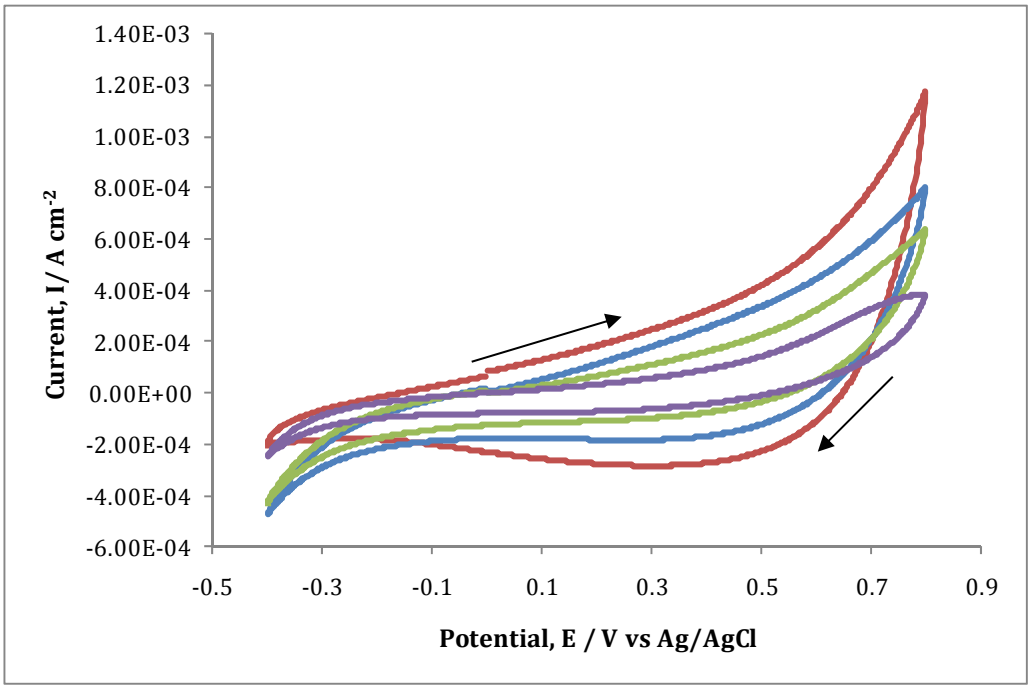

Figure 6.12: Characterisation CV, cycle 3 of 5, of — pTS doped PPy in 0.10 mol dm^{-3} $NaNO_3$ with the addition of — 0.06 mol dm^{-3} NaVPA, — 0.10 mol dm^{-3} NaVPA and — 0.14 mol dm^{-3} NaVPA cycled between –0.450 V vs Ag|AgCl and +0.800 V vs Ag|AgCl at 25 mV s^{-1}.

To investigate further how the currents were affected, the number of cycles was increased. Figure 6.13 shows cyclic voltammograms recorded for PPypTS with added NaVPA after 5, 10, 15 and 20 cycles. There is a clear decrease in the current with continuous cycling. This is more evident in the inset in Figure 6.13 where the currents measured at +0.700 V vs Ag|AgCl are plotted as a function of the cycle number.

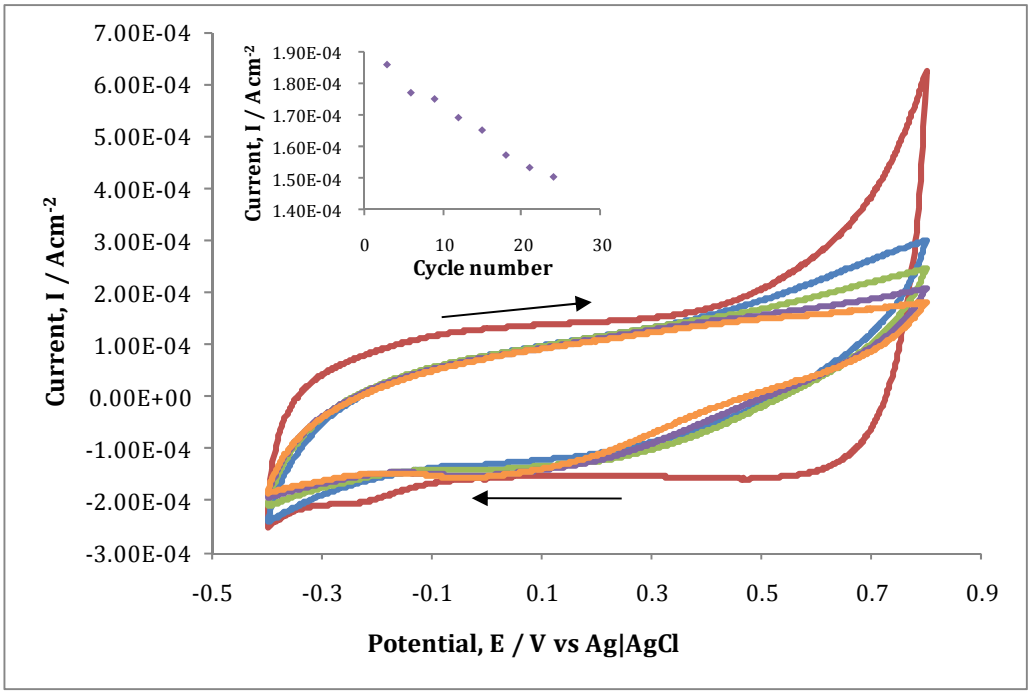

Figure 6.13: CV plot of — PPypTS in 0.10 mol dm^{-3} $NaNO_3$ and in 0.50 mol dm^{-3} NaVPA, scanning between –0.450 V vs Ag|AgCl and +0.800 V vs Ag|AgCl at 25 mV s^{-1}, at — cycle 5, — cycle 10, — cycle 15 and — cycle 20. Inset shows clearly how the currents are decreasing with increasing cycle number.

However, it can also be seen that there is very little change in the oxidation and reduction currents at potentials below +0.500 V vs Ag|AgCl and above – 0.100 V vs Ag|AgCl. The window was then confined between – 0.200 V vs Ag|AgCl and +0.500V vs Ag|AgCl and it can be seen in Figure 6.14 that the opposite trend occurred with a slight increase in the current with repeated cycling. This trend implies that ion exchange between the VPA^- and the pTS^- already doped on the polymer occurs.

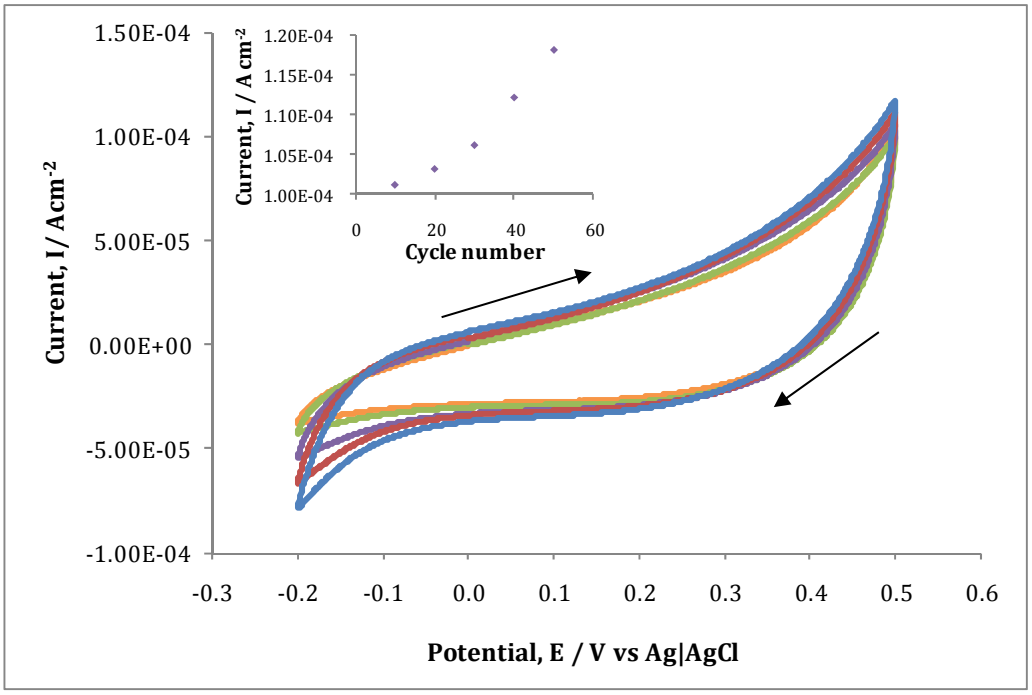

Figure 6.14: CV plots, scanning between –0.200 V and +0.500 V at 25 mV s^{-1}, of PPypTS in 0.50 mol dm^{-3} NaVPA at — cycle 10, — cycle 20, — cycle 30, — cycle 40 and — cycle 50. Inset shows how currents increase with increasing cycle number, currents measured at +0.500 V vs Ag|AgCl.

The success of the post-doping was measured in terms of the amount of drug released from the polymer. Preliminary studies were carried out in which the thickness of the PPypTS film and the number of times the film was cycled in 0.50 mol dm^{-3} NaVPA were varied. More promising release profiles were measured with a thin polymer (2.5 min growth) than when a thick polymer (5 min growth) was post-doped with VPA^-. The polymer was also immersed in the 0.50 mol dm^{-3} NaVPA solution for the precise length of time it took to complete 75 cycles to survey whether the release of VPA^- is associated with cycling the polymer in the NaVPA solution or merely due to the polymer being immersed in the NaVPA solution for a long period of time. Post-doping was also performed on films of $PPyNO_3$ to investigate the use of a more mobile dopant[35] to increase the amount of drug that could be post-doped. All polymers were grown in triplicate and released passively over a 4 h period with samples taken at 2 h and 4 h. Figure 6.15 shows the amount of VPA^- measured during these release studies.

For both the pTS^- and NO_3^- doped polymers, a similar relationship between the number of cycles and the amount of VPA^- released was observed. The optimum number of cycles in NaVPA was found to be 50 times. It seems that when the polymer was cycled for 25 cycles there was not sufficient time for the VPA^- to become doped within the polymer. In contrast, cycling for 75 or 100 cycles seems to suggest that the VPA^- is given too much time to exchange with the dopant and starts to exchange back out of the polymer. The fact that very little VPA^- was measured from the polymer that was immersed in the 0.50 mol dm^{-3} NaVPA solution for a length of time, provides further evidence that by cycling the polymer in NaVPA some ionic exchange occurs. However, in all cases there is very little difference between the amount of drug measured at 2 h and 4 h which suggests that the majority of the drug is released within the first 2 h. This, in turn, indicates that the ionic exchange occurs only at the polymer-solution interface.

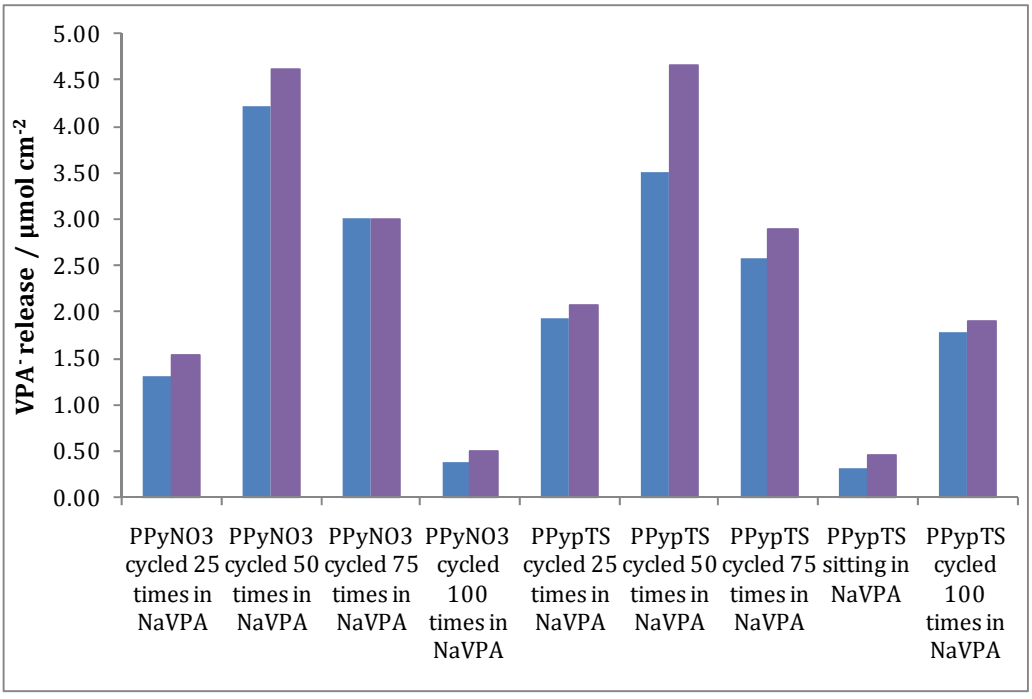

Figure 6.15: Release studies carried out passively on $PPyNO_3$ and PPypTS post-doped with VPA^-. Samples were taken at ■ 2 h and ■ 4 h. (n=3, % error = 6.4 %)

6.3.4 Post-doping PPy deposited onto a pre-layer

As mentioned in Section 6.3.2.3, the presence of a pre-layer, such as polyterthiophene (PTTh) doped with ClO_4^-, on the electrode surface provides a larger surface area on which a PPy doped film can be deposited and therefore

enables enhanced polymer growth[29]. As the post-doping occurs at the solution interface of the polymer, an increased polymer size would therefore increase the amount of post-doping sites. For these initial studies with the pre-layer, only the PPypTS polymer was used. The pre-layer (PTTh) was grown, as described in Section 6.3.2.3, for 33.5 min and the polymer 'post-layer' (PPypTS) was grown for 33.5 min upon this. The polymer was also grown for 2.5 min on a pre-layer grown for 2.5 min. To monitor the effect of the pre-layer, the polymer was also deposited directly onto the electrode for 2.5 min and 33.5 min. In all cases the post-doping was carried out by sweeping the potential between – 0.200 V vs Ag|AgCl and +0.500 V vs Ag|AgCl, at a scan rate of 25 mV s^{-1} for 50 cycles, in the presence of 0.50 mol dm^{-3} NaVPA. The release profiles from these polymer films are shown in Figure 6.16.

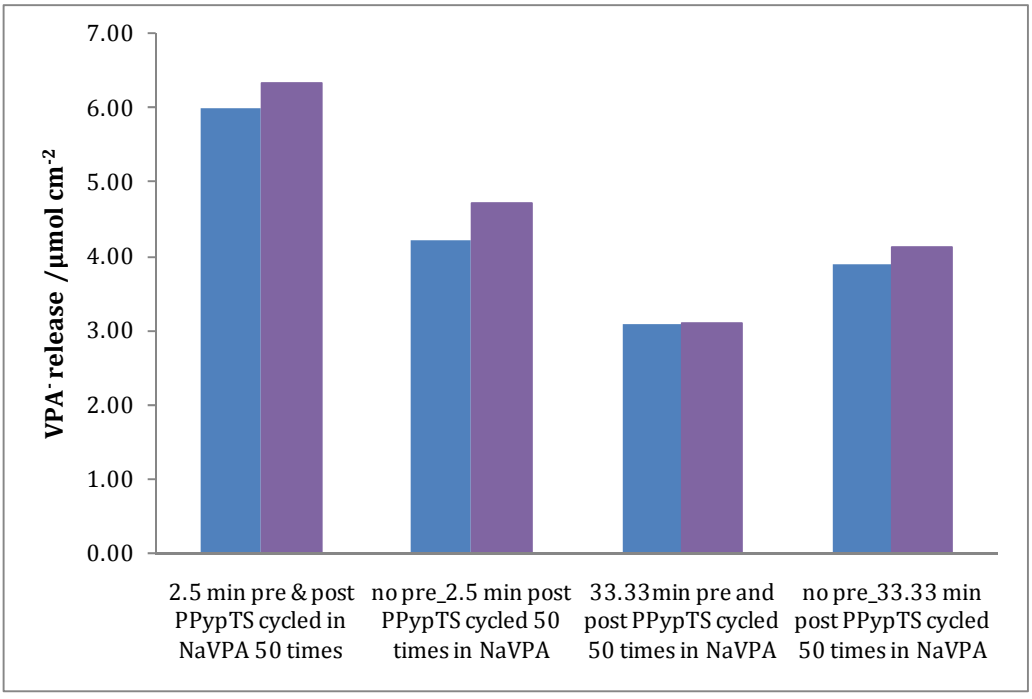

Figure 6.16: Release profiles of VPA^- recorded when varying the prelayer and polymer growth. Samples were taken at ■ 2 h and ■ 4 h. (n=3, % error = 7.8 %)

The optimum release profile was observed when a 2.5 min PTTh pre-layer was grown with a 2.5 min PPypTS polymer. Polymers were then grown under these optimum conditions using both NO_3^- and pTS^- as dopants in the post-layer and cycled in NaVPA under the same conditions as before for 50 and 75 cycles. The

release studies are shown in Figure 6.17. The polymers deposited onto the pre-layer release a higher amount of VPA^- than those grown directly onto the electrode, as shown previously in Figure 6.16. Even though NO_3^- is a more mobile dopant, the polymer doped with pTS^- displays higher VPA^- release and therefore all subsequent release studies were performed on two different polymers; PPypTS grown on the PTTh pre-layer and PPypTS grown directly onto the electrode.

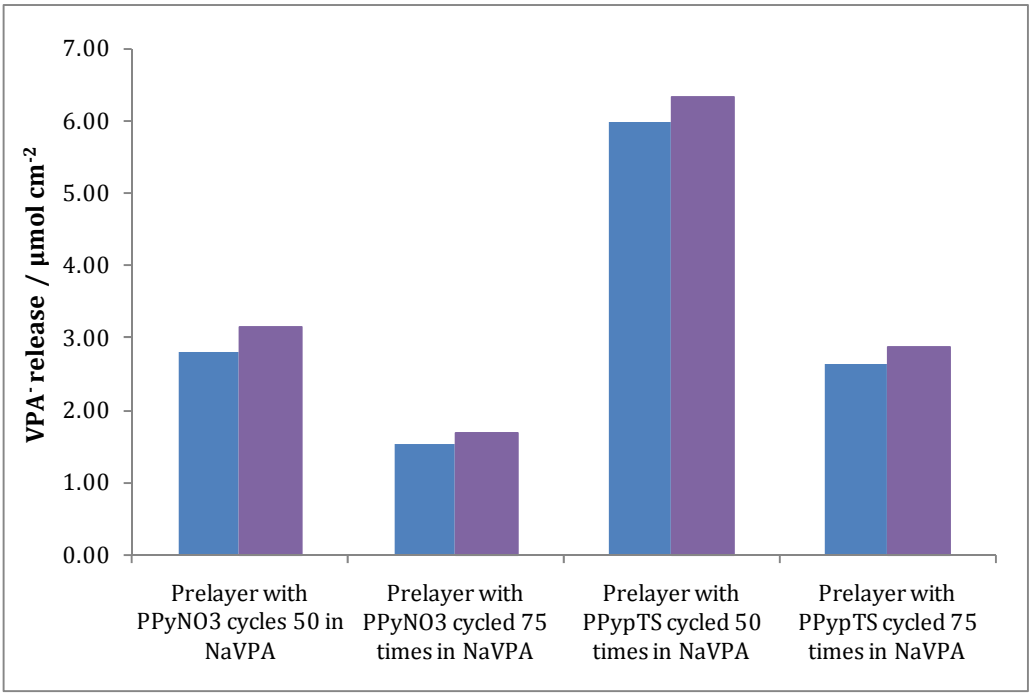

Figure 6.17: Amount of VPA^- recorded from release studies of polymers deposited on a pre-layer of PPTh doped with ClO_4^-. Samples were taken at ■ 2 h and ■ 4 h. (n=3, % error = 8.6 %)

Passive release was then carried out for a longer period of time and samples were taken more frequently. It is apparent from Figure 6.18A that more VPA^- is released from the polymer deposited on the pre-layer. Stimulated release was then carried out at –0.500 V vs Ag|AgCl, –0.250 V vs Ag|AgCl and +0.500 V vs Ag|AgCl and the release profiles are shown in Figure 6.18 B, C and D, respectively.

It is clear from these plots that the majority of the drug is released within the first 10 min and it is difficult to identify which applied potential gives the highest release. By examining the release profiles in the first 10 min, the difference between the release profiles may be more obvious.

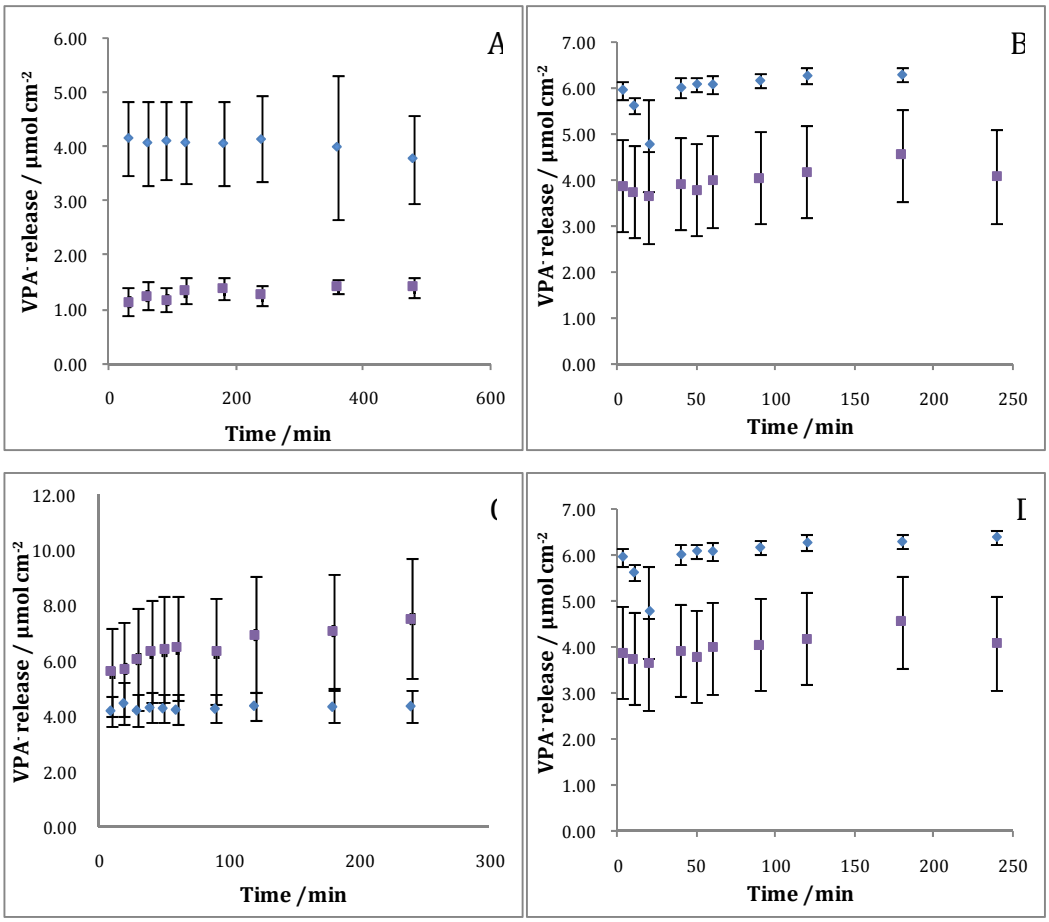

Figure 6.18: VPA^- release studies carried out from two polymers; ■ grown directly onto the electrode and ♦ grown on the pre-layer of ClO_4^- doped PPTh. The release potentials were **A** passive, **B** –0.500 V vs Ag|AgCl, **C** –0.250 V vs Ag|AgCl and **D** +0.500 V vs Ag|AgCl. (n=3).

The release studies were then repeated with a sample being taken every minute for the first 10 min to determine the best release parameters. These results are shown in Figure 6.19. From these release profiles, it is clear that the majority of the drug is released within the 1st minute and again the amount of drug released is independent of the potential applied. This was unexpected since VPA^- has a negative charge due to the sodium salt and typical release profiles for an anionic drug, as seen in the release studies discussed in Chapters 3, 4 and 5, display an increase in drug release as the polymer is reduced. The fact that the amount of drug released has no relationship to the applied potential suggests that controlled release of VPA^- from the polymer does not occur.

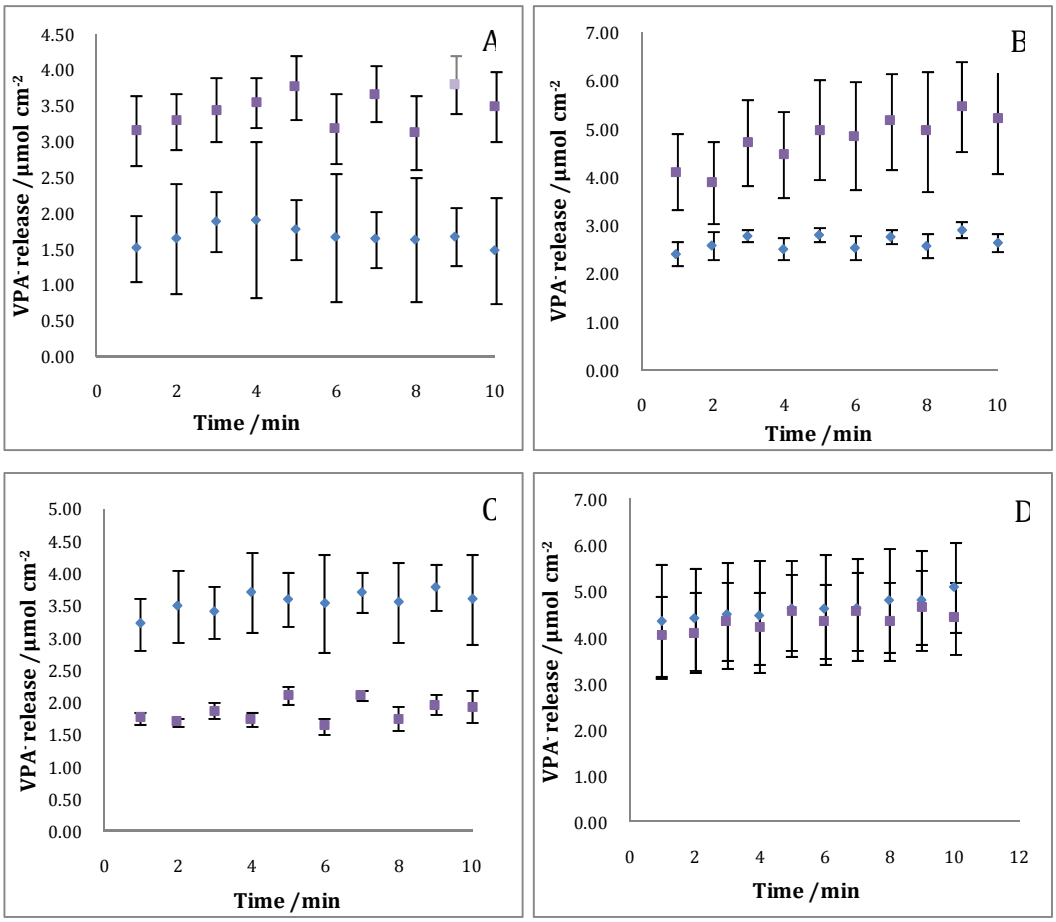

Figure 6.19: VPA^- release measurements of the first 10 min at **A** passive, **B** –0.500 V vs Ag|AgCl, **C** –0.250 V vs Ag|AgCl and **D** +0.500 V vs Ag|AgCl. The drug was released from two polymers; ■ grown directly onto the electrode and ♦ grown on the pre-layer of ClO_4^- doped PPTh. (n=3).

6.3.5 Characterisation of the post-doped polymer

6.3.5.1 Characterisation by CV

CV was utilised to explore the redox properties of the PPypTS, deposited directly onto the gold mylar, and to monitor any changes in redox properties as result of post-doping the polymer with VPA^-. Figure 6.20 shows the cyclic voltammograms recorded by scanning between – 0.400 V vs Ag|AgCl and +0.800 V vs Ag|AgCl in $NaNO_3$ at 25 mV s^{-1}. CV was firstly performed on the PPypTS polymer, the polymer was then cycled in 0.50 mol dm^{-3} NaVPA for 5 cycles scanning between –0.400 V vs Ag|AgCl and +0.800 V vs Ag|AgCl before it was then replaced in the $NaNO_3$ and another CV was performed. It was then placed back into the NaVPA and the process was repeated. Figure 6.20A shows three cyclic voltammograms; the

PPypTS polymer, the PPypTS polymer after it was cycled in NaVPA and the PPypTS polymer after it was cycled in NaVPA a second time. There is a significant difference in the cyclic voltammogram of PPypTS before and after it is cycled in NaVPA with the development of two oxidation peaks at –0.200 V vs Ag|AgCl and +0.350 V vs Ag|AgCl and a reduction peak at –0.100 V vs Ag|AgCl becomes more pronounced. These suggest that the composition of the polymer has been altered as a result of being cycled in the NaVPA, giving further confirmation that some kind of ionic exchange occurs. Figure 6.20B shows two cyclic voltammograms; the polymer cycled in the NaVPA before it was replaced back into the $NaNO_3$ and the polymer cycled a second time in NaVPA. There is very little change in the shape of the CVs with the exception that the currents have increased from the first to the second.

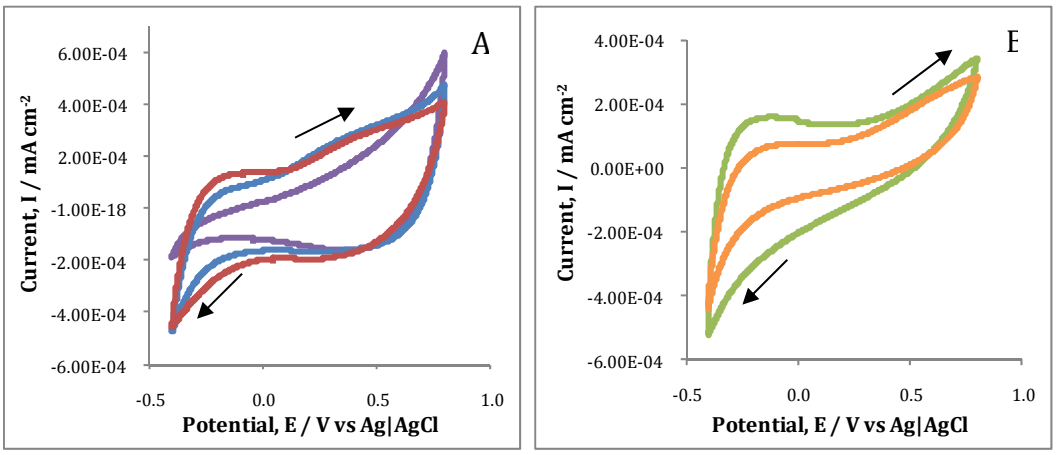

Figure 6.20: Cyclic voltammograms of PPypTS, scanning between – 0.400 V vs Ag|AgCl and +0.800 V vs Ag|AgCl at a scan rate of 25 mV s^{-1}, in the presence of **A** 0.10 mol dm^{-3} $NaNO_3$ for the — first time, — second time after 5 cycles in NaVPA and — third time after 5 cycles in NaVPA and **B** 0.50 mol dm^{-3} NaVPA for the — first time and — second time after 5 cycles in $NaNO_3$.

6.3.5.2 Morphology of the post-doped polymer

Scanning electron microscopy (SEM) was performed in order to obtain information on the morphology of the PPypTS film, deposited on the PTTh pre-layer, before and after the post-doping. The films were first synthesised and in some cases cycled in NaVPA with release studies carried out, washed thoroughly with distilled water and dried by exposure to a gentle air flow for 30 s. Figure 6.21

shows SEM micrographs of the PPypTS polymer grown on the pre-layer before and after cycling in NaVPA and after 8 hours of passive release. The morphology of the polymer, presented in Figure 6.21, does not have the globular cauli-flower morphology of the PPy films seen in Chapters 3 and 5 and characteristically seen for PPy[36, 37]. These films are more porous and typical of those seen for PTTh[29, 38]. This suggests the presence of the pre-layer has a profound effect on the morphology of the polymer. There are similarities in the polymer before it was cycled and after the passive release. In Figure 6.21B, the globular shapes of the VPA^- on the surface of the polymer can be seen. The cross sections of the polymer were also measured and were found to be approximately 8 μm including the prelayer and < 1 μm, on its own, without the prelayer.

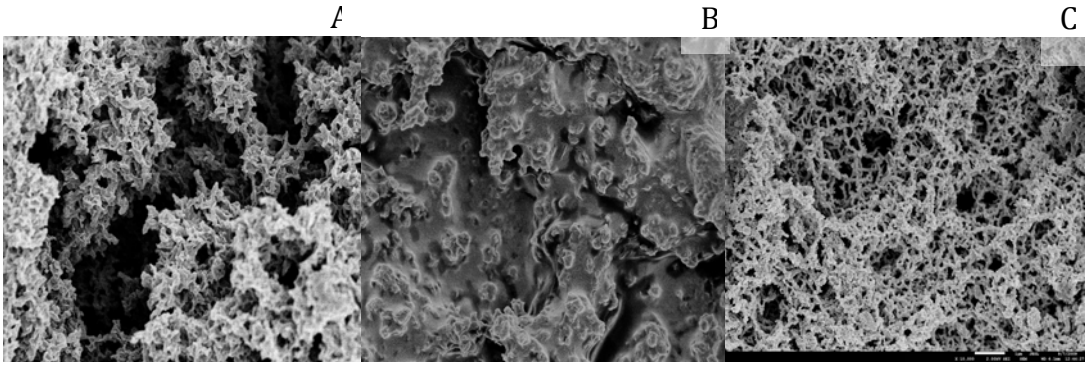

Figure 6.21: SEM micrographs of **A** PPypTS on PPTh doped with ClO_4^-. **B** cycled in 0.50 mol dm^{-3} NaVPA between –0.250 V vs Ag|AgCl and +0.500 V vs Ag|AgCl for 50 cycles and **C** after passive release for 8 hours. All micrographs are at a magnification of 10,000.

Further SEM micrographs of the polymers were performed after stimulated release was carried out at –0.500 V vs Ag|AgCl, –0.200 V vs Ag|AgCl and +0.500 V vs Ag|AgCl. To investigate whether the change in morphology seen in Figure 6.21B was due to the presence of the VPA^- or merely due to cycling the polymer in a solution, a polymer of PPypTS was cycled in sodium para-toluene sulfonate (NapTS) under the same parameters and released passively. These micrographs are all shown in Figure 6.22. There are similarities between the polymer after release in Figure 6.21C and Figure 6.22D indicating that this appearance in morphology may just be a result of the polymer left sitting in either the NaVPA or NapTS solutions for a long period of time. Figure 6.22C has features similar to both Figure 6.21B and Figure 6.22D, as there is still evidence of the drug

on the polymer surface and the morphology is similar. Reduction potentials were applied to the polymers in Figure 6.22A and B and this may be why their appearance is different to the others. Figure 6.22A has the traits of a typical PPy film with globular shapes[39, 40] whereas Figure 6.22B has the appearance that the polymer has been wiped from the electrode. None of these images, however, give any verification as to how the VPA^- is incorporated into the polymer.

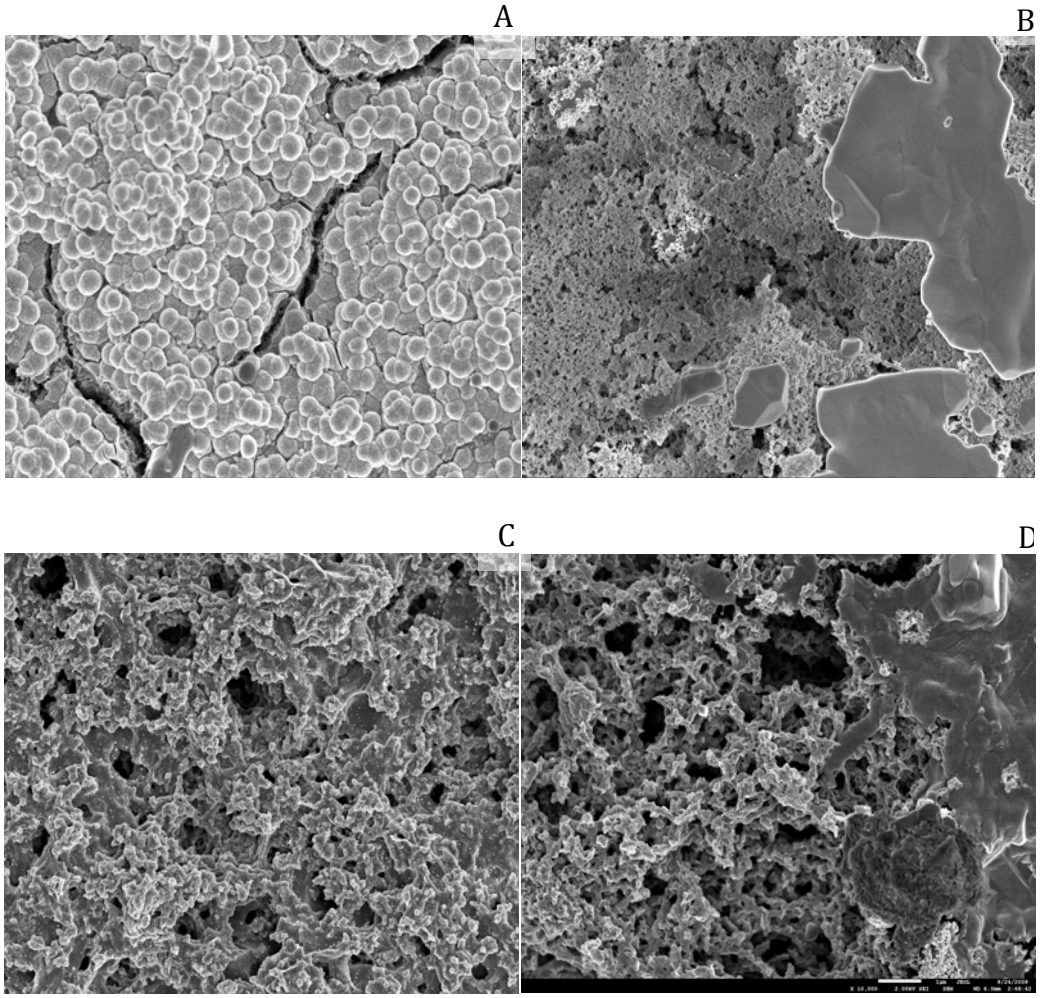

Figure 6.22: SEM micrographs of stimulated release of PPypTS cycled in 0.50 mol dm^{-3} NaVPA between –0.250 V vs Ag|AgCl and +0.500 V vs Ag|AgCl for 50 cycles and released at potentials of **A** –0.500 V vs Ag|AgCl, **B –**0.250 V vs Ag|AgCl and **C** +0.500 V vs Ag|AgCl and **D** is PPypTS cycled in NapTS and released passively. All PPypTS films were deposited on a layer of PPTh doped with ClO_4^-. All micrographs are at a magnification of 10,000.

6.3.6 Measuring pTS⁻ exchange

To investigate the post-doping further, the amount of pTS⁻ expelled from the polymer during the ion exchange was measured using UV-vis spectroscopy. The polymer was grown as before directly onto the gold mylar and the polymer was cycled in the presence of 0.20 mol dm^{-3} NaCl. The potential was swept between –0.200 V vs SCE and +0.500 V vs SCE for 60 cycles with a sample of the solution taken every 10 cycles. The polymers were also held at three different potentials; –0.500 V vs SCE, –0.200 V vs SCE and +0.500 V vs SCE. Samples were taken every 5 min over the course of 30 min. The amount of pTS⁻ released from the polymer is shown in Figure 6.23.

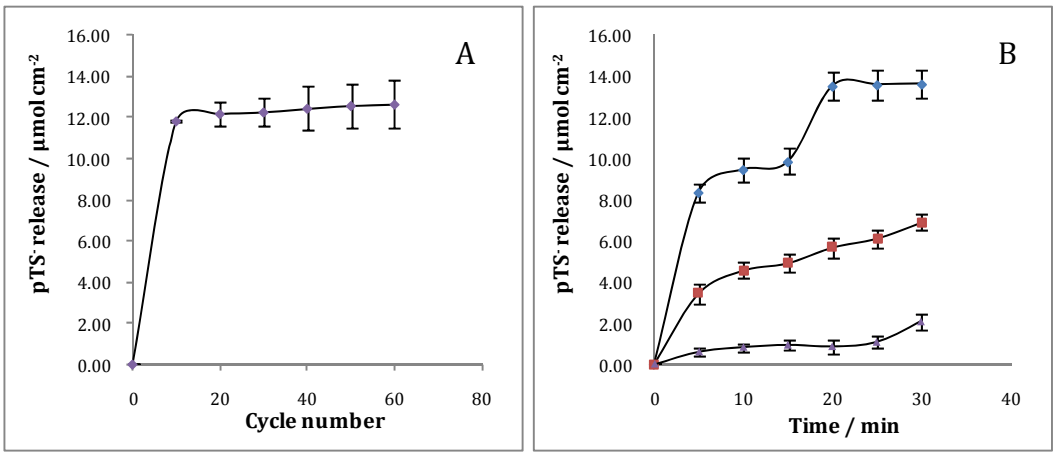

Figure 6.23: A is the amount of pTS⁻ measured as pTS⁻ doped PPy was cycled in 0.20 mol dm^{-3} NaCl 60 times, scanning between –0.200 V and +0.500 V at 25 mV s^{-1}. **B** is the amount of pTS⁻ detected when pTS⁻ doped PPy was held at ♦ –0.500 V vs SCE, ■ –0.200 V vs SCE and ▲ +0.500 V vs SCE. (n=2)

On comparing Figure 6.23 with Figure 6.19, it is clear that the amount of pTS⁻ released is higher than the concentration of VPA⁻ released. It is also clear that when a reduction potential is applied higher concentrations of pTS⁻ are released. This is consistent with Equation 6.5.

$$PPy^{+}pTS^{-} + e^{-} \rightarrow PPy^{0} + pTS^{-} \qquad 6.5$$

PPy doped with pTS⁻ is a polymer that has been comprehensively investigated and documented[41-43]. The ion exchange process of PPy has also received significant

interest[33, 35, 42-45] and there is a general agreement that for an anion of medium-large size, such as pTS^-, there is mixed ion transport across the polymer during discharge. During a redox process, PPypTS, in a solution of NaCl, shows a combination of both anion and cation exchange processes due to the insertion and expulsion of both Na^+ and Cl^- with a small amount of pTS^- anions leaking out of the polymer matrix. The expulsion and insertion of cations, Na^+, are shown in Equation 6.6 and Equation 6.7, respectively, while the incorporation and expulsion of Cl^- anions are shown in Equations 6.8 and 6.9, respectively. Although these equations are not balanced, they illustrate how the charged ions move across the polymer membrane.

$$PPy_n^0 pTS^- Na^+ - e^- \rightarrow PPy_n^0 PPy_n^+ pTS^- + Na^+ \quad 6.6$$

$$PPy_n^0 PPy_n^+ pTS^- + Na^+ + e^- \rightarrow PPy_n^0 pTS^- Na^+ + pTS^- \quad 6.7$$

$$PPy_n^0 PPy_n^+ pTS^- + Cl^- - e^- \rightarrow PPy_n^+ pTS^- Cl^- \quad 6.8$$

$$PPy_n^+ pTS^- Cl^- + e^- \rightarrow PPy_n^0 PPy_n^+ pTS^- + Cl^- + pTS^- \quad 6.9$$

However, in a solution of NapTS, only the exchange of Na^+ takes place because pTS^- cannot be exchanged due to its large size[42, 43]. VPA^- is only slightly smaller in size than pTS^-. It may be that it is too large a counterion for VPA^- exchange to take place. Nevertheless, some VPA^- was measured from the polymers during the release studies which suggests that some exchange did take place. The amount of pTS^- being expelled from the polymer during ionic exchange in the VPA^- was measured over 50 cycles and is shown in Figure 6.24. The amount is much lower compared to that in Figure 6.23A which indicates that VPA^- may be too large for sufficient anion exchange to take place.

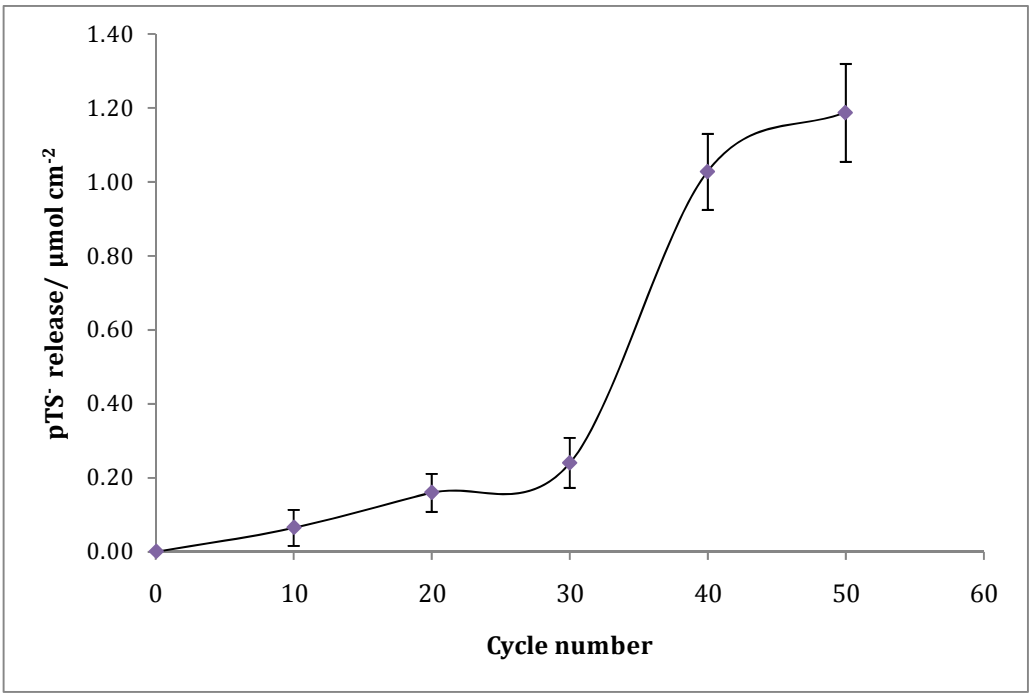

Figure 6.24: The amount of pTS^- measured as pTS^- doped PPy was cycled in 0.50 mol dm^{-3} NaVPA 50 times, scanning between **–**0.200 V vs SCE and +0.500 V vs SCE at 25 mV s^{-1}. (n=2)

It could be that a small amount of VPA^- is exchanged on the surface of the polymer and that could account for the VPA^- that was measured during the release studies. If the drug was on the surface of the polymer then its release could not be controlled by applying a potential, be it reduction or oxidation, and this may explain the ambiguous relationship the VPA^- release has with the release potential.

A final experiment was then performed in an attempt to completely expel pTS^- from the polymer and dope it with VPA^-. PPypTS was grown galvanostatically as before on the bare gold mylar. A potential of –0.700 V vs SCE was then applied for 2 h in the presence of NaVPA with the aim of completely removing all pTS^- from the PPy. It was then placed in a fresh electrolyte of NaVPA and a potential of +0.500 V vs SCE was applied for 1 h. The polymer was then placed in an electrolyte of 0.20 mol dm^{-3} NaCl and a reduction potential of –0.500 V vs SCE was then applied. As discussed in Section 2.5.1, a calibration curve of the NaVPA was obtained by UV-vis spectroscopy and the concentrations of the VPA^- in these samples were calculated using the slope of the calibration curve. Representative data are shown in Figure 6.25. The amount of VPA^- measured was similar to that of

pTS^-, as shown from a comparison of Figure 6.25 and Figure 6.23B, but the polymer had to have one dopant entirely expelled before it could be doped with another. Though this method showed some promise, it was very time consuming and not an ideal way of doping PPy with VPA^-.

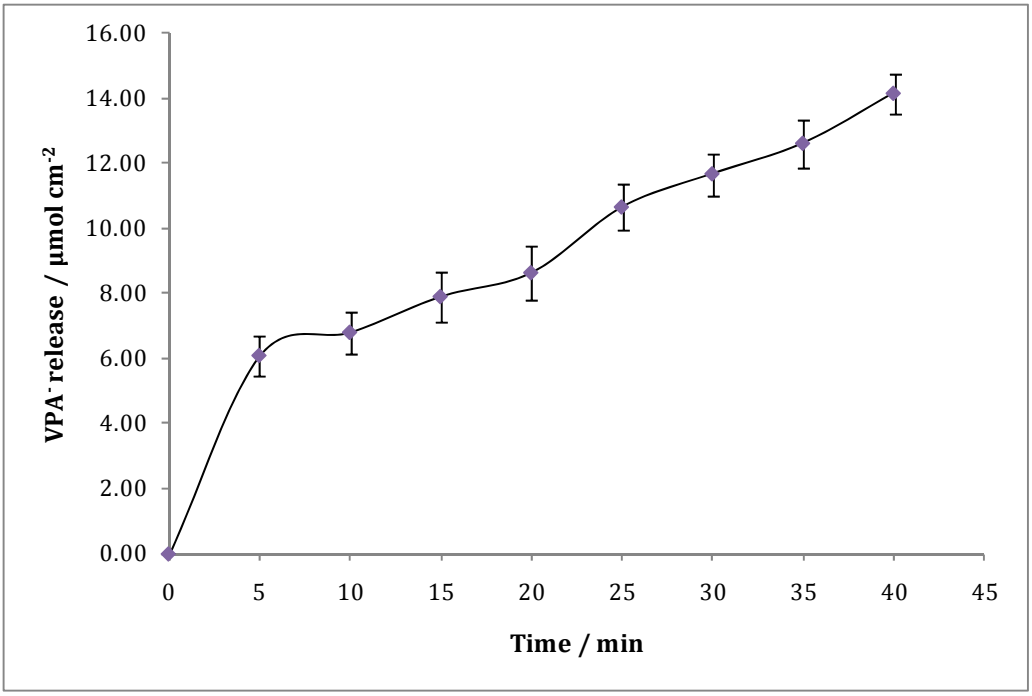

Figure 6.25: Amount of VPA^- measured, in 0.20 mol dm^{-3} NaCl, from the polymer at a reduction potential of –0.500 V vs SCE. All pTS^- was expelled from the PPypTS polymer by applying a potential of –0.700 V vs SCE for 2 h in the presence of 0.50 mol dm^{-3} NaVPA, before doping the polymer with VPA^- by applying a potential of +0.500 V vs SCE for 1 h in the presence of 0.50 mol dm^{-3} NaVPA. (n=2)

6.3.7 Vapour phase polymerisation (VPP)

Since the successful deposition of PPy doped with VPA^- by means of electrochemistry proved difficult, an alternative approach was investigated. Vapour phase polymerisation (VPP) is a simple way to polymerise Py before incorporating molecules into the polymer. Bjorn Winther- Jensen *et al.*[46] reported the successful VPP of Py and the same protocol was followed in this work. Once the polymerisation process was optimised, the next step was to investigate how much VPA^- could be immobilised into the polymer. The polymers were collapsed and 'stuffed' with three different percentages of NaVPA in ethanol (EtOH); 0.5 %, 1.0 % and 2.0 %. Characterisation studies were carried out on the polymer during the

VPP process. CV was carried out in $NaNO_3$ before and after the polymer was rinsed with 0.5 % NaVPA in EtOH. These were then compared to cyclic voltammograms of a polymer rinsed with 0.5 % $NaNO_3$ in EtOH. All cyclic voltammograms can be seen in Figure 6.26. The cyclic voltammogram of NO_3^- 'stuffed' in the polymer is very similar to that of VPA^- 'stuffed' in the polymer suggesting that there is indeed VPA^- incorporated into the PPy.

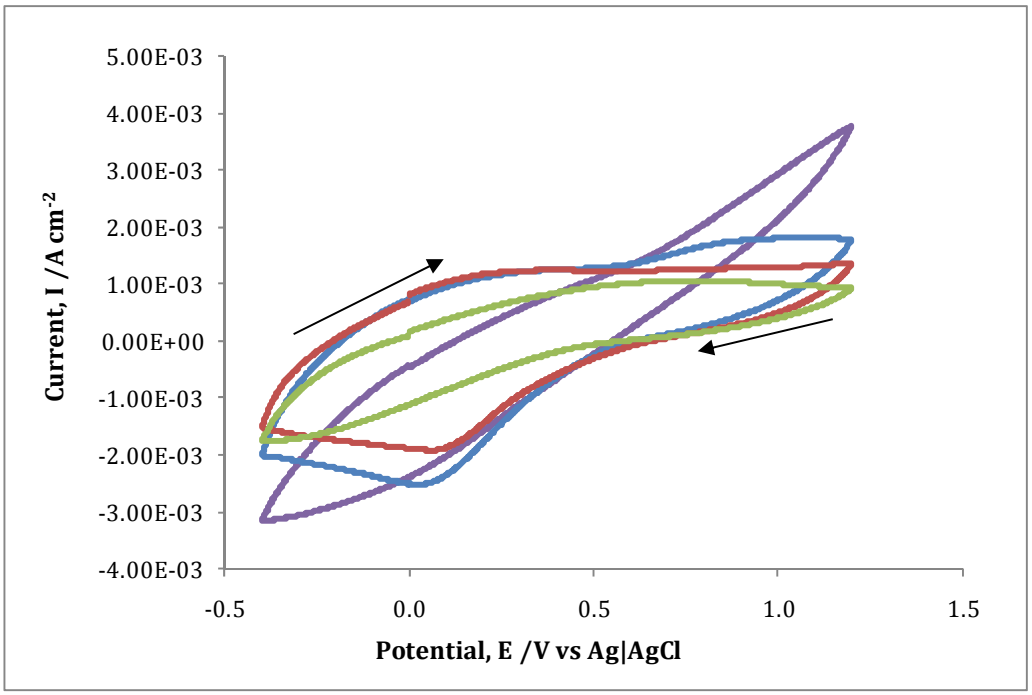

Figure 6.26: CV plot, scanning between – 0.400 V vs Ag|AgCl and +1.200 V vs Ag|AgCl at a scan rate of 25 mV s^{-1} in 0.10 mol dm^{-3} $NaNO_3$, of — PPy before collapse, — PPy 'stuffed' with 0.5 % NaVPA, — PPy ' stuffed' with 0.5 % $NaNO_3$ and — PPy rinsed in EtOH.

Release studies were carried out at –0.100 V vs Ag|AgCl, –0.600 V vs Ag|AgCl and passively and were monitored over a 4 h period from the polymers with 1.0 % VPA^- and 2.0 % VPA^-. The amount of VPA^- released is shown in Figure 6.27. The amount of drug measured after the 4 h release periods was quite low. No other release potentials were investigated as these preliminary results indicated that VPA^- release from these loading levels would be minimal.

VPP is quite a hard technique to achieve consistent reproducibility. The two main concerns were; the adhesion of the polymer to the ITO glass surface during the rinsing process and optimising how much Fe(III) [TOS] was applied to the

substrate. VPP is a technique that could be used for releasing lower doses of VPA^- but achieving a higher amount of VPA^- release from VPP polymers is thought to be extremely difficult from the experiments that were carried out in these studies.

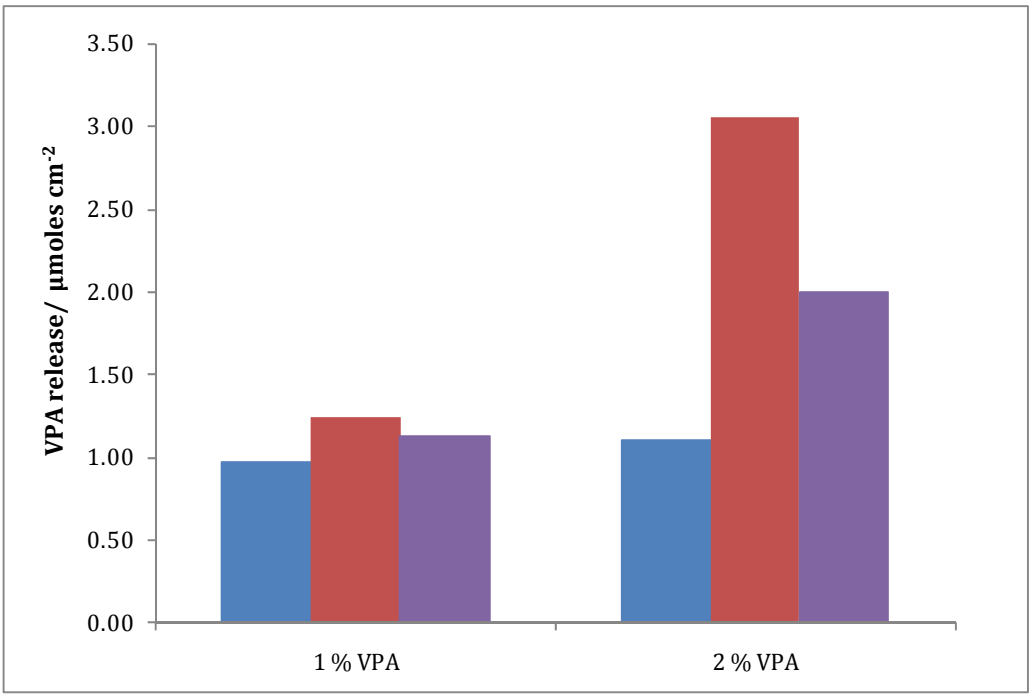

Figure 6.27: VPA^- release measurements from polymers incorporated with VPA^- by VPP. Samples were taken after 4 h and drug release took place at ■ –0.100 V vs Ag|AgCl, ■ passively and ■ at +0.600 V vs Ag|AgCl. (n=2, % error = 6 %)

6.4 Summary of results

This work demonstrates that the electropolymerisation of Py to generate PPy doped with VPA^- is not possible. Several methods of depositing the polymer by electrochemical means were tried and tested, including constant potential, pulsed galvanostatic technique, cyclic voltammetry and depositing onto a pre-layer on the electrode surface. All failed to provide positive results and the reason for this is believed to be associated with the pH of the drug. The lowest pH value where VPA^- is soluble is 5.6. As the monomer oxidises, there is an increase in the concentration of protons in the vicinity of the electrode and the equilibrium is shifted towards the insoluble form of HVPA. As seen in Chapter 4 with the electrodeposition of PPyDF, the local acidity at the electrode causes insoluble drug crystals to form which hinders the rate of polymerisation and it is possible that the difference in pKa between VPA and DF, even though small, means that this local acidity is having

an even greater effect on the formation of PPy doped with VPA^- in that it is preventing any deposition from taking place. It appears that although the monomer is oxidised, there are no soluble anions available at the electrode interface to dope the polymer.

Ionic exchange of the VPA anion with an anion already doped within the PPy was also investigated and release studies of the VPA^- were carried out, however, the amount of VPA^- released from the polymer was independent of the applied potential. Characterisation studies of polymers before and after post-doping were carried out and there was evidence to suggest that VPA^- was exchanged into the polymer. However, upon further investigation it seems that the VPA^- may be too large a counterion for the exchange to occur with efficiency. The anion exchange that was observed occurred only with anions at the polymer-solution interface.

VPP was offered as an alternative to incorporate the VPA^- into the PPy. The release of VPA^- from the polymer was studied and only small amounts of VPA^- were measured. It seems that this is a technique that would be better suited to very low levels of VPA^- release.

6.5 References

1. F. S. Abbott, J. M. Orr, S. M. Ferguson, and R. W. Burton, *Journal of Pharmaceutical Sciences,* **14** (1881).
2. E. Volzke and H. Doose, *Epilepsia,* **14**:185 (1973).
3. P. M. Jeavons and J. E. Clark, *Br Med J,* **2**:584 (1974).
4. H. Meunier, Carraz, G., Meunier, Y., and Eymard, M., *Therapie,* **18**:435 (1963).
5. A. Pellegrini, P. Gloor, and A. L. Sherwin, *Epilepsia,* **19**:351 (1978).
6. S. Daniel and J. K. Penry, *Epilepsia,* **16**:549 (1975).
7. K. Vasudev, S. Das, U. Goswami, and G. Tayal, *Journal of Psychopharmacology,* **15**:187–190 (2001).
8. K. Vasudev, U. Goswami, and K. Kohli, *Psychopharmacology,* **150**:15 (2000).
9. R. Baselt and R. Cravey, *Disposition of Toxic Drugs and Chemicals in Man,*Biomedical Publications, 2004.
10. Y. Godin, L. Heiner, J. Mark, and P. Mandel, *Journal of Neurochemistry,* **16**:869 (1969).
11. S. Simler, L. Ciesielski, M. Maitre, H. Randrianarisoa, and P. Mandel, *Biochemical Pharmacology,* **22**:1701 (1973).
12. T. Wiegand, K. R. Olson, and H. E. Hern, *Emedicine,* (2009).

13. G. Zaccara, A. Messori, and F. Moroni, *Clinical Pharmacokinetics,* **15**:367 (1988).
14. R. B. Carr and K. Shrewsbury, *American Journal of Psychiatry,* **164**:1020 (2007).
15. E. Perucca, R. Grimaldi, G. Gaytfi, S. Pirracchio, F. Crema, and G. M. Frigo, *British Journal of Clinical Pharmacology,* **17**:665 (1984).
16. R. Gugler and G. E. von Unruh, *Clinical Pharmacokinetics,* **5**:67 (1980).
17. R. Gugler, A. Schell, M. Eichelbaum, W. Fröscher, and H. U. Schulz, *European Journal of Clinical Pharmacology,* **12**:125 (1977).
18. C. Lucarelli, P. Villa, E. Lombaradi, P. Prandini, and A. Brega, *Chromatograph,* **33**:37 (1992).
19. S. Cooreman, E. Cuypers, M. De Doncker, P. Van Hee, W. Uyttenbroeck, and H. Neels, *Immuno-analyse & Biologie Spécialisée,* **23**:240 (2008).
20. K. Kondo, M. Nakamura, R. Nishioka, and S. Kawai, *Analytical Sciences,* **1**:385 (1985).
21. J. P. Moody and S. M. Allan, *Clinica Chimica Acta,* **127**:263 (1983).
22. T. Kinoshita and O. Nakajima, *Journal of Tokyo Women Medical College,* **60**:1043 (1990).
23. A. Peterson, T. Lopez, E. O. Islas, and R. D. Gonzalez, *Applied Surface Science,* **253**:5767 (2007).
24. T. Lopez, R. Alexander-Katz, M. G. P.Castillo, J. Manjearrez, R. D. Gonzalez, L. IlHarco, A. Fidalgo, and J. Rieumont, *Journal of Material Science,* **44**:5449 (2009).
25. S. Sadki, P. Schottland, N. Brodie, and G. Sabourand, *Royal Society of Chemistry,* **29**:283 (2000).
26. S. Sabah, M. Aghamohammadi, and N. Alizadeh, *Sensors and Actuators B: Chemical,* **114**:489 (2005).
27. P. Canizares, J. García-Gómez, J. Lobato, and M. A. Rodrigo, *Industrial & Engineering Chemistry Research,* **42**:956 (2003).
28. A. F. Diaz and K. K. Kanazawa, *J.C.S. Chem*:635 (1979).
29. S. E. Moulton, M. D. Imisides, R. L. Shepherd, and G. G. Wallace, *Journal of Materials Chemistry,* **18**:3608 (2008).
30. D. E. Tallman, C. Vang, G. G. Wallace, and G. P. Bierwagen, *Journal of Electrochemical Society,* **149**:C173 (2002).
31. H. A. De Abreu, W. B. De Almeida, and H. A. Duarte, *Chemical Physics Letters,* **383**:47 (2004).
32. S. Shimoda and E. Smela, *Electrochimica Acta,* **44**:219 (1998).
33. A. F. Diaz, J. I. Castillo, J. A. Logan, and W.-Y. Lee, *Journal of Electroanalytical Chemistry,* **129**:115 (1981).
34. S. Aeiyach, B. Zaid, and P. C. Lacaze, *Electrochimica Acta,* **44**:2889 (1999).
35. P. M. M.R. Gandhi, G.M. Spinks, G.G. Wallace, *Synthetic Metals,* **73**:247 (1995).
36. J. M. Ko, H. W. Rhee, S. M. Park, and C. Y. Kim, *Journal of Electrochemistry Society,* **137** (1990).
37. A. S. Liu and M. A. S. Oliveira, *Journal of Brazilian Chemistry Society,* **18**:143 (2007).
38. G. Stevenson, S. E. Moulton, P. C. Innis, and G. G. Wallace, *Synthetic Metals,* **160**:1107 (2010).

39. C. W. Han Xu, Chunlei Wang, Jim Zoval, Marc Madou, *Biosensors and Bioelectronics,* **21**:2094 (2005).
40. T. Hernandez-Perez, M. Morales, N. Batina, and M. Salmon, *Journal of The Electrochemical Society,* **148**:C369 (2001).
41. S. Jing, T.-S. Jadranka, C. Shu Yi, L. Kwong Chi, and A. K. Paul, *Journal of Applied Polymer Science,* **111**:876 (2009).
42. J. Chengyou, Y. Fenglin, and Y. Weishen, *Journal of Applied Polymer Science,* **101**:2518 (2006).
43. L. Sheng, Q. Yubing, and G. Xingpeng, *Journal of Applied Polymer Science,* **114**:2307 (2009).
44. C. Arbizzani, M. Mastragostino, L. Nevi, and L. Rambelli, *Electrochimica Acta,* **52**:3274 (2007).
45. H. Masuda and D. K. Asano, *Synthetic Metals,* **135-136**:43 (2003).
46. J. C. Bjorn Winther - Jenson, Keld West and Gordon Wallace, *Macromolecules,* **37**:5930 (2004).

Chapter 7

Conclusion

7.1 General conclusions

The main objective of this research work was to develop and characterise a controllable drug delivery system for the release of anionic drugs. The biomaterial employed, to allow the incorporation and release of the drugs, was a polypyrrole (PPy) membrane film.

The first drug chosen for investigation was dexamethasone 21-disodium phosphate (NaDex). This drug is effective in a number of treatments and is medium to large in size and highly soluble in aqueous solution. It was easily immobilised into the polymer during the polymerisation process and four methods of deposition were presented. These methods involved a mixture of constant potential, cyclic voltammetry (CV) and depositing a pre-layer of PPyCl onto the electrode prior to deposition of PPyDex. The optimum method of polymerisation was found to be a two step constant potential practice, whereby a constant potential of +0.900 V vs SCE was applied until 0.8 C cm^{-2} of charge was consumed. This was then followed by further growth to 2.0 C cm^{-2} at +0.800 V vs SCE. The total charge consumed during the growth of the polymer was 2.8 C cm^{-2}.

The amount of Dex^{2-} released was measured at several potentials from +0.100 V vs SCE to –1.200 V vs SCE over a period of 60 min, using UV-vis spectroscopy. Release studies were also carried out at open-circuit potential (OCP) and it was clear that the amount of Dex^{2-} released was dependent on the potential applied and was not purely a result of the drug diffusing across the polymer membrane. The fastest release occurred at an applied potential of –0.900 V vs SCE with approximately 27 µmol cm^{-2} of Dex^{2} released after 60 min. The rate of release, at this potential, for the first 5 min was calculated as 2.50 µmol cm^{-2} min^{-1}. The release rate thereafter was 0.531 µmol cm^{-2} min^{-1}, which was significantly higher than the rate of release at any of the other potentials applied. In previous reports[1-3] on the controlled release of Dex^{2-}, the amount of Dex^{2-} released was measured between 3 µg cm^{-2} to 16 µg cm^{-2}. In this study, 13.9 mg cm^{-2} was released after 60 min at –0.900 V vs SCE, which is three-orders of magnitude higher than these literature values. In the aforementioned reports, the PPy was either over-oxidised,

stimulated by connecting to a magnesium anode or an alternative polymer material to PPy was examined which may account for the lower release of Dex^{2-} reported.

With the use of electrochemical quartz crystal microbalance (EQCM), a doping level of 0.30 was calculated for the PPyDex. It was estimated that 89% of the drug was released after 1 h at –0.900 V vs SCE, while approximately 17% was released at OCP. It was found that it was possible to oxidise the reduced polymer so that further Dex^{2-} could be incorporated. These release/incorporation experiments were carried out several times with the same polymer. EQCM measurements indicated that more Dex^{2-} was incorporated each time the oxidation potential was applied, which implies that more PPy^{0} was oxidised back to PPy^{+}. Investigations into the possibility of switching 'on and off' the Dex^{2-} release, by applying oxidation and reduction potentials, were carried out. It was found that the rate of release was considerably mired with the application of an oxidation potential, but the release of Dex^{2-} could not be completely prevented.

Furthermore, the morphology of the PPy film doped with Dex^{2-} was found to be typical of that observed for PPy as reported in the literature[4-6]. However, this was not the case for PPy doped with DF^{-}, the anion form of diclofenac sodium salt (NaDF), the second drug studied and discussed in Chapter 4. At concentrations of 0.10 mol dm^{-3} and higher, the NaDF was insoluble in water and the deposition of PPy doped with DF^{-} was only possible under heated conditions. Direct electrodeposition of the polymer onto the bare electrode proved difficult and therefore it was deposited upon a thin film of PPyCl. With the use of optical imaging and scanning electron microscopy (SEM), crystal-like shards were observed on the surface and embedded within the PPy. Electrochemical impedance spectroscopy (EIS) and cyclic voltammetry (CV) were used to measure the electrochemical activity and conductivity of the polymer. It was found that the PPyDF was not highly conductive due to the crystal-like shards in the polymer. These crystal-like shards were identified as insoluble forms of the drug encased in the polymer and their presence at the surface limited the growth of the PPyDF film.

The formation of these insoluble crystals was explained in terms of the pKa of the drug. The pH of the drug-monomer solution was measured as 7.4. Using the well-known Henderson Hasselbalch equation, the % of anions in solution at this pH was calculated as 99 %. However, according to the mechanism for the electropolymerisation of pyrrole, proposed by Diaz *et al.*[7], there is a loss of protons to form the neutral polymer chains. This loss in protons causes a local acidity at the interface of the electrode which subsequently shifts the equilibrium from the soluble DF^- anions towards the insoluble HDF.

Release studies for DF^- were carried out and the highest amount of DF^- released was measured at –0.700 V vs SCE. Using EQCM the doping level of DF^- within the polymer was estimated at 0.33. The total amount of DF^- released over a 60 min period was about 7.0 μmol cm^{-2} yet only a slightly higher amount, 9.0 μmol cm^{-2}, was measured over a period of 5 h. This is not thought to be an accurate reflection of the amount of DF^- doped within the polymer as the release of the insoluble forms of the drug increased the amount of drug being measured on release. SEM micrographs taken of the polymer after the release studies showed that the majority of the insoluble HDF crystals were removed from the polymer and this would contribute to the final concentration of DF^- in the release electrolyte. It was observed that after the release of these crystals, higher amounts of DF^- could be doped onto the polymer and this meant the successful release of larger amounts of DF^- was possible. This was attributed to the exposure of a more porous polymer structure, the underlying PPyCl, which became doped with DF^- in the presence of the oxidation potential and this resulted in higher uptake and doping by the DF^- anions.

In Chapter 5, the successful electrodeposition of PPy doped with either indomethacin or sulindac in the presence of EtOH is described. Tetrabutylammonium perchlorate (TBAP) was added to the EtOH to increase the conductivity of the electropolymerisation solution. The PPy films were deposited at elevated temperatures to ensure the solubility of the drugs in the ethanol solution. The concentration of the TBAP was kept to a minimum so that the anionic

ClO_4^- would not be preferentially doped within the polymer over the drugs. All polymers were deposited at a constant potential to a charge of 2.8 C cm^{-2} and it was found that the rate of polymerisation was dependent on the temperature at which deposition occurred.

During the release studies it was found that approximately 260 µmol cm^{-2} of $Indo^-$ was doped within the polymer at optimum conditions and after 60 min at an applied potential of –0.800 V vs SCE, 82 % of the $Indo^-$ was released. At –0.900 V vs SCE, 54 µmol cm^{-2} of Sul^- was released from PPySul after 60 min which is equivalent to 90 % of the total amount of Sul^- estimated to be doped within the polymer. Again, the rate of drug release could be controlled with the application of an oxidation potential. It was calculated that between 2.04 x 10^{-6} mol cm^{-2} and 2.19 x 10^{-6} mol cm^{-2} of ClO_4^- was also incorporated into the polymers during deposition. However, this ClO_4^- can be released with the application of a reduction potential and the polymer can be re-oxidised to incorporate only Sul^- or $Indo^-$. On application of the optimum reduction potentials, large amounts of $Indo^-$ or Sul^-, in the absence of ClO_4^- , can be released.

Although there have been no reports in the literature of the electrochemical release of either $Indo^-$ or Sul^-, their release has been documented using other methods. Lee *et al.*[8] reported the release of Indo transdermally across skin that was pretreated with an erbium:YAG laser and observed an average rate of release of 27.53 µg cm^{-2} h^{-1}. Taking the rate of release of $Indo^-$ in this work to be 2.70 µmol cm^{-2} min^{-1}, this corresponds to 54.1 mg cm^{-2} h^{-1} which is higher than that of the transdermal release. Kim *et al.*[9, 10] reported a 42 % release of Indo from micelles and nanospheres but it is not clear how much Indo was initially entrapped, while Liu *et al.*[11], who also reported the release of Indo from micelles, calculated the encapsulation of approximately 9 to 10 drug molecules per micelle. Benson and co-workers[12] reported the release of 7 mg Sul from polymer mircocarriers over a 20 h period and this equated to 90 % of the drug entrapped within the polymer. This is much lower than the amount of Sul^- incorporated and released from PPy in this work, which is approximately 20 mg.

EIS, EQCM and SEM were employed to characterise these polymer films. It was found that PPy films deposited in EtOH are less conductive than those electrosynthesised under aqueous conditions. In particular, the PPyIndo film exhibits poor conducting properties, as evidenced from both CV data and EIS. From EQCM analysis, the average doping level of $Indo^-$ within the polymer was calculated as 0.24 which indicates a ratio of 4:1 for monomer-to-dopant. A similar doping ratio has been reported for PPy doped with camphorsulfonate (CS^-)[13]. For PPySul, a doping level of 0.075 was determined which is the lowest for any of the polymers studied in this work. Indeed, a doping level this low is unusual for PPy, with even polymers of low electrical conductivity having doping levels of 0.25–0.28[13, 14]. Doping levels as low as 0.14 and 0.15 have only been documented for pyrrole derivatives of poly(N-butylpyrrole) and poly(2-cyanoethyl)pyrrole[15]. Using SEM, the morphology of the polymers was found to be typical of PPy electrodeposited in the presence of an organic media, such as acetonitrile.

Finally in Chapter 6, the incorporation of a small soluble drug, valproic acid sodium salt (NaVPA), was investigated. There is only one report in the literature on the doping of PPy with VPA^-. Sabah *et al.*[16] reported the electrodeposition of a PPy film doped with VPA^- using pulsed galvanostatic technique. However, they did not show any data proving this polymer was formed. This method along with several other electrochemical methods of depositing the polymer were tried and tested, including constant potential, CV and depositing onto a pre-layer on the electrode surface. All failed to provide positive results and the reason for this is believed to be associated with the pH of the drug. The lowest pH value where VPA^- is soluble is 5.6. As the monomer oxidises, there is an increase in the concentration of protons in the vicinity of the electrode and the equilibrium is shifted towards the insoluble form of HVPA. As seen with the electrodeposition of PPyDF, the local acidity at the electrode causes insoluble drug crystals to form which hinders the rate of polymerisation. It is possible that the difference in pKa between VPA (4.95) and DF (4.0), even though small, means that this local acidity is having an even greater effect on the formation of PPy doped with VPA^- in that it is preventing any deposition from taking place. It seems that although the monomer is oxidised,

there are no soluble anions available at the electrode interface to dope the polymer.

Ionic exchange of the VPA^- anion with an anion already doped on the PPy was also investigated and release studies of the VPA^- were carried out, however, the amount of VPA^- released from the polymer was independent of the applied potential. Characterisation studies of polymers before and after post-doping were carried out and there was evidence to suggest that VPA^- was exchanged into the polymer, but when this was further investigated it seems that the VPA^- may be too large a counterion for the exchange to occur with efficiency. It seems that the anion exchange occurs only with anions at the polymer-solution interface. Vapour phase polymerisation was offered as an alternative to incorporate the VPA^- into the PPy. The release of VPA^- from the polymer was studied, but only small amounts of VPA^- were measured. It seems that this is a technique that would be better suited to very low levels of VPA^- release.

In many of the articles published about drug delivery, emphasis is generally placed on the size and charge of the dopant. Although size and charge are important the pKa of the drug is often overlooked. The studies of VPA^- and DF^- in this work highlight that a small difference in pKa can have significant effects on the success of a drug delivery system and a small dopant with a negative charge does not guarantee a successful dopant.

Overall, the main goals of this research work have been achieved and in general the amount of drug that was incorporated and released from the polymers is higher than those currently reported in the literature. To further develop these systems with the aim of implantation, the size of the electrode would need to be reduced significantly, which in turn would affect the amount of drug being doped and released. Other future studies include *in vitro* biocompatibility studies followed by *in vivo* studies. These would include completing release studies in the presence of proteins, lipids and other active ingredients of body tissue. It would also be necessary to monitor the shelf-life of the implants over an extended period of time and to study the drug release properties to confirm that after weeks or

months of implantation the polymer is still capable of allowing controlled drug release.

7.2 References

1. G. Stevenson, S. E. Moulton, P. C. Innis, and G. G. Wallace, *Synthetic Metals,* **160**:1107 (2010).
2. S. E. Moulton, M. D. Imisides, R. L. Shepherd, and G. G. Wallace, *Journal of Materials Chemistry,* **18**:3608 (2008).
3. R. Wadhwa, C. F. Lagenaur, and X. T. Cui, *Journal of Controlled Release,* **110**:531 (2005).
4. J. M. Ko, H. W. Rhee, S. M. Park, and C. Y. Kim, *Journal of Electrochemical Society,* **137** (1990).
5. A. S. Liu and M. A. S. Oliveira, *Journal of Brazilian Chemistry Society,* **18**:143 (2007).
6. M. Bazzaoui, E. A. Bazzaoui, L. Martins, and J. I. Martins, *Synthetic Metals,* **130**:73 (2002).
7. E. M. Genies, G. Bidan, and A. F. Diaz, *Journal of Electroanalytical Chemistry,* **149**:101 (1983).
8. A. F. Diaz, J. I. Castillo, J. A. Logan, and W.-Y. Lee, *Journal of Electroanalytical Chemistry,* **129**:115 (1981).
9. S. Y. Kim, Y. M. Lee, H. J. Shin, and J. S. Kang, *Biomaterials,* **22**:2049 (2001).
10. S. Y. Kim, I. L. G. Shin, Y. M. Lee, C. S. Cho, and Y. K. Sung, *Journal of Controlled Release,* **51**:13 (1998).
11. M. Liu, K. Kono, and J. M. J. Fréchet, *Journal of Controlled Release,* **65**:121 (2000).
12. W. Landgraf, N.-H. Li, and J. R. Benson, *Drug Delivery Technology* **3**(2003).
13. A. O. V. Syritski, O. Forsen, *Electrochimica Acta* **48**:1409 (2003).
14. M. C. Pedro, C. Milagros, O. Estibalitz, C. Elena, and A. P. José, *Surface and Interface Analysis,* **39**:26 (2007).
15. Z. Deng, D. C. Stone, and M. Thompson, *Analyst,* **122**:1129 (1997).
16. M. A. Simin Sabah, Naader Alizadeh, *Sensors and Actuators,* **114**:489 (2005).
17. D. A. LaVan, T. McGuire, and R. Langer, *Nature Biotechnology,* **21**:1184 (2003).